

DYNAMIC BEHAVIOR OF WATER AND AIR CHEMISTRY IN INDOOR POOL FACILITIES

by

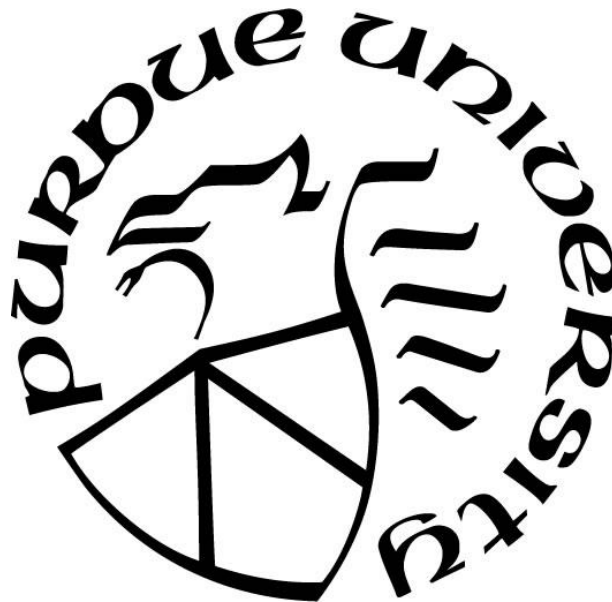
Lester Ting Chung Lee

A Dissertation

Submitted to the Faculty of Purdue University

In Partial Fulfillment of the Requirements for the degree of

Doctor of Philosophy



Lyles School of Civil Engineering

West Lafayette, Indiana

December 2021

THE PURDUE UNIVERSITY GRADUATE SCHOOL
STATEMENT OF COMMITTEE APPROVAL

Dr. Ernest R. Blatchley III, Chair

Lyles School of Civil Engineering

Dr. Chad T. Jafvert

Lyles School of Civil Engineering

Dr. Loring F. Nies

Lyles School of Civil Engineering

Dr. Melissa Millerick-May

College of Human Medicine, Michigan State University

Approved by:

Dr. Dulcy M. Abraham

To my family, for their love, patience, understanding, and support.

ACKNOWLEDGMENTS

Great appreciation is extended to my advisor Dr. Ernest R. Blatchley III for his expertise, guidance, encouragement, and support. Also, sincere gratitude is given to my advising committee, Dr. Chad Jafvert, Dr. Loring Nies, and Dr. Melissa Millerick-May for devoting time to serving on my research committee.

Many thanks to the National Swimming Pool Foundation (now Pool & Hot Tub Alliance) and the Council for the Model Aquatic Health Code (CMAHC) for their financial support.

Much appreciation is offered to my colleagues in the research group for their cooperation in the laboratory and field. Special thanks are for Dr. Nadezhda N. Zyaykina for her assistance in our laboratory.

Special thanks go to swimming pool facility personnel and staff members who aided in sampling of pool water and air. Specials thanks go to Steve Mueller from PoolPak for assisting the Phase I study. Also, many thanks go to Frederic Hammel from Ethera Labs for providing indoor air quality monitoring devices used in this study. Also, thanks go to Hiden Analytical for providing a portable MIMS instrument for use in this study.

TABLE OF CONTENTS

LIST OF TABLES	7
LIST OF FIGURES	8
ABSTRACT	19
1. INTRODUCTION	22
2. LITERATURE REVIEW	29
2.1 Swimming Pool Treatment	29
2.2 Chlorine Chemistry	32
2.3 Volatile Disinfection By-product (DBP) Formation.....	33
2.4 Health Effects of Exposure to Volatile DBPs.....	38
2.5 Indoor Air Quality (IAQ) Model	40
3. METHODS AND MATERIALS	42
3.1 Analytical Methods	42
3.1.1 Chemtrac HydroAct 4.....	42
3.1.2 DPD/KI	44
3.1.3 Membrane Introduction Mass Spectrometry (MIMS).....	45
3.1.4 Digestion/colorimetric Method for Urea Analysis	48
3.1.5 Air Quality Monitor	48
3.2 Sampling	49
3.2.1 Pool Characteristics	49
3.2.2 Water Sampling	52
3.2.3 Air Sampling.....	59
3.2.4 Flow rate measurements at pool facility B	63
3.3 IAQ Model	65
3.3.1 Model Assumptions	65
3.3.2 IAQ Model Governing Equation	70
4. PHASE 1.....	74
4.1 Phase 1	74
4.1.1 Trends of Chlorine, ORP, and pH	74
4.1.2 Trends of Turbidity.....	78

4.1.3	Trends of Volatile DBPs.....	80
4.1.4	Trend of Urea.....	93
4.1.5	Trend of Gas-phase NCl_3	95
4.2	Summary and conclusions	103
5.	PHASE 2.....	104
5.1	Measurements at Pool facility B	104
5.1.1	Measurements in February 2019	104
5.1.2	Measurements in March 2019	117
5.1.3	Measurements in April 2019	127
5.1.4	Measurements in June 2019.....	135
5.1.5	Measurements in November 2019	146
5.2	Measurements at Pool facility C	156
5.3	Measurements at Pool facility D.....	162
5.4	Measurements at Pool facility E	174
5.5	Summary of liquid-phase volatile DBP measurements	182
5.6	Summary of gas-phase NCl_3 and CO_2 measurements.....	191
6.	PHASE 3 (IAQ MODEL).....	196
6.1	Derivation of the governing equations.....	196
6.2	Estimation of parameters	199
6.3	Results of NCl_3 IAQ model	202
6.4	Results of CO_2 IAQ model	223
7.	SUMMARY AND CONCLUSIONS	234
	REFERENCES	238
	APPENDIX A. SAMPLE SPREAD SHEET FOR NCl_3 MODEL.....	249
	APPENDIX B. SAMPLE SPREAD SHEET FOR CO_2 MODEL.....	251

LIST OF TABLES

Table 2.1. Typical concentrations of nitrogenous compounds in human sweat and urine.	36
Table 3.1. Limits of detection for volatile DBPs by benchtop MIMS system based on a signal:noise ratio of 2:1.....	47
Table 3.2. Limits of detection for volatile DBPs by benchtop MIMS system based on a signal:noise ratio of 2:1.....	48
Table 3.3. Summarized of the characteristics of all the studied pools.....	51
Table 3.4. Summary of meet schedules, timing of sample collection, and measurements.....	61
Table 3.5. NEMo device placement in pools.....	62
Table 5.1. Arithmetic mean DBP concentrations plus minimum and maximum concentration values for pool facility A to E.....	188
Table 5.2. Correlation matrix for DBPs in water samples collected at pool facility B.	190
Table 5.3. The Arithmetic mean gas-phase NCl_3 concentrations plus minimum and maximum concentration values for pool facility B to E.	193
Table 5.4. The correlation coefficients between NCl_3 and CO_2 in each NEMo devices.....	195
Table 6.1. Input parameters used in NCl_3 IAQ model spreadsheet.	204
Table 6.2. Summary of conditions of each experiment and corresponding estimates of mass transfer coefficients for NCl_3	212
Table 6.3. Input parameters used in CO_2 IAQ model spreadsheet.	225
Table 6.4. Calculated and estimated liquid-phase mass transfer coefficients of CO_2 for Facility B during the June 2019 and November 2019 experiments.....	228

LIST OF FIGURES

Figure 3.1. HydroAct 4 with each sensor and recirculation lines set up in control room.....	44
Figure 3.2. PalinTest portable photometer.....	45
Figure 3.3. MIMS system. (a) Photo of Agilent 6850 GC with 5975C MSD and pumping system: (b) schematic of membrane device, as installed in the GC.....	46
Figure 3.4. Portable MIMS system.	47
Figure 3.5. NEMo air quality monitor.	49
Figure 3.6. Layout of Pool facility A during phase 1 study.....	54
Figure 3.7. Layout of Pool facility B during February 2019 measurements.	54
Figure 3.8. Gas-phase NCl_3 CFD profile of Pool facility B.	55
Figure 3.9. Layout of Pool facility B during March 2019 measurements.	55
Figure 3.10. Layout of Pool facility C during March 2019 measurements.	56
Figure 3.11. Layout of Pool facility B during April 2019 measurements.	56
Figure 3.12. Layout of Pool facility B during June 2019 measurements.	57
Figure 3.13. Layout of Pool facility D during August 2019 measurements.	57
Figure 3.14. Layout of Pool facility B during November 2019 measurements.....	58
Figure 3.15. Layout of Pool facility E during January 2020 measurements.....	58
Figure 3.16. Air flow rates with fitting curves as functions of their respective damper opening settings for five air handling units in pool facility B.	64
Figure 3.17. Schematic representation of two-film model for gas-liquid transfer.....	70
Figure 3.18. Schematic illustration of control region and relevant parameters of IAQ model.....	71
Figure 4.1. Time-course monitoring of free chlorine, total chlorine and ORP at pool A.....	76
Figure 4.2. Time-course monitoring of pH at pool A.	77
Figure 4.3. Time-course monitoring of turbidity at pool A.	79
Figure 4.4. Time-course monitoring of liquid-phase NH_2Cl at pool A measured by MIMS. Red triangle symbols represent the water sample collected from the pool. Blue circle symbols represent water samples collected after filtration. The black dashed line represents the detection limit. Empty circle symbols represent measurements before swimming practices. Empty triangle symbols represent measurements after swimming practices. Pink vertical bars represent swimmer counts.	81

Figure 4.5. Time-course monitoring of liquid-phase NHCl_2 at pool A measured by MIMS. Red triangle symbols represent the water sample collected from the pool. Blue circle symbols represent water samples collected after filtration. The black dashed line represents the detection limit. Empty circle symbols represent measurements before swimming practices. Empty triangle symbols represent measurements after swimming practices. Pink vertical bars represent swimmer counts. 82

Figure 4.6. Time-course monitoring of liquid-phase NCl_3 at pool A measured by MIMS. Red triangle symbols represent the water sample collected from the pool. Blue circle symbols represent water samples collected after filtration. The black dashed line represents the detection limit. Empty circle symbols represent measurements before swimming practices. Empty triangle symbols represent measurements after swimming practices. Pink vertical bars represent swimmer counts. 83

Figure 4.7. Combined chlorine measured by MIMS and DPD. Triangle red line represents combined chlorine measured by MIMS collected at pool. Circle blue line represents combined chlorine measured by MIMS collected after filtration. Pink square line represents combined chlorine measured by DPD collected at the pool. 85

Figure 4.8. Time-course monitoring of CHCl_3 at pool A measured by MIMS. Red triangle symbols represent water samples collected from the pool. Blue circle symbols represent water samples collected after filtration. The black dashed line represents the detection limit. Empty circle symbols represent measurements before swimming practices. Empty triangle symbols represent measurements after swimming practices. Pink vertical bars represent swimmer counts. 87

Figure 4.9. Time-course monitoring of CNCl at pool A measured by MIMS. Red triangle symbols represent water samples collected from the pool. Blue circle symbols represent water samples collected after filtration. The black dashed line represents the detection limit. Empty circle symbols represent measurements before swimming practices. Empty triangle symbols represent measurements after swimming practices. Pink vertical bars represent swimmer counts. 89

Figure 4.10. Time-course monitoring of CNCHCl_2 at pool A measured by MIMS. Red triangle symbols represent water samples collected from the pool. Blue circle symbols represent water samples collected after filtration. The black dashed line represents the detection limit. Empty circle symbols represent measurements before swimming practices. Empty triangle symbols represent measurements after swimming practices. Pink vertical bars represent swimmer counts. 91

Figure 4.11. Time-course monitoring of CH_3NCl_2 at pool A measured by MIMS. Red triangle symbols represent water samples collected from the pool. Blue circle symbols represent water samples collected after filtration. The black dashed line represents the detection limit. Empty circle symbols represent measurements before swimming practices. Empty triangle symbols represent measurements after swimming practices. Pink vertical bars represent swimmer counts. 92

Figure 4.12. Time-course monitoring of urea. Red triangle symbols represent water samples collected from the pool. Blue circle symbols represent water samples collected after filtration. Empty circle symbols represent measurements before swimming practices. Empty triangle symbols represent measurements after swimming practices. Pink vertical bars represent swimmer counts. 94

Figure 4.13. Time-course monitoring of air samples from 11/13/2017 to 11/19/2017. Red line represents the relative humidity at the pool facility. Blue line represents the gas-phase NCl_3 collected by NEMo. Two horizontal lines represent relative humidities of 30% and 60%. Pink vertical bars represent swimmer counts.	96
Figure 4.14. Time-course monitoring of air samples from 11/20/2017 to 11/26/2017. Red line represents the relative humidity at the pool facility. Blue line represents the gas-phase NCl_3 collected by NEMo. Two horizontal lines represent relative humidities of 30% and 60%. Pink vertical bars represent swimmer counts.	97
Figure 4.15. Time-course monitoring of air samples from 11/27/2017 to 12/3/2017. Red line represents the relative humidity at the pool facility. Blue line represents the gas-phase NCl_3 collected by NEMo. Two horizontal lines represent relative humidities of 30% and 60%. Pink vertical bars represent swimmer counts. Vertical dark blue line represents the date of a filter media change.	98
Figure 4.16. Time-course monitoring of air samples 12/11/2017 to 12/17/2017. Red line represents the relative humidity at the pool facility. Blue line represents the gas-phase NCl_3 collected by NEMo. Two horizontal lines represent relative humidities of 30% and 60%. Pink vertical bars represent swimmer counts.	99
Figure 4.17. Time-course monitoring of air samples from 12/18/2017 to 12/24/2017. Red line represents the relative humidity at the pool facility. Blue line represents the gas-phase NCl_3 collected by NEMo. Two horizontal lines represent relative humidities of 30% and 60%. Pink vertical bars represent swimmer counts.	100
Figure 4.18. Time-course monitoring of air samples from 12/25/2017 to 12/31/2017. Red line represents the relative humidity at the pool facility. Blue line represents the gas-phase NCl_3 collected by NEMo. Two horizontal lines represent relative humidities of 30% and 60%. Pink vertical bars represent swimmer counts.	101
Figure 4.19. Time-course monitoring of air samples from 1/1/2018 to 1/7/2018. Red line represents the relative humidity at the pool facility. Blue line represents the gas-phase NCl_3 collected by NEMo. Two horizontal lines represent relative humidities of 30% and 60%. Pink vertical bars represent swimmer counts.	102
Figure 5.1. Time-course monitoring of NH_2Cl at pool facility B during swimming meet in February 2019. Light blue regions indicate when swimmers were present in the pool. Horizontal line represents the detection limit.	106
Figure 5.2. Time-course monitoring of NHCl_2 at pool facility B during swimming meet in February 2019. Light blue regions indicate when swimmers were present in the pool. Horizontal line represents the detection limit.	107
Figure 5.3. Time-course monitoring of NCl_3 at pool facility B during swimming meet in February 2019. Light blue regions indicate when swimmers were present in the pool. Horizontal line represents the detection limit.	108
Figure 5.4. Time-course monitoring of CHCl_3 at pool facility B during swimming meet in February 2019. Light blue regions indicate when swimmers were present in the pool. Horizontal line represents the detection limit.	109

Figure 5.5. Time-course monitoring of CNCl at pool facility B during swimming meet in February 2019. Light blue regions indicate when swimmers were present in the pool. Horizontal line represents the detection limit.	110
Figure 5.6. Time-course monitoring of CHCHCl_2 at pool facility B during swimming meet in February 2019. Light blue regions indicate when swimmers were present in the pool. Horizontal line represents the detection limit.	111
Figure 5.7. Time-course monitoring of CH_3NCl_2 at pool facility B during swimming meet in February 2019. Light blue regions indicate when swimmers were present in the pool. Horizontal line represents the detection limit.	112
Figure 5.8. Time-course monitoring of urea at pool facility B during swimming meet in February 2019. Light blue region indicates when swimmers were present in the pool.	113
Figure 5.9. Time-course monitoring of gas-phase NCl_3 and RH measured by NEMo devices at pool facility B during swimming meet in February 2019. Blue regions indicate when swimmers were present in the pool.	115
Figure 5.10. Time-course monitoring of gas-phase NCl_3 and gas-phase CO_2 measured by NEMo devices at pool facility B during swimming meet in February 2019. Blue regions indicate when swimmers were present in the pool.....	116
Figure 5.11. Time-course monitoring of free chlorine, total chlorine, and combined chlorine at pool facility B during regular operating hours in March 2019. Vertical bars represent the swimmer number in the pool.	119
Figure 5.12. Time-course monitoring of NH_2Cl at pool facility B during regular operating hours in March 2019. Vertical bars represent the swimmer number in the pool.....	119
Figure 5.13. Time-course monitoring of NHCl_2 at pool facility B during regular operating hours in March 2019. Vertical bars represent the swimmer number in the pool. Horizontal line represents the detection limit.	120
Figure 5.14. Time-course monitoring of NCl_3 at pool facility B during regular operating hours in March 2019. Vertical bars represent the swimmer number in the pool. Horizontal line represents the detection limit.	120
Figure 5.15. Time-course monitoring of CHCl_3 at pool facility B during regular operating hours in March 2019. Vertical bars represent the swimmer number in the pool. Horizontal line represents the detection limit.	121
Figure 5.16. Time-course monitoring of CNCl at pool facility B during regular operating hours in March 2019. Vertical bars represent the swimmer number in the pool. Horizontal line represents the detection limit.	121
Figure 5.17. Time-course monitoring of CNCHCl_2 at pool facility B during regular operating hours in March 2019. Vertical bars represent the swimmer number in the pool. Horizontal line represents the detection limit.	122

Figure 5.18. Time-course monitoring of CH_3NCl_2 at pool facility B during regular operating hours in March 2019. Vertical bars represent the swimmer number in the pool. Horizontal line represents the detection limit.	122
Figure 5.19. Time-course monitoring of urea at pool facility B during regular operating hours in March 2019. Vertical bars represent the swimmer number in the pool.	123
Figure 5.20. Time-course monitoring of gas-phase NCl_3 and RH measured by NEMo devices at pool facility B during regular operating hours in March 2019. Vertical bars represent the swimmer number in the pool.	125
Figure 5.21. Time-course monitoring of gas-phase NCl_3 and gas-phase CO_2 measured by NEMo devices at pool facility B during regular operating hours in March 2019. Vertical bars represent the swimmer number in the pool.	126
Figure 5.22. Time-course monitoring of NH_2Cl at pool facility B during regular operating conditions in April 2019. Vertical bars represent the swimmer number in the pool. Horizontal line represents the detection limit.	128
Figure 5.23. Time-course monitoring of NHCl_2 at pool facility B during regular operating conditions in April 2019. Vertical bars represent the swimmer number in the pool. Horizontal line represents the detection limit.	128
Figure 5.24. Time-course monitoring of NCl_3 at pool facility B during regular operating conditions in April 2019. Horizontal line represents the detection limit.	129
Figure 5.25. Time-course monitoring of CHCl_3 at pool facility B during regular operating conditions in April 2019. Horizontal line represents the detection limit.	129
Figure 5.26. Time-course monitoring of CNCl at pool facility B during regular operating conditions in April 2019. Horizontal line represents the detection limit.	130
Figure 5.27. Time-course monitoring of CNCHCl_2 at pool facility B during regular operating conditions in April 2019. Horizontal line represents the detection limit.	130
Figure 5.28. Time-course monitoring of CH_3NCl_2 at pool facility B during regular operating conditions in April 2019. Horizontal line represents the detection limit.	131
Figure 5.29. Time-course monitoring of urea at pool facility B during regular operating conditions in April 2019. Vertical bars represent the swimmer number in the pool.	131
Figure 5.30. Time-course monitoring of gas-phase NCl_3 and RH measured by NEMo devices at pool facility B during regular operating hours in April 2019. Vertical bars represent the number of swimmers in the pools.	133
Figure 5.31. Time-course monitoring of gas-phase NCl_3 and gas-phase CO_2 measured by NEMo devices at pool facility B during regular operating hours in April 2019. Vertical bars represent the number of swimmers in the pools.	134
Figure 5.32. Time-course monitoring of free and total at pool facility B during swimming meet in June 2019. Vertical bars represent the number of swimmers in the pools.	137

Figure 5.33. Time-course monitoring of pH at pool facility B during swimming meet in June 2019.	137
Figure 5.34. Time-course monitoring of alkalinity at pool facility B during swimming meet in June 2019.....	138
Figure 5.35. Trend of calculated aqueous-phase CO ₂ at pool facility B during swimming meet in June 2019.	138
Figure 5.36. Time-course monitoring of aqueous-phase NH ₂ Cl at pool facility B during swimming meet in June 2019. Vertical bars represent the number of swimmers in the pools. Horizontal line represents the detection limit.	139
Figure 5.37. Time-course monitoring of aqueous-phase NHCl ₂ at pool facility B during swimming meet in June 2019. Vertical bars represent the number of swimmers in the pools. Horizontal line represents the detection limit.	139
Figure 5.38. Time-course monitoring of aqueous-phase NCl ₃ at pool facility B during swimming meet in June 2019. Vertical bars represent the number of swimmers in the pools. Horizontal line represents the detection limit.	140
Figure 5.39. Time-course monitoring of aqueous-phase CHCl ₃ at pool facility B during swimming meet in June 2019. Vertical bars represent the number of swimmers in the pools. Horizontal line represents the detection limit.	140
Figure 5.40. Time-course monitoring of aqueous-phase CNCl at pool facility B during swimming meet in June 2019. Vertical bars represent the number of swimmers in the pools. Horizontal line represents the detection limit.	141
Figure 5.41. Time-course monitoring of aqueous-phase CNCHCl ₂ at pool facility B during swimming meet in June 2019. Vertical bars represent the number of swimmers in the pools. Horizontal line represents the detection limit.	141
Figure 5.42. Time-course monitoring of aqueous-phase CH ₃ NCl ₂ at pool facility B during swimming meet in June 2019. Vertical bars represent the number of swimmers in the pools. Horizontal line represents the detection limit.	142
Figure 5.43. Time-course monitoring of aqueous-phase urea at pool facility B during swimming meet in June 2019. Vertical bars represent the number of swimmers in the pools.....	142
Figure 5.44. Time-course monitoring of gas-phase NCl ₃ and RH, as measured by NEMo devices at pool facility B during swimming meet in June 2019. Vertical bars represent the number of people in each area of pool facility B.	144
Figure 5.45. Time-course monitoring of gas-phase NCl ₃ and gas-phase CO ₂ , as measured by NEMo devices at pool facility B during swimming meet in June 2019. Vertical bars represent the number of people in each area of pool facility B.....	145
Figure 5.46. Time-course monitoring of free and total chlorine at pool facility B during swimming meet in November 2019. Vertical bars represent the number of swimmers in the pools.	147

Figure 5.47. Time-course monitoring of pH at pool facility B during swimming meet in November 2019.....	148
Figure 5.48. Time-course monitoring of alkalinity at pool facility B during swimming meet in November 2019.....	148
Figure 5.49. Trend of calculated aqueous-phase CO ₂ at pool facility B during swimming meet in November 2019.....	149
Figure 5.50. Time-course monitoring of CHCl ₃ at pool facility B during swimming meet in November 2019. Vertical bars represent the number of swimmers in the pools. Horizontal line represents the detection limit.	149
Figure 5.51. Time-course monitoring of urea at pool facility B during swimming meet in November 2019. Vertical bars represent the number of swimmers in the pools.....	150
Figure 5.52. Time-course monitoring of gas-phase NCl ₃ and relative humidity (RH) measured by NEMo devices at pool facility B during swimming meet in November 2019. Vertical bars represent the number of people in each area of pool facility B.	153
Figure 5.53. Time-course monitoring of gas-phase NCl ₃ with gas-phase CO ₂ measured by NEMo devices at pool facility B during swimming meet in November 2019. Vertical bars represent the number of people in each area of pool facility B.....	154
Figure 5.54. Time-course monitoring of gas-phase CO ₂ measured by LI-830 Trace Gas Analyzer at pool facility B during swimming meet in November 2019. Vertical bars represent the number of people in each area of pool facility B.	155
Figure 5.55. Time-course monitoring of free and total chlorine at pool facility C during swimming meet in March 2019. Vertical bars represent the number of swimmers in the pools.	157
Figure 5.56. Time-course monitoring of pH at pool facility C during swimming meet in March 2019.....	157
Figure 5.57. Time-course monitoring of urea at pool facility C during swimming meet in March 2019. Vertical bars represent the number of swimmers in the pools.....	158
Figure 5.58. Time-course monitoring of gas-phase NCl ₃ and RH measured by NEMo devices at pool facility C during swimming meet in March 2019. Vertical bars represent the swimmer number in the pool area.....	160
Figure 5.59. Time-course monitoring of gas-phase NCl ₃ with gas-phase CO ₂ measured by NEMo devices at pool facility C during swimming meet in March 2019. Vertical bars represent the swimmer number in the pool area.....	161
Figure 5.60. Time-course monitoring of free and total chlorine at pool facility D during swimming meet in August 2019. Vertical bars represent the number of swimmers in the pools.	163
Figure 5.61. Time-course monitoring of pH at pool facility D during swimming meet in August 2019.....	164
Figure 5.62. Time-course monitoring of alkalinity at pool facility D during swimming meet in August 2019.....	165

Figure 5.63. Trend of calculated aqueous-phase CO ₂ at pool facility D during swimming meet in August 2019.	166
Figure 5.64. Time-course monitoring of liquid-phase NCl ₃ concentration by portable MIMS at pool facility D during swimming meet in August 2019. Vertical bars represent the number of swimmers in the pools. Horizontal line represents the detection limit.	167
Figure 5.65. Time-course monitoring of aqueous-phase CHCl ₃ by portable MIMS at pool facility D during swimming meet in August 2019. Vertical bars represent the number of swimmers in the pools. Horizontal line represents the detection limit.	168
Figure 5.66. Time-course monitoring of aqueous-phase CNCl by portable MIMS device at pool facility D during swimming meet in August 2019. Vertical bars represent the number of swimmers in the pools. Horizontal line represents the detection limit.	169
Figure 5.67. Time-course monitoring of urea at pool facility D during swimming meet in August 2019. Vertical bars represent the number of swimmers in the pools.	170
Figure 5.68. Time-course monitoring of gas-phase NCl ₃ and RH measured by NEMo devices at pool facility D during swimming meet in August 2019. Vertical bars represent the number of people in each area of pool facility D.	172
Figure 5.69. Time-course monitoring of gas-phase NCl ₃ with gas-phase CO ₂ measured by NEMo devices at pool facility D during swimming meet in August 2019. Vertical bars represent the number of people in each area of pool facility D.	173
Figure 5.70. Time-course monitoring of free and total chlorine at pool facility E during study in January 2020. Vertical bars represent the number of swimmers in the pools.	175
Figure 5.71. Time-course monitoring of pH at pool facility E during study in January 2020. ..	176
Figure 5.72. Time-course monitoring of alkalinity at pool facility E during study in January 2020.	176
Figure 5.73. Trend of calculated aqueous-phase CO ₂ at pool facility E during study in January 2020.	177
Figure 5.74. Time-course monitoring of CHCl ₃ by portable MIMS at pool facility E during study in January 2020. Vertical bars represent the number of swimmers in the pools. Horizontal line represents the detection limit.	177
Figure 5.75. Time-course monitoring of urea at pool facility E during study in January 2020. Vertical bars represent the number of swimmers in the pools.	178
Figure 5.76. Time-course monitoring of gas-phase NCl ₃ and RH measured by NEMo devices at pool facility E during study in January 2020. Vertical bars represent the number of people in each area of pool facility E.	180
Figure 5.77. Time-course monitoring of gas-phase NCl ₃ with gas-phase CO ₂ measured by NEMo devices at pool facility E during study in January 2020. Vertical bars represent the number of people in each area of pool facility E.	181

Figure 5.78. Comparison of ranged of liquid-phase NH_2Cl concentration measured in this study with previous studies in chlorinated swimming pools.....	184
Figure 5.79. Comparison of ranged of liquid-phase NHCl_2 concentration measured in this study with previous studies in chlorinated swimming pools.....	184
Figure 5.80. Comparison of ranged of liquid-phase NCl_3 concentration measured in this study with previous studies in chlorinated swimming pools.....	185
Figure 5.81. Comparison of ranged of liquid-phase CHCl_3 concentration measured in this study with previous studies in chlorinated swimming pools.....	185
Figure 5.82. Comparison of ranged of liquid-phase CNCl concentration measured in this study with previous studies in chlorinated swimming pools.....	186
Figure 5.83. Comparison of ranged of liquid-phase CNCHCl_2 concentration measured in this study with previous studies in chlorinated swimming pools.....	186
Figure 5.84. Comparison of ranged of liquid-phase CH_3NCl_2 concentration measured in this study with previous studies in chlorinated swimming pools.....	187
Figure 5.85. Comparison of ranged of gas-phase NCl_3 concentration measured in this study with previous studies in chlorinated swimming pools. Colored vertical lines represent the concentration ranged of measured gas-phase NCl_3 in each study. Colored circles represent the mean concentration of gas-phase NCl_3 in each study. Horizontal dark blue dotted line represents the guideline level of gas-phase NCl_3 recommended by WHO (2006). Horizontal pink dotted line represents the guideline level of gas-phase NCl_3 recommended by Bernard (2006).	194
Figure 6.1. Fitting curve of the selection for best-fit value of K' from NEMo A from March 2019 study at pool facility B. $\text{RSS} = \text{Residual sum of (measured gas-phase } \text{NCl}_3 \text{ concentration – model gas-phase } \text{NCl}_3 \text{ concentration)}^2$. $K' = \text{liquid to gas phase of } \text{NCl}_3 \text{ mass transfer coefficient}$	205
Figure 6.2. Fitting curve of the selection for best-fit value of K' from NEMo B from March 2019 study at pool facility B. $\text{RSS} = \text{Residual sum of (measured gas-phase } \text{NCl}_3 \text{ concentration – model gas-phase } \text{NCl}_3 \text{ concentration)}^2$. $K' = \text{liquid to gas phase of } \text{NCl}_3 \text{ mass transfer coefficient}$	206
Figure 6.3. Fitting curve of the selection for best-fit value of K' from NEMo C from March 2019 study at pool facility B. $\text{RSS} = \text{Residual sum of (measured gas-phase } \text{NCl}_3 \text{ concentration – model gas-phase } \text{NCl}_3 \text{ concentration)}^2$. $K' = \text{liquid to gas phase of } \text{NCl}_3 \text{ mass transfer coefficient}$	207
Figure 6.4. Fitting curve of the selection for best-fit value of K' from NEMo B from April 2019 study at pool facility B. $\text{RSS} = \text{Residual sum of (measured gas-phase } \text{NCl}_3 \text{ concentration – model gas-phase } \text{NCl}_3 \text{ concentration)}^2$. $K' = \text{liquid to gas phase of } \text{NCl}_3 \text{ mass transfer coefficient}$	208
Figure 6.5. Fitting curve of the selection for best-fit value of K' from NEMo C from April 2019 study at pool facility B. $\text{RSS} = \text{Residual sum of (measured gas-phase } \text{NCl}_3 \text{ concentration – model gas-phase } \text{NCl}_3 \text{ concentration)}^2$. $K' = \text{liquid to gas phase of } \text{NCl}_3 \text{ mass transfer coefficient}$	209

Figure 6.6. Fitting curve of the selection for best-fit value of K' from NEMo A from June 2019 study at pool facility B. RSS = Residual sum of (measured gas-phase NCl_3 concentration – model gas-phase NCl_3 concentration) ² . K' = liquid to gas phase of NCl_3 mass transfer coefficient.....	210
Figure 6.7. Fitting curve of the selection for best-fit value of K' from NEMo B from June 2019 study at pool facility B. RSS = Residual sum of (measured gas-phase NCl_3 concentration – model gas-phase NCl_3 concentration) ² . K' = liquid to gas phase of NCl_3 mass transfer coefficient.....	211
Figure 6.8. Time-course monitoring of gas-phase NCl_3 by NEMo device A and liquid-phase NCl_3 with model gas-phase NCl_3 , and trend of air flow rate in pool facility B during experiment in March 2019. Vertical bars represent the number of swimmers in pool facility B.	214
Figure 6.9. Time-course monitoring of gas-phase NCl_3 by NEMo device B and liquid-phase NCl_3 with model gas-phase NCl_3 , and trend of air flow rate in pool facility B during experiment in March 2019. Vertical bars represent the number of swimmers in pool facility B.	215
Figure 6.10. Time-course monitoring of gas-phase NCl_3 by NEMo device C and liquid-phase NCl_3 with model gas-phase NCl_3 , and trend of air flow rate in pool facility B during experiment in March 2019. Vertical bars represent the number of swimmers in pool facility B.	216
Figure 6.11. Time-course monitoring of gas-phase NCl_3 by NEMo device C and liquid-phase NCl_3 with model gas-phase NCl_3 , and trend of air flow rate in pool facility B during experiment in April 2019. Vertical bars represent the number of swimmers in pool facility B.	217
Figure 6.12. Time-course monitoring of gas-phase NCl_3 by NEMo device C and liquid-phase NCl_3 with model gas-phase NCl_3 , and trend of air flow rate in pool facility B during experiment in April 2019. Vertical bars represent the number of swimmers in pool facility B.	218
Figure 6.13. Time-course monitoring of gas-phase NCl_3 by NEMo device A and liquid-phase NCl_3 with model gas-phase NCl_3 , and trend of air flow rate in pool facility B during study in June 2019. Vertical bars represent the number of swimmers in pool facility B.	220
Figure 6.14. Time-course monitoring of gas-phase NCl_3 by NEMo device B and liquid-phase NCl_3 with model gas-phase NCl_3 , and trend of air flow rate in pool facility B during study in June 2019. Vertical bars represent the number of swimmers in pool facility B.	221
Figure 6.15. Fitting curve of the selection for best-fit value of K' from NEMo A for June 2019 study at pool facility B. RSS = Residual sum of the (measured gas-phase CO_2 concentration – model gas-phase CO_2 concentration) ² . K' = liquid to gas phase of CO_2 mass transfer coefficient.	226
Figure 6.16. Fitting curve for selection of best-fit value of K' from LI-COR CO_2 analyzer for November 2019 study at pool facility B. RSS = Residual sum of the (measured gas-phase CO_2 concentration – model gas-phase CO_2 concentration) ² . K' = liquid to gas phase of CO_2 mass transfer coefficient.	227
Figure 6.17. Time-course monitoring of gas-phase CO_2 by NEMo A and liquid-phase CO_2 with model gas-phase CO_2 , and trend of air flow rate in pool facility B during study in June 2019. Vertical bars represent the number of swimmers and non-swimmer in pool facility B.	229

Figure 6.18. Time-course monitoring of gas-phase CO₂ by LI-COR CO₂ analyzer and liquid-phase CO₂ with model gas-phase CO₂, and trend of air flow rate in pool facility B during study in November 2019. Vertical bars represent the number of swimmers and non-swimmer in pool facility B..... 230

Figure 6.19. Time-course monitoring of gas-phase CO₂ by NEMo A and liquid-phase CO₂ with model gas-phase CO₂ in pool facility B during study in June 2019. Vertical bars represent the number of swimmers and non-swimmer in pool facility B. Gray dash line represents the gas-phase NCl₃ measurement by NEMo A and green dash line represent the model gas-phase NCl₃ from NEMo a..... 232

Figure 6.20. Time-course monitoring of gas-phase CO₂ by LI-COR CO₂ analyzer and liquid-phase CO₂ with model gas-phase CO₂ in pool facility B during study in November 2019. Vertical bars represent the number of swimmers and non-swimmer in pool facility B. Pink line represents the gas-phase NCl₃ measurement by NEMo B device. 233

ABSTRACT

Swimming is the second most common form of recreational activity in the U.S. Swimming pool water and air quality should be maintained to allow swimmers, pool employees, and spectators to use the pool facility safely. One of the major concerns regarding the health of swimmers and other pool users is the formation of disinfection by-products (DBPs) in swimming pools. Previous research has shown that volatile DBPs can adversely affect the human respiratory system. DBPs are formed by reactions between chlorine and other compounds that are present in water, most of which are introduced by swimmers, including many that contain reduced nitrogen. Some of the DBPs formed in pools are volatile, and their transfer to the gas phase in pool facilities is promoted by mixing near the air/water interface, caused by swimming and pool features.

Swimming pool water treatment processes can play significant roles in governing water and air quality. Thus, it is reasonable to hypothesize that water and air quality in a swimming pool facility can be improved by renewing or enhancing one or more components of water treatment.

The first phase of the study was designed to identify and quantify changes in water and air quality that are associated with changes in water treatment at a chlorinated indoor pool facility. Reductions of aqueous NCl_3 concentration were observed following the use of secondary oxidizer with its activator. This inclusion also resulted in significant decreases in the concentrations of cyanogen chloride (CNCl) and dichloroacetonitrile (CNCHCl_2) in pool water. The concentration of urea, a compound that is common in swimming pools and that functions as an important precursor to NCl_3 formation, as well as a marker compound for introduction of contaminants by swimmers, was also reduced after the addition of activator.

The second phase of this study involved field measurements to characterize and quantify the dynamic behavior of indoor air quality (IAQ) in indoor swimming pool facilities, particularly as related to volatile compounds that are transferred from swimming pool water to air. Measurements of water and air quality were conducted before, during, and after periods of heavy use at several indoor pool facilities. The results of a series of measurements at different swimming pool facilities allowed for examination of the effects of swimmers on liquid-phase DBPs and gas-phase NCl_3 . Liquid-phase NCl_3 concentrations were observed to gradually increase during periods of high swimmer numbers (*e.g.*, swimming meets), while liquid-phase CHCl_3 concentration was nearly constant in the same period. Concentrations of urea displayed a steady increase each day during

these periods of intensive use. In general, the highest urea concentrations were measured near the end of each swimming meet.

Measurements of IAQ dynamics during phase 2 of the study demonstrated the effects of swimmers on the concentrations of gas-phase NCl_3 and CO_2 , especially during swimming meets. The measured gas-phase NCl_3 concentration often exceeded the suggested upper limits of $300 \mu\text{g}/\text{m}^3$ or $500 \mu\text{g}/\text{m}^3$ during swimming meets, especially during and immediately after warm-up periods, when the largest numbers of swimmers were in the pool. Peak gas-phase NCl_3 concentrations were observed when large numbers of swimmers were present in the pools; measured gas-phase concentrations were as high as $1400 \mu\text{g}/\text{m}^3$. Concentrations of gas-phase NCl_3 rarely reached above $300 \mu\text{g}/\text{m}^3$ during regular hours of operation. Furthermore, the types of swimmers were shown to affect the transfer of volatile compounds, such as NCl_3 , from water to air in pool facilities. In general, adult competition swimmers promoted more rapid transfer of these compounds than youth competition swimmers or adult recreational swimmers. The measured gas-phase CO_2 concentration often exceeded 1000 ppm_v during swimming meets, whereas the gas-phase CO_2 concentration during periods of non-use of the pool tended to be close to the background (ambient) CO_2 concentration or slightly more than 400 ppm_v . This phenomenon was largely attributed to the activity of swimmers (mixing of water and respiratory activity) and the normal respiratory activity of spectators.

IAQ models for gas-phase NCl_3 and CO_2 were developed to relate the characteristics of the indoor pool environment to measurements of IAQ dynamics. Several assumptions were made to develop these models. Specifically, pool water and indoor air were assumed to be well-mixed. The reactions that were responsible for the formation and decay of the target compounds were neglected. Two-film theory was used to simulate the net mass-transfer rate of volatile compounds from the liquid phase to the gas phase. Advective transport into and out of the air space of the pool were accounted for. The IAQ model was able to simulate the dynamic behavior of gas-phase NCl_3 during regular operating hours. Predictions of gas-phase NCl_3 dynamics were generally less accurate during periods of intensive pool use; however, the model did yield predictions of behavior that were qualitatively correct. Strengths of the model include that it accounts for the factors that are believed to have the greatest influence on IAQ dynamics and is simple to use. Model weaknesses include that the model did not account liquid-phase reactions that are responsible for formation and decay of the target compounds. The IAQ model for NCl_3 dynamics could still be a

useful tool to form the basis for recommendations regarding the design and operation of indoor pool facilities so as to optimize IAQ.

Measurements of CO₂ dynamics indicated qualitatively similar dynamic behavior as NCl₃. Because of this, it was hypothesized that CO₂ may represent a surrogate for NCl₃ for monitoring and control of IAQ dynamics. To examine this issue in more detail, a conceptually similar model of CO₂ dynamics was developed and applied. The model was developed to allow for an assessment of the relative contributions of liquid→gas transfer and respiration by swimmers and spectators to CO₂ dynamics. The results of this modeling effort indicated that the similarity of CO₂ transfer behavior to NCl₃ may allow use of CO₂ as a surrogate during periods with few to no spectators in the pool; however, when large numbers of spectators are present, the behavior of CO₂ dynamics may not be representative of NCl₃ dynamics because of spectator respiration.

1. INTRODUCTION

Swimming is a popular recreational activity in the U.S. Swimming can provide a whole-body workout, as nearly all muscles are used during swimming. Also, swimming can provide many human health benefits in the form of endurance, muscle strength, and cardiovascular fitness. In addition, swimming can reduce blood pressure, risk of heart disease, diabetes, and stroke (Tanaka et al., 1997). In recent years, swimming pool facilities have been used for therapeutic exercise for some injuries and medical conditions, such as spinal cord injuries and chronic low back pain.

Swimming is considered as a year-around activity in temperate and cold regions due to the construction of indoor swimming pools. Swimming pool water must undergo treatment in order to achieve clean and clear water as well as eliminate harmful substances, including waterborne microbial pathogens such as viruses, bacteria, and protozoa. Most swimming pool water treatment systems are based on water recirculation through treatment processes that include filtration and disinfection.

Filtration systems commonly applied in swimming pool facilities are used to control colloidal particles. Coagulation and flocculation can be applied to improve the performance of filters in these systems. The number of times pool water can be filtered through a filter system in a 24-hour period is governed by the turnover rate of the pool. Under the assumption of a well-mixed pool, a 6-hour turnover rate will result in 98% clarification if the pool and filter are designed properly (CDC, 2006). According to the World Health Organization, the pH should be maintained between 7.2 and 7.8 in chlorinated swimming pools (WHO, 2006). Total alkalinity should be maintained at 60-180 ppm (CDC, 2006).

Chlorine is the most frequently used disinfectant in swimming pools because of its relatively low cost and ease to use (Glauner et al., 2005; Judd and Black, 2000; Li and Blatchley, 2007). However, chlorine (and other chemical disinfectants) can also react with various organic and inorganic compounds to produce disinfection by products (DBPs) in swimming pools (Li and Blatchley, 2007). Chlorine has been demonstrated to react with several compounds that are attributed to the (poor) hygiene practices of swimmers, leading to formation of DBPs in chlorinated pools. Numerous organic-N compounds that are found in human sweat and urine have been identified as precursors of volatile DBPs that are common in swimming pools. These precursor compounds include urea, creatinine, amino acids, and uric acid (Li and Blatchley, 2007; Weaver

et al., 2009; Zwiener et al., 2007). Several DBPs in pool water and air are associated with adverse health effects for swimmers and swimming pool patrons (Font-Ribera et al., 2010; Glauner et al., 2005; Loos and Barceló, 2001; Villanueva et al., 2007; Weisel et al., 2009). Li and Blatchley (2007) identified eleven volatile DBPs that are formed in chlorinated swimming pools. Weaver *et al.* (2009) illustrated that these eleven DBPs are common in chlorinated indoor pool water samples. Swimmers are subjected to DBPs through three main pathways: inhalation, dermal absorption/contact, and ingestion (Whitaker et al., 2003).

Among swimming pool DBPs, trichloramine (NCl_3) has been researched most extensively due to its association with irritation of the respiratory system in chlorinated swimming pools (Héry et al., 1995; Jacobs et al., 2007; Massin et al., 1998; Thickett et al., 2002). NCl_3 is particularly volatile compared with other volatile DBPs that are common to pools, including the other inorganic chloramines (monochloramine (NH_2Cl) and dichloramine (NHCl_2)) (Sander, 1999). Several human-associated compounds, such as urea, uric acid, creatinine, and amino acids, have been demonstrated to function as precursors for NCl_3 formation in chlorinated pools (Blatchley and Cheng, 2010; Li and Blatchley, 2007; Lian et al., 2014). Also, gas-phase NCl_3 is largely responsible for the chlorine odor in indoor swimming pool facilities. NCl_3 can irritate the eyes, skin, and the respiratory system (Massin et al., 1998; Parrat et al., 2012; Thickett et al., 2002). Several studies have shown positive correlations between irritation symptoms among swimmers and pool workers with high gas-phase NCl_3 concentration at indoor pool facilities (Bowen et al., 2007; Kaydos-Daniels et al., 2008). Long-term studies of gas-phase NCl_3 concentration in indoor chlorinated swimming pools have been conducted in recent years (Lévesque et al., 2015; Zare Afifi and Blatchley, 2016, 2015). However, there are still no comprehensive data available to define the factors that affect gas-phase NCl_3 dynamics of indoor swimming pools. In part, investigations of gas-phase NCl_3 dynamics have been limited by analytical methods.

Several studies have utilized a method developed by Héry *et al.* (1995) for measuring gas-phase NCl_3 (Font-Ribera et al., 2016; Fornander et al., 2013; Lévesque et al., 2015; Nordberg et al., 2012; Seys et al., 2015). This method is based on reduction of NCl_3 to chloride, which is followed by ion chromatography to quantify chloride production. An air sample containing gas-phase NCl_3 is pumped at a known volumetric flow rate through a glass fiber filter that has been saturated with a solution of sodium carbonate and diarsenic trioxide. The +1-valent chlorine in

NCl_3 will promote oxidation of arsenic, resulting in reduction of chlorine to the chloride ion. However, this method is known to be vulnerable to interference by oxygen (Héry et al. 1995).

An alternative wet-chemical method was applied by Weng *et al.* (2011). The method was developed as a modification of a DPD/KI colorimetric method that includes air sparging for measuring gas-phase NCl_3 . Air is pumped at a known volumetric flow rate through two sequential gas-washing bottles, each equipped with a glass stem possessing coarse fritted ends. Both gas-washing bottles will contain 30 mL of an aqueous DPD/KI solution. This method was designed to trap gas-phase inorganic chloramines in the DPD/KI solution; however, because NCl_3 is roughly two orders of magnitude more volatile than the other inorganic chloramines (based on Henry's law constants), the majority of the color change from the DPD/KI is attributable to NCl_3 . Based on previous studies, NCl_3 is likely the dominant inorganic chloramine in air above chlorinated indoor pools, and likely the major cause of the change of color in this approach (Héry et al., 1995; Weaver et al., 2009; Weng et al., 2011). However, several other compounds can promote the color change of DPD/KI, including the other inorganic chloramines and volatile organic chloramines (*e.g.*, CH_3NCl_2). These compounds represent sources of interference in this analytical method. Molecular oxygen can also contribute to the color change in the DPD/KI solution; however, because almost all NCl_3 is trapped in the first of the two gas washing bottles, the O_2 signal developed in the second bottle can be used to estimate gas-phase NCl_3 concentration by subtraction of the O_2 signal (2nd bottle) from the total color change signal (1st bottle).

In this study, the gas-phase concentration of NCl_3 was monitored using NEMo IAQ monitors (Ethera Labs, Crolles, France). The NEMo device is a passive IAQ monitor that can be configured to measure gas-phase NCl_3 (Ethera, 2018; Nguyen et al., 2013). Details of the principles of this analytical method are presented in the Methods section.

This research was divided into 3 phases. Phase 1 involved an investigation of the effects of several water treatment process changes on air and water quality in a chlorinated, indoor swimming pool. Phase 2 involved examination of the effects of pool design, operational characteristics, type of swimmers, and swimmer activity on air and water quality in indoor swimming pool facilities. Phase 3 involved the development and application of an IAQ model for swimming pool facilities.

Phase 1

Swimming pool water treatment processes can play significant roles in water and air quality. Moreover, because several important constituents of swimming pool water (including several DBPs) are volatile, there are strong links between water quality and air quality in indoor pool facilities. Thus, it is reasonable to hypothesize that water and air quality in indoor swimming pools can be improved by adjusting one or more components of the pool water treatment.

In this phase of study, three treatment components were selected to examine this hypothesis: filter media, coagulant/flocculant chemicals, and secondary oxidizers. Activated filter media (AFM), all poly flocc (APF), and secondary oxidizers were applied to an existing pool treatment system to investigate their effects on water and air quality in an indoor swimming pool facility.

AFM and APF were developed specifically for pool water treatment. AFM is an amorphous alumino-silicate manufactured from green glass that was developed as a direct replacement for filter sand media. APF contains 6 different electrolytes and polyelectrolytes to promote coagulation. APF was designed for use with AFM in swimming pool applications.

The secondary oxidizers were applied and acted as a shocking agent at the beginning of the experiment and then applied continuously in the tested swimming pool. These compounds were designed to oxidize reduced organic contaminants in pool water, thereby reducing chlorine use, while maintaining oxidation-reduction potential (ORP). On-line (real-time) measurements of ORP are often used to control oxidant addition to pool water.

Phase 1 of this project was conducted to characterize and quantify the effects of sequential treatment component changes on water and air quality in a chlorinated, indoor swimming pool.

Three modes of pool treatment process were examined:

- Original operation functioned as the baseline of this study (*i.e.*, experimental control) and was monitored for roughly three weeks.
- Original operation while replacing sand filter media to AFM for roughly four weeks.
- Filter operation with AFM, coagulant feed terminated, feeding of secondary oxidant and activator initiated for a period of eight weeks.

The time frames applied for each stage were selected to allow the performance of each process change to approach a stable condition to examine the effects of these treatment process changes over a range of operating conditions. For each stage of operation, samples of water and air were

collected on a regular schedule. Water samples were subjected to a series of analytical procedures to allow characterization and quantification of chemical constituents. IAQ was monitored using a NEMo device, which allowed near real-time quantification of gas-phase NCl_3 , VOCs, CO_2 , and humidity.

The purpose of this phase was to examine long-term behavior of several water quality parameters (residual chlorine, pH, turbidity, ORP, DBPs, and urea) and air quality parameters (concentrations of NCl_3 , VOCs, CO_2 , as well as relative humidity) after each process change.

Phase 2

Phase 2 of this study involved measurements of air and water quality in indoor swimming pool facilities before, during, and after periods of heavy use. Experiments focused on periods of heavy use at pool facilities because these tend to represent the circumstances that yield the poorest water and air quality in indoor pool facilities. As such, measurements of these attributes of system behavior will allow for improvements in our understanding of the design and operational characteristics that optimize the indoor swimming environment.

Concentrations of gas-phase NCl_3 , CO_2 , and relative humidity were monitored using NEMo devices. For each experiment, NEMo devices were installed near the pool deck area. As in phase 1 of the study, the gas-phase concentrations of NCl_3 with CO_2 were positively correlated and showed similar dynamic behavior.

Several relevant water quality parameters were also measured in this phase of the work. Liquid-phase volatile DBPs were quantified using a bench top MIMS system in some experiments and a portable MIMS system in other experiments. pH and alkalinity were also measured and later were applied to calculate the liquid-phase CO_2 concentration. Free and total chlorine were measured using the DPD/KI colorimetric method with a portable photometer. The numbers of swimmers and spectators were counted every hour during the study periods as swimming activity was hypothesized to promote the transfer of volatile compounds from the liquid phase to the gas phase. All people in the facility (swimmers and spectators) will affect the concentration of gas-phase CO_2 .

In total, eight experiments were conducted in indoor swimming pool facilities in Indiana and Michigan during a 12-month span. Five experiments were conducted at a university swimming pool in Indiana, among them three were experiments that were conducted during swimming meets;

two experiments were conducted during regular operation hours. One study was conducted during a swimming meet at a high school swimming pool in Indiana. Two experiments were conducted at university swimming pools in Michigan during swimming meets. Age groups of the swimmers for the swimming meets were recorded because type and size of swimmers could affect the dynamics of transfer of volatile compounds from water to air.

The measurements of liquid-phase volatile DBPs in this study were compared with the literature. The data were also statistically analyzed by Pearson correlation to identify potential (linear) associations between individual DBP compounds. The measurements of gas-phase NCl_3 were also compared with those reported in previous investigations (Fornander et al., 2013; Lévesque et al., 2015; Nordberg et al., 2012; Seys et al., 2015; Weng et al., 2011; Zare Afifi and Blatchley, 2016). When possible, the characteristics and operating conditions of the heating, ventilation, and dehumidification (HVAC) system operating conditions were recorded or measured at the pool facility.

The purpose of this phase was to collect data to quantify the dynamic behavior of pool water and IAQ in indoor swimming pool facilities. The experiments were conducted to allow collection of measurements that defined typical behavior of these indoor pool facilities, as well as behavior during periods of heavy use, when water and air quality were expected to be poorest.

Phase 3

A mass-balance based model was developed to describe the dynamic behavior of air quality in indoor swimming pool facilities. The fundamental governing mass-balance was based on several assumptions. First, two-film theory was used to simulate the dynamics of liquid→gas transfer of volatile compounds. Second, the air above the pool was assumed to be well-mixed. Third, the pool water was also assumed to be well-mixed. The model also accounted for advective transport of the target compound into and out of the air space above the pool.

The governing mass-balance equations were developed to include terms to quantify the effects of the factors that are known to affect IAQ. Input parameters to the model included the numbers of swimmers and spectators in the pool facility, (outside) air flow rate into the building, pool surface area, and air volume in the building. Regression analysis was used to estimate mass transfer coefficients for NCl_3 and CO_2 . Mass transfer coefficient estimates were compared with previous studies.

The mass transfer coefficients coupled with the governing equation and liquid-phase measurements were then used to simulate IAQ dynamics in terms of gas-phase NCl_3 and CO_2 concentrations. A comparison of measured concentrations and model predictions was then conducted. This phase of the study also involved an investigation of the parameters that affect IAQ dynamics and model performance.

Experiments and numerical simulations were conducted to examine gas-phase CO_2 as a potential surrogate for gas-phase NCl_3 in indoor swimming pool facilities. This was motivated in part by the fact that there are many inexpensive, simple, commercially available CO_2 sensors that could be applied for monitoring and control of IAQ dynamics in indoor pool facilities.

The model of IAQ dynamics was applied to simulate IAQ dynamics in indoor swimming pools under various hypothetical scenarios. The IAQ model was developed for use by pool operators to use for optimization of HVAC systems and for evaluation of the effects of remediation measures, such as air stripping systems. HVAC systems are used to control air temperature and humidity, as well as control the rate of air exchange. The IAQ model provides a tool to optimize IAQ and HVAC system operation.

2. LITERATURE REVIEW

2.1 Swimming Pool Treatment

General indicators of a healthy environment in indoor pools include clear water and the absence of strong odors. In most pool systems, water is recirculated through a treatment system that will include one or more physical separation processes, along with one or more processes that will promote oxidation and disinfection. The temperature of water and air of the pool facility should be maintained for bather comfort and for the comfort of pool employees and spectators (Bullock, 2003). Also, pool water pH should be controlled to a slightly alkaline value to promote activity on the part of chlorine as an oxidant and a disinfectant, while providing corrosion control (Bullock, 2003). Since swimming pools often contain a large volume of water, it is not practical or economical to frequently replace the pool water (Kanan, 2010). Thus, it is common for a pool to recirculate essentially a fixed volume of water through its treatment system for a period of several months to several years, with replacement only to compensate for evaporative losses between complete water replacements. Common swimming pool water treatment processes include filtration, coagulation and flocculation, pH and temperature control, disinfection, circulation (turnover), and shock treatment with oxidants (Bullock, 2003; Kanan, 2010).

Filtration is essential to maintain water clarity and remove suspended particulates from water; these particulates are usually introduced to pools by swimmers. However, filtration is generally ineffective for control of dissolved materials in pool water. The turbidity of pool water, an optical measurement that serves as a proxy for particle concentration, should be low enough to allow a lifeguard to be able to clearly see through the entire depth of water in the pool. A upper-limit guideline recommended by World Health Organization (WHO) for turbidity is 0.5 nephelometric turbidity units (NTU) compared with upper-limit of 5 NTU for drinking water (WHO, 2017). For comparison, the upper-limit on turbidity defined by the U.S EPA is 0.3 NTU for drinking water in at least 95% of the water samples in any month (U.S EPA, 2006).

Filtration systems commonly applied in swimming pools include sand filters, cartridge filters, and diatomaceous earth filters (DE filter) (CDC, 2006). In the U.S, the most common filters used in swimming pool facilities are sand filters (Griffiths, 2003).

Coagulation promotes separation of suspended materials largely by the mechanisms of charge neutralization and bridging so that small particles can agglomerate to form flocs. In turn, floc formation can improve particle removal during filtration. Coagulation can also be applied to promote removal of some microorganisms, such as *Giardia* and *Cryptosporidium*, both of which are resistant to chlorine (PWTAG, 2016). Coagulation and flocculation are not required treatment processes in the swimming pool industry in the U.S. but are commonly applied in western Europe.

The pH and temperature of pool water are controlled for swimmer comfort and for optimization of water chemistry. HOCl is the dominant form of free chlorine when pH is below the pK_a of HOCl, while OCl^- is the dominant form at pH above the pK_a of HOCl. Notably, HOCl tends to be much more effective than OCl^- as a disinfectant (White, 1999). The temperature of pool water depends upon its use, but is generally maintained in the range 26 to 30°C. Although a warmer pool may be more comfortable for the bathers (excluding competitive swimmers), elevated temperature increases relative humidity, the tendency for volatile compounds to be transferred from the liquid phase to the gas phase, and microbial growth rates. For each 10°C rise in pool water temperature, microbial growth rates approximately double, thereby promoting biofilm formation in the pool and its recirculation system. For perspective, the water temperature in therapeutic hot tubs and spas can be as high as 40°C (Bullock, 2003).

Disinfection process usually involve strong oxidizers to decompose detrimental materials and inactivate waterborne microbial pathogens. There are several types of disinfectants available for use in swimming pools. Chlorine is the most frequently used disinfectant in swimming pools because of its relatively low cost and ease to use. Also, control hardware can be used to maintain consistent residual chlorine concentration in pool water (Glauner et al., 2005; Judd and Black, 2000).

Continuous circulation (turnover) in swimming pools is required to maintain acceptable water quality (Zwiener et al., 2007). Water is removed from the pool and then treated water is reintroduced back to the pool. Pool turnover of 4-6 hours is common. At a turnover rate of once per 4 hours, water in a pool will be subjected to treatment roughly 6 times per day. However, it is important to recognize that pools are generally not well-mixed systems. Therefore, a portion of the water in a pool is likely to experience treatment at a lower frequency than this average value.

Shock treatment generally involves the application of a high concentration of an oxidizing chemical (often chlorine) to promote oxidation of organic compounds and prevent algal growth.

Routine shock treatment commonly involves raising the free chlorine concentration to 10-20 mg/L (as Cl₂) for one to four hours for pools. Shock treatment is also applied after accidental fecal release, when water clarity is a problem, and when algal blooms occur in pools. Under these conditions, the free chlorine concentration may be increased to 20 mg/L for a period of eight hours when swimmers are not present (Chrostowski and Foster, 2004). Shock chlorination is generally followed by dechlorination to reduce the free chlorine concentration to an acceptable value, before swimmers are allowed back in a pool.

Ultraviolet (UV) irradiation has been applied as a secondary disinfection process in conventional chlorinated pools because UV is known to be effective for control of *C. parvum* and *G. lambia* (Craik et al., 2001; Hijnen et al., 2006). UV-based processes have been demonstrated to be effective for photodegradation of inorganic chloramines (Li and Blatchley, 2009). UV irradiation has also been identified as an efficient treatment for nitrosamine compounds, which are potent carcinogens that could be found in chlorinated swimming pools (Lee et al., 2005). Zare-Afifi and Blatchley (2016) reported the concentrations of several volatile disinfection by-products decreased in a chlorinated swimming pool after the installation of UV-based systems (medium and low pressure).

Air stripping systems are used to separate volatile compounds from liquid-phase water. Among indoor pool facilities, air stripping has been accomplished by air bubbling in the pool's surge tank; however, a dedicated air stripping device (*e.g.* a tower or tray-based system) may also be incorporated into the recirculation system of a pool. There are several processes that could be considered as air stripping methods including mechanical surface aeration, diffused aeration, spray fountains, spray or tray towers, and countercurrent packed towers (Srinivasan et al., 2008). These approaches recognize that the vast majority of the mass of any volatile compound contained in a swimming pool facility at any time is likely to exist in the liquid phase. Tardif *et al.* (2017) and Tsamba *et al.* (2020) reported the positive effects of air stripping on the DBPs in pool water and air. However, air stripping systems may also result in increases in energy consumption (Tsamba et al., 2020) and will also promote transfer of CO₂. CO₂ transfer from pool water is relevant in that it can significantly alter pool water pH. Also, CO₂ is commonly applied in pools for pH control.

2.2 Chlorine Chemistry

Most swimming pools in the U.S and other developed countries apply chlorine as a primary disinfectant (Griffiths, 2003). Chlorine is generally added to pools as a hypochlorite salt (sodium or calcium hypochlorite). Sodium hypochlorite is added as an aqueous solution (i.e., bleach). Calcium hypochlorite is generally added as a dry solid (tablets and briquettes). Hypochlorite salt forms are used in most pool water treatment facilities because they eliminate the need for storage of gaseous chlorine and a gas-phase chlorine feeding device.

Regardless of the form of chlorine, these salts dissolve in water to yield the hypochlorite ion (OCl^-). In turn, OCl^- will participate in protonation and disproportionation reactions to yield hypochlorous acid (HOCl), molecular chlorine (Cl_2), and chlorine monoxide (Cl_2O). The concentration of Cl_2 is generally assumed to be negligible, largely because the equilibrium for Cl_2 trends to be shifted toward HOCl production. In most situations, the concentration of Cl_2O is also small, relative to the concentrations of HOCl and OCl^- . However, there are some reactions that depend on one or both of these forms of chlorine. So, despite the fact that Cl_2 and Cl_2O do not contribute appreciably to the residual chlorine concentration in pools, they can play important roles with respect to swimming pool chemistry (Blatchley and Cheng, 2010; Sivey and Roberts, 2012).

For most practical applications, the sum of the concentrations of HOCl and OCl^- will represent free available chlorine; the distribution of free chlorine among these forms is dependent on pH, temperature, and total chlorine concentration as illustrated by equations 2.1 to 2.3 (at temperature 25°C). HOCl is the predominant form of free chlorine as it is the more germicidal of the two (AWWA, 1999).



The National Swimming Pool Foundation has recommended that free available chlorine in pools and spas should be maintained between 1-5 mg/L as Cl_2 , with an ideal range between 2-4 mg/L as Cl_2 (NSPF, 2006). The World Health Organization (WHO) also recommend a minimum

free chlorine concentration for swimming pools of 1 mg/L as Cl_2 with good circulation and dilution (WHO, 2006). In western Europe, the suggested free chlorine range in the swimming pools is often lower. For example, in Germany the concentration of free chlorine in swimming pools must be kept in the range of 0.3-0.6 mg/L as Cl_2 (Zwiener et al., 2007).

2.3 Volatile Disinfection By-product (DBP) Formation

Chlorine is a strong oxidizer and is the most commonly applied disinfectant in swimming pool facilities. However, studies have shown that there are several drawbacks of chlorination in pools including low effectiveness against some microbial pathogens (e.g., *Cryptosporidium parvum*) (Hijnen et al., 2006) and the formation of disinfection by-products (DBPs). DBPs are generally attributable to reactions of chlorine with various organic and inorganic compounds in pool water.

Recent research related to DBP formation and behavior in swimming pools has improved our understanding of this topic. The first studies of trihalomethanes (THMs) in the water of indoor public swimming pools were published in 1980 (Bätjer et al., 1980; Beech et al., 1980). In these studies, chloroform and other halomethanes were measured in public indoor swimming pools in Germany and in the U.S. Mean THM concentrations in the water of eight swimming pools ranged from 104 to 472 $\mu\text{g/L}$ and mean chloroform concentration in the air ranged from 36 to 241 $\mu\text{g/m}^3$ in Bremen, Germany (Bätjer et al., 1980). The average total THM concentration found in 101 fresh water pools was 125 $\mu\text{g/L}$ in the Miami area (Beech et al., 1980). THMs are an important marker of DBP formation, but DBP chemistry is much broader than just THMs.

More than 100 DBPs have been identified in chlorinated swimming pool waters, including haloacetic acids (HAAs), haloacids, halodiacids, haloaldehydes, haloacetonitriles (HANs), haloketones (HKs), halonitromethanes (HNMs), bromate, haloamides, haloalcohols, nitrosamines, combined chlorine, 3-chloro-4-(dichloromethyl)-5-hydroxy-2(5H)-furanone (MX), and MX homologues (Boorman, 1999; Richardson et al., 2007). The most common DBPs in swimming pools are generally the inorganic chloramines, THMs, and HAAs (Chu and Nieuwenhuijsen, 2002; Kim et al., 2002).

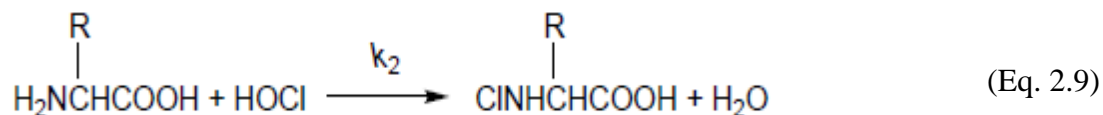
Chloramines are common to pools and they include inorganic chloramine and organic forms. Formation of inorganic chloramines (monochloramine (NH_2Cl), dichloramine (NHCl_2), and trichloramine (NCl_3)) has been studied extensively. Jafvert and Valentine (1992) reported a

comprehensive summary of the reactions and their kinetics to describe the dynamics of the chloramination and breakpoint chlorination processes, which are performed by reacting free chlorine with ammonia (NH₃). A more recent paper provided an updated summary of these reactions, as well as an on-line model that incorporates these reactions and reported rate constants to provide detailed simulations of the dynamic behavior of inorganic chloramines (Wahman, 2018). The yields of NH₂Cl, NHCl₂, and NCl₃ are dependent on the ratio of chlorine to ammonia-nitrogen concentration, pH, temperature, and time. When ammonia is present as the form of reduced-N in the system, a reaction sequence is initiated by a series of substitution reactions, and then proceeds to a series of oxidation/reduction (redox) reactions. The forward and reverse substitution reactions are relatively rapid, and as such equilibrium between inorganic chloramines is established quickly (Jafvert and Valentine, 1992). These reversible reactions involve substitution of +1-valent chlorine for hydrogen on ammoniacal nitrogen as illustrated in equations 2.4 to 2.6.



The formation of inorganic chloramines in swimming pools generally follows chemical pathways that are somehow different than the reactions listed above, largely because there is little or no ammonia-N in most pools. Rather, pool water is often characterized by relatively high concentrations of reduced-N in the forms of organic-N compounds, including urea, creatinine, uric acid, and amino acids. These compounds have all been demonstrated to function as precursors for NCl₃ formation (Li and Blatchley, 2007). It is likely that hydrolysis of NCl₃ then leads to formation of NHCl₂ and NH₂Cl.

Like ammonia, organic amino nitrogen compounds can react with chlorine in pool water. These compounds will undergo substitution reactions similar to those described above. Several organic N-chlorinated amines have been identified from this reaction under chlorination conditions (Isaac and Morris, 1980; Nweke and Scully, 1989; Snyder and Margerum, 1982). These organic chloramines are also considered as DBPs. One reaction is illustrated in equation 2.9 (Morris, 1967).



Precursors of DBP formation in swimming pools are commonly introduced by bathers. The precursors are introduced to pools by human activity through excretion of body fluids (sweat, urine, and saliva). Weng and Blatchley (2011) estimated that among competitive swimmers, as much as 823-1760 mL sweat and 55-117 mL of urine are introduced into swimming pool water by each swimmer per day. As described above, body fluids are known to contain many nitrogenous compounds. Human urine and sweat are generally regarded as the primary sources of organic-N introduced to pool waters. The Guidelines for Safe Recreational Water Environment from the World Health Organization (WHO, 2006) stated that the five most abundant nitrogen compounds or compound groups in human urine and sweat by mass concentration are urea, ammonia, creatinine, uric acid and amino acids. Table 2.1 illustrates typical concentrations of urea, ammonia, creatinine, and amino acids in urine and sweat. Previous research has indicated that these compounds will react with free chlorine to yield several volatile DBPs, including trichloramine (NCl_3), dichloroacetoneitrile (CNCHCl_2), cyanogen chloride (CNCl), and dichloromethylamine (CH_3NCl_2) (Judd and Bullock, 2003; Kim et al., 2002; Li and Blatchley, 2007; Shang et al., 2000). CH_3NCl_2 has been identified as a product of chlorination of creatinine and CNCHCl_2 was identified as a product of chlorination of L-Histidine and L-Arginine (Weng et al., 2012). Both uric acid and L-Histidine have been identified as precursors of CNCl formation (Li and Blatchley, 2007; Lian et al., 2014). Also, NCl_3 appeared to be a common product of chlorination of urea, uric acid, creatinine, L-Histidine and L-Arginine (Li and Blatchley, 2007; Lian et al., 2014).

Precursors of THM formation in pools may also originate from humic substances, lotion, skin, and saliva (Judd and Jeffrey, 1995; Kim et al., 2002; Lee, 2016). The presence and formation of THMs are related to the disinfectant used and chloramine concentrations (Jolley and Carpenter, 1983). For instance, THM production has been observed to be low when the breakpoint is not achieved and the residual chlorine is largely represented as combined chlorine (Jolley and Carpenter, 1983). When free chlorine is the main disinfectant, chloroform (CHCl_3) is often the dominant THM by weight.

Table 2.1. Typical concentrations of nitrogenous compounds in human sweat and urine.
WHO (2006), and b) *Geigy Scientific Tables* (Magos, 1987).

a)

Nitrogen-Containing compounds	Sweat		Urine	
	Mean content	Portion of total nitrogen	Mean content	Portion of total nitrogen
	(mg/L)	(%)	(mg/L)	(%)
Urea	680	68	10240	84
Ammonia	180	18	560	5
Amino acids	45	5	260	2
Creatinine	7	1	640	5
Other compounds	80	8	500	4
Total nitrogen	992	100	12200	100

b)

Nitrogen-Containing compounds	Sweat	Urine
	Mean content	Mean content
	(mmol/L)	(mmol/d)
Urea	19.6	343
Ammonia	3.02	42.7
Creatinine	41	13.2
Amino acids	3.6	--
<i>Glycine</i>	--	1.4
<i>L-Histidine</i>	--	1.29
<i>L-Arginine</i>	--	0.03

Note: Volume of urine is estimated at 1360 mL/day for male adult, and the sweat rate of an adult is 7.2 g min⁻¹m⁻².

Several investigations have provided measurements of volatile DBPs in chlorinated swimming pool facilities. Weaver et al. (2009) measured aqueous inorganic chloramine (NH_2Cl , NHCl_2 , and NCl_3) concentrations in 11 chlorinated swimming pools that ranged from undetectable to 1880 $\mu\text{g/L}$ as Cl_2 , undetectable to 417 $\mu\text{g/L}$ as Cl_2 , and undetectable to 377 $\mu\text{g/L}$ as Cl_2 , respectively. Zare-Afifi (2016) observed aqueous NH_2Cl , NHCl_2 , and NCl_3 concentrations in an indoor swimming pool that ranged from undetectable to 620 $\mu\text{g/L}$ as Cl_2 , undetectable to 250 $\mu\text{g/L}$ as Cl_2 , and undetectable to 2190 $\mu\text{g/L}$ as Cl_2 .

Weaver et al. (2009) observed that chloroform concentrations in 11 chlorinated pools that ranged from undetectable to 298 $\mu\text{g/L}$. Zare-Afifi (2016) reported that aqueous chloroform concentrations ranged from 12.2 to 282 $\mu\text{g/L}$ at a chlorinated indoor swimming pool. Weaver et al. (2009) reported that aqueous CNCl concentration ranged from below detection limit to 194 $\mu\text{g/L}$. Zare-Afifi (2016) reported that aqueous CNCl concentrations ranged from 1.07 to 203 $\mu\text{g/L}$ at a chlorinated indoor swimming pool.

Dichloromethylamine (CH_3NCl_2) and dichloroacetonitrile (CNCHCl_2) are organic chloramine and haloacetonitrile (HAN) species, respectively, that have been identified in chlorinated swimming pools. Weaver et al. (2009) measured the concentrations of CH_3NCl_2 and CNCHCl_2 in public swimming pools; they ranged from undetectable to 51.0 $\mu\text{g/L}$ as Cl_2 and 0.575 to 87.1 $\mu\text{g/L}$, respectively. Zare Afifi (2016) reported that aqueous CH_3NCl_2 and CNCHCl_2 concentrations ranged from undetectable to 1900 $\mu\text{g/L}$ as Cl_2 and 0.67 to 30.5 $\mu\text{g/L}$, respectively.

Gas-phase NCl_3 is often the focal point of indoor swimming pool air quality. According to the measured concentrations of inorganic chloramines in pool water and their respective Henry's law constants, NCl_3 is the likely to be present at the highest gas-phase concentration of the chloramine compounds (Holzwarth et al., 1984; Weng et al., 2011). The gas-phase NCl_3 concentration is influenced by aqueous NCl_3 concentration in pool water, temperature, air circulation, and mixing behavior at the liquid:gas interface (Schmalz et al., 2011; Weng et al., 2011). Massin et al. (1998) monitored 46 public pools and found the mean gas-phase NCl_3 concentration as 0.24 mg/m^3 . Thickett et al. (2002) reported measurements of gas-phase NCl_3 that ranged from 0.1 to 0.57 mg/m^3 in a pool area. Weng et al. (2011) reported gas-phase NCl_3 concentrations at a pool that ranged from 0.1 to 0.7 mg/m^3 . One study revealed that the concentrations of NCl_3 ranged from 0.017 to 0.15 mg/m^3 in the swimming pools at Taiwan (Chu

et al., 2013). Lévesque et al. (Lévesque et al., 2015) reported that the mean concentration of gas-phase NCl_3 was 0.38 mg/m^3 in a pool at Canada.

2.4 Health Effects of Exposure to Volatile DBPs

DBPs are important for swimming pool water quality because they can lead to human health risks, including possible damage to the respiratory system (Lévesque et al., 1994; Massin et al., 1998), induction of asthmatic response (Bernard et al., 2003; Thickett et al., 2002), irritation of eyes and skin (Fantuzzi et al., 2012; Font-Ribera et al., 2010), and an increased risk of bladder cancer (Villanueva et al., 2007). Swimmers are exposed to DBPs through three main pathways: inhalation, dermal absorption/contact, and ingestion (Whitaker et al., 2003). Lindstrom *et al.* (1997) estimated dermal absorption by swimmers comprised 80% of total THM uptake from swimming pools. Villanueva *et al.* (2007) identified an association between THM exposure in swimming pools and an increased risk of bladder cancer risk. Also, studies have shown that children have higher potential risk of respiratory problems than adults because of the immaturity of their respiratory systems (Bernard et al., 2007, 2003; Carbone et al., 2002). The US EPA has established a maximum contaminant level of 80 ppb ($\mu\text{g/L}$) for the total THM (TTHM) in treated drinking water; however, the EPA have not developed a guideline or regulation for THMs in swimming pools.

CNCl is a highly toxic compound, which was used as a chemical warfare agent in the first world war because it can cause immediate organ injury upon contact (Reid, 1940). Exposure to high concentrations of CNCl is harmful to several organ systems including the lungs, heart, and central nervous system via inhalation and could be fatal with extended exposure (Soltani et al., 2015). CNCl has also been reported to cause irritation of the skin, eyes, and the nasal system (NIOSH, 2003). CNCl is a highly volatile compound. The National Institute for Occupational Safety and Health (NIOSH) has suggested an occupational exposure limit of 0.6 mg/m^3 for gas-phase CNCl (NIOSH, 2003). To date, there have been no studies of human exposure and toxicity of CNCl in swimming pools, but it is ubiquitous in chlorinated indoor swimming pools, although liquid-phase concentrations are typically low. On the other hand, it is plausible that a relatively high liquid-phase concentration of CNCl could exist for a short period of time under some conditions; specifically, the presence of high CNCl precursor concentration and a low concentration of free chlorine could yield high liquid-phase CNCl concentration, probably as a

transient event. In turn, this could lead to acute exposure to gas-phase CNCl under these conditions. The WHO has not established a CNCl guideline value in drinking water because CNCl typically occurs in drinking water at concentrations well below those of health concern (WHO, 2017). No recommended guideline of CNCl concentration has been established for the swimming pool environment.

CH₃NCl₂ (dichloromethylamine) is an organic chloramine compound and its toxicity toward humans remains largely undefined. CH₃NCl₂ is characterized by an odor similar to NCl₃ and along with NCl₃ is probably responsible for the “chlorine odor” that is commonly observed around swimming pools. Currently, there are no regulatory standards or guideline values for CH₃NCl₂ in swimming pools or drinking water.

CNCHCl₂ belongs to the haloacetonitrile (HAN) group. Compared with other DBPs (THMs and HAAs), HANs generally display higher genotoxicity and cytotoxicity (Plewa et al., 2011). The U.S. Environmental Protection Agency has defined a Health Advisory value for CNCHCl₂ in drinking water of 6 µg/L (U.S EPA, 2009a). To date, there is no regulation or guideline value for CNCHCl₂ concentration in swimming pools.

Among health effects associated with exposure to inorganic chloramines, NCl₃ has been researched most extensively due to its association with irritation of the human respiratory system; these symptoms are commonly reported in chlorinated swimming pools (Bernard et al., 2003; Fantuzzi et al., 2012; Jacobs et al., 2007; Massin et al., 1998). Also, NCl₃ is largely responsible for the chlorine odor in indoor swimming pool facilities and is an important contributor to corrosion of metal surfaces (including stainless-steel) in indoor swimming pool settings.

Massin *et al.* (1998) reported irritation of the eyes, nasal passages, and throat as common symptoms among lifeguards after exposure to gas-phase NCl₃. Thickett *et al.* (2002) revealed the development of occupational asthma in swimming pool workers caused by exposure to gas-phase NCl₃ at a swimming pool in Switzerland. Their results also indicated that asthma symptoms occurred among pool workers who did not enter the pool water. Parrat *et al.* (2012) suggested an increasing risk of irritative symptoms following the exposure of gas-phase NCl₃ at concentration around 0.2-0.3 mg/m³ for swimming pool workers at United Kingdom. One study demonstrated potential correlations between irritation symptoms among swimmers and patrons in and near the pool with high concentration of chloramines in the indoor pools (Kaydos-Daniels et al., 2008). Jacobs *et al.* (2007) and Dang *et al.* (2010) both reported that cumulative, long-term NCl₃ exposure

is correlated with upper respiratory symptoms and atopy in swimming patrons, pool workers, and elite swimmers. In another study, pool workers exposed to gas-phase NCl_3 concentrations above 0.5 mg/m^3 experienced ocular symptoms, runny noses, and loss of voice (Fantuzzi et al., 2012). Also, studies have suggested possible associations between long term exposure to NCl_3 and the occurrence of severe asthma in highly trained swimmers (Goodman and Hays, 2008; Uyan et al., 2009).

Two recommend reference levels have been reported for gas-phase NCl_3 concentration in recreational pool facilities. One recommend upper limit of 0.5 mg/m^3 was established by WHO based on stationary measurements as a guideline for safe recreational water environments (WHO, 2006). Bernard *et al.* (2006) suggested an upper limit of 0.3 mg/m^3 in swimming pool facilities because when gas-phase NCl_3 concentration in pool air exceeded 0.3 mg/m^3 , an almost immediate increase in lung epithelium permeability was observed while applying surfactant-associated proteins as epithelial permeability markers.

2.5 Indoor Air Quality (IAQ) Model

In contemporary societies in developed countries, it is common for people to spend more than 90% of their time indoors: at home, at work, in transition, and in many other public and private places (Guo, 2017). Human health can be adversely affected by the air we breathe in these indoor environments. Indoor air can also contain a variety of air pollutants, often at concentrations well above those that are observed outdoors.

Indoor Air Quality (IAQ) generally refers to the air quality within and around buildings and structures and especially related to the health and comfort of people near the buildings (U.S EPA, 2014). The characteristics of IAQ for one setting can change with time and space, and certainly vary among various settings within buildings. Furthermore, risks of some diseases can be increased by indoor air pollution. Evidence of diseases associated with indoor air pollutants has identified radon, environmental tobacco smoke, formaldehyde, asbestos, latex, and other natural and synthetic allergens as the causative agents (Guo, 2017). Thus, improving indoor air quality has become an important issue.

Two approaches have been developed for assessing IAQ in buildings: measurements and modeling. Measurements of IAQ generally rely on IAQ monitoring devices/instruments. Some of these measurements are conducted *in-situ*, while others are performed in a laboratory using air

samples that have been collected at the target location. On-site, long-term measurements can provide opportunities to observe and quantify the dynamic behavior of indoor air pollutants. However, these measurements tend to be expensive and require periodic calibration and maintenance. Thus, short-term measurements are more often conducted to assess IAQ dynamics.

IAQ models offer ways to link sources, sinks, and building factors to simulate the dynamic behavior of indoor air pollutants. Also, IAQ models can be used to help solve IAQ problems. IAQ models can provide information on the factors that govern IAQ dynamics and can help to determine the system parameters (state variables) that must be measured to characterize and control system performance. Common uses of IAQ models include estimation of pollutant concentration and evaluation of the impact of individual sources. IAQ models can act as important tools to study various indoor environments and can also be used to simulate the effects of changes in state variables.

IAQ models range from very simple to complex, and from being able to simulate the behavior of a single component to multiple components. IAQ models should consider physical processes (emission and ventilation) and chemical processes that govern the dynamic behavior of target compound concentrations. IAQ models often fall into one of three categories: statistical, mass-balance, and computational fluid dynamic (CFD) models.

Statistical models are based on empirical formulas that are defined using measurements. Many of these models have been used to estimate the distribution of indoor pollutant exposure and potential dose distribution for building occupants or sensitive sub-populations using Monte Carlo methods (Guo, 2017).

Mass-balance models are based on the concept of mass conservation. They often provide the tools best suited for studying general IAQ problems. Under some circumstances, these models can accurately predict indoor compound concentrations and their responses to changes in state variables. Also, they can be used to evaluate the impact of the source, sink, and IAQ parameters on indoor compound concentrations.

CFD models are spatially-detailed mass-balance models that are used to predict air velocity and target compound concentrations on a local scale, and in a dynamic sense in indoor air spaces. The transport of compounds from one point to another can be accurately simulated by these models. When properly validated, these models can be effective for estimation of personal exposure to indoor air pollutants (Spengler et al., 2001).

3. METHODS AND MATERIALS

The Chapter provides descriptions of the analytical methods used in phases 1 and 2 of the study including Chemtrac HydroAct 4, DPD/KI method, Membrane Introduction Mass Spectrometry (MIMS), the digestion/colorimetric method for urea analysis, and the air quality monitor (NEMo). Also, this chapter lays out the characteristics of each of the studied pools, usage of these swimming pools, and locations of water and air sample collection. In addition, the basic concept of the IAQ model and governing equation are defined in this chapter.

3.1 Analytical Methods

3.1.1 Chemtrac HydroAct 4

The Chemtrac HydroAct 4 is an electronic communication and control system. It functions as an analyzer and a controller with multiple sensors. It is also able to store measurements for subsequent analysis. In this phase of the study, a HydroAct 4 was used to collect data from five sensors that were included in the recirculating line of an indoor pool including, free chlorine, total chlorine, pH/ORP, particle count, and turbidity. The HydroAct 4 was installed in the control room of the pool and filtered water samples flowed past the chlorine, pH, and ORP sensors. A valve was used to select unfiltered and filtered water samples for diversion to the turbidimeter and particle counter as shown in Figure 3.1. Data from each sensor were collected every 10 minutes and uploaded to cloud storage.

A potentiastatic sensor insulated from the liquid by a hydrophilic membrane was installed within the recirculation line. The potentiostatic method is an amperometric measurement with constant potential, made through 2 metal electrodes and a reference electrode dipped in a cell. The gold cathode functioned as the working electrode, the stainless-steel anode was the counter electrode, and a silver/silver halide electrode was used as the reference electrode. Free chlorine (HOCl and OCl^-) diffused through the hydrophilic membrane and was reduced at the cathode while generating a small current that was proportional to the concentration of free chlorine. The free chlorine sensor applied in this project had a measurement range from 0 to 5 mg/L as Cl_2 (ppm). Calibration was done with the DPD colorimetric method.

Another three-electrode amperometric sensor was used to measure the concentration of total chlorine. The sensor measured the current that was generated from free chlorine (HOCl and OCl^-) and chloramines when these compounds passed through membrane and were reduced at the cathode. The current was proportional to the concentration of total chlorine (free chlorine and chloramines). The total chlorine sensor applied in this project had a measurement range of 0 to 5 mg/L (ppm). As with the free and total chlorine measurements, calibration was by the DPD colorimetric method.

The pH and ORP sensors applied in this project were able to measure pH and ORP continuously with temperature readout. The ORP sensor operated by measuring the potential between two electrodes. The ORP signal provides a measure of the tendency of pool water to promote oxidation of reduced compounds. The detection range for pH was 0-14 and the measured range for ORP was -1999 to +1999 mV. In this study, a Chemtrac pH 1 sensor and a Chemtrac ORP 1 sensor were used to monitor water in the recirculating line at the target pool. The readings from this pH/ORP sensor were compared to the sensor that was already in use at the pool.

The Chemtrac turbidity sensor used in this study included an LED light source for a nephelometric (90 degree) light scatter measurement of turbidity (NTU). The range of measurement was established as 0.01 to 100 NTU. Single-point calibration was used for this instrument. Water from the recirculation line was pumped through the turbidity sensor at a flow rate of 1 gallon per minute (3.8 L/min). Both filtered and unfiltered sample data were collected.

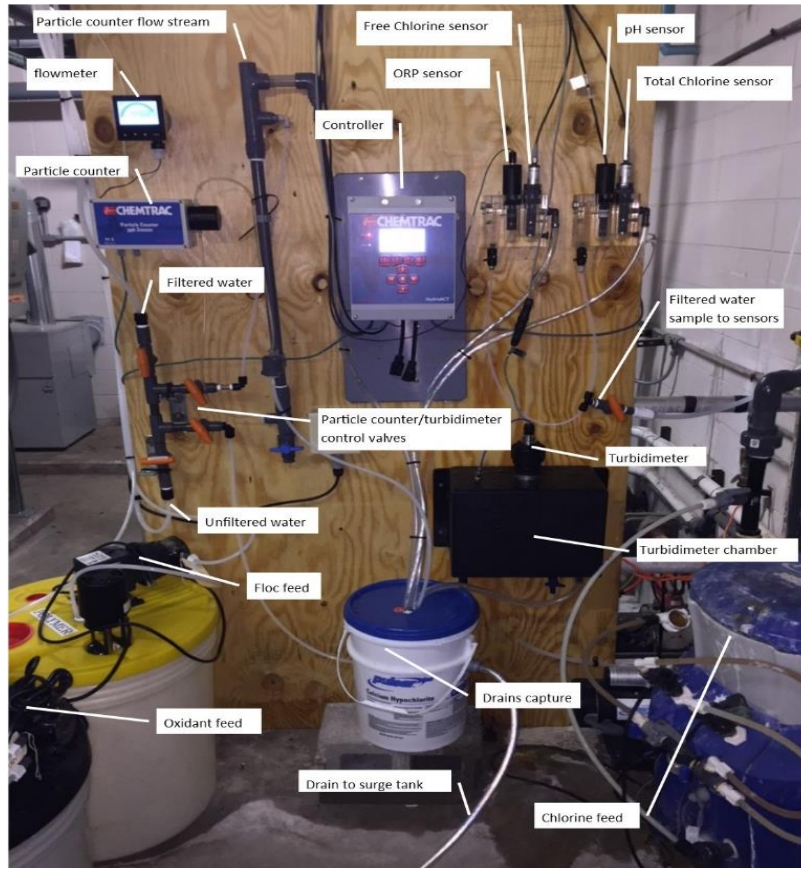


Figure 3.1. HydroAct 4 with each sensor and recirculation lines set up in control room.

3.1.2 DPD/KI

Concentrations of free chlorine in aqueous grab samples were measured daily by method 4500-Cl G, DPD Colorimetric Method, described in *Standard Methods for the Examination of Water and Wastewater* (APHA-AWWA-WEF, 1998). DPD XF (Free chlorine) and DPD XT (Total chlorine) tablets were used to develop the colorimetric signals for measurement of chlorinated pool water samples. Absorbance (A_{515}) was measured with a PalinTest 9 portable photometer (Figure 3.2). DPD Oxystop tablets were applied to prevent interference of chlorine reading during the addition of secondary oxidizer period.



Figure 3.2. Palintest portable photometer.

3.1.3 Membrane Introduction Mass Spectrometry (MIMS)

MIMS has proved to be a suitable method for quantifying and characterizing volatile DBPs in aqueous solution. Simplicity, speed, and sensitivity are key features of the MIMS (Davey et al., 2011; Johnson et al., 2000; Ketola et al., 2002) as it can analyze aqueous samples with little or no pre-treatment. MIMS is based on gas:liquid separation of volatile compounds from a solvent by a pervaporation membrane. Separation can be viewed as a three step process: (i) adsorption of hydrophobic compounds at the membrane:solution interface, with hydrophilic (polar or ionic) compounds being rejected by the membrane; (ii) diffusion of hydrophobic, volatile compounds through the membrane; and (iii) desorption into a low-pressure gaseous (inert) carrier stream such as helium or N_2 . Once in the gas phase, compounds are swept directly into a mass spectrometer (Weng, 2013).

MIMS has been applied for monitoring and identifying inorganic chloramines (Kotiahio et al., 1991). Shang and Blatchley (1999) demonstrated MIMS to be effective for measurement of inorganic chloramine concentrations in chlorinated water. Additionally, Li and Blatchley (2007)

applied MIMS to measure chloroform, dichloroacetonitrile, dichloromethylamine, and cyanogen chloride in swimming pool samples. Weaver *et al.* (2009) measured 11 volatile DBPs in chlorinated indoor swimming pools using MIMS.

The MIMS system used in this study comprised an Agilent GC-MS system (5975C mass-selective detector (MSD) and 6850 gas chromatograph (GC)) with a membrane injection device (Figure 3.3), as described by Shang and Blatchley (1999). The GC was used only for temperature control of the membrane interface (i.e., no chromatography was used). The membrane injection device was constructed around small-diameter medical/pharmaceutical silicone tubing (0.25 mm i.d., 0.47 mm o.d., 60 mm long, Baxter, IL), and operated under a liquid sample flow rate of 0.7 mL/min with an auxiliary gas (He) flow rate of 0.5 mL/min (Weng, 2013).

The MIMS system was operated with electron ionization (70 eV). Volatile DBPs were identified using mass spectrum scan mode ($49 \leq m/z \leq 200$) and further quantified with selected ion monitoring (SIM). Each volatile DBP in this study had at least one unique m/z peak for quantifying their abundance. Ions at m/z 53, 61, 74, 88, 89, 98 were used to quantify NH_2Cl , CNCl , CNCHCl_2 , NCl_3 , NHCl_2 , CH_3NH_2 , respectively, following the method described in Li and Blatchley (2007). CHCl_3 was quantified from ions at m/z 83. In order to account for changes in MIMS behavior, an external standard curve of CHCl_3 was evaluated weekly to characterize the performance of the MIMS system. These data were used to adjust the calibration curves for the other 7 volatile DBPs, as described by Weaver *et al.* (2009). Limits of detection for each target compound were defined on the basis of a 2:1 signal:noise ratio. Numbers are shown in Table 3.1.

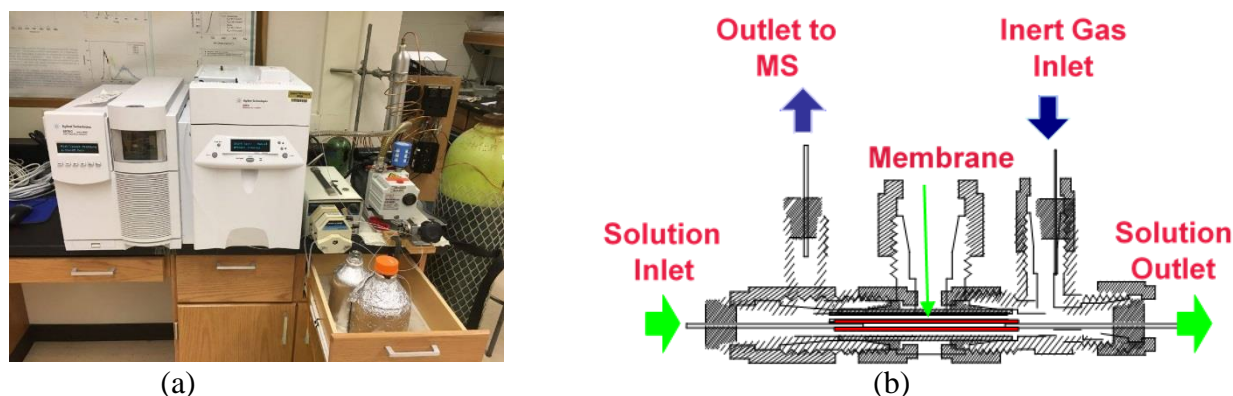


Figure 3.3. MIMS system. (a) Photo of Agilent 6850 GC with 5975C MSD and pumping system: (b) schematic of membrane device, as installed in the GC.

Table 3.1. Limits of detection for volatile DBPs by benchtop MIMS system based on a signal:noise ratio of 2:1.

Compound	NH ₂ Cl	NHCl ₂	NCl ₃	CHCl ₃	CNCl	CNCHCl ₂	CH ₃ NCl ₂
Detection Limit (µg /L)	60	28	3.6	3.7	0.8	2.0	1.6

A portable MIMS system was made available for some experiments by loan of an instrument from the manufacturer (Hiden Analytical, Livonia, MI). The portable MIMS system used in this study was an HPR-40 quadrupole mass spectrometer with through flow membrane cell, as shown in Figure 3.4. Due to its design and configuration, it is operated without a carrier gas. As such, it was possible to transport it to study sites with a personal vehicle. Specifically, this MIMS system was transported to Pools D, E, and F (described below) for use during the experiments that were conducted at each facility. The system operates in a similar manner as the bench top MIMS, but the detection limits for the portable MIMS system were higher than those of the bench top instrument for targeted volatile DBP compounds in this study, as illustrated in Table 3.2. As a result, not every targeted volatile DBP was detectable in swimming pool D, E, and F water samples using this instrument.



Figure 3.4. Portable MIMS system.

Table 3.2. Limits of detection for volatile DBPs by benchtop MIMS system based on a signal:noise ratio of 2:1.

Compound	NCl ₃	CHCl ₃	CNCl
Detection Limit (µg /L)	100	6.5	10

3.1.4 Digestion/colorimetric Method for Urea Analysis

Prescott and Jones (1969) described a method of urea measurement that included a digestion procedure involving antipyrine and colorimetric analysis. Two reagent solutions were prepared separately for this measurement: 1) antipyrine/H₂SO₄ reagent, which comprised 4 g/L antipyrine in 40% (v/v) sulfuric acid and 2) oxime reagent, which included 5 g/L 2,3-butanedione oxime in 5% (v/v) acetic acid. The two reagents were prepared as a mixture with 2 parts of antipyrine/H₂SO₄ reagent and one part of oxime reagent. The digestion reagent was prepared immediately before use. 2 mL of digestion solution were added to 2 mL of swimming pool water sample, then the mixture was placed in a 60°C water bath for 150 minutes for digestion. The yellow color that developed from this digestion process has been demonstrated to be proportional to the concentration of urea in the original sample (Prescott and Jones, 1969). A series of urea standard solutions was prepared by gravimetric addition, then subjected to the same digestion procedure for development of a standard curve. Absorbance of each digestion sample and standard were measured at the wavelength of 466 nm. Water samples and standard samples were analyzed in triplicate.

3.1.5 Air Quality Monitor

Air quality monitoring devices (NEMo, Ethera Labs, Crolles, France, Figure 3.5) were made available for these experiments. The devices were installed at fixed locations within the studied pools. This device is a passive air monitor that accomplishes measurements of gas-phase constituents using a proprietary SolGel nanoporous material on a sensor slide, which has the capacity to concentrate very low level (ppb) chemical compounds (600 m² of air exchange per gram material), then use an electronic/optical system to measure the concentration of target compounds, such as NCl₃ in air. For measurements of gas-phase NCl₃ concentration, the sol-gel material was infused with KI. The reaction between NCl₃ and KI results in formation of molecular

iodine (I_2). Real-time measurements of opacity (based on I_2) are then used to estimate the gas-phase NCl_3 concentration in the air that surrounds the sensor.

Other sensors were also installed in the monitor's chamber to measure temperature, relative humidity, and CO_2 concentration in air. The NEMo device can store measurements collected over a 24-hr period, so that slide replacement was required every day.



Figure 3.5. NEMo air quality monitor.

3.2 Sampling

3.2.1 Pool Characteristics

Five indoor pools located in Indiana and Michigan were sampled. Facilities monitored in this phase of the research were all indoor pools that are used by people with from a wide range of ages. These pools are all public pools that either belong to a public recreational center, university, or local high school. A summary of basic pool characteristics is presented in Table 3.3. All pools used chlorine as the disinfectant. All pools except Pool A also have UV disinfection systems in place. In general, the pools used the local water distribution system for filling and makeup water. Pool B used groundwater from a local well. Pool A was sampled only during Phase 1 of the study. Pools B, C, D, and E were investigated during Phase 2 of the study.

Pool facility A was in a public recreational center with plan dimensions of 10-yards wide and 25-yards long. The pool was used by daily lap swimmers, a group swimming course, swim team practice, and a water Zumba class. The swimming pool was managed by the pool staff, and no modifications were made to the heating, ventilation, and dehumidification system.

Pool facility B was located at a public university with two main water bodies: a competition pool with dimension of 25-yards wide and 50-meters long, and a diving well with dimension of 25-yards wide and 25-yards long. There is a moveable bulkhead that divides the competition pool into two sides. During short-course swimming meets (competitions of 25-yd or 25-m), one side was used as the “competition side” where actual swimming races are held, while the other side was used for warm-up/warm-down activities. Water samples were collected only from the competition pool. Pool and HVAC system operations were unchanged throughout the sampling periods.

Pool facility C was also located at a public university with pool dimensions of 25-yards wide and 50-meters long. A floating bulkhead separates the pool into two sides, one for competition and one for warm-up/warm-down. Water samples were collected from the competition side. Unexpectedly, the HVAC system stopped functioning for roughly two hours during the sample collection period from 8:00 am on 3/16/2019 to 7:00 am on 3/17/2019. Pool operation was normal during the sample period.

Pool facility D is located in a high school with pool dimensions of 25-yards wide and 50-meters long. The pool also included a bulkhead to separate the pool into two sides. Water samples were collected from the warm-up/warm-down area, near the bulkhead. The Pool and HVAC system were operated normally during the swimming meet.

Pool facility E belongs to a public university with pool dimensions of 15-yards wide and 40-yards long. A moveable bulkhead separates the pool into lap swimming side and diving side. Water samples were collected from the lap swimming side. Pool and HVAC system operations were unchanged during the sampling period. Also, this project did not include any measures to influence the hygiene practices of swimmers in any of the pools.

Table 3.3. Summary of the characteristics of all the studied pools.

Pool facilities	Number of pools in facility	Pool dimension	Chlorination method	UV	pH control	Types of swimmers	Age groups of swimmers
A	1	10 yard × 25 yard	Sodium hypochlorite	No	Sodium bisulfate	daily lap swimmers, a group swimming course, swim team practice, and a water Zumba class	Adults and children
B Feb	2	25 yard × 25 yard and 50 meter × 25 yard	Calcium hypochlorite	Y	CO ₂	Swimming meet	14 and under
B Mar	2	25 yard × 25 yard and 50 meter × 25 yard	Calcium hypochlorite	Y	CO ₂	daily lap swimmers and swim team practice	Adults and College students
B April	2	25 yard × 25 yard and 50 meter × 25 yard	Calcium hypochlorite	Y	CO ₂	daily lap swimmers and swim team practice	Adults and College students
B June	2	25 yard × 25 yard and 50 meter × 25 yard	Calcium hypochlorite	Y	CO ₂	Swimming meet	8 and under
B Nov	2	25 yard × 25 yard and 50 meter × 25 yard	Calcium hypochlorite	Y	CO ₂	Swimming meet	Adults and College students
C	1	50 meter × 25 yard	Sodium hypochlorite	Y	Muriatic acid	Swimming meet	13 to 18
D	1	50 meter × 25 yard	Sodium hypochlorite	Y	Sodium bisulfate	Swimming meet	14 and under
E	1	15 yard × 40 yard	Calcium hypochlorite	Y	CO ₂	daily lap swimmers and swim team practice and swimming meet	Adults and College students

3.2.2 Water Sampling

During Phase 1, swimming pool water samples were collected from Pool Facility A in 230 mL polyethylene terephthalate bottles with screw caps. No headspace was allowed for water samples. Two kinds of water sample were collected every weekday morning. One was collected directly from the pool taken approximately 20 cm below the water surface; this sample was referred to as “pool water.” The other sample was collected downstream of filtration from the recirculation line; this sample was referred to as “filtered water.” Water samples were transported to the Environmental Engineering Laboratory at Purdue University and analyzed within 1 hour of collection. Additional sampling included water samples that were collected before the evening swim team practice (5:00 pm) and the other was collected after practice (9:00 pm) on Monday and Thursday, both samples were collected from the pool. Also, after introduction of the oxidant process, extra water samples were collected from the pool before any swimmers entered the pool for morning lap swimming. The sampling methods were designed in a manner that would not interfere with or change the operation of the pool.

During Phase 2, water samples were collected at Pool facility B during swimming meets that were held in February, June, and November 2019. Sample collection was also conducted in March and April 2019 during regular pool operating hours. Pool water sample pairs were collected periodically depending on swimming meet schedules and times when the pool was open to the public. Samples were collected in 50 mL terephthalate bottles with screw caps. Samples were transported to the Environmental Engineering Laboratory at Purdue University as soon as possible after collection for analysis. One water sample was analyzed for volatile DBPs by MIMS. The other water sample was used to measure chlorine and pH, and for urea analysis.

Measurements were conducted at Pool facility C during a swimming meet in March 2019. Sample pairs were collected in 25 mL terephthalate bottles with screw caps. No headspace was allowed for water samples. One sample was used immediately to measure chlorine and pH with a portable UV photometer. The other sample was stored in a travel cooler and transported back to the Environmental Engineering Laboratory at Purdue University for urea analysis after the meet. It was not possible to measure liquid-phase volatile DBP concentrations during this swimming meet.

Experiments were conducted at Pool facility D during a two-day swimming meet in August 2019. Samples were collected every hour in a 200 mL bottles and analyzed immediately for volatile

DBP concentration using the portable MIMS device. Water samples were also collected to conduct chlorine, pH, and alkalinity measurements. Extra samples were stored in a travel cooler and transported back to the Environmental Engineering Laboratory at Purdue University each day for urea analysis.

Water measurements were conducted at Pool facility E during 5-day period including a half-day swimming meet in January 2020. Samples were collected every hour in a 300 mL bottles and immediately subjected to volatile DBP analysis with the portable MIMS instrument. Water samples were also collected to conduct chlorine and alkalinity measurements. In addition, pH was recorded with a portable pH probe. Extra samples were stored in a travel cooler and transported back to the Environmental Engineering Laboratory at Purdue University after the sampling period for urea analysis.

Water sampling points for each measurement are illustrated in Figures 3.6 to Figure 3.14.

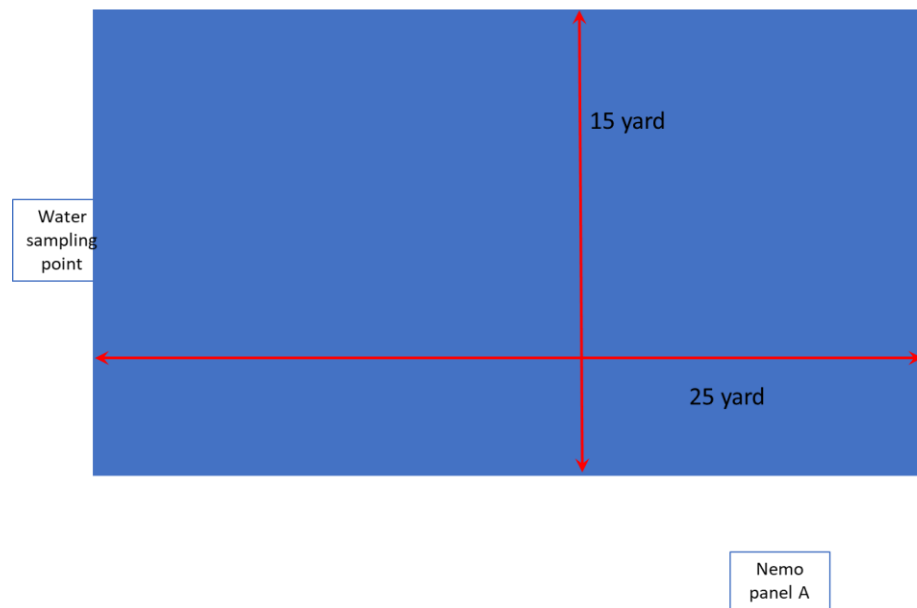


Figure 3.6. Layout of Pool facility A during Phase 1 study. Also included are locations of water sample collection and NEMO placement.

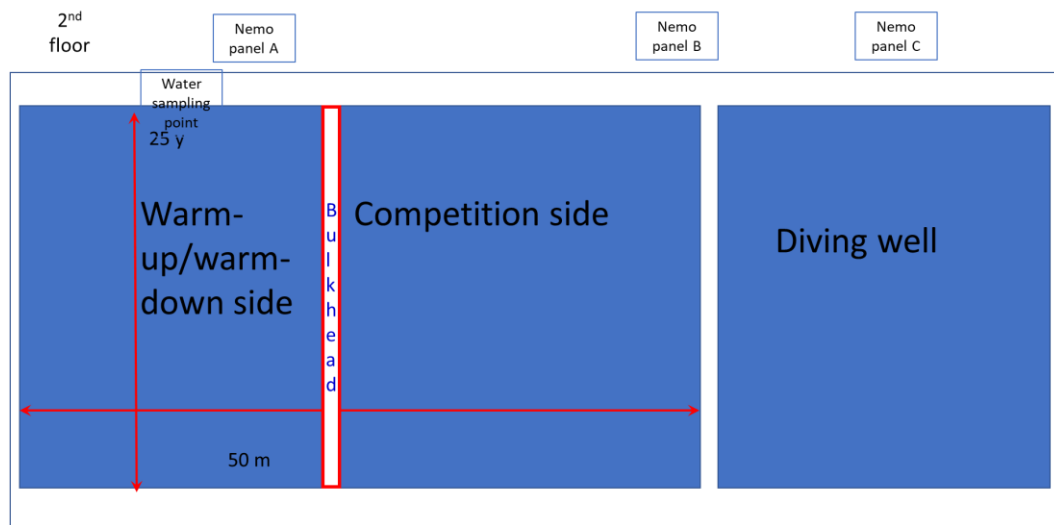
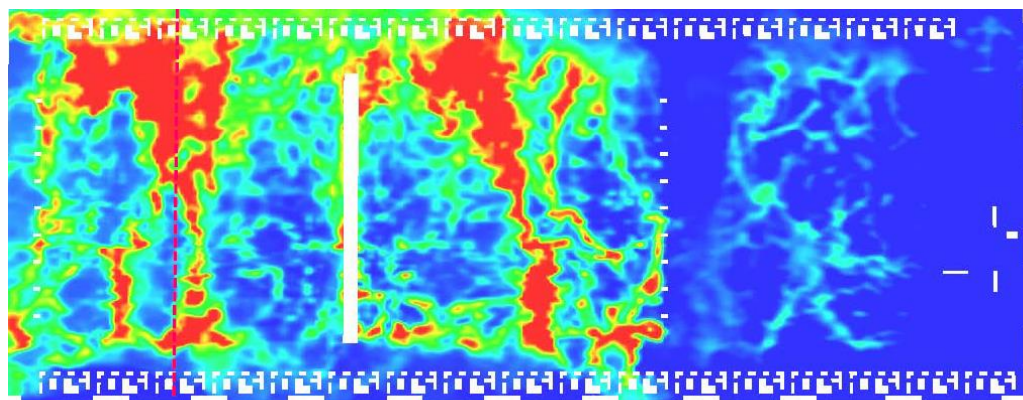


Figure 3.7. Layout of Pool facility B during February 2019 measurements. Also included are locations of water sample collection and NEMO placement.



Horizontal Plane located at Height = 1ft above pool deck

Figure 3.8. Gas-phase NCl_3 CFD profile of Pool facility B.

The red shading indicates regions of elevated gas-phase NCl_3 concentration.
 The green/yellow shading indicates regions of intermediate gas-phase NCl_3 concentration.
 The blue shading indicated regions of low gas-phase NCl_3 concentration.

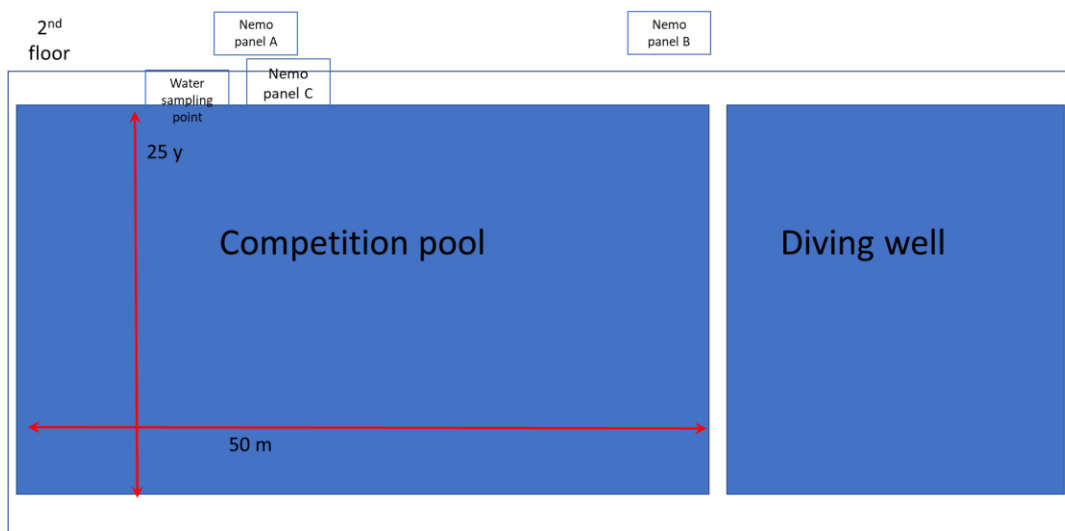


Figure 3.9. Layout of Pool facility B during March 2019 measurements. Also included are locations of water sample collection and NEMO placement.

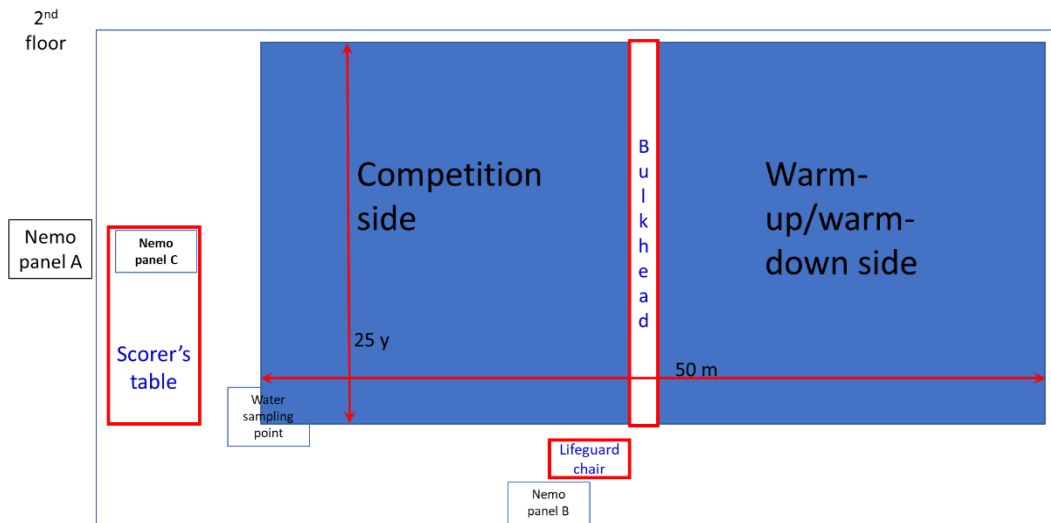


Figure 3.10. Layout of Pool facility C during March 2019 measurements. Also included are locations of water sample collection and NEMo placement.

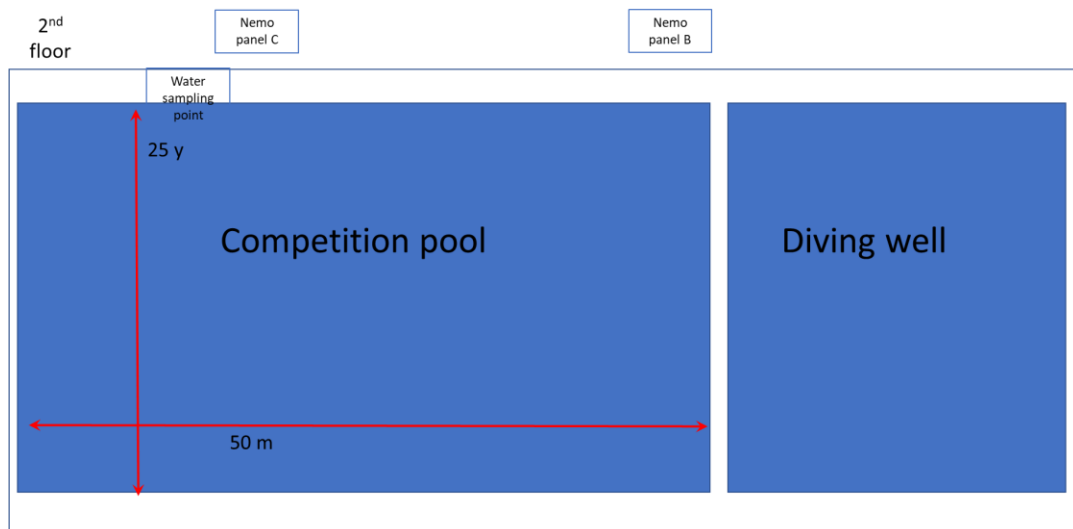


Figure 3.11. Layout of Pool facility B during April 2019 measurements. Also included are locations of water sample collection and NEMo placement.

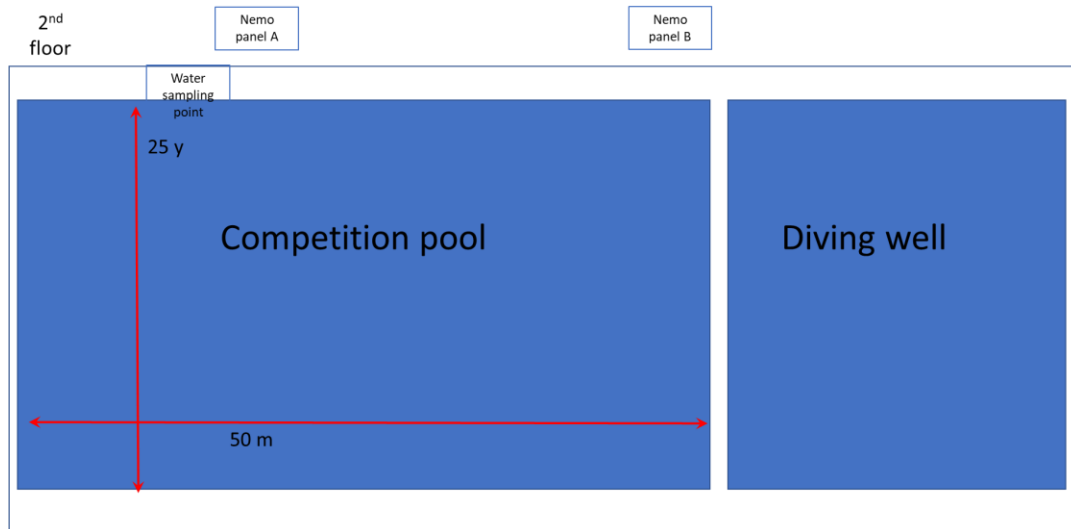


Figure 3.12. Layout of Pool facility B during June 2019 measurements. Also included are locations of water sample collection and NEMO placement.

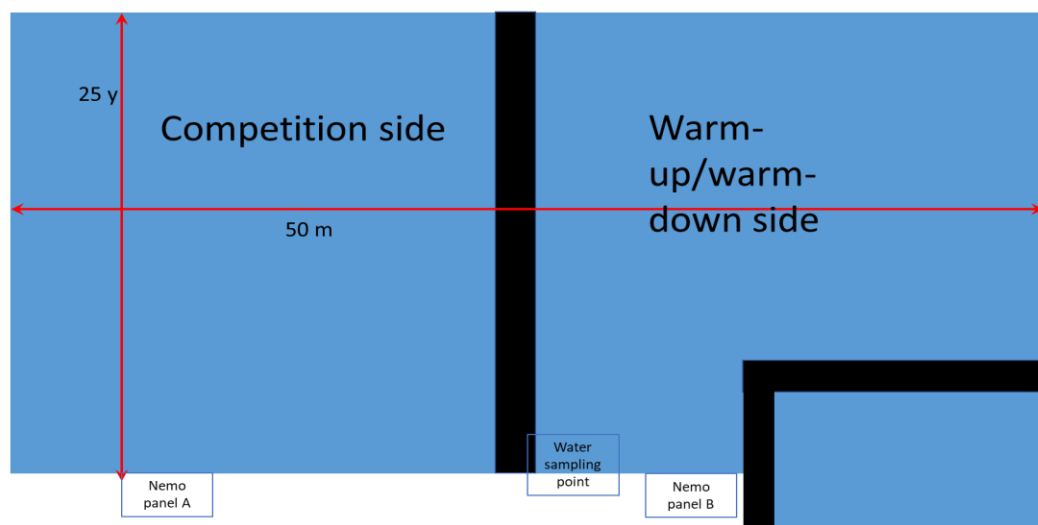


Figure 3.13. Layout of Pool facility D during August 2019 measurements. Also included are locations of water sample collection and NEMO placement.

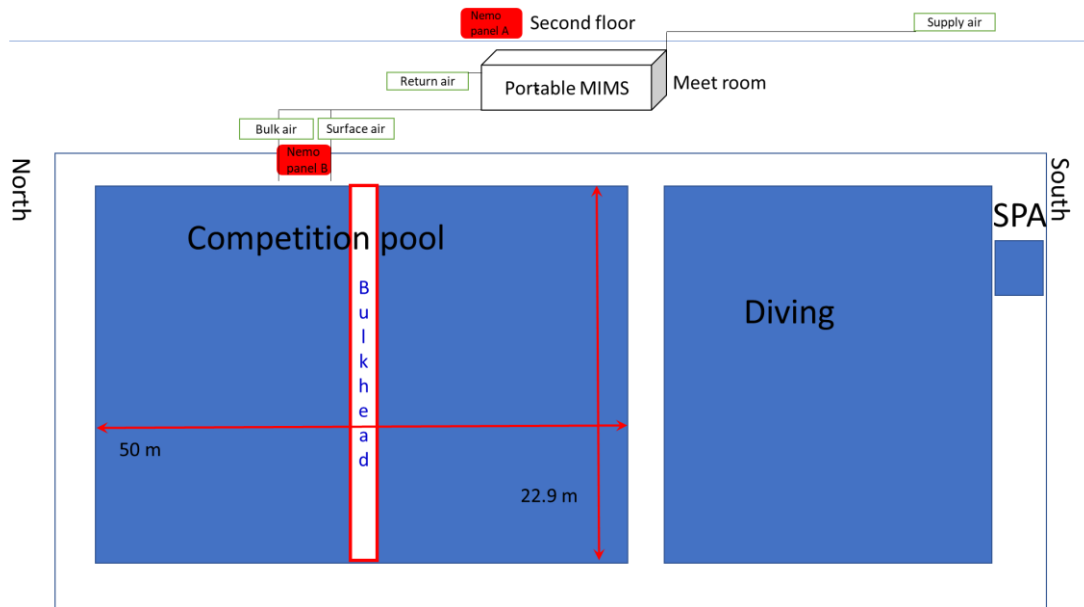


Figure 3.14. Layout of Pool facility B during November 2019 measurements. Also included are locations of water sample collection and NEMo placement.

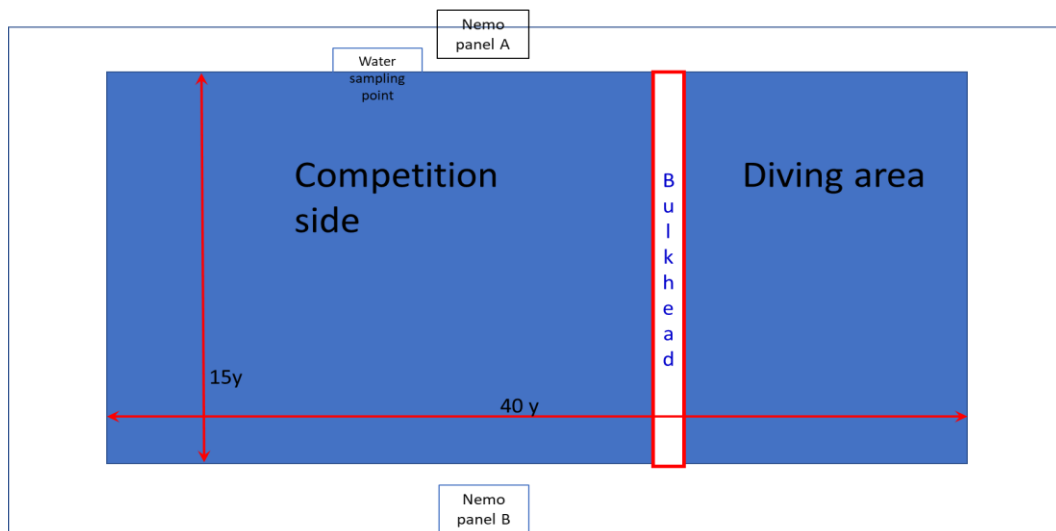


Figure 3.15. Layout of Pool facility E during January 2020 measurements. Also included are locations of water sample collection and NEMo placement.

3.2.3 Air Sampling

One air quality monitoring device (NEMo) was installed on the wall of pool facility A. It was placed roughly 2.5 meters above the swimming pool surface and 4 meters away the swimming pool edge. The layout of the pool area is illustrated in Figure 3.6.

Three NEMo devices were applied during the swimming meet on February 2019 at pool facility B and their locations in the pool area are illustrated in Figure 3.7. NEMo panel A was placed near the warm-up/warm-down side, NEMo panel B was placed between the competition side and the diving well, and NEMo panel C was located across from the center of the diving well. All three NEMo devices were placed approximately 4.5 meters above the pool deck and 5 meters away from pool surface. These locations were selected based on a computational fluid dynamic (CFD) profile of gas-phase NCl_3 behavior in pool facility B. The CFD profile was established by Novus Environmental Inc (Guelph, Ontario, Canada). The CFD results are presented in Figure 3.8. A summary of swimming meet schedules, timing of sample collection, and water/air measurements at all studied facilities are illustrated in Table 3.4.

Three NEMo devices were installed during March 2019 at Pool facility B and their locations in the pool area are illustrated in Figure 3.9. Only NEMo panel C was moved to a new location from the previous experiment, as it was placed approximately 1.5 meters above the pool deck and 1 meter away the pool surface.

Three NEMo devices were installed during a swimming meet in March 2019 at pool facility C and their positions in the pool area are shown in Figure 3.10. Nemo panel A was located on the second floor, approximately 4 meters above pool deck and 4 meters away from pool surface. NEMo panel B was placed under a lifeguard chair roughly 1.5 meters above the pool deck and 4 meters away from the pool surface. NEMo panel C was located near the scorer's table, roughly 1 meter above pool deck and 2 meters away from the pool surface.

Two NEMo devices were applied during the April 2019 experiment at pool facility B as NEMo panel A was undergoing maintenance and was not available for this experiment. Locations of the NEMo devices in the pool area are illustrated in Figure 3.11.

Two NEMo devices were installed during a swimming meet pool facility B in June 2019 and their locations within the pool area are illustrated in Figure 3.12. NEMo devices were placed approximately 4 meters above the pool deck and 5 meters away from pool surface.

Two NEMo devices were installed during a swimming meet at pool facility D in August 2019 and their locations around the pool area are shown in Figure 3.13. Both NEMo devices were placed 1.5 meters above the pool deck and 1 meter away from the pool surface.

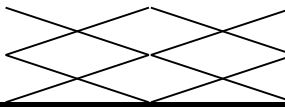
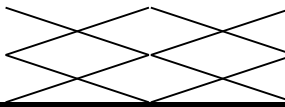
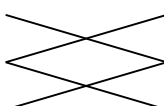
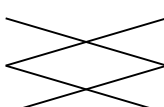

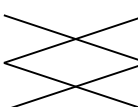
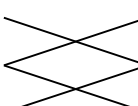
Two NEMo devices were installed during a swimming meet at pool facility B in November 2019 and their location around the pool area are shown in Figure 3.14. NEMo A was placed near the middle of the competition side and approximately 4.5 meters above the pool deck and 5 meters away from pool surface. NEMo B was placed approximately near 1.5 meters above the pool deck and 1 meter away from the pool surface.

Two NEMo devices were installed during measurements at pool facility E in January 2020 and their locations around the pool area are shown in Figure 3.15. Both NEMo devices were positioned roughly 1.8 meters above pool deck and 1.7 meters away from pool surface. All NEMo device locations relative to the pool surface are shown in Table 3.5.

Table 3.4. Summary of meet schedules, timing of sample collection, and measurements.

Pool facilities	First day of meet	Second day of meet	Third day of meet	Fourth day of meet	Measurements of liquid phase	Timing of water sample collection	Measurement of gas phase
B Feb 1 to Feb 3	4:30 pm to 8:30 pm	8:00 am to 1:00 pm; 4:30 pm to 8:30 pm	7:30 am to 2:30 pm		Volatile DBPs and urea.	Meet event start, during the meet and after the meet	Time-course NCl_3 and CO_2 concentration
B June 21 to June 23	5:00 pm to 8:00 pm	8:30 am to 6:30 pm	8:00 am to 4:00 pm		DPD, pH, Alkalinity, volatile DBPs and urea	Every two hours throughout the meet	Time-course NCl_3 and CO_2 concentration
B Nov 21 to Nov 24	8:00 am to 1:30 pm; 4:30 pm to 9:30 pm	8:00 am to 1:30 pm; 4:30 pm to 9:30 pm	8:00 am to 1:30 pm; 4:30 pm to 9:30 pm	9:00 am to 12:00 pm	DPD, pH, Alkalinity, volatile DBPs and urea	Every hour throughout the meet	Time-course NCl_3 and CO_2 concentration
C	7:30 am to 12:30 pm; 4:30 pm to 8:30 pm	8:30 am to 1:00 pm	8:30 am to 1:00 pm		DPD, pH and urea.	Mostly Every 3 hour throughout the meet	Time-course NCl_3 and CO_2 concentration
D	7:00 am to 8:00 pm	7:00 am to 7:00 pm			DPD, pH, Alkalinity, volatile DBPs and urea	Every hour throughout the meet	Time-course NCl_3 and CO_2 concentration
E	2:00 pm to 3:30 pm				DPD, pH, Alkalinity, volatile DBPs and urea	Every hour throughout the meet	Time-course NCl_3 and CO_2 concentration

Table 3.5. NEMo device placement in pools.

Pool facilities	NEMo A	NEMo B	NEMo C
A 11/2018~4/2019			
Distance away pool surface (m)	4		
Distance above pool surface (m)	2.5		
B 02/2019			
Distance away pool surface (m)	5	5	5
Distance above pool surface (m)	4.5	4.5	4.5
B 03/2019			
Distance away pool surface (m)	5	5	1
Distance above pool surface (m)	4.5	4.5	1.5
B 04/2019			
Distance away pool surface (m)		5	5
Distance above pool surface (m)		4.5	4.5
B 06/2019			
Distance away pool surface (m)		5	5
Distance above pool surface (m)		4.5	4.5
B 11/2019			
Distance away pool surface (m)		1	5
Distance above pool surface (m)		1.5	4.5
C 03/2019			
Distance away pool surface (m)	4	4	2
Distance above pool surface (m)	4	1.5	1
D 08/2019			
Distance away pool surface (m)	1	1	
Distance above pool surface (m)	1.5	1.5	
E 01/2020			
Distance away pool surface (m)	1.7	1.7	
Distance above pool surface (m)	1.8	1.8	

3.2.4 Flow rate measurements at pool facility B

Outdoor air flow rate into pool facility B was automatically controlled by dampers in each of five air handling units. During normal operations, damper openings were automatically adjusted based on relative humidity and temperature inside the facility. Each unit was operated independently. When the damper opening reading was 100%, it corresponded with 100% of air coming into the building being outdoor air; this also corresponded to the maximum flow rate of outdoor air through the air handling unit. When the damper reading was 80%, that corresponded to a condition in which 80% of air coming into the building was outdoor air and 20% was return air. The minimum damper reading was 30% for pool facility B. Collectively, the sum of the inlet air flow rates was assumed to be the same as the outlet air flow rate.

Facility B maintains time-course records of damper settings. However, outdoor air flow rate as a function of damper setting had not been measured previously. Thus, measurements of air flow rate in the heating ventilation and air conditioning (HVAC) system were conducted at pool facility B. For each of the five air handling units, air velocities were measured at the supply air duct for damper opening settings of 30%, 65%, and 100%. For each air handler, air velocity profiles were measured with an air data multimeter model ADM-860 connected with a standard pitot probe (Shortridge Instruments, Inc, Scottsdale, Arizona). Air velocities were recorded for a regular grid of horizontal and vertical positions across the cross section of the supply air duct air, then averaged (21 to 40 locations, depending on the size of the duct). The averaged air velocities were multiplied by the cross-sectional area of the air duct to obtain an estimate of the air flow rate. The same procedure was followed for each of the five air handling units.

Air flow rates as a function of damper opening setting for each of the air handling units were estimated by fitting smooth curves to the data, as shown in Figure 3.16. By visual inspection, an order 2 polynomial trendline appeared to provide a good fit the collected data; fitting curve equations are shown in Figure 3.16 as well. Total outdoor air flow rates were calculated as the sum of the calculated air flow rates from the five air handling units.

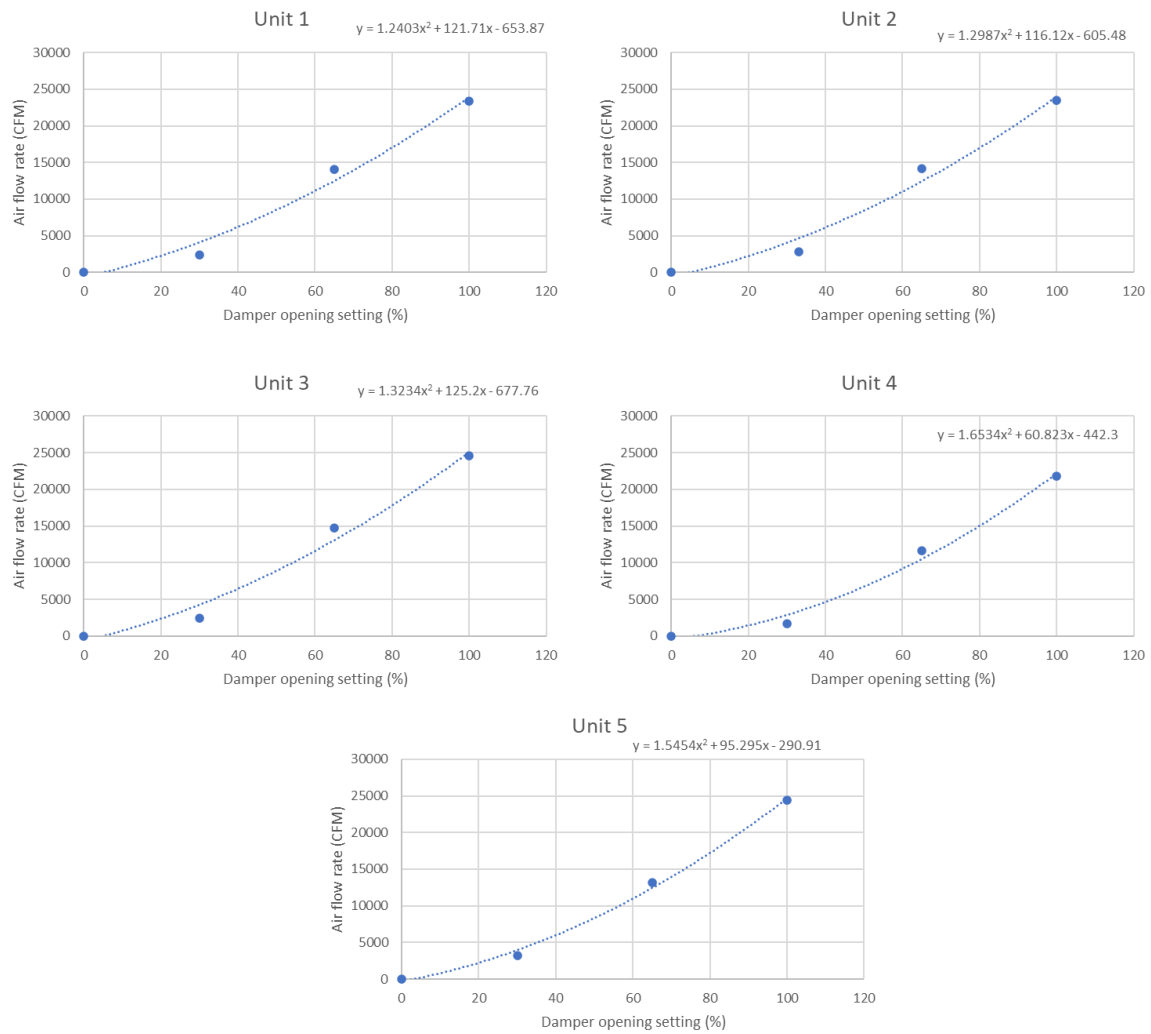


Figure 3.16. Air flow rates with fitting curves as functions of their respective damper opening settings for five air handling units in pool facility B.

3.3 IAQ Model

3.3.1 Model Assumptions

The IAQ model was developed based on three major assumptions:

- Two-film theory was used to simulate the net mass-transfer rate of volatile compounds from the liquid phase to the gas phase. Two-film theory includes an implicit assumption of the mechanics of molecule transfer from the liquid phase to the gas phase. Specifically, two-film theory assumes that net transport is limited by diffusive transport across a thin boundary layer on the liquid side of the gas:liquid interface, a similar layer on the gas side of the interface, or both. This assumption is mechanistically plausible, but represents a simplification of the actual mechanics of transfer.
- The air space was well-mixed in each pool facility. This assumption is not likely to be strictly correct; however, measurements of IAQ dynamics at Facility B indicated similar behavior among sampling locations. Also, if this assumption is not made, then an alternative model to describe mixing/transport behavior in the gas phase must be applied. This model is likely to be much more complicated than our model based on the well-mixed assumption, and considerably more difficult (and expensive) to apply.
- Well-mixed liquid-phase; this assumption also is probably not valid. In general, swimmers spend most of their time near the free surface of water. The majority of the mechanical mixing and precursor introduction attributable to swimmers is confined to the top 30-50 cm of water. However, if this assumption is not made, then an alternative model to describe mixing/transport behavior in the liquid phase must be applied.

Two-film theory is often used to describe (net) transport of compounds between the gas and liquid phases. Figure 3.17 illustrates the transport of a molecule from the liquid phase to the gas phase at a microscopic scale, as hypothesized by the two-film model. During interphase transport processes, a molecule in the bulk liquid will first move to the edge of the liquid film. The molecule will then be transported across the liquid film by diffusion, then transport across liquid:gas

interface. The molecule will then undergo diffusive transport across the gas film. Lastly, the molecule will be transported from the edge of the gas film to the bulk gas phase.

In two-film theory, it is assumed that mass transfer across the liquid:gas interface between gas and liquid is instantaneous; the interface itself is assumed to provide no resistance; therefore, the interfacial concentrations of gas and liquid phases are in local equilibrium as defined by Henry's law. Net mass transfer is assumed to be controlled by diffusion across the hypothetical liquid film, the gas film, or both. Mathematically, Fick's law links the net flux across these films to linear concentration and pressure profiles in the liquid and gas films, respectively. The flux, F , across these films can be expressed as:

$$F = -\frac{D_G}{RT} \frac{dP}{dx} = -D_L \frac{dC}{dx} \quad (\text{eq.3.1})$$

Where,

D_G = gas-phase diffusivity [=] L^2/t

R = gas constant

T = absolute temperature

P = partial pressure of gas being transported

x = distance of direction of transport

D_L = liquid-phase diffusivity [=] L^2/t

C = liquid-phase concentration

However, some parameters in gas and liquid phase in eq 3.1 are difficult to measure thus an empirical approach were developed following the similar mathematical form. In the empirical form, flux is represented as the product of a “driving force” and a constant of proportionality. The empirical form is:

$$F = \frac{k_G}{RT} (p_b - p_i) = k_L (c_i - c_b) \quad (\text{eq. 3.2})$$

Where,

k_G = gas-phase mass transfer coefficient [=] L/t

p_b = bulk gas-phase pressure

p_i = gas interface pressure

k_L = liquid-phase mass transfer coefficient [=] L/t

c_i = liquid interface concentration

c_b = bulk liquid-phase concentration

An implicit assumption of the two-film model is that the concentration/pressure gradients in each film are constant. Therefore, we can re-write these gradients as follows:

$$\frac{dp}{dx} = \frac{\Delta p}{\Delta x} = \frac{p_b - p_i}{\delta_G}, \quad \frac{dc}{dx} = \frac{\Delta c}{\Delta x} = \frac{c_i - c_b}{\delta_L} \quad (\text{eq 3.3})$$

By comparison of above equations with Fick's law, another definition of local mass transfer-coefficient could be expressed as:

$$k_G = \frac{D_G}{\delta_G}, \quad k_L = \frac{D_L}{\delta_L} \quad (\text{eq 3.4})$$

Where,

δ_G = thickness of gas film [=] L

δ_L = thickness of liquid film [=] L

Equation 3.2 is often modified to another empirical form that is based on the “overall” resistance model, rather than local resistance. The “overall” resistance model is presented in two forms:

$$F = \frac{K_G}{RT} (p_b - p^*) = K_L (c^* - c_b) \quad (\text{eq. 3.5})$$

Henry's law can be used to substitute equilibrium liquid-phase concentration with their equivalent equilibrium gas partial pressure, thus the flux across liquid film can also be expressed to partial pressure. A common form of Henry's law is:

$$P = HX, \text{ where } X \approx \frac{c_b}{c_{H_2O}} \quad (\text{eq 3.6})$$

Where, $c_{H_2O} \approx 55.6$ mole/L, and c_b is expressed in molar unit. To apply Henry's law into the overall resistance model, it is more convenient to use a following form:

$$P = H_m C_b, \text{ where } H_m \approx \frac{H}{c_{H_2O}} \quad (\text{eq 3.7})$$

We can expand the overall liquid-phase flux equation to include the interface liquid concentration:

$$(c^* - c_b) = (c^* - c_i) + (c_i - c_b) \quad (\text{eq 3.8})$$

From equation 3.2, 3.5 and 3.7, we can rearrange the form as follows:

$$F = K_L(c^* - c_b), \text{ or } (c^* - c_b) = \frac{F}{K_L} \quad (\text{eq 3.9})$$

$$F = \frac{k_G}{RT}(p_b - p_i) = \frac{H_m k_G}{RT}(c^* - c_i), \text{ or } (c^* - c_i) = \frac{FRT}{H_m k_G} \quad (\text{eq 3.10})$$

$$F = k_L(c_i - c_b), \text{ or } (c_i - c_b) = \frac{F}{k_L} \quad (\text{eq. 3.11})$$

The terms on the right-hand sides of equations 3.9 to 3.11 can then be substituted into equation 3.8 to yield:

$$\frac{F}{K_L} = \frac{FRT}{H_m k_G} + \frac{F}{k_L} \quad (\text{eq. 3.12})$$

Flux F can be removed as the common term in the equation:

$$\frac{1}{K_L} = \frac{RT}{H_m k_G} + \frac{1}{k_L} \quad (\text{eq. 3.13})$$

A similar manipulation starting with the overall flux equation based on gas-phase concentration will be expressed as:

$$\frac{1}{K_G} = \frac{1}{k_G} + \frac{H_m}{RTk_L} \quad (\text{eq. 3.14})$$

Equations 3.13 and 3.14 can be viewed as “resistance” expressions, where $1/K_L$ or $1/K_G$ represent total resistance to mass transfer based on liquid or gas phase concentration, respectively. These equations also imply the effect of the Henry’s law constant on mass transfer resistance. In general, compounds with low H_m tend to have high affinity for the liquid phase. For these compounds, the liquid-film will not provide substantial resistance to transport. Therefore, for compounds with low H_m , mass transfer is controlled by gas-phase film resistance. On the other hand, for compounds with large H_m (*i.e.*, volatile compounds), mass transfer tends to be controlled by liquid-film resistance.

Two-film theory was applied to simulate the transfer of volatile compounds (NCl_3 and others) from the liquid phase to the gas phase in the swimming pool environment. This model suggests that mixing in the liquid phase can be expected to enhance the rate of transfer of volatile compounds (*i.e.*, compounds with relatively large values of H_m), while mixing of the gas-phase is expected to have less effect on transfer of volatile compounds from the liquid phase to the gas phase.

Gas and liquid phase well-mixed assumptions were applied in the model as a means of simplifying the analysis and allowing for reasonable estimates of dynamic behavior in the gas phase, as well as links between IAQ, system design, and system operating characteristics.

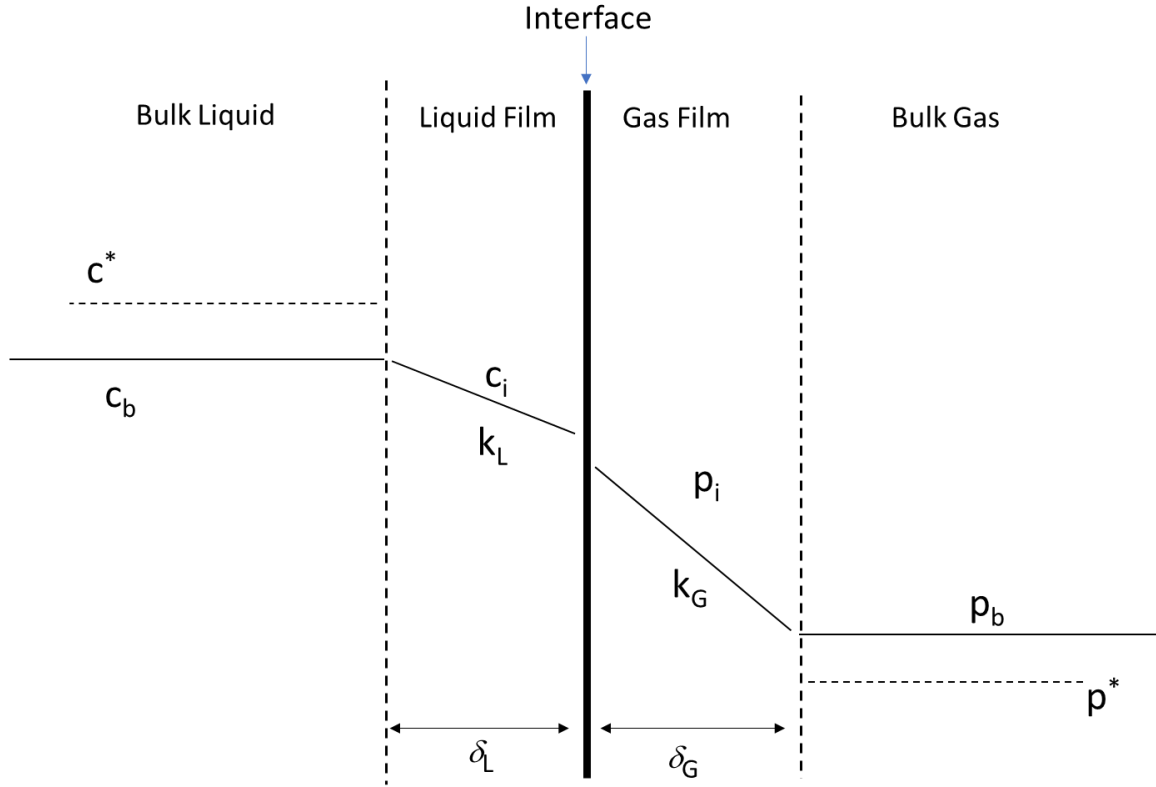


Figure 3.17. Schematic representation of two-film model for gas-liquid transfer.

3.3.2 IAQ Model Governing Equation

The fundamental equation that was used to define this IAQ model is presented below as equation 3.15. This model is based on principles of mass-balance, with a control region of the (well-mixed) indoor air space above a pool. A schematic illustration of control region and relevant parameters of the IAQ model are presented in Figure 3.18.

$$V_g \frac{dc_g}{dt} = Q_g C_{g,in} - Q_g C_g + \Phi_B + \sum_{i=1}^n \Phi_{S,i} \quad (\text{eq. 3.15})$$

Where,

V_g : volume of gas phase (air volume in indoor pool facility).

C_g : concentration of contaminant in air space, and leaving air space.

t : time.

Q_g : volumetric flow rate of air into (and out of) the air space.

$C_{g,in}$: concentration of contaminant in outside air entering the air space.

Φ_B : (net) rate of mass transfer of contaminant from liquid→gas under baseline conditions.

$\Phi_{S,i}$: (net) rate of mass transfer of contaminant from liquid→gas attributable to i^{th} swimmer.

n : number of swimmers.

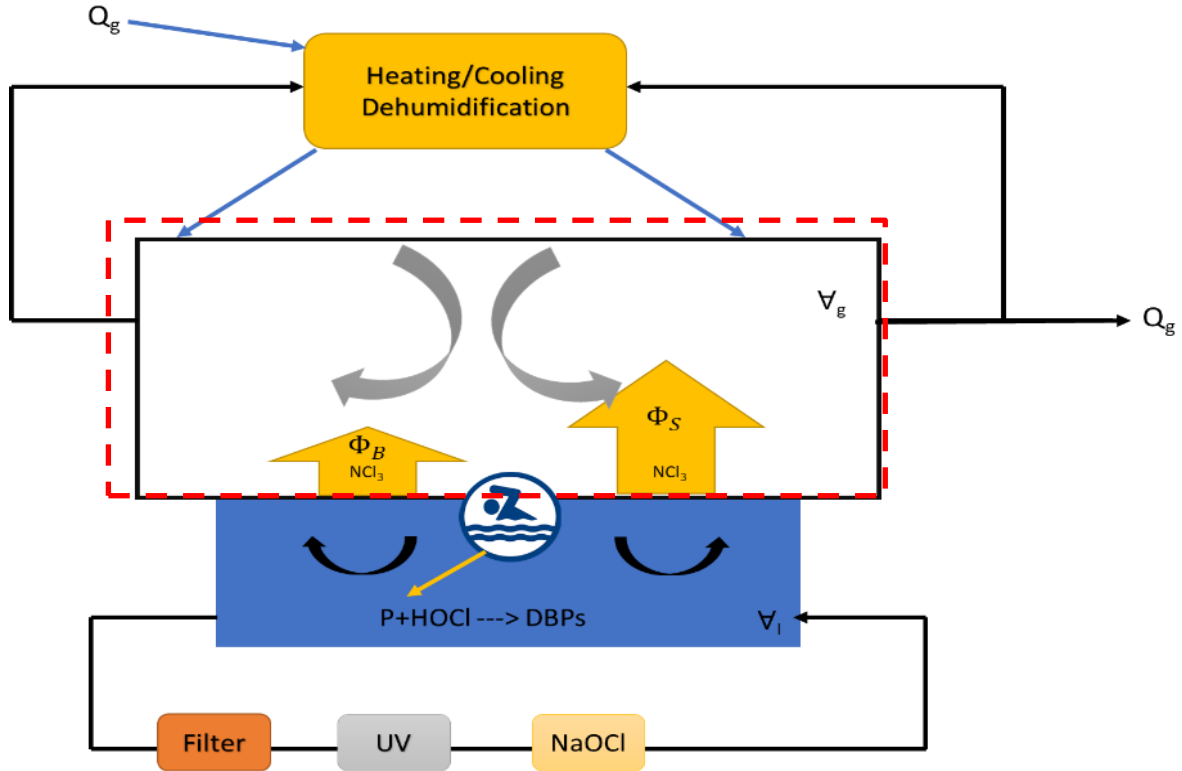


Figure 3.18. Schematic illustration of control region and relevant parameters of IAQ model.

Red dashed line represents the control region and it is assumed to be well-mixed.

Φ_B : (net) rate of mass transfer of contaminant from liquid→gas under baseline conditions.

Φ_S : (net) rate of mass transfer of contaminant from liquid→gas attributable to swimmer

C_g : concentration of contaminant in air space, and leaving air space.

Q_g : volumetric flow rate of air into (and out of) the air space.

V_g : volume of gas phase.

V_l : volume of water phase.

The logic and assumptions behind this equation are as follows:

- The product on the left-hand side of equation describes the time rate-of change of the mass of volatile DBP/contaminant in the control region.
- Outside air is brought into the air space by an air handling system, where it is subjected to heating, cooling, and/or dehumidification. The first term on the right-side of the governing equation represents the rate of mass transport of contaminant that is brought into the control region. The treated (conditioned) air is then distributed into the air space. Some of this air is returned to the air handling system for additional treatment and recirculation. A portion of the air from the air space is vented to the outside; the volumetric rate of air flow from the system is equal to the volumetric rate at which outside air is brought into the control region. The second term on the right-side of the governing equation indicates the rate of mass transport of contaminant that is released from the control region.
- Volatile DBPs are all assumed to be generated in water exclusively; it is assumed that no other sources of these compounds exist in the system. Schematically, reactions between precursors (P) that are introduced by swimmers and free chlorine are shown in Figure 3.17. At present, it is not possible to accurately simulate DBP formation/degradation dynamics in pool water because the kinetics of many of the participating reactions are complex and incompletely defined. However, in some cases analytical tools are available to quantify the liquid-phase concentrations of volatile DBPs in a pool.
- Under baseline conditions (*i.e.*, when the pool facility is closed and water circulation/mixing are entirely attributable to water recirculation through the treatment system), net liquid→gas transfer of volatile compounds takes place at a rate of Φ_B ; this rate of mass transport $\left(\frac{\text{mass or moles}}{\text{time}}\right)$ can be related to other aspects of system behavior through the two-film theory. The contribution of this process to IAQ dynamics is described by the third term on the right-side of the governing equation.
- When swimmers are in the water, they introduce DBP precursors (see step 3) and also mix water in the immediate vicinity of the air:water interface. This mixing behavior promotes net transport of volatile compounds (including some DBPs) from

water→air. Each swimmer is assumed to contribute to water→air transport independently at a rate of $\Phi_{S,i}$. The overall rate of water→air transport attributable to swimmers $\left(\frac{\text{mass or moles}}{\text{time}}\right)$ is defined as the sum of their individual contributions and each swimmer is assumed to contribute equally to this process. Therefore, if there are n swimmers in the water, the net rate of water→air transfer due to these swimmers is defined by the sum: $\sum_{i=1}^n \Phi_{S,i}$ as described by the fourth term in the right-side of the governing equation. As with the baseline water→air transfer process, the rate of transport by swimmers was simulated using two-film theory.

- The processes that contribute to IAQ dynamics are assumed to operate independently; therefore, their effects are additive.

4. PHASE 1

Time-course monitoring of free chlorine, total chlorine, ORP, pH, and turbidity were conducted using the Chemtrac HydroAct 4 device at the target indoor swimming pool. Measurements of the concentrations of volatile DBPs in water samples were conducted by MIMS. Seven different volatile DBPs were investigated in this project: monochloramine (NH_2Cl), dichloramine (NHCl_2), trichloramine (NCl_3), chloroform (CHCl_3), cyanogen chloride (CNCl), dichloroacetonitrile (CNCHCl_2), and dichloromethylamine (CH_3NCl_2). Each of these compounds have been previously identified as a volatile DBP in swimming pools. Urea in pool water samples was measured by the digestion/colorimetric method. Concentrations of gas-phase NCl_3 were monitored by NEMo.

The goals of this experiment were to quantify the effects of changes in water treatment processes on water and air quality in an indoor pool. The pool chosen for this investigation was used by recreational and competition swimmers.

4.1 Phase 1

4.1.1 Trends of Chlorine, ORP, and pH

The National Swimming Pool Foundation recommends that free chlorine in pools and spas should be maintained between 1-5 mg/L as Cl_2 (NSPF, 2006). The World Health Organization has also suggested a minimum free chlorine concentration for swimming pools of 1 mg/L as Cl_2 with proper circulation and dilution (WHO, 2006).

Time-course measurements of free chlorine, total chlorine, and ORP are presented in Figure 4.1. The Figure should be interpreted as follows. The vertical solid lines indicate treatment process changes during the study. Dates identified on the horizontal axis represent every Monday during the study.

Free chlorine concentrations were not expected to change substantially after replacing the filter media to AFM and the initiation of APF feed; however, some variations of the free chlorine signal were observed. The first significant free chlorine concentration decrease was observed on 11/13/2017; this abrupt change was due to re-calibration of the free chlorine sensor. Gradual

decreases of free chlorine concentration were observed when the chlorine feed tank was empty, including the holiday periods for Thanksgiving (starting 11/23/2017) and Christmas (starting 12/24/2017). During free chlorine concentration decreases, corresponding reductions of ORP were also observed, as anticipated. Total chlorine concentrations did not change substantially after replacing sand filter media with AFM and starting to feed APF, compared to the baseline stage.

Notable changes of free chlorine and total chlorine concentrations were observed after the introduction of secondary oxidizers into the pool. The secondary oxidant is a persulfate-based oxidizer in the presence of an activator that generates sulfate free radicals. The activator is a water-soluble Metal-Porphyrin that allowed the oxidizer to be applied as liquid form. For the period following introduction of the secondary oxidant and the activator, ORP was consistent with measurements conducted in the earlier stages of this project.

The trends of total chlorine concentration followed the trends of free chlorine concentration during the study period. However, after addition of secondary oxidizers, the difference between total chlorine and free chlorine (analytically defined as combined chlorine) was smaller than during the previous stages. Previous research has demonstrated that the combined chlorine signal includes contributions from inorganic chloramines and organic chloramines (Jensen and Johnson, 1990; Weaver et al., 2009). The observation of a decrease in the difference between total and free chlorine implies that the addition of the secondary oxidant may have caused a decrease in chloramine formation, degradation of chloramine precursors to prevent their participation in chloramine formation reactions, or both.

According to the Centers for Disease Control and Prevention (CDC), the pH of the pool water should be maintained between 7.2 and 7.8. Time-course measurements of pH during the study period are presented in Figure 4.2. Generally, pH was within the guideline range. Exceptions occurred when the acid feed tank was not filled. For instance, the acid feed tank was empty during Thanksgiving weekend, resulting in an increase of pH. The acid feed tank was observed to be empty several times during the study period.

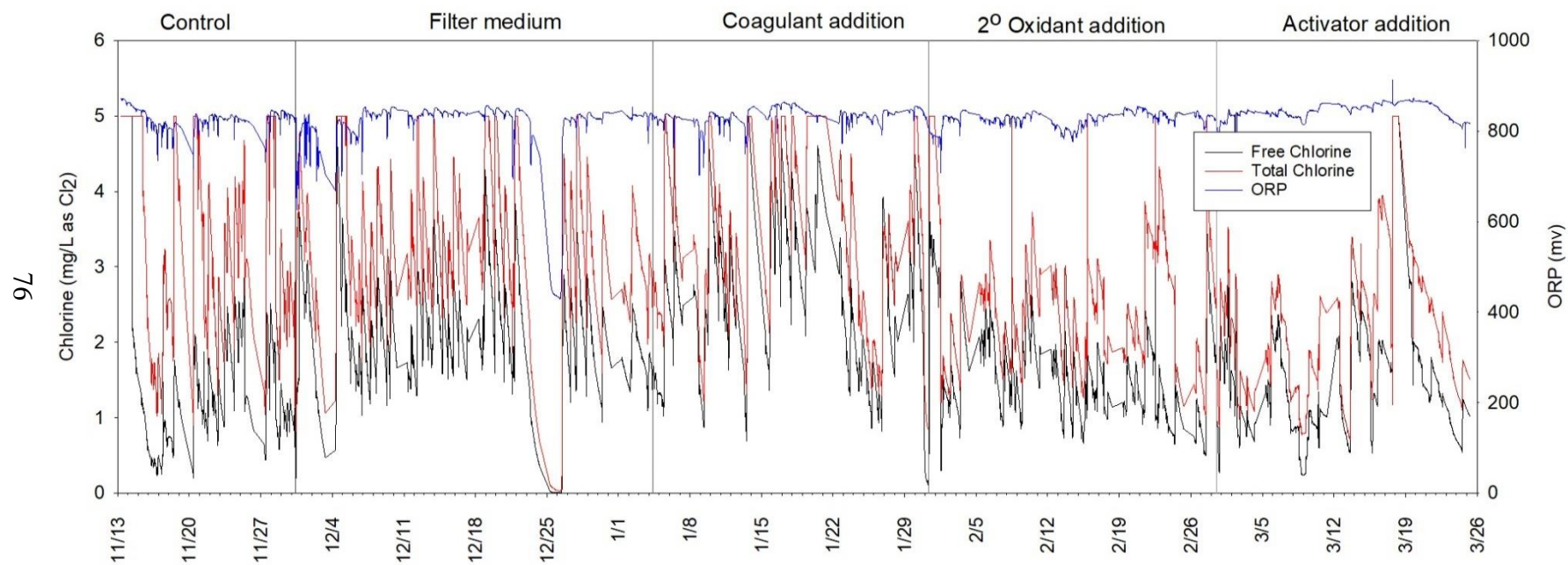


Figure 4.1. Time-course monitoring of free chlorine, total chlorine and ORP at pool A.

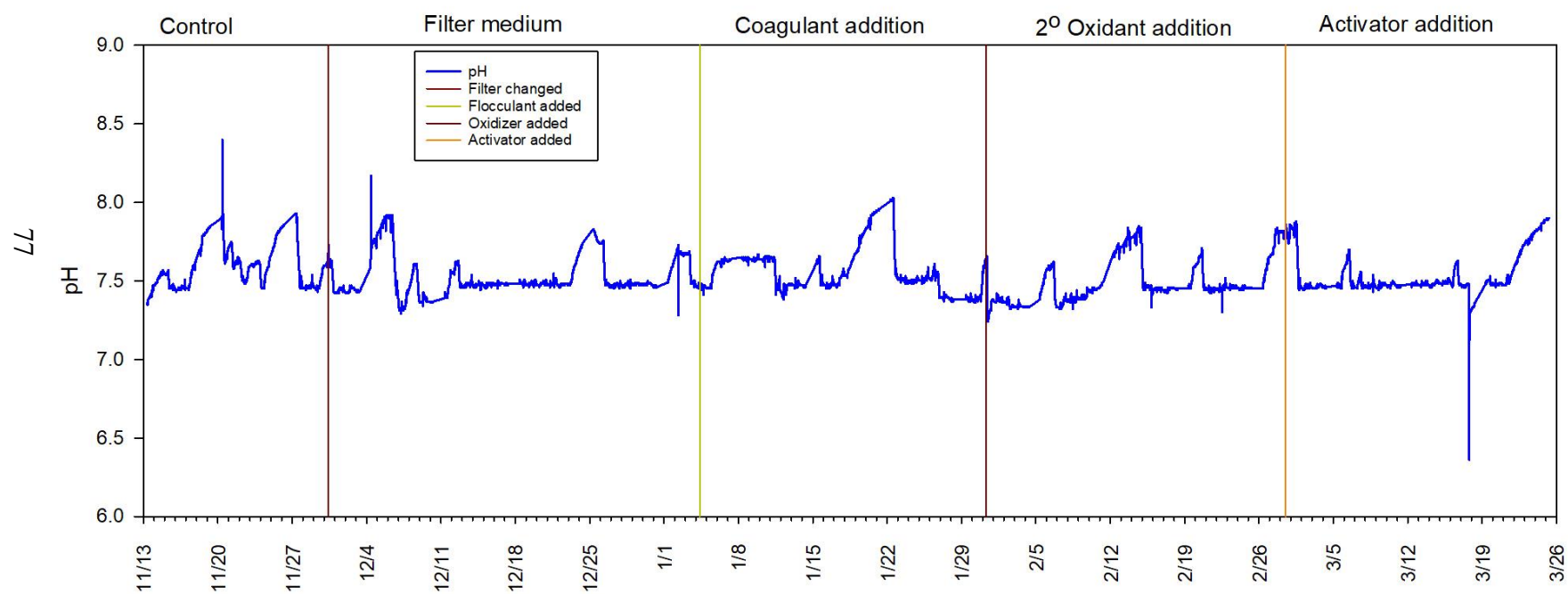


Figure 4.2. Time-course monitoring of pH at pool A.

4.1.2 Trends of Turbidity

According to the Pool Water Treatment Advisory Group, turbidity in swimming pool water should be maintained below 0.5 NTU (PWTAG, 2016). The *Guidelines for Safe Recreational Water Environments* call for 0.5 NTU as an upper limit for pools (WHO, 2006). Time-course measurements of turbidity are summarized in Figure 4.3. The gray vertical lines represent the swimmer counts as record by the lifeguard (hourly) at the pool. The sharp increases of turbidity generally coincided with filter backwash events. Small increases of turbidity were also identifiable immediately after heavy bather loads in the pool, providing an indication of swimmer impacts on particle concentration.

It was hypothesized that replacement of the sand filter medium with AFM and introduction of the coagulant chemical would reduce turbidity, relative to the baseline stage of pool operation. During the baseline stage, the turbidity was measured to be close to 0.05 NTU when there were no or few swimmers in the pool. After replacing filter media, similar readings were observed when swimmers were in the pool except the week after Christmas when a pool operator modified ORP and pH to standard levels (by addition of sodium bisulfate granules and sodium bisulphate salt) into the pool. After introduction of coagulant (APF), turbidity improved to below 0.05 NTU immediately. However, APF was mixed inappropriately on 1/11/2018, causing turbidity to exceed 0.5 NTU on 1/12/2018. The turbidity returned to roughly 0.05 NTU within a couple of days.

The aim of the APF evaluation was to improve turbidity to below 0.03 NTU, but turbidity could only be measured as low as 0.04 NTU; this occurred when the bather load in the pool typically less than 5 swimmers. Therefore, the APF evaluation was discontinued (*i.e.*, coagulant feeding to the pool was terminated) on 1/28/2018. Overall, the turbidity was still maintained around 0.05 NTU, even in the absence of coagulant feeding.

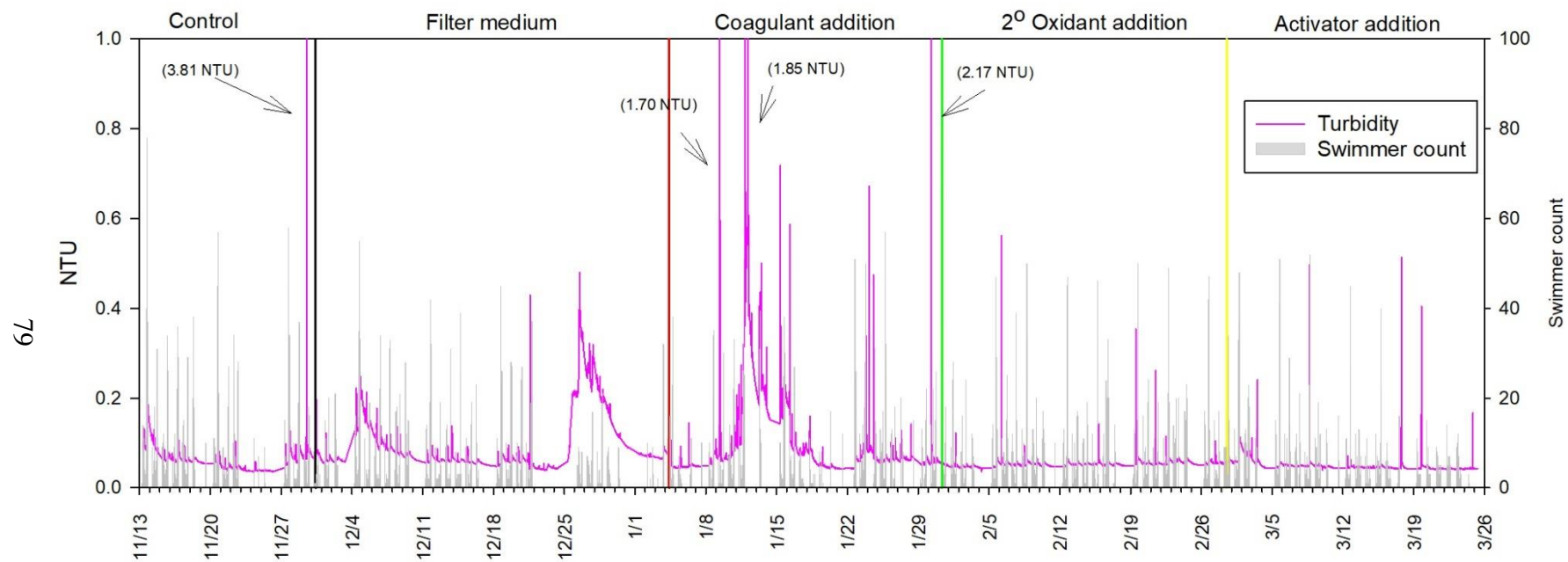


Figure 4.3. Time-course monitoring of turbidity at pool A.

4.1.3 Trends of Volatile DBPs

The term “combined chlorine” is commonly understood to refer to inorganic chloramines: monochloramine (NH_2Cl), dichloramine (NHCl_2), and trichloramine (NCl_3). Inorganic chloramines in pools are mainly the products of reactions between free chlorine and organic-N compounds. Previous research has revealed typical concentrations of NH_2Cl , NHCl_2 , and NCl_3 found in public swimming pools from below detection limit to 1880 $\mu\text{g/L}$ as Cl_2 , below detection to 417 $\mu\text{g/L}$ as Cl_2 , and below detection limit to 377 $\mu\text{g/L}$ as Cl_2 respectively (Weaver et al., 2009).

Time-course monitoring of NH_2Cl is illustrated in Figure 4.4. The concentration of NH_2Cl gradually increased after the replacement of filter media and started to decrease after the application of the coagulant chemical. In general, swimmer number did not correlate strongly with measured concentrations of NH_2Cl . Significant reductions in NH_2Cl concentration were observed after the introduction of the activator; in many cases, the concentration of NH_2Cl dropped below the limit of detection.

As shown in Figure 4.5, no obvious trends in NHCl_2 concentration were observed in the time-course data set for this compound. NHCl_2 is a generally unstable compound, and its concentration was generally lower than the concentration of NH_2Cl .

Time-course measurements of liquid-phase NCl_3 concentration are illustrated in Figure 4.6. After replacing sand filter to AFM, a slight improvement of NCl_3 concentration was observed for a period of about two weeks, but the NCl_3 concentration increased afterward. After addition of secondary oxidizers, concentrations of NCl_3 reduced moderately and remained stable for four weeks. The implication is that rates of formation and decay of NCl_3 had approached a steady-state condition during these weeks. Further reduction of NCl_3 concentration was detected following the application of the activator.

Concentrations of liquid-phase NCl_3 after swimming practice were generally higher than before practice, suggesting a swimmer impact on NCl_3 in pool water. The difference of NCl_3 concentrations between before and after practice became minor after the introduction of the activator, suggesting that it might reduce the swimmer impact on NCl_3 concentrations in the pool.

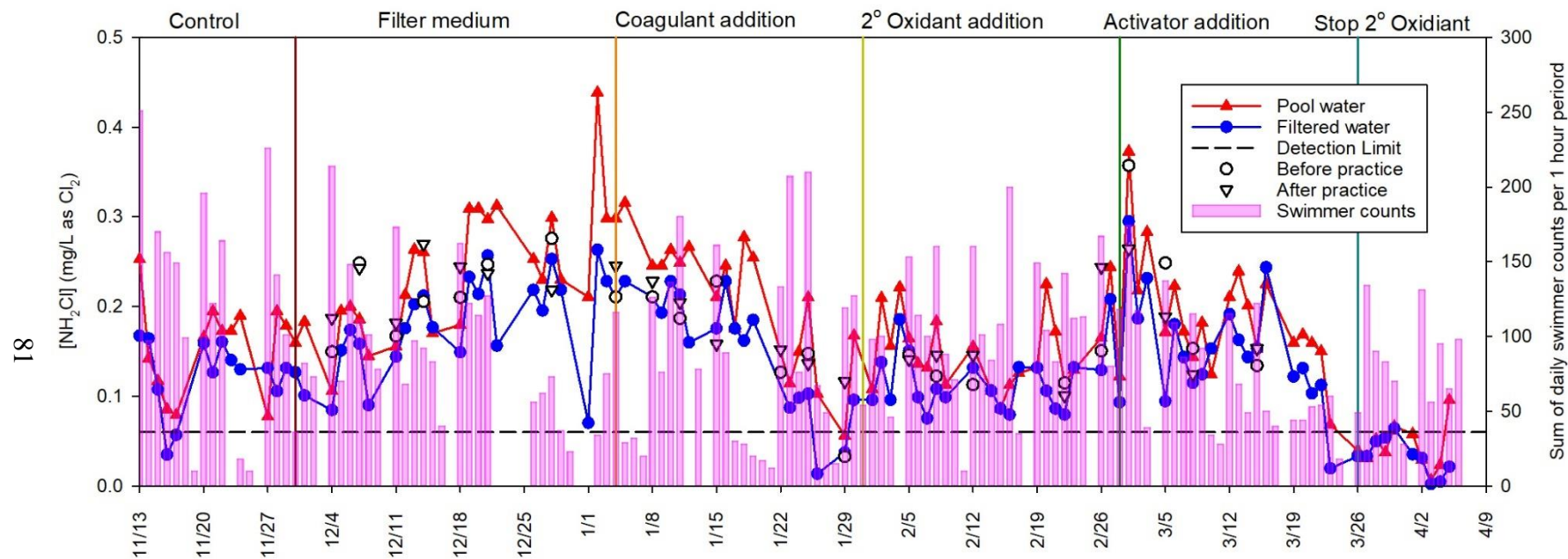


Figure 4.4. Time-course monitoring of liquid-phase NH_2Cl at pool A measured by MIMS. Red triangle symbols represent the water samples collected from the pool. Blue circle symbols represent water samples collected after filtration. The black dashed line represents the detection limit. Empty circle symbols represent measurements before swimming practices. Empty triangle symbols represent measurements after swimming practices. Pink vertical bars represent swimmer counts.

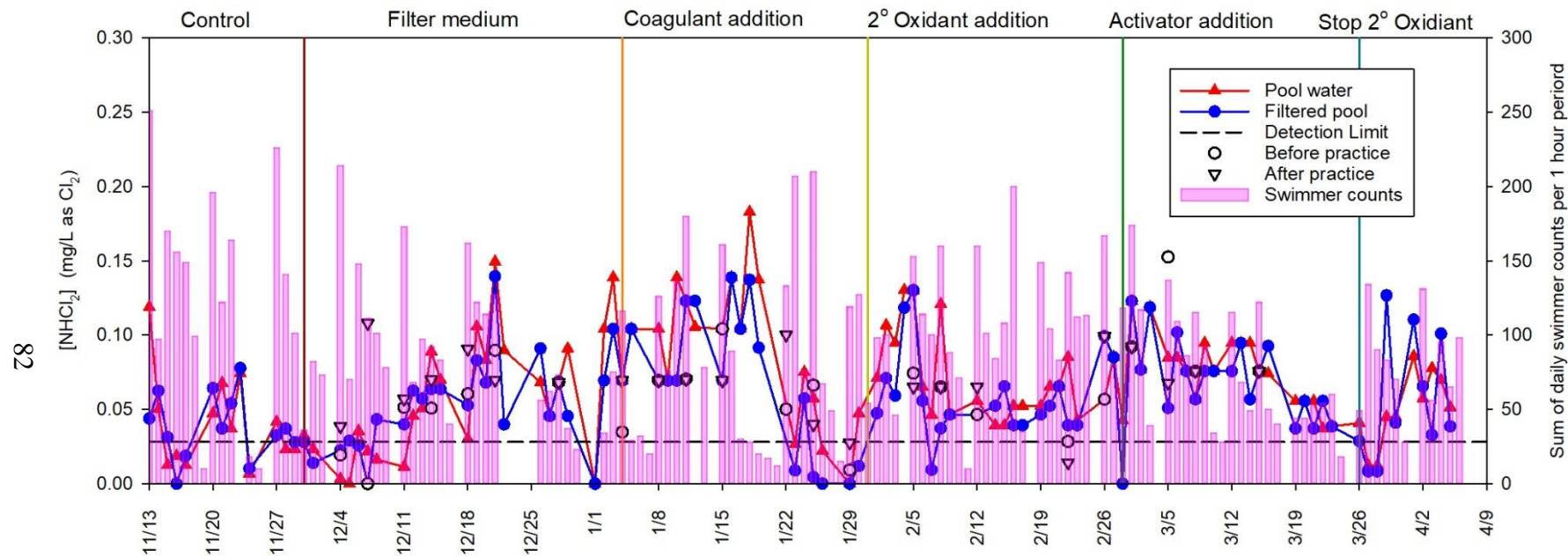


Figure 4.5. Time-course monitoring of liquid-phase NH_4Cl_2 at pool A measured by MIMS. Red triangle symbols represent the water samples collected from the pool. Blue circle symbols represent water samples collected after filtration. The black dashed line represents the detection limit. Empty circle symbols represent measurements before swimming practices. Empty triangle symbols represent measurements after swimming practices. Pink vertical bars represent swimmer counts.

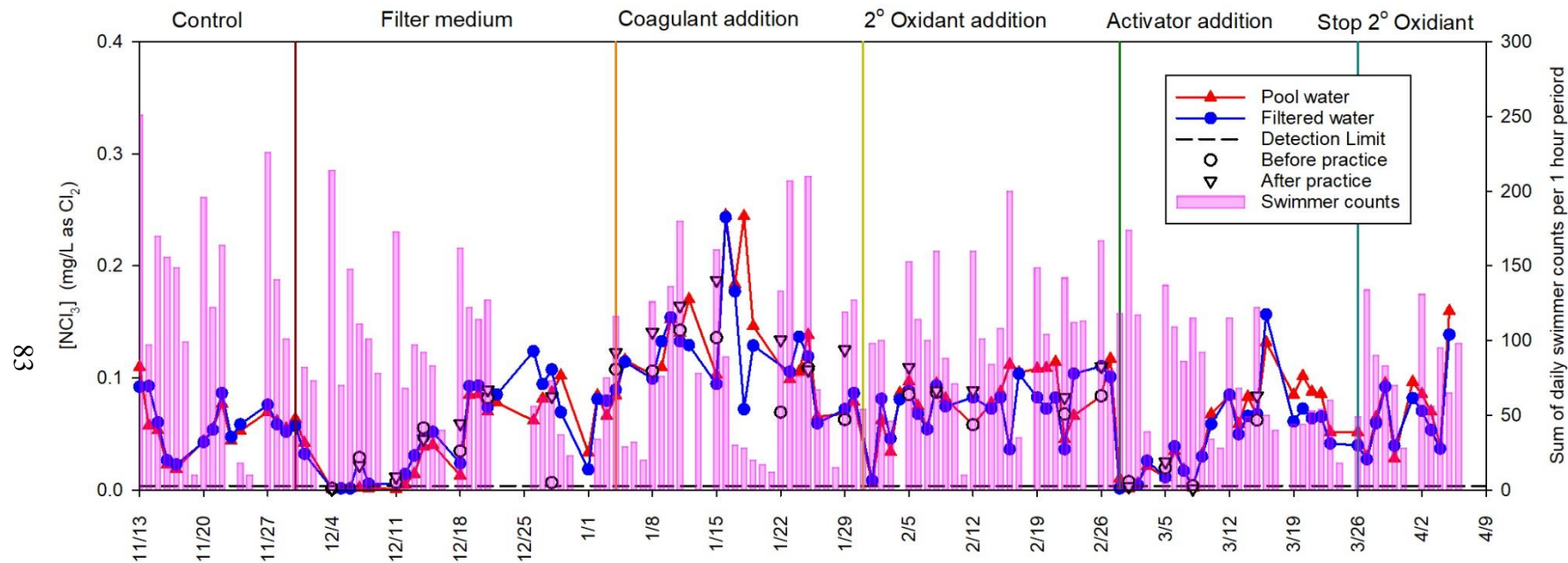


Figure 4.6. Time-course monitoring of liquid-phase NCl_3 at pool A measured by MIMS. Red triangle symbols represent the water samples collected from the pool. Blue circle symbols represent water samples collected after filtration. The black dashed line represents the detection limit. Empty circle symbols represent measurements before swimming practices. Empty triangle symbols represent measurements after swimming practices. Pink vertical bars represent swimmer counts.

Combined chlorine was measured daily by the MIMS method (sum of the concentrations of NH_2Cl , NHCl_2 , and NCl_3) and the DPD method (total chlorine - free chlorine). The results of these measurements are shown in Figure 4.7. In general terms, the difference between the DPD measurement of combined chlorine and the MIMS measurement of combined chlorine is probably attributable to organic chloramines. However, with the exception of CH_3NCl_2 , none of the organic chloramines were identifiable or quantifiable using the methods that were applied in this research.

The DPD-based measurements showed substantial changes across the duration of the study period. Also, the DPD readings were generally higher than the corresponding measurements by MIMS. As described above, this suggests that organic chloramines comprised a substantial fraction of the chloramine signal by DPD. On average, DPD signals were roughly twice as high as the corresponding MIMS signals. This behavior is consistent with previous research (Weaver et al., 2009).

Interference in the DPD signal is relevant to pool operation, especially since the conventional method for reducing the chloramine signal is shock chlorination. Swimming pool shock chlorination treatment is based on conventional “breakpoint chlorination” chemistry, wherein it is assumed that the combined chlorine signal is attributable to inorganic chloramines. However, the chemistry of reactions between free chlorine and organic-N compounds is not as well-defined as that of chlorination of ammoniacal-N. Moreover, the reactions between free chlorine and urea are remarkably slow, suggesting that conventional shock chlorination treatment may actually be detrimental to pool water quality (Blatchley and Cheng, 2010).

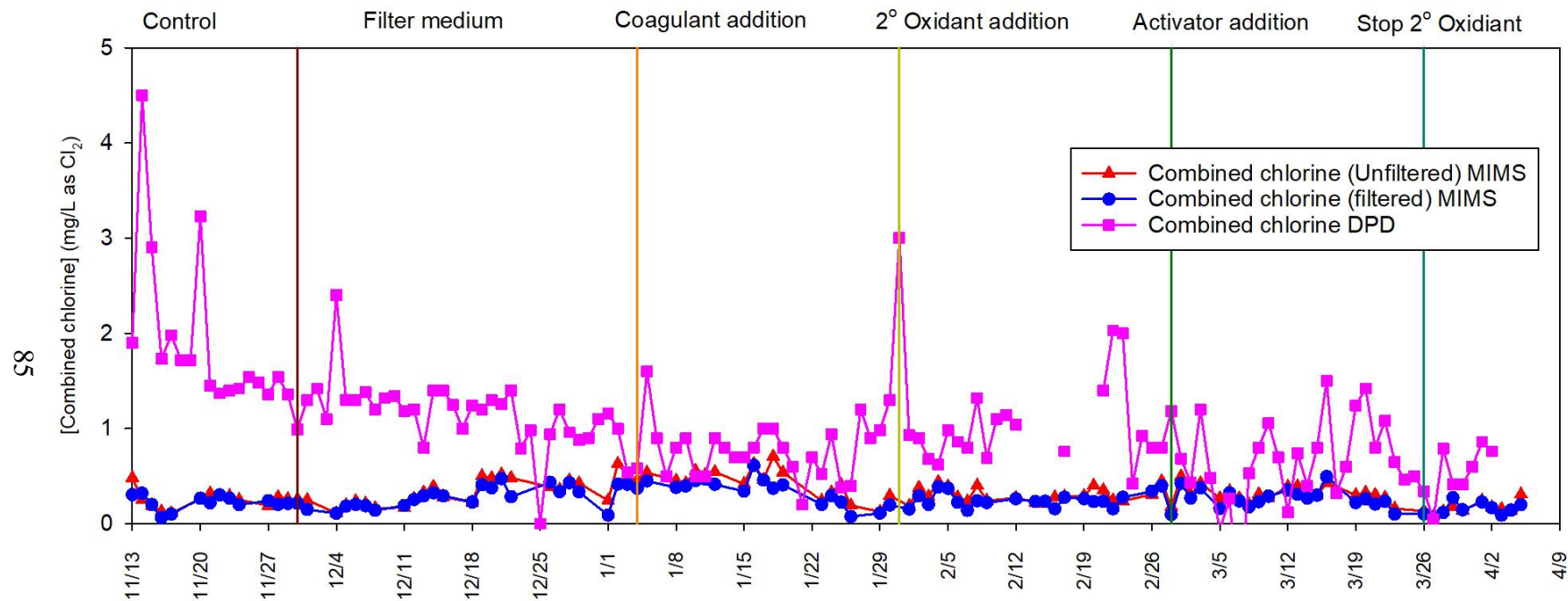


Figure 4.7. Combined chlorine measured by MIMS and DPD. The red triangles represent combined chlorine measured by MIMS collected at the pool. The blue circles represent combined chlorine measured by MIMS collected after filtration. The pink squares represent combined chlorine measured by DPD collected at the pool.

Chloroform (CHCl_3) is often the dominant compound in chlorinated water samples from the trihalomethane (THM) group. The US EPA has established a maximum contaminant level (MCL) of 80 ppb ($\mu\text{g/L}$) for the total THM (TTHM) in treated drinking water (U.S EPA, 2009b). Among exposure pathways, inhalation and dermal absorption/contact are believed to be more important than ingestion for THMs in swimming pools (Gordon et al., 2006; Nuckols et al., 2005; Whitaker et al., 2003). Weaver et al. (2009) reported that chloroform concentrations in several chlorinated pools that ranged from 16.3 to 138 $\mu\text{g/L}$.

The concentration of CHCl_3 was generally consistent until the application of activator, after which a substantial reduction of CHCl_3 concentration was observed (see Figure 4.8). However, CHCl_3 concentration increased after 3/9/2018 when the secondary oxidizer pump was adjusted to reduce the feeding rate; a similar trend was observed with the concentration of NCl_3 during this period. The mechanism of CHCl_3 reduction is still unclear but probably is linked to reduction in the concentration of CHCl_3 precursors caused by reactions with the secondary oxidants and the activator.

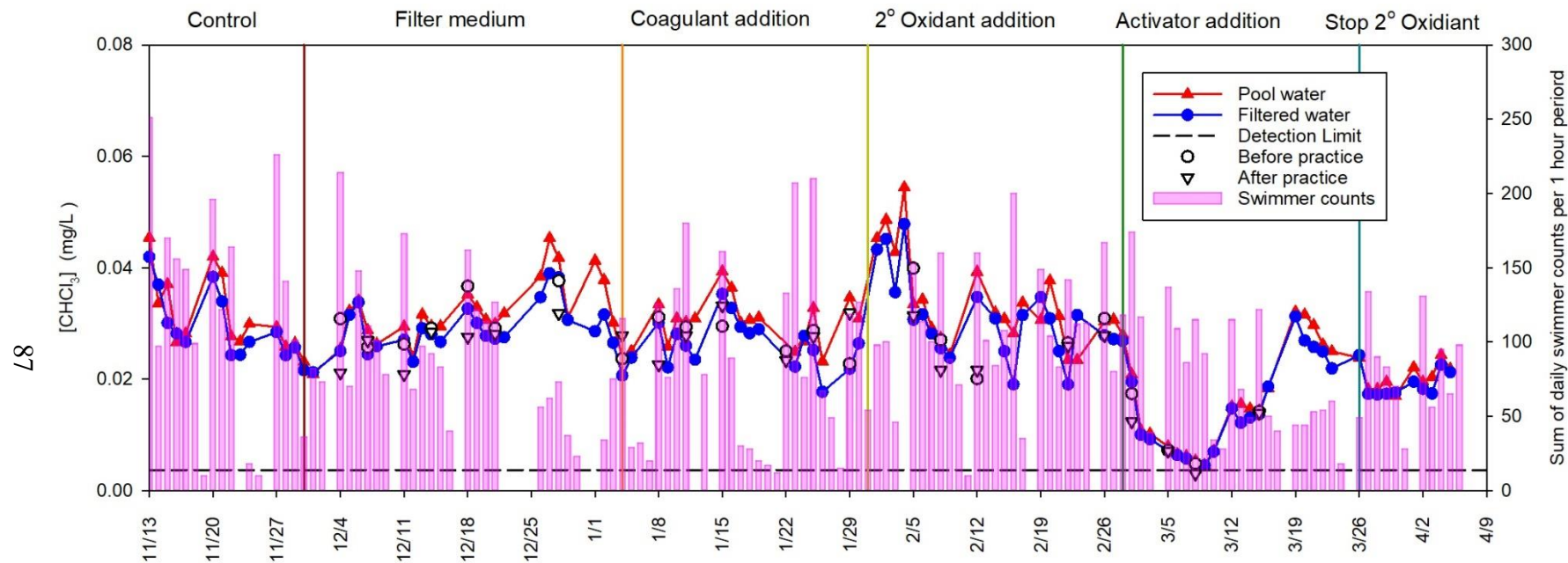


Figure 4.8. Time-course monitoring of CHCl_3 at pool A measured by MIMS. Red triangle symbols represent water samples collected from the pool. Blue circle symbols represent water samples collected after filtration. The black dashed line represents the detection limit. Empty circle symbols represent measurements before swimming practices. Empty triangle symbols represent measurements after swimming practices. Pink vertical bars represent swimmer counts.

Previous studies have shown that CNCl and free chlorine in water samples tend to be negatively correlated (Na and Olson, 2004; Weaver et al., 2009; Zare Afifi and Blatchley, 2016) that is to say, maintaining high free residual chlorine can be used to limit the concentration of CNCl because free chlorine plays a critical role in the decay of CNCl; specifically, the hypochlorite ion is believed to catalyze the oxidation of CNCl to cyanate (Na and Olson, 2004). However, it is important to recognize that chlorine is also critical for the formation of CNCl from reactions with amino acids and uric acid (Li and Blatchley III, 2007; Lian et al., 2014). At a free chlorine concentration of 0.5 mg/L (as Cl_2) at 25°C and pH=7, the half-life of CNCl in water has been reported to be roughly 60 minutes (Na and Olson, 2004). Weaver et al. (2009) measured CNCl in several public swimming pool water samples and the concentrations ranged from below detection limit to 194 $\mu\text{g/L}$.

Time-course monitoring of CNCl is shown in Figure 4.9. The CNCl concentrations in filtered water were relatively consistent and low during the study period. However, substantial variation and higher concentrations of CNCl were observed in the pool water samples. It is hypothesized that oxidation of CNCl occurred during the time spent by water in the recirculation line where the residual free chlorine concentration would be relatively high; however, CNCl reformation occurred in the pool. Substantial reduction of CNCl concentration in the pool was observed after the addition of secondary oxidizers, and the concentrations of CNCl in pool and filtered water samples were almost equal after that time.

The concentration of CNCl after swimming practice was typically about twice as high as the concentration in a water sample collected before practice. Swimmer impact on CNCl concentration in pool water was obvious until the addition of activator. This behavior reinforced the relatively rapid rates of CNCl formation and decay, as well as the importance of the activator for decomposition of precursors or DBPs, as similar trends were observed on NCl_3 and CHCl_3 in the pool.

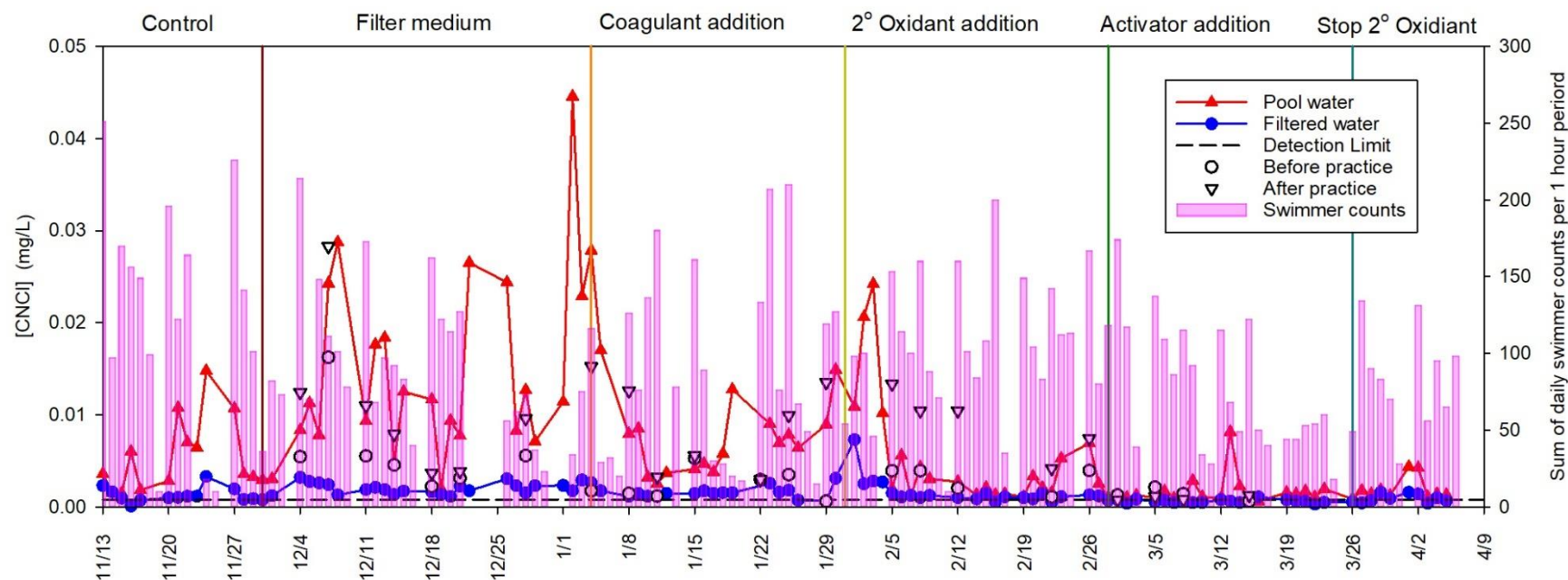


Figure 4.9. Time-course monitoring of CNCl at pool A measured by MIMS. Red triangle symbols represent water samples collected from the pool. Blue circle symbols represent water samples collected after filtration. The black dashed line represents the detection limit. Empty circle symbols represent measurements before swimming practices. Empty triangle symbols represent measurements after swimming practices. Pink vertical bars represent swimmer counts.

Dichloroacetonitrile (CNCHCl_2) is a haloacetonitrile (HAN) compound. It is known that HANs generally present higher genotoxicity and cytotoxicity than THMs (Plewa et al., 2011). CNCHCl_2 can act as an irritant to the skin and the respiratory system and it is a possible mutagenic compound (Osgood and Sterling, 1991). Time-course monitoring of CNCHCl_2 is illustrated in Figure 4.10. Concentrations of CNCHCl_2 were stable until the use of secondary oxidizers; further reduction was evident after the addition of the activator, after which the CNCHCl_2 concentration was reduced to below the limit of detection (0.002 mg/L). The relationship of the activator to the concentration of CNCHCl_2 is undefined at this time and will require further study. In addition, no clear effect of swimmers was evident on CNCHCl_2 concentrations, as the concentration of CNCHCl_2 was not always higher after the swimming practice. However, it is generally understood that the reactions that are responsible for formation and decay of CNCHCl_2 tend to be slower than those that are responsible for CNCl formation (Reckhow et al., 2001).

Dichloromethylamine (CH_3NCl_2) belongs to organic chloramine group. The toxicity of CH_3NCl_2 remains undefined, but it produces an odor like NCl_3 . Currently, there are no regulatory standards for CH_3NCl_2 in swimming pools or drinking water. Weaver et al. (2009) measured CH_3NCl_2 in several public swimming pool water samples and the concentrations ranged from below detection limit to 51.0 $\mu\text{g/L}$.

Time-course monitoring of CH_3NCl_2 is illustrated in Figure 4.11. The concentration of CH_3NCl_2 was consistent until the addition of the activator, after which a sharp increase in CH_3NCl_2 concentration was observed, followed by a period of steady decay of CH_3NCl_2 concentration. The mechanism responsible for this behavior has not been defined.

Previous research has indicated that CH_3NCl_2 formation is favored under high pH conditions (Li and Blatchley III, 2007). It is possible that the use of activator coupled with a relatively high pH condition (Figure 4.2) may have contributed to the behavior of CH_3NCl_2 as an intermediate in the pool. The concentrations of CH_3NCl_2 were essentially identical between filtered and pool water samples. This suggests that the rates of formation and decay of this compound were relatively slow. Also, swimmer impact did not affect CH_3NCl_2 concentrations in the pool.

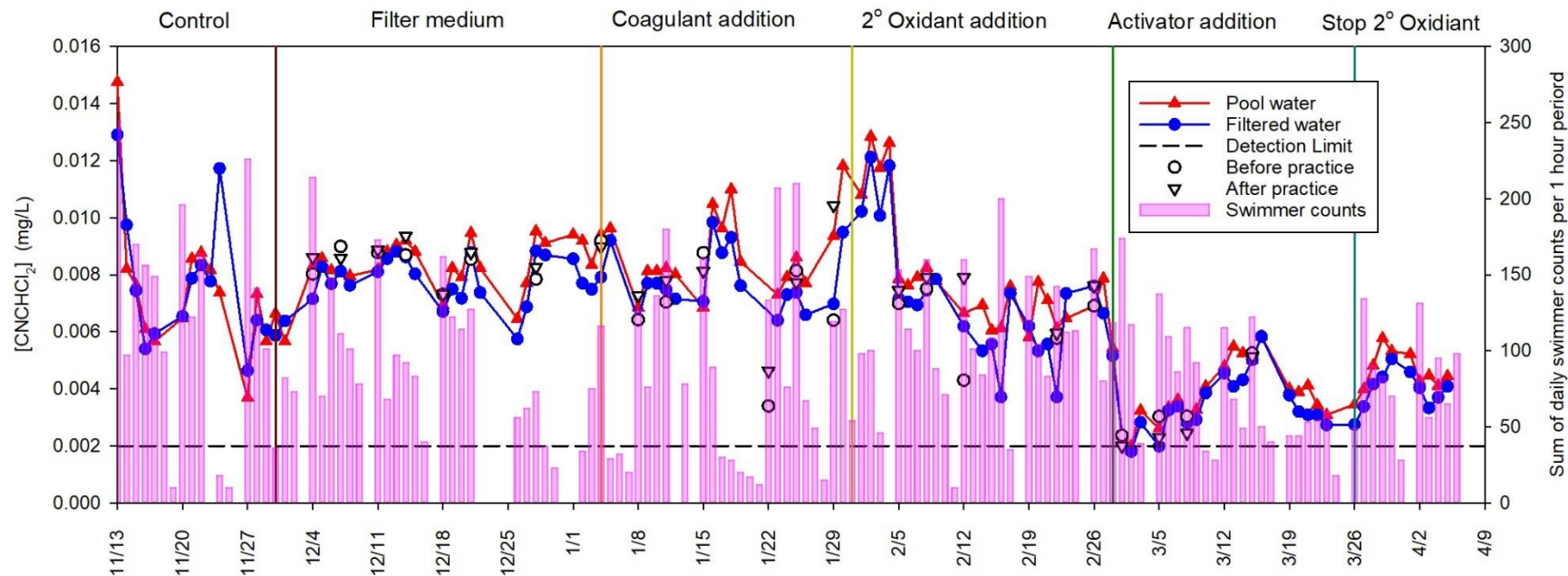


Figure 4.10. Time-course monitoring of CNCHCl_2 at pool A measured by MIMS. Red triangle symbols represent water samples collected from the pool. Blue circle symbols represent water samples collected after filtration. The black dashed line represents the detection limit. Empty circle symbols represent measurements before swimming practices. Empty triangle symbols represent measurements after swimming practices. Pink vertical bars represent swimmer counts.

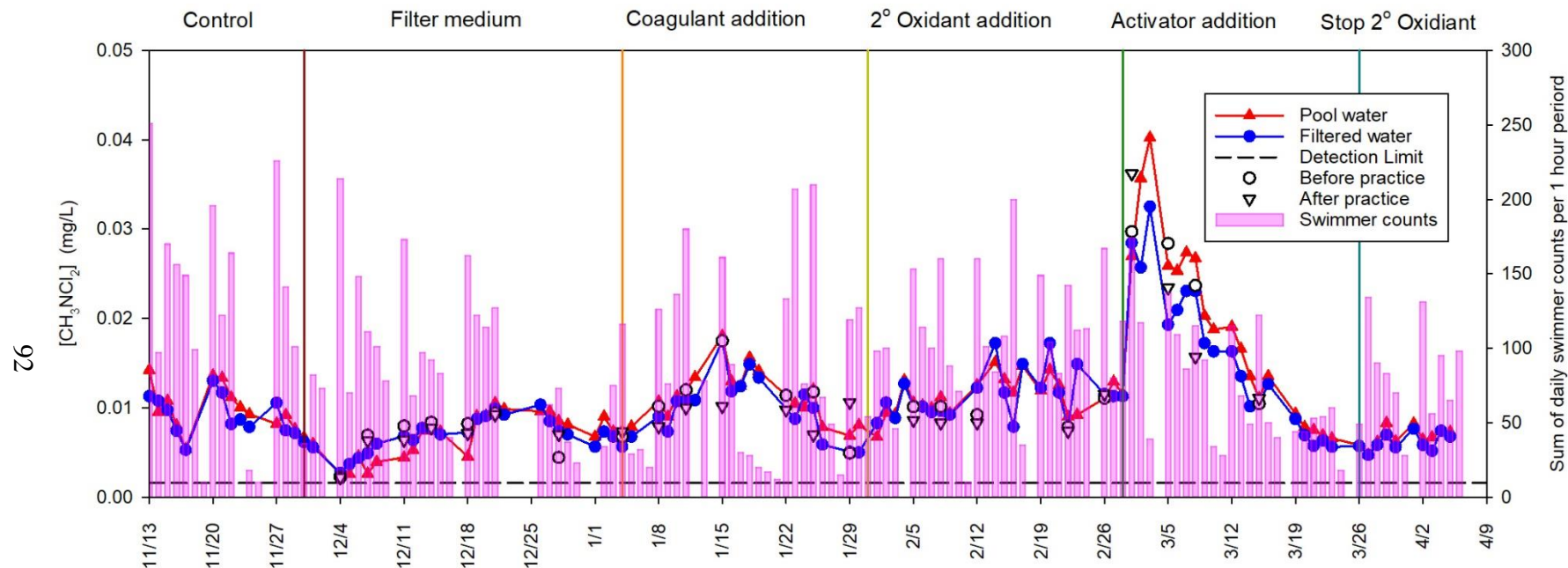


Figure 4.11. Time-course monitoring of CH_3NCl_2 at pool A measured by MIMS. Red triangle symbols represent water samples collected from the pool. Blue circle symbols represent water samples collected after filtration. The black dashed line represents the detection limit. Empty circle symbols represent measurements before swimming practices. Empty triangle symbols represent measurements after swimming practices. Pink vertical bars represent swimmer counts.

4.1.4 Trend of Urea

Urea is the dominant organic-N compound in human urine and sweat by mass. Also, urea is a component of “natural moisturizing factor,” a group of chemicals that is produced in skin tissues to maintain skin moisture (Erdinger et al., 1997; Gunkel and Jessen, 1986). A large fraction of NCl_3 in swimming pool water is assumed to be attributable to the reactions of free chlorine and urea (Hansen et al., 2012; Schmalz et al., 2011). Urea has been considered as an effective precursor to NCl_3 formation, although the reaction of urea with free chlorine is slow (Blatchley and Cheng, 2010). De Laat et al. (2011) reported the urea concentration in swimming pools to range from 0.12 - 3.6 mg/L. Weng and Blatchley (2011) reported urea concentration to range from 0.07 - 0.15 mg/L in an indoor swimming pool under conditions of heavy use. It is known that urea concentrations are related to the bather load in the swimming pool, as well as water replacement practices. Large numbers of swimmers and slow water replacement rates generally correspond with high urea concentration (Weng and Blatchley, 2011).

Time-course monitoring of urea concentration is summarized in Figure 4.12. Overall, urea concentrations in filtered water samples were slightly lower than pool water samples; the reasons for this behavior are not entirely clear. A regular, weekly pattern emerged wherein the urea concentration was generally lowest on Monday and gradually increased through the remainder of the week. Since urea is slow to react with chlorine, this behavior suggested that urea was slowly accumulating during periods of heavy pool use (weekdays), but degraded over the weekend when the pool was used only sparingly. The fact that the concentration of urea in water samples collected after practice was consistently higher than the concentration in samples collected at the same location immediately before practice supports this hypothesis.

Urea concentration decreased after the filter media was changed, as shown in Figure 4.12. The lowest concentrations observed during this stage were found during the Christmas and New Year holiday periods, when almost no swimmers used the pool. Urea concentration was not diminished after the addition of secondary oxidizers, but effective urea reductions were observed after the use of activator, when urea concentration was reduced to as low as 0.05 mg/L. However, the chemistry of the activator is still undefined.

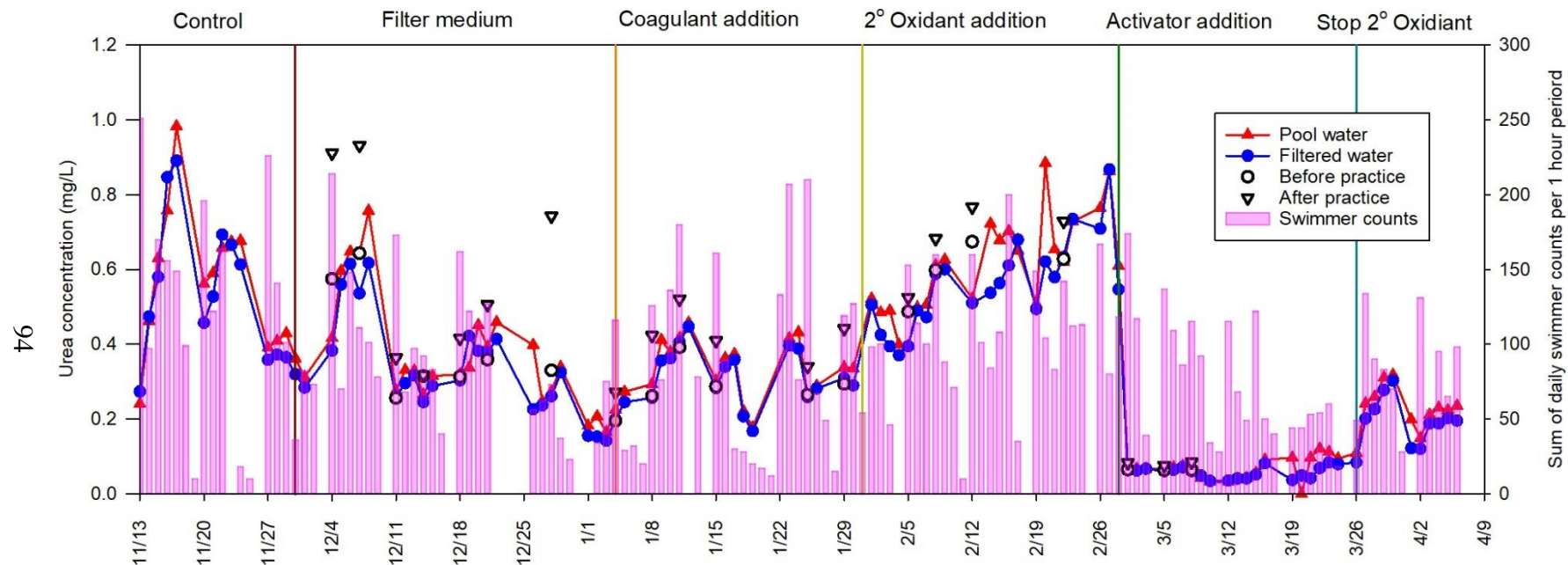


Figure 4.12. Time-course monitoring of urea. Red triangle symbols represent water samples collected from the pool. Blue circle symbols represent water samples collected after filtration. Empty circle symbols represent measurements before swimming practices. Empty triangle symbols represent measurements after swimming practices. Pink vertical bars represent swimmer counts.

4.1.5 Trend of Gas-phase NCl_3

Weekly time-course monitoring of humidity and NCl_3 measured by the air quality monitor are displayed in Figures 4.13 - 4.19. It should be noted that the manufacturer of the air quality monitor indicated that the device will only provide accurate measurements of gas-phase NCl_3 concentration when relative humidity (RH) is within 30-60%. The heating, ventilation, and air conditioning (HVAC) system in the pool facility was unable to maintain consistent humidity for an extended period. The design of the HVAC system in the target pool involved the use of outdoor air to help control the RH in the pool facility. Rapid changes of humidity are often observed in the upper Midwest, especially during cold winter months. The RH constraint of the NEMo device limited access to reliable measurements of gas-phase NCl_3 during the study period to only those times where the RH condition was satisfied.

For the periods in which RH was within the specified range, high gas-phase NCl_3 concentrations were generally observed immediately after a period of heavy bather load (see Figures 4.13, 4.14, and 4.15). When large numbers of swimmers were present in the pool, they enhanced the mixing of near-surface pool water causing highly volatile compounds like NCl_3 to be transported from water to air. The surge of gas-phase NCl_3 concentration was most evident after periods when more than 40 swimmers were in the pool; gas-phase NCl_3 concentrations during these times were as high as 1.2 mg/m^3 . For perspective, an upper limit for gas-phase NCl_3 concentration of 0.5 mg/m^3 was recommended by WHO (WHO, 2006), and 0.3 mg/m^3 as suggested by Bernard et al. (2006). The high concentrations of gas-phase NCl_3 observed in the studied pool could potentially cause health risks for swimmers and pool workers.

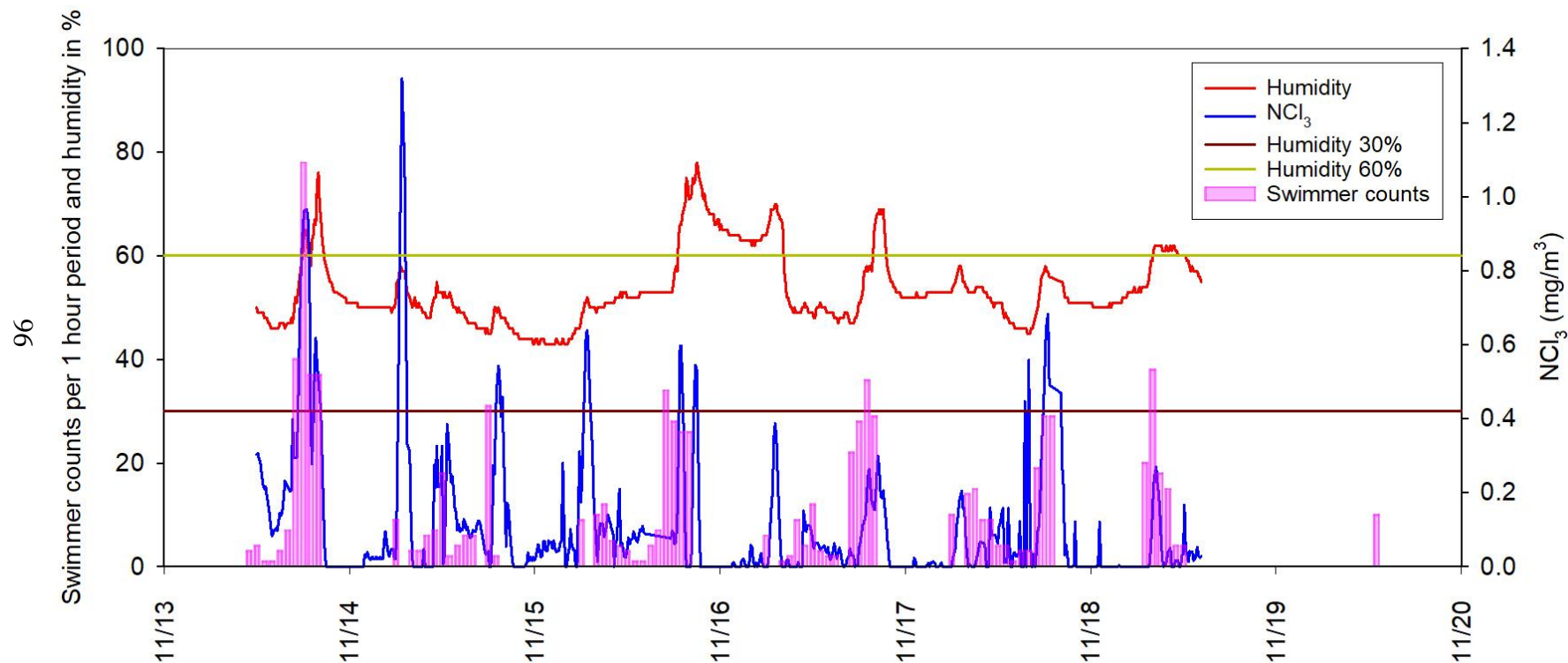


Figure 4.13. Time-course monitoring of air samples from 11/13/2017 to 11/19/2017. Red line represents the relative humidity at the pool facility. Blue line represents the gas-phase NCl₃ collected by NEMo. Two horizontal lines represent relative humidities of 30% and 60%. Pink vertical bars represent swimmer counts.

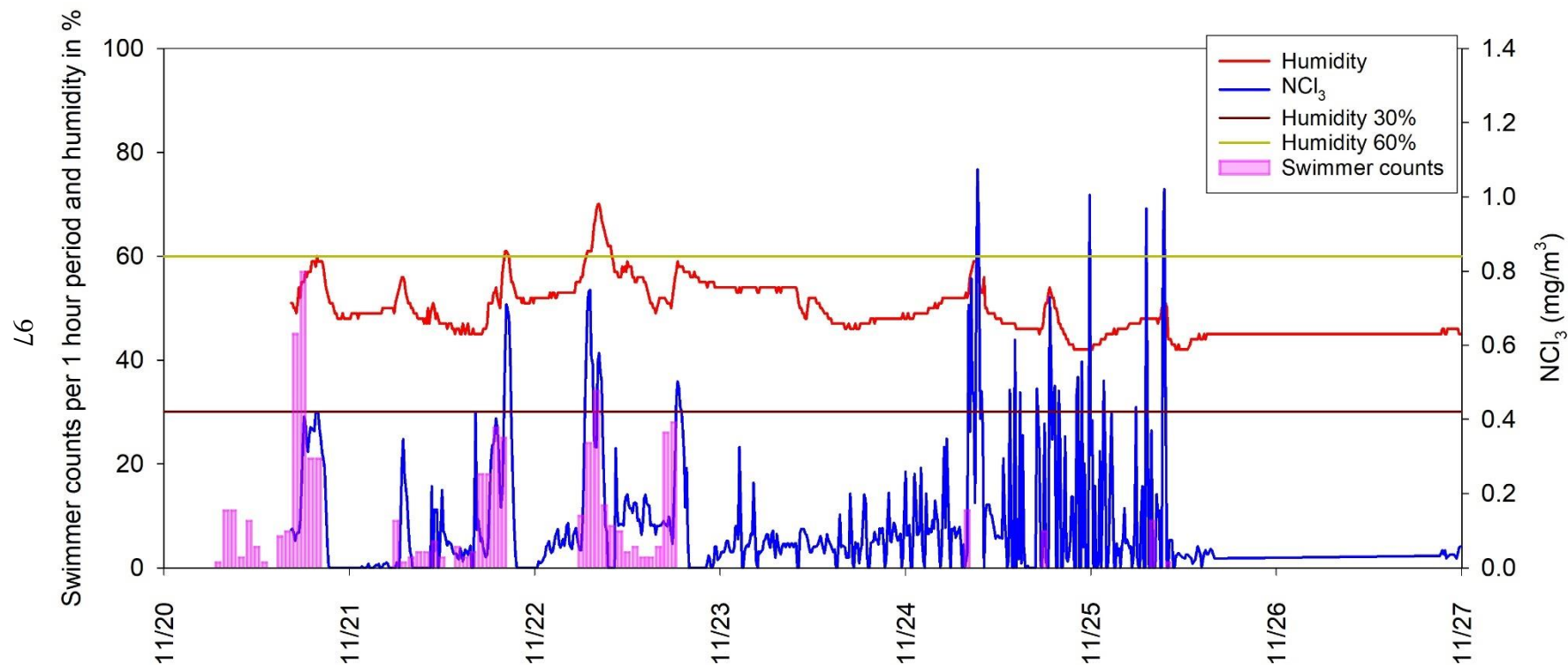


Figure 4.14. Time-course monitoring of air samples from 11/20/2017 to 11/26/2017. Red line represents the relative humidity at the pool facility. Blue line represents the gas-phase NCl₃ collected by NEMo. Two horizontal lines represent relative humidities of 30% and 60%. Pink vertical bars represent swimmer counts.

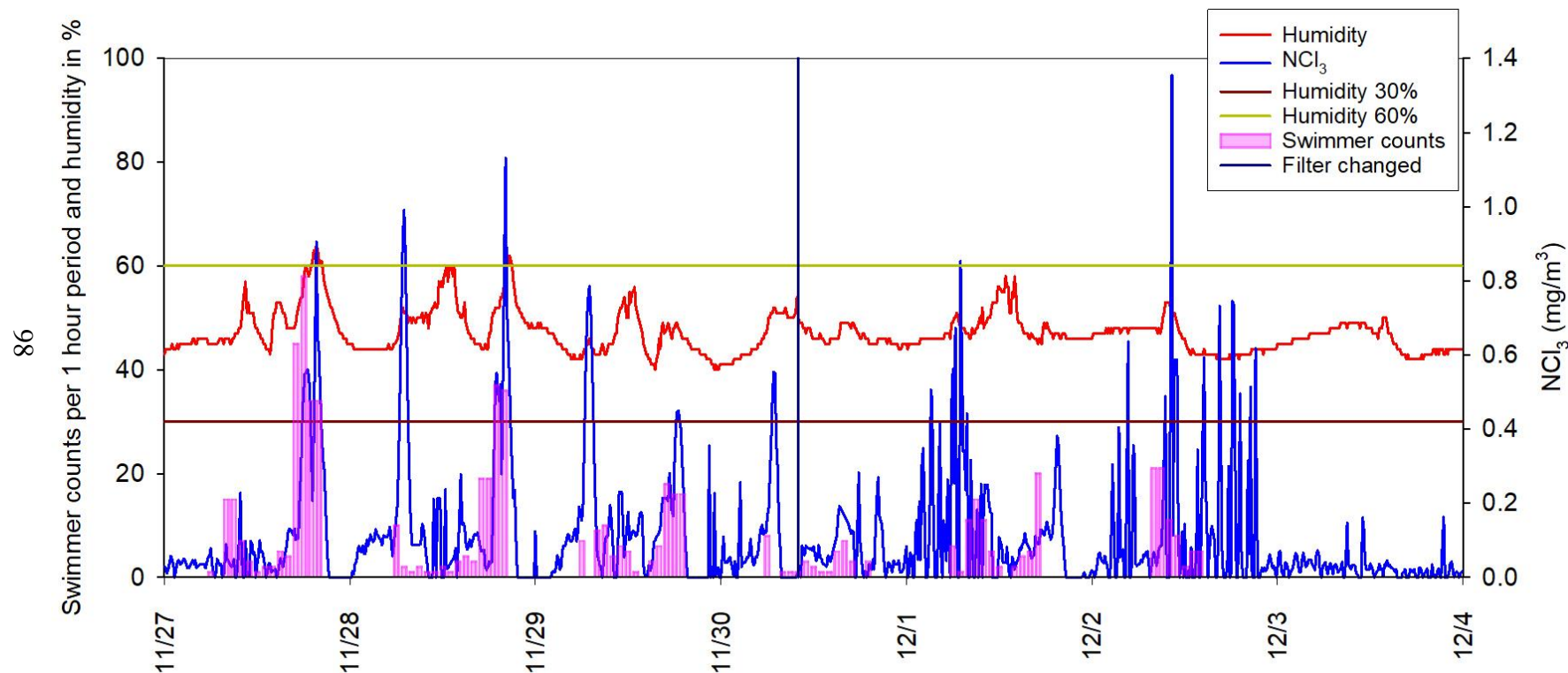


Figure 4.15. Time-course monitoring of air samples from 11/27/2017 to 12/3/2017. Red line represents the relative humidity at the pool facility. Blue line represents the gas-phase NCl₃ collected by NEMo. Two horizontal lines represent relative humidities of 30% and 60%. Pink vertical bars represent swimmer counts. Vertical dark blue line represents the date of a filter media change.

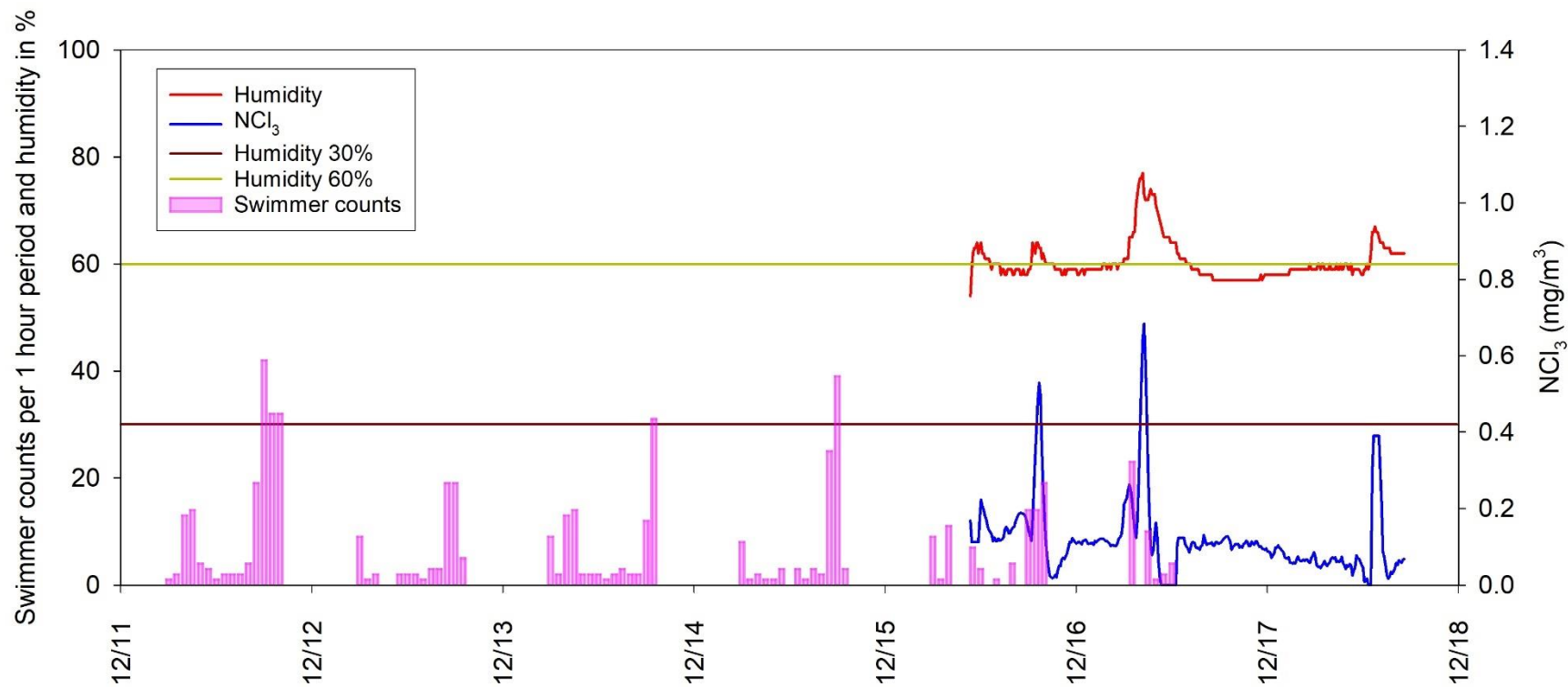


Figure 4.16. Time-course monitoring of air samples 12/11/2017 to 12/17/2017. Red line represents the relative humidity at the pool facility. Blue line represents the gas-phase NCl₃ collected by NEMo. Two horizontal lines represent relative humidities of 30% and 60%. Pink vertical bars represent swimmer counts.

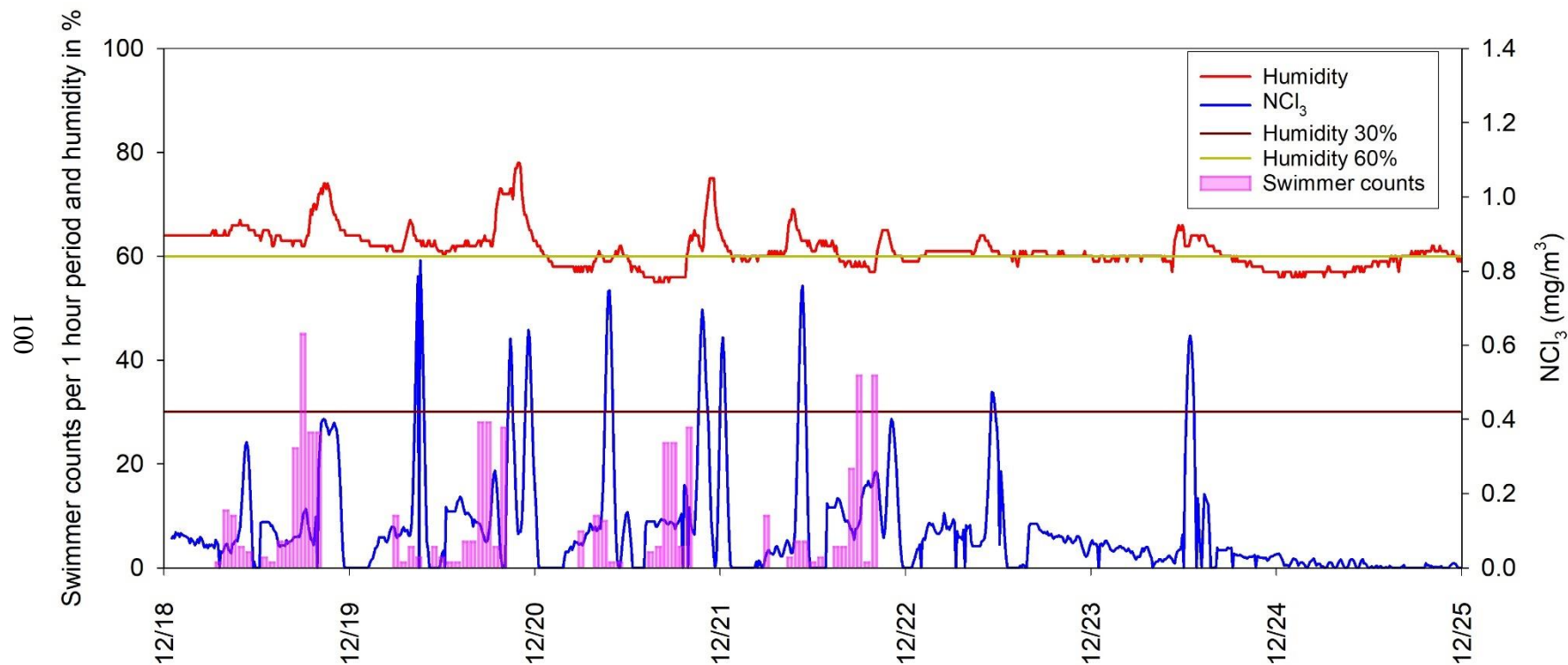


Figure 4.17. Time-course monitoring of air samples from 12/18/2017 to 12/24/2017. Red line represents the relative humidity at the pool facility. Blue line represents the gas-phase NCl_3 collected by NEMo. Two horizontal lines represent relative humidities of 30% and 60%. Pink vertical bars represent swimmer counts.

Pink vertical bars represent swimmer counts.

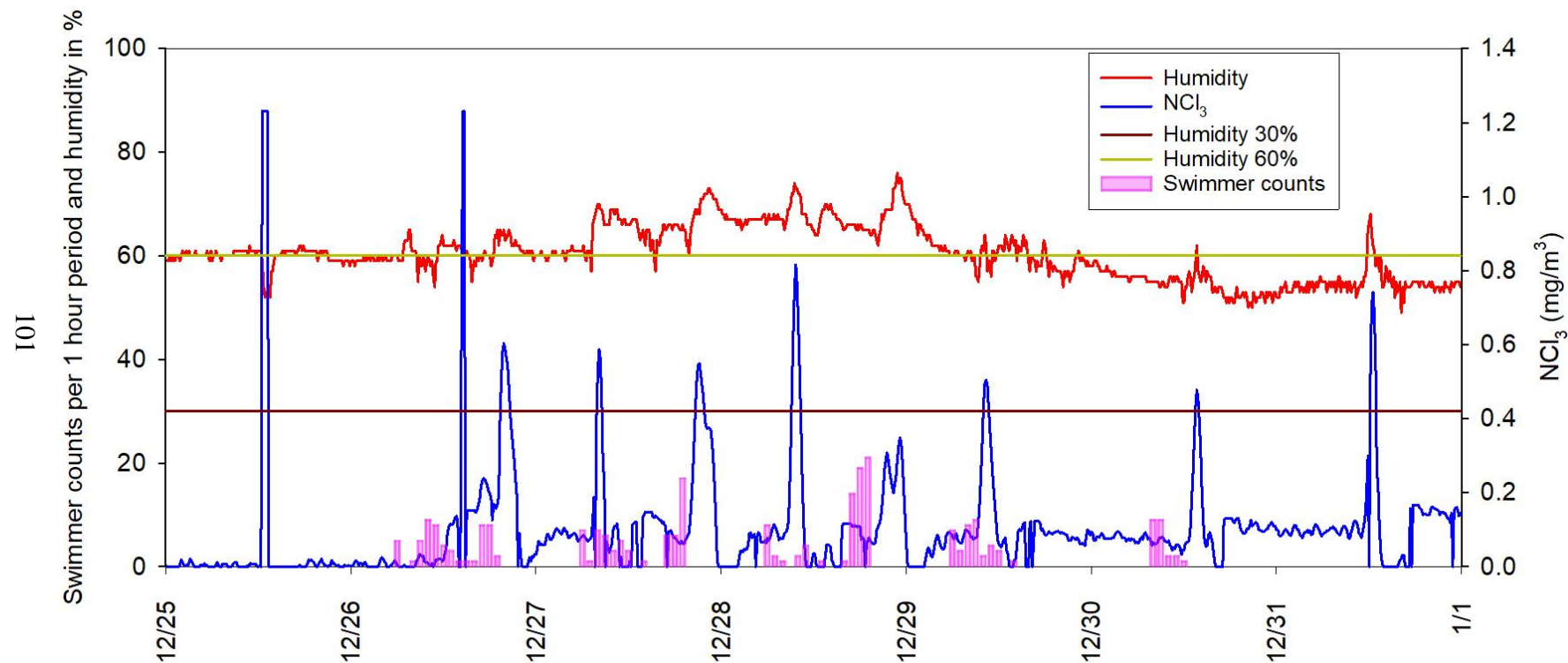


Figure 4.18. Time-course monitoring of air samples from 12/25/2017 to 12/31/2017. Red line represents the relative humidity at the pool facility. Blue line represents the gas-phase NCl₃ collected by NEMo. Two horizontal lines represent relative humidities of 30% and 60%. Pink vertical bars represent swimmer counts.

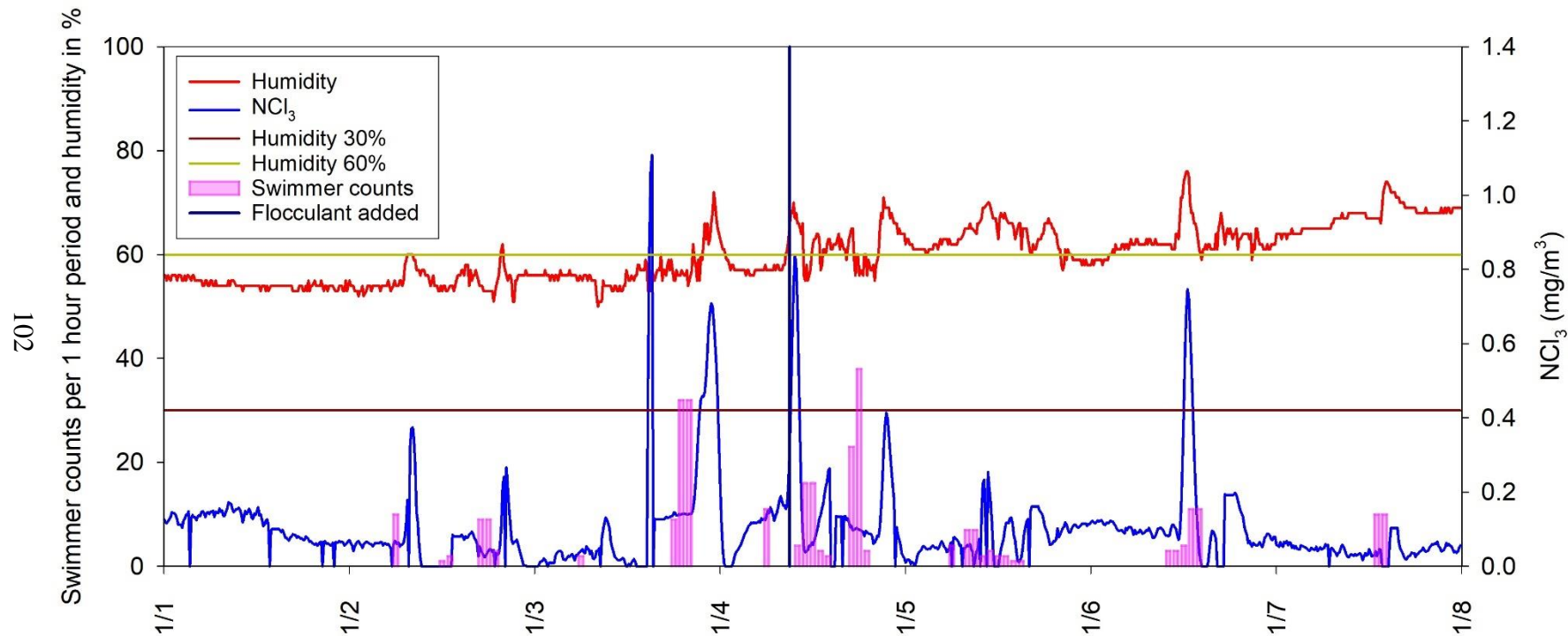


Figure 4.19. Time-course monitoring of air samples from 1/1/2018 to 1/7/2018. Red line represents the relative humidity at the pool facility. Blue line represents the gas-phase NCl_3 collected by NEMo. Two horizontal lines represent relative humidities of 30% and 60%. Pink vertical bars represent swimmer counts.

4.2 Summary and conclusions

After application of secondary oxidizers, reductions of free chlorine and total chlorine in the swimming pool water were observed. CNCl concentration was reduced substantially after addition of the oxidizers. The concentrations of NCl_3 , CHCl_3 , and CNCHCl_2 also declined after introduction of the secondary oxidizers. The degradation of these compounds apparently depended on the presence of the secondary oxidant, as increases of the concentrations of these DBPs were seen once the secondary oxidant feed rate was reduced. The addition of the activator also resulted in small reductions of the concentrations of several volatile DBPs including NCl_3 , CNCl, and CNCHCl_2 . The introduction of the activator in the pool also diminished the concentration of urea. Secondary oxidizers coupled with the activator could be an effective treatment process to limit the accumulation of DBPs and their precursors in swimming pools.

There was clear evidence that swimmer's activity could impact the concentrations of gas-phase NCl_3 . Also, NEMo could be a reliable air quality monitor when relative humidity is within 30% to 60%. NEMo devices had been applied constantly during the phase 2 study.

5. PHASE 2

Time-course measurements of volatile DBPs and urea in water samples from eight experiment periods at four different swimming pool facilities located at Indiana and Michigan are present in this chapter. In addition, the results of time-course monitoring of air quality parameters including concentrations of gas-phase NCl_3 and gas-phase CO_2 are displayed in this chapter. The numbers of swimmers in the pools were recorded throughout the experiment periods. Trends of volatile DBPs and urea concentrations during the experiment periods were investigated.

5.1 Measurements at Pool facility B

5.1.1 Measurements in February 2019

Measurements were conducted during a swimming meet at pool facility B that was held in February 2019. The meet started Friday (2/1/2019) afternoon and lasted until Sunday (2/3/2019) noon. Competition on 2/1/2019 was held from 4:30 pm to 8:30 pm; the early session on 2/2/2019 was held from 8:00 am to 1:00 pm and a second session was held from 4:30 pm to 8:30 pm. The session on 2/3/2019 was held from 7:30 am to 2:30 pm. This swimming meet was for 14 and under boys and girls, with approximately 250 swimmers participating. Water samples were collected from the pool when the meet started and continued at a regular interval until the facility closed each day from 2/1/2019 to 2/5/2019. In addition to the competition, the facility was used by citizen lap swimmers through the period of the meet and afterward. No counts of swimmers were collected during this experiment, but the times of pool use by swimmers in the meet were well-defined by the meet schedule.

Time-course measurements of volatile DBPs and urea in water samples are shown in Figures 5.1-5.8. Inorganic chloramines (NH_2Cl and NCl_3) represented the dominant volatile DBPs in the pool. Concentrations of NH_2Cl reached their highest value at the start of the second day of the meet and gradually decreased afterward. A distinctly different trend was observed for the measurements of liquid-phase NCl_3 , with concentrations starting near the limit of detection at the beginning of the meet, then rising slowly to almost 0.1 mg/L (as Cl_2) within about two days.

Concentrations of CHCl_3 decreased slightly during the study period. Concentrations of CNCl and CNCHCl_2 behaved similarly to each other, in that both decreased gradually throughout the meet. Concentrations of CH_3NCl_2 increased during first two days of the meet then slowly decreased after the meet concluded. Concentrations of urea ranged from 0.15 to 0.3 mg/L. No clear trend was observed for the measurement for urea.

The factors that are likely to contribute the dynamic behavior of DBPs in pools include bather load, reactivity of these compounds, location of sample collection, mixing in the pool, free chlorine concentration, and pH. The increase of inorganic chloramines and CH_3NCl_2 during first two days of the meet may be attributed to the swimmers that introduced DBP precursors to the pool. Free chlorine and pH were not measured, either. Thus, the data from this study does not reveal the impacts of free chlorine and pH on the dynamic behavior of DBPs.

The trends of CHCl_3 , CNCl , and CNCHCl_2 suggest that their rates of their formation were faster than their rates of decay. The trends could also be the result of the mixing in the pool. Swimmers' activity caused the mixing, which then led to the liquid to gas transfer of these compounds.

The trend of urea suggests an effect of swimmers. Also, the fluctuation could be affected by the sample location and mixing in the pool. The water samples were collected at the same sample point throughout the study period. However, the mixing behavior by swimmer and water recirculation could likely influence the measurement of urea.

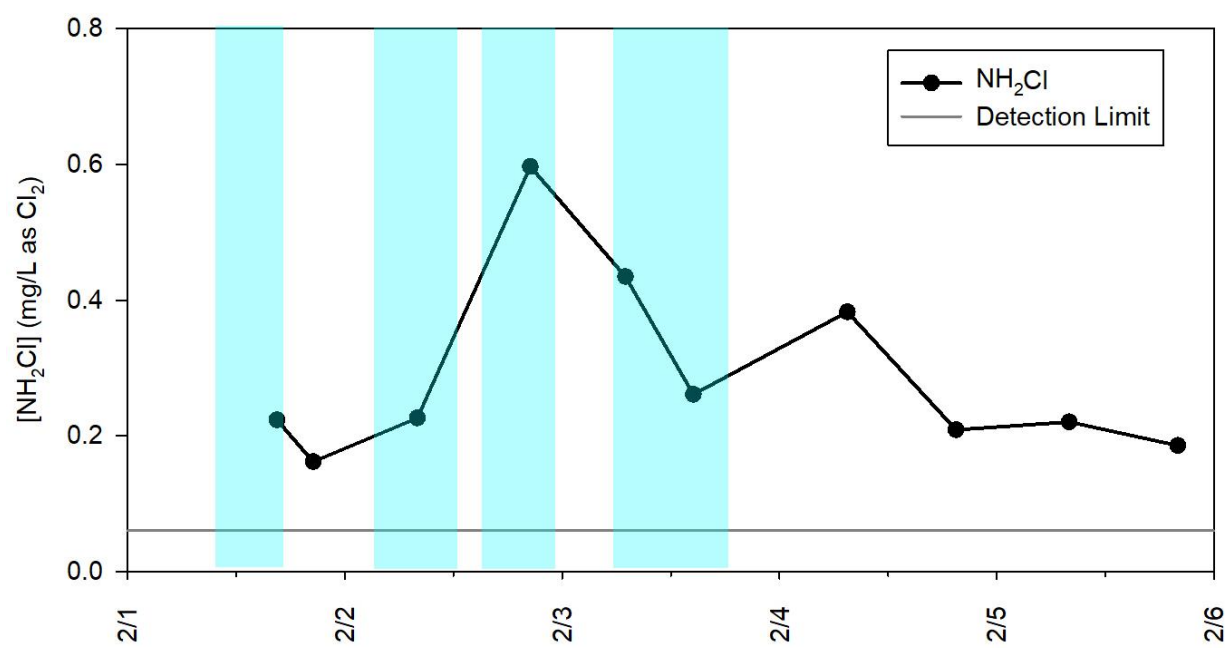


Figure 5.1. Time-course monitoring of NH_2Cl at pool facility B during swimming meet in February 2019. Light blue regions indicate when swimmers were present in the pool. Horizontal line represents the detection limit.

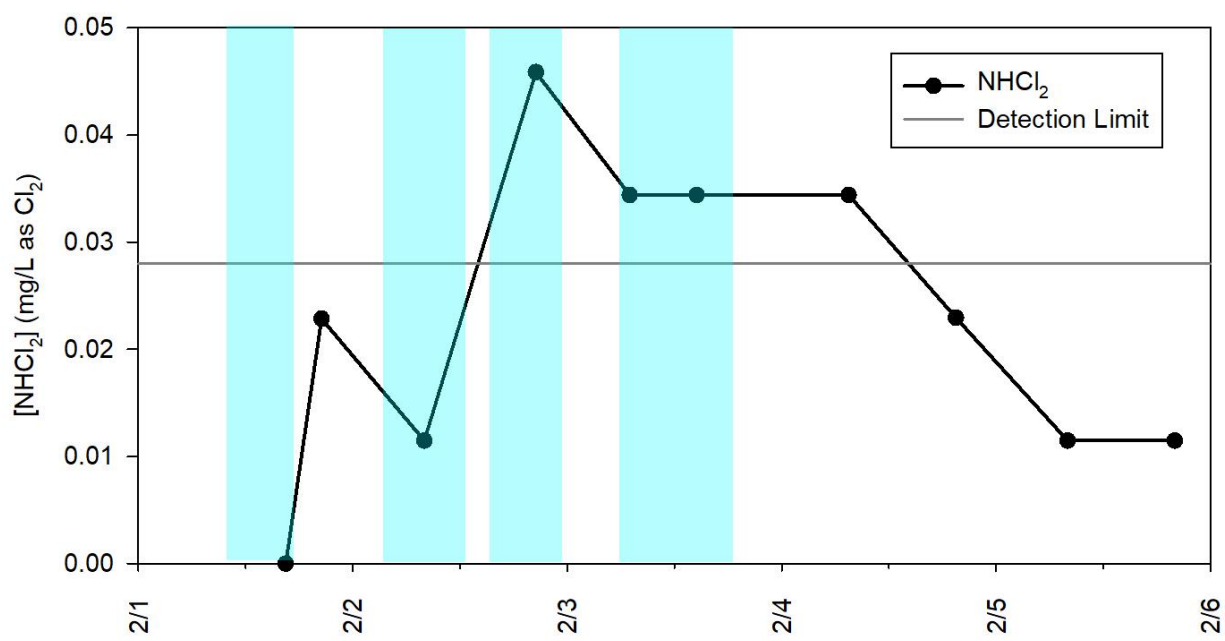


Figure 5.2. Time-course monitoring of NHCl_2 at pool facility B during swimming meet in February 2019. Light blue regions indicate when swimmers were present in the pool. Horizontal line represents the detection limit.

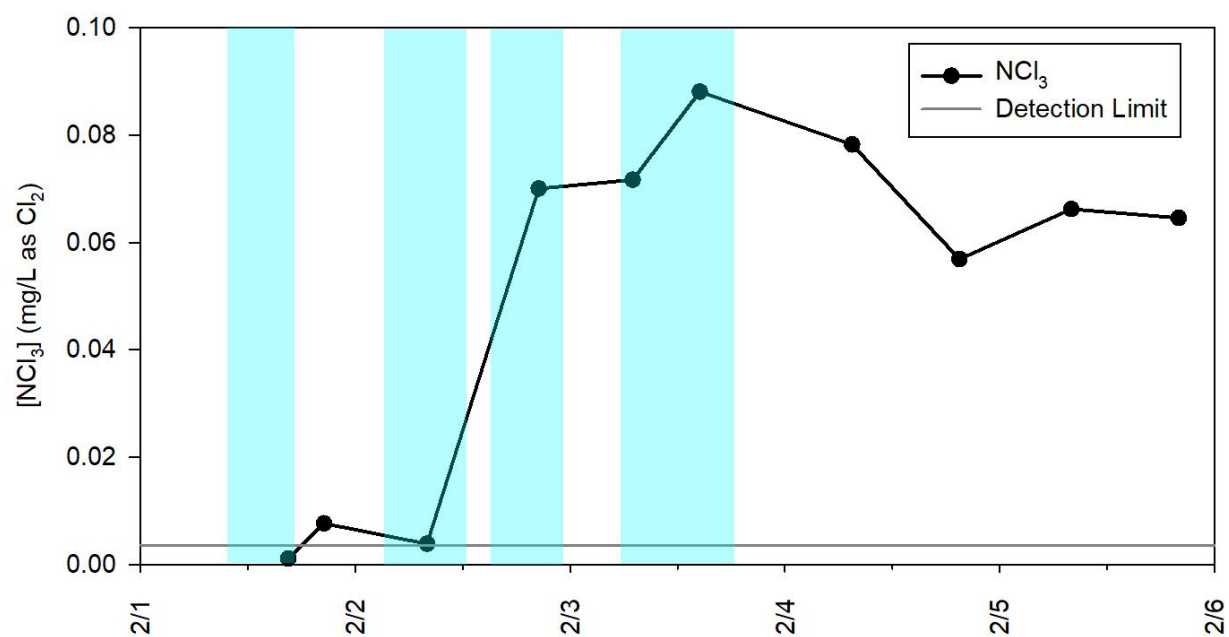


Figure 5.3. Time-course monitoring of NCl_3 at pool facility B during swimming meet in February 2019. Light blue regions indicate when swimmers were present in the pool. Horizontal line represents the detection limit.

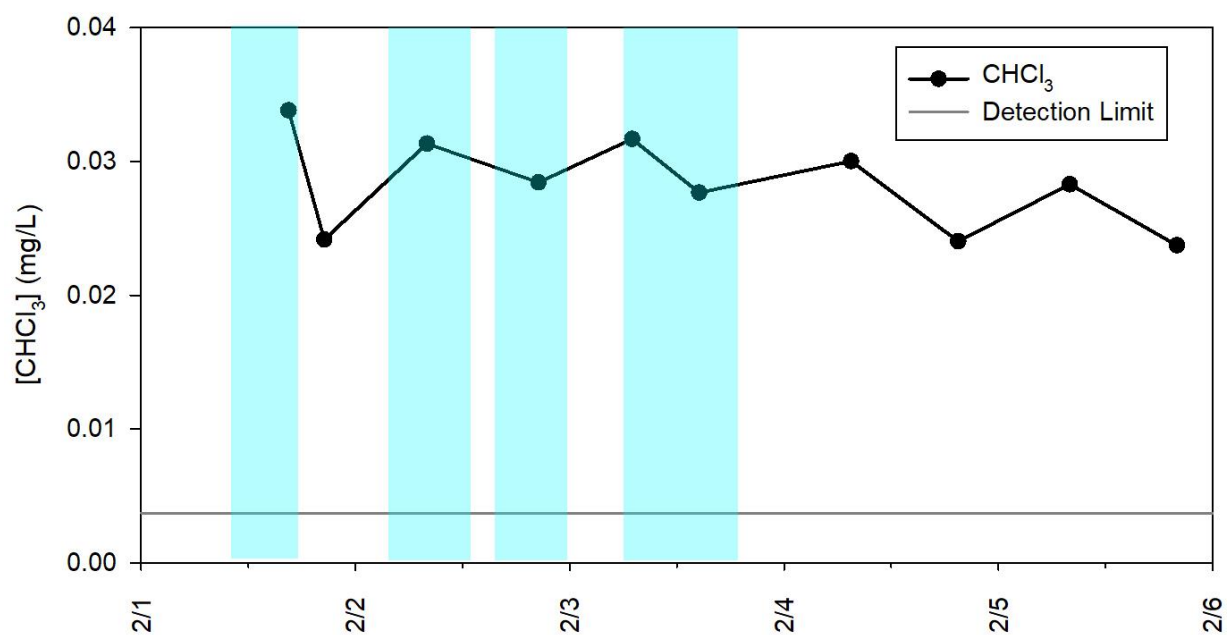


Figure 5.4. Time-course monitoring of CHCl_3 at pool facility B during swimming meet in February 2019. Light blue regions indicate when swimmers were present in the pool. Horizontal line represents the detection limit.

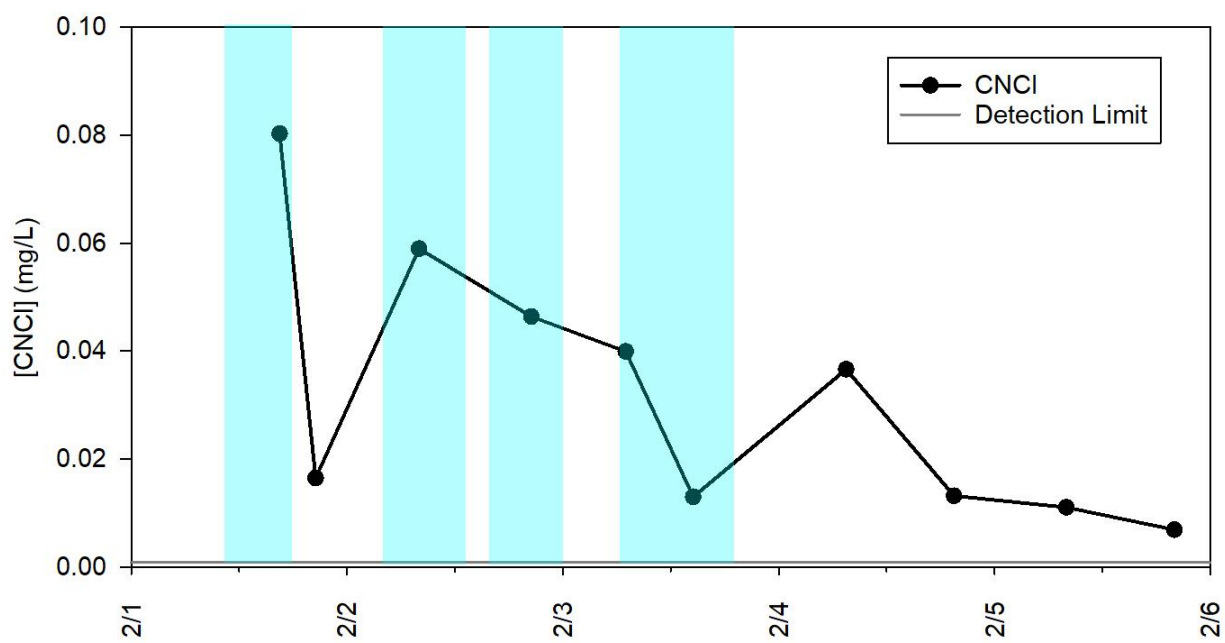


Figure 5.5. Time-course monitoring of CNCl at pool facility B during swimming meet in February 2019. Light blue regions indicate when swimmers were present in the pool. Horizontal line represents the detection limit.

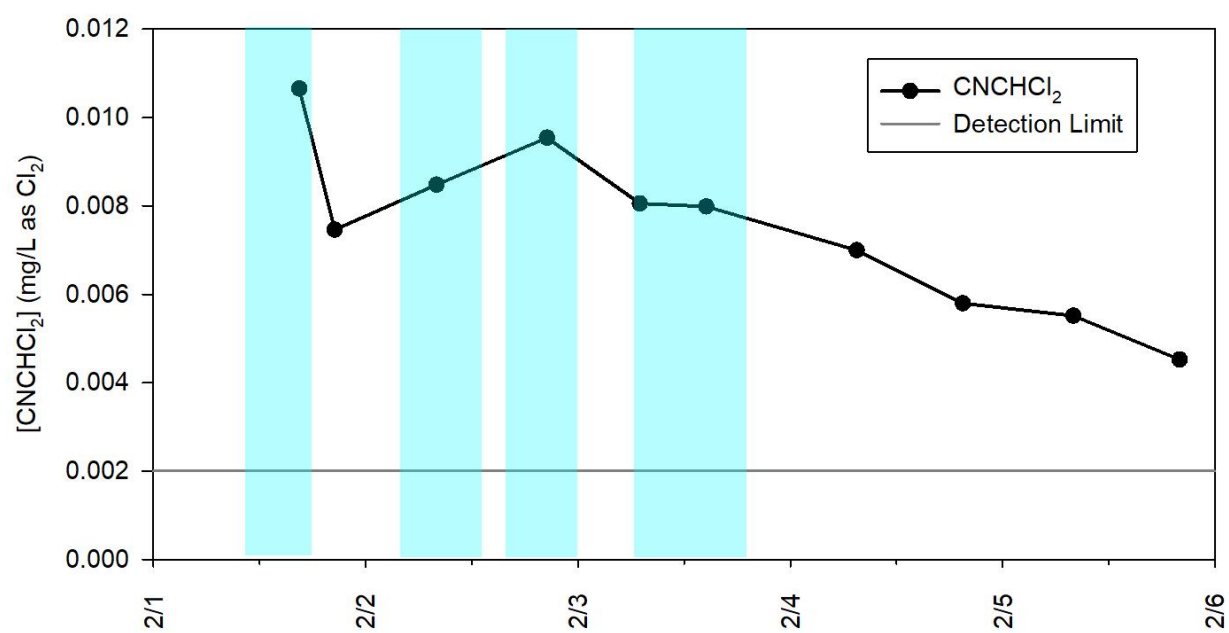


Figure 5.6. Time-course monitoring of CHCHCl_2 at pool facility B during swimming meet in February 2019. Light blue regions indicate when swimmers were present in the pool. Horizontal line represents the detection limit.

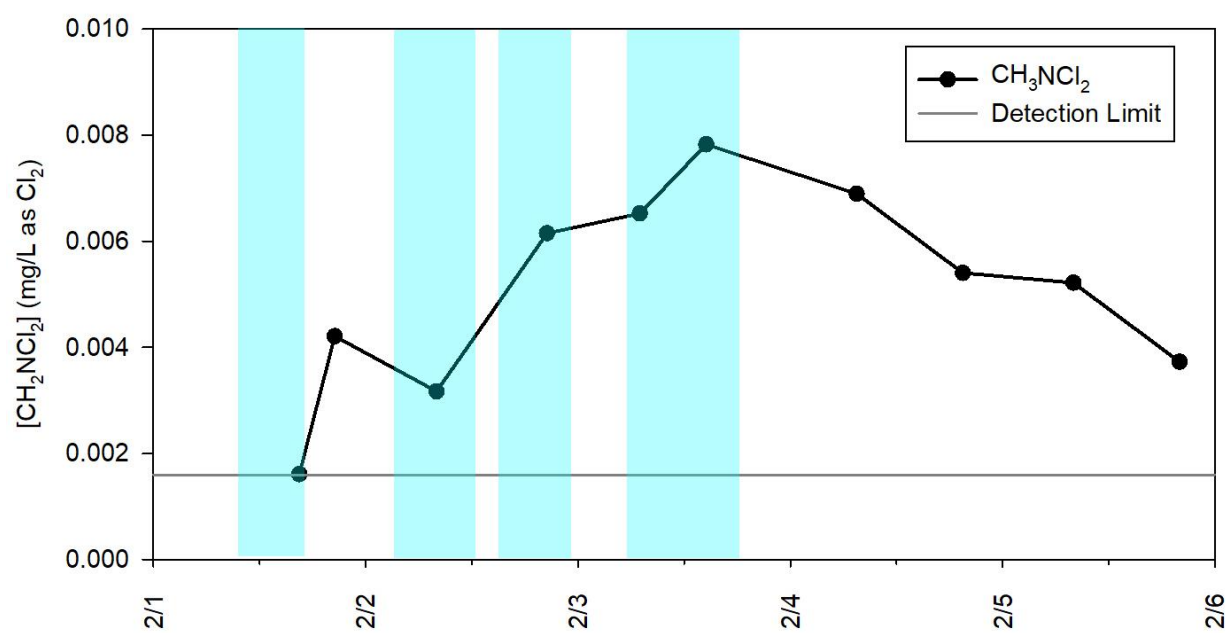


Figure 5.7. Time-course monitoring of CH_3NCl_2 at pool facility B during swimming meet in February 2019. Light blue regions indicate when swimmers were present in the pool. Horizontal line represents the detection limit.

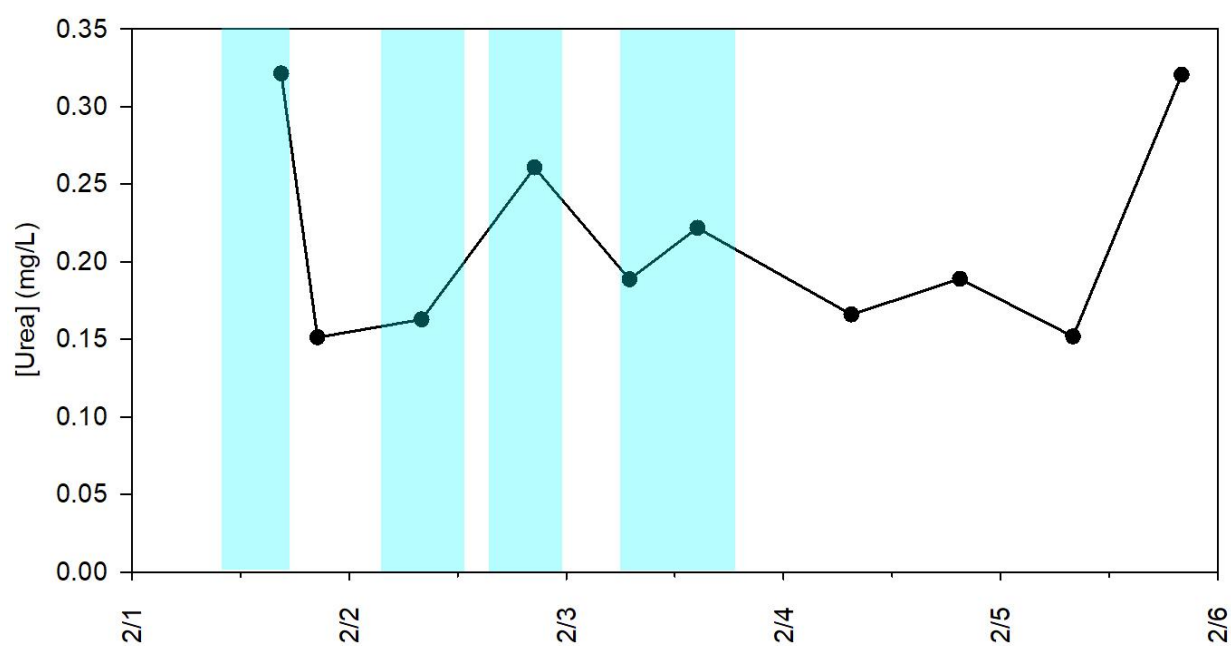


Figure 5.8. Time-course monitoring of urea at pool facility B during swimming meet in February 2019. Light blue region indicates when swimmers were present in the pool.

Time-course monitoring of gas-phase NCl_3 and relative humidity (RH) are illustrated in Figure 5.9. For this experiment, the actual number of swimmers in the pool during this swimming meet was not counted. Therefore, the blue regions in Figure 5.9 were included to indicate when swimmers were present in the pool, based on the schedule of events for the meet. It should be noted that the manufacturer of the air quality monitor has indicated that the device will only provide accurate measurements of gas-phase NCl_3 concentration when RH is within the range 30-60%. As shown in Figure 5.9, RH was within this range for measurements collected by NEMo panels A and B. RH from NEMo panel C indicated several measurements that were above 60%. Generally, the manufacturer of the NEMo devices has indicated that measurements of gas-phase NCl_3 should be viewed as underestimates if RH is higher than 60% and overestimates if RH is lower than 30%. This is because water vapor interferes with the opacity measurement that is the basis of NCl_3 concentration measurements.

High gas-phase NCl_3 concentrations were generally observed at the beginning of each session, especially during warm-up periods, when the number of swimmers in the pool were highest. Gas-phase NCl_3 concentrations reached as high as $700 \mu\text{g}/\text{m}^3$ for all three NEMo devices. For perspective, an upper limit for acceptable gas-phase NCl_3 is $500 \mu\text{g}/\text{m}^3$ as recommended by WHO (WHO, 2006) and $300 \mu\text{g}/\text{m}^3$ as suggested by Bernard et al. (2006). At these concentrations, humans begin to demonstrate adverse respiratory responses to NCl_3 exposure.

Time-course monitoring of gas-phase NCl_3 with gas-phase CO_2 is illustrated in Figure 5.10. Gas-phase CO_2 reached as high as 900 ppm_v for panels A and B during the swimming meet. Readings from panel C indicated CO_2 above 2000 ppm_v, probably because this NEMo device was located close to the SPA that operates adjacent to the diving well in this facility. In general, gas-phase CO_2 concentration is related to several factors, including the number of swimmers, number of people in the audience, and the liquid-phase concentration of CO_2 . The time-course behaviors of CO_2 and NCl_3 appear to be strongly correlated during and after this swimming meet at pool facility B.

Measurements of gas-phase NCl_3 and CO_2 from around the pool facility B also suggested that the air approaches a well-mixed condition, with the possible exception of locations near the spa. The assumption of a well-mixed air space is critical to the development and application of the mass-balance based IAQ model.

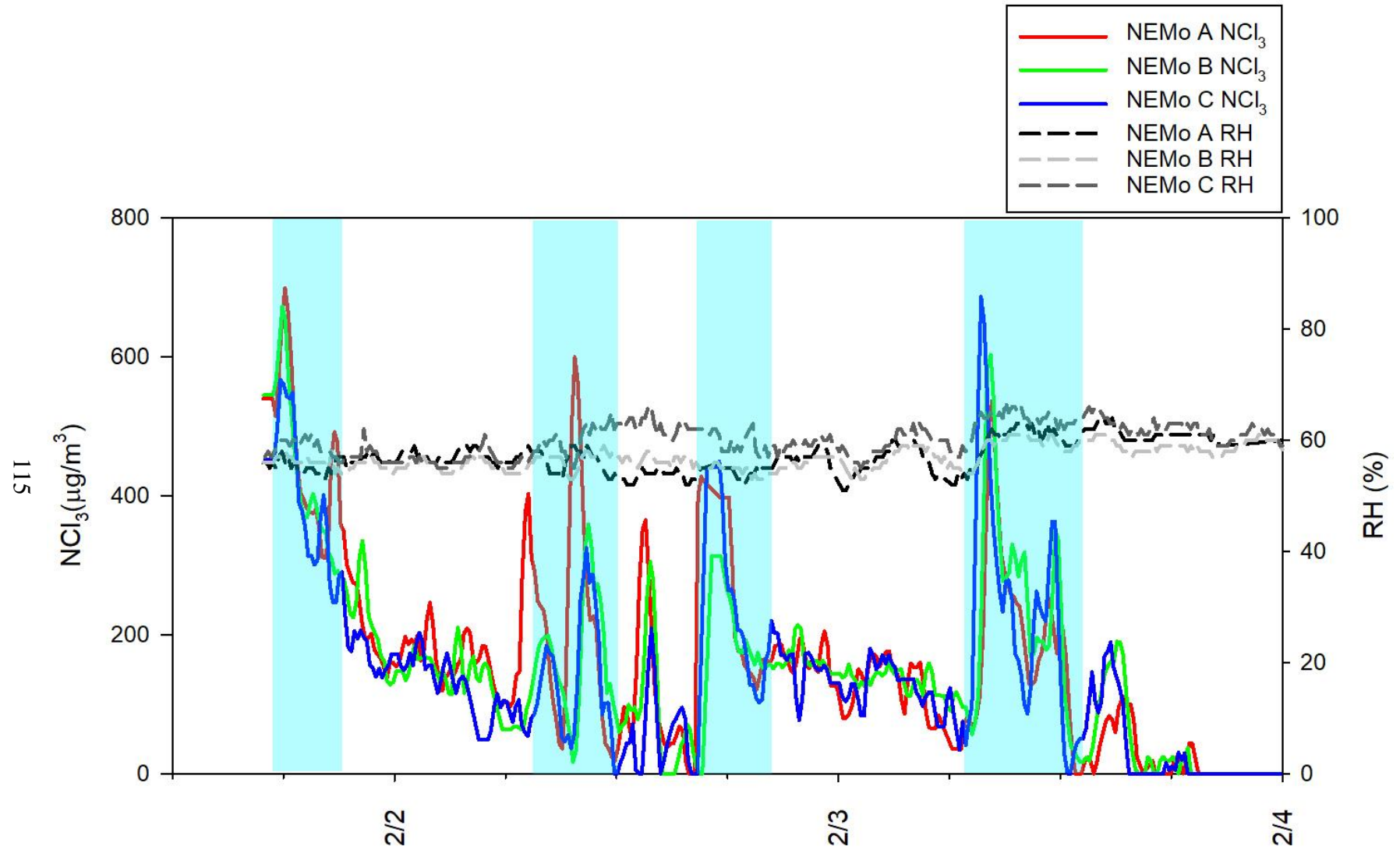


Figure 5.9. Time-course monitoring of gas-phase NCl_3 and RH measured by NEMo devices at pool facility B during swimming meet in February 2019. Blue regions indicate when swimmers were present in the pool.

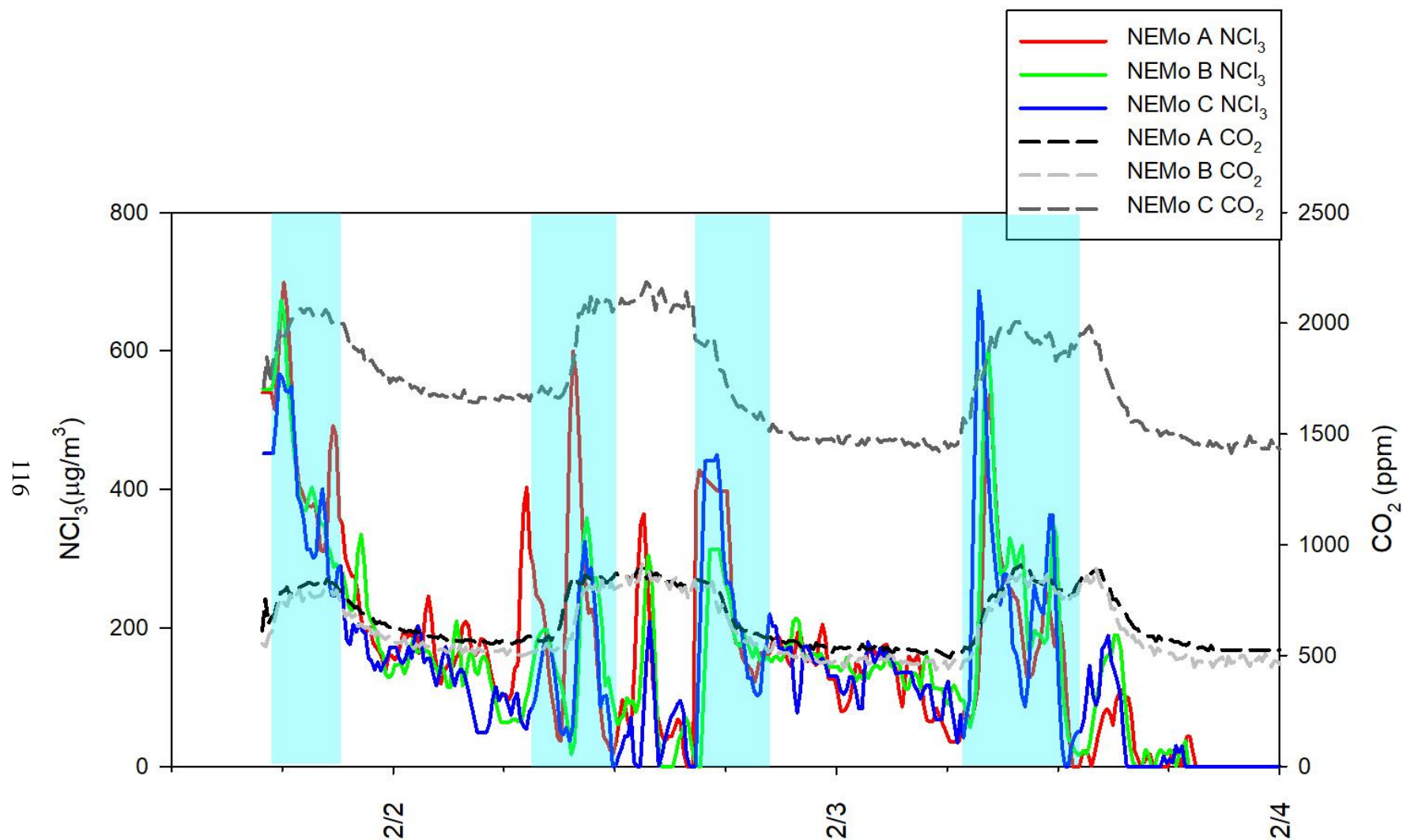


Figure 5.10. Time-course monitoring of gas-phase NCl_3 and gas-phase CO_2 measured by NEMo devices at pool facility B during swimming meet in February 2019. Blue regions indicate when swimmers were present in the pool.

5.1.2 Measurements in March 2019

Measurements were conducted during regular operating hours at pool facility B from 3/6/2019 to 3/8/2019. This experiment was conducted during normal operations of the pool to allow a comparison of the dynamic behavior of volatile DBPs with the swimming meet period. During regular hours, the pool is used by lap swimmers, practice for competition teams, and swimming lessons. The locations of the NEMO devices and water sample collection point are illustrated in Figure 3.9. For this experiment, swimmer count was recorded every hour by lifeguards at the pool.

Trends of free chlorine and total chlorine, as measured by DPD, are presented in Figure 5.11. Combined chlorine (total chlorine-free chlorine) concentrations were consistent throughout the experiment period. The concentrations of combined chlorine were mostly lower than 0.3 mg/L (as Cl_2). It is important to point out that although numbers of swimmer were recorded on the competition side and the warm up side of the pool, the swimmers were in the same water body that was separated by a floating bulkhead.

Measurements of volatile DBPs and urea in water samples are shown in Figures 5.12-5.19. NH_2Cl and NCl_3 represented the dominant volatile DBPs in the pool. The peak concentrations for these two compounds were observed around 0.2 mg/L (as Cl_2). Concentrations of CHCl_3 were consistent during the study period. CNCHCl_2 and CH_3NCl_2 showed similar trends to CHCl_3 . The trends of NH_2Cl and NHCl_2 were similar, which suggests that their respective rates of formation and decay were similar. The fluctuations of these measurements were likely affected by water mixing behavior near the sample location.

The concentrations of NCl_3 in this experiment were slightly higher than those from the study of February. A relatively small number of swimmers would be expected to lead to less NCl_3 precursors in the pool water. However, fewer swimmers will also result in reduced mixing of near-surface water, which is believed to be largely responsible for liquid to gas transfer of NCl_3 .

A trend of NCl_3 behavior was observed such that the concentration usually increased through the day, during periods of swimmer activity. A sharp decrease was noted for the first measurements of each day. The factors that contributed this behavior could include recirculation of pool water during the night, resulting in mixing of near-surface water and water from deeper locations during the overnight period.

The stable concentration of CHCl_3 is probably attributable to its relatively slow rate of formation and lack of any significant mechanism of decay. More generally, it is likely that the rate for CHCl_3 formation was similar to its rate of liquid→gas transfer during this period. The dynamic behavior of CNCl was influenced by its reactivity with free chlorine and pH. The fluctuation of CNCl could also be influenced by the mixing behavior of swimmers and location of sample collection.

The concentrations of CNCHCl_2 and CH_3NCl_2 were lower than their corresponding measurements during the February study, which suggests that the concentrations of the precursors to these compounds were lower in March than in February. Both of their trends were similar to CHCl_3 , which suggests that their dynamic behaviors were similar to CHCl_3 at that point of location during the study period.

Concentrations of urea ranged from 0.05 to 0.4 mg/L. When no swimmers were present in the pool, degradation of urea could take place during the overnight period. A diurnal pattern of behavior was observed for urea concentration during this study. This pattern of behavior is consistent with previous reports of the dynamic behavior of urea (Weng and Blatchley, 2011). Urea is known to react slowly with free chlorine (Blatchley and Cheng, 2010). The decrease of urea concentration overnight was believed to be attributable to mixing of near surface water from recirculation of the pool that brings deep water up to the surface; deep water is assumed to have far less urea than near-surface water because swimmers spend the vast majority of their time in pools in the near-surface region.

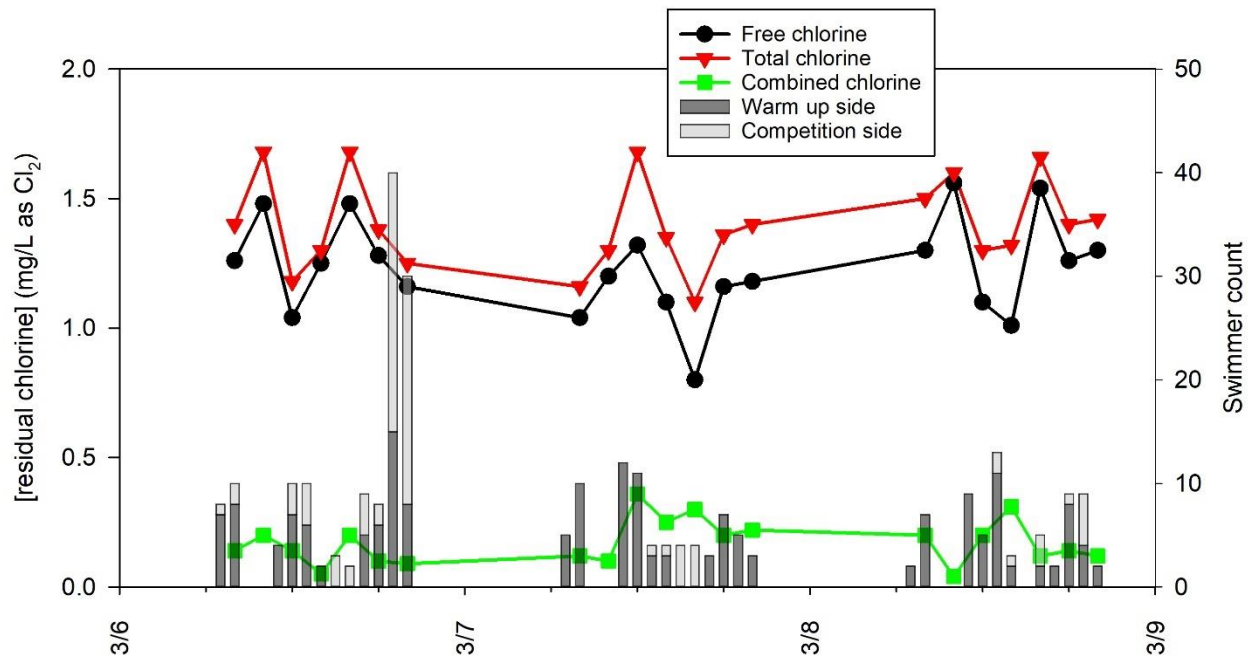


Figure 5.11. Time-course monitoring of free chlorine, total chlorine, and combined chlorine at pool facility B during regular operating hours in March 2019. Vertical bars represent the swimmer number in the pool.

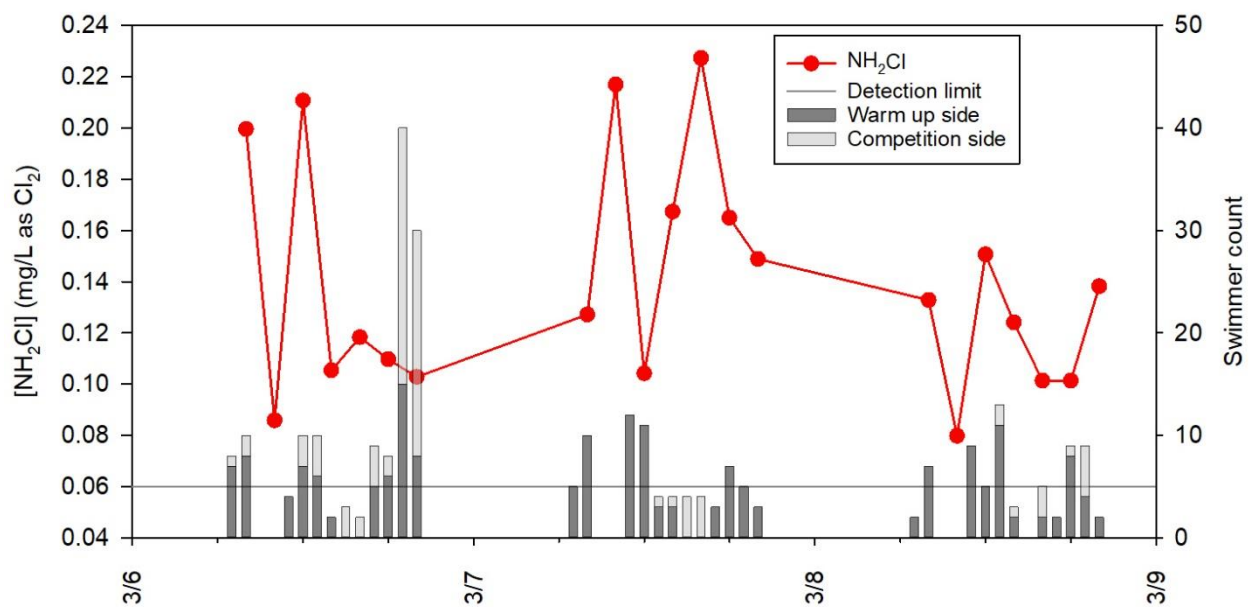


Figure 5.12. Time-course monitoring of NH_2Cl at pool facility B during regular operating hours in March 2019. Vertical bars represent the swimmer number in the pool. Horizontal line represents the detection limit.

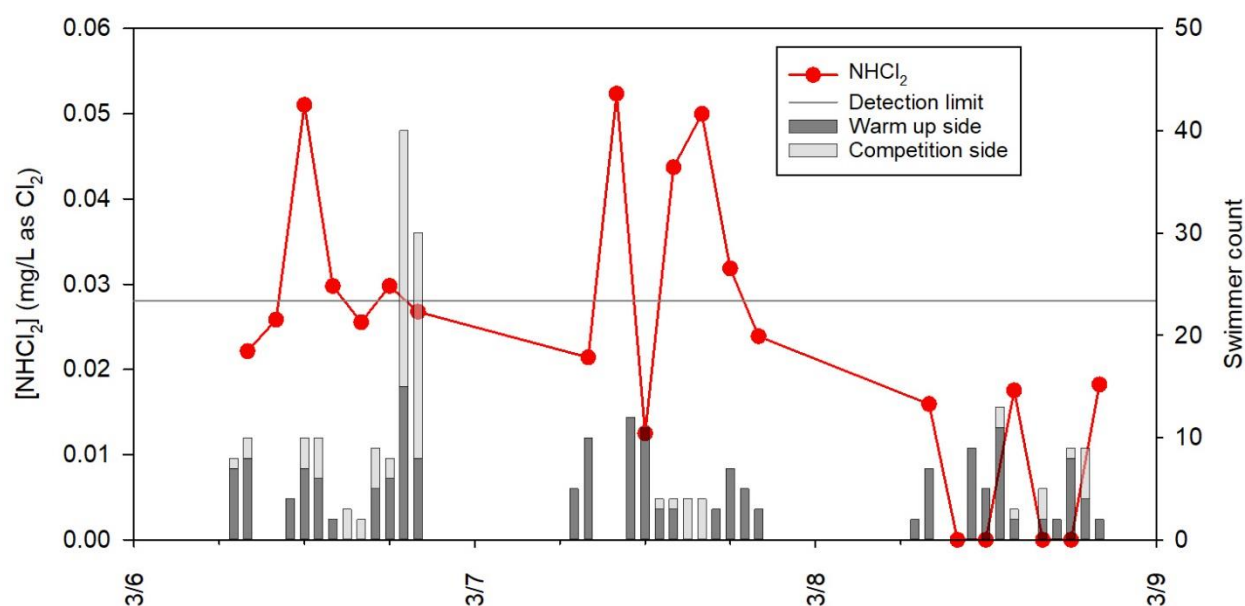


Figure 5.13. Time-course monitoring of NHCl_2 at pool facility B during regular operating hours in March 2019. Vertical bars represent the swimmer number in the pool. Horizontal line represents the detection limit.

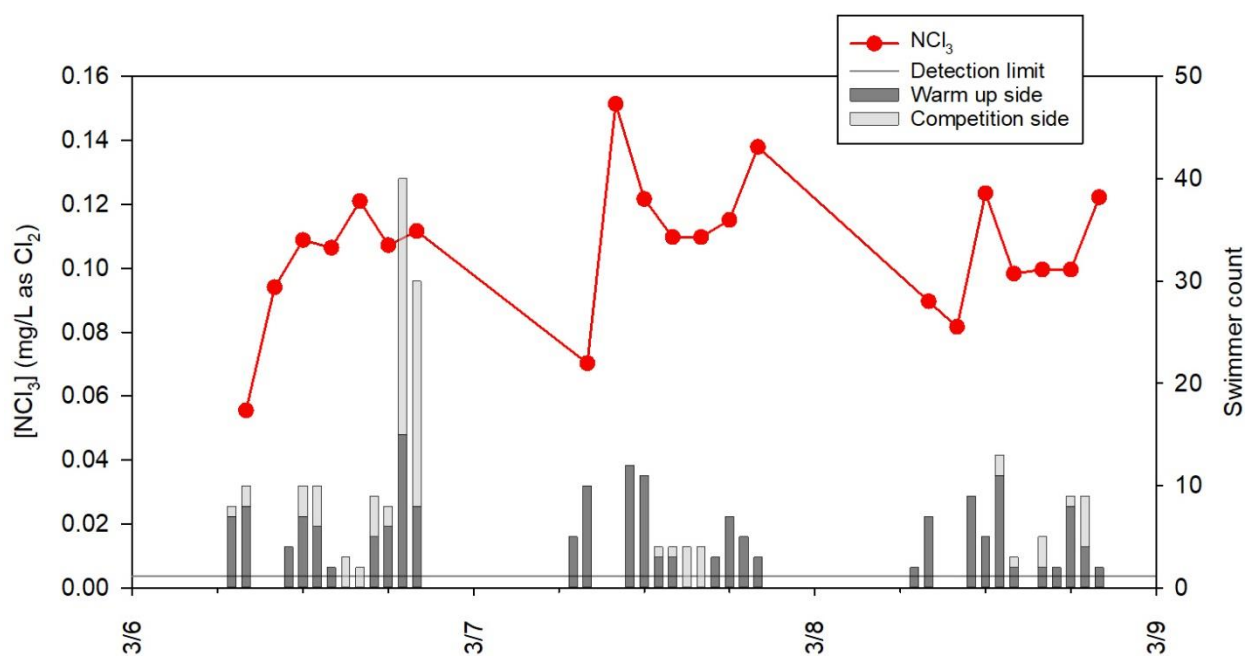


Figure 5.14. Time-course monitoring of NCl_3 at pool facility B during regular operating hours in March 2019. Vertical bars represent the swimmer number in the pool. Horizontal line represents the detection limit.

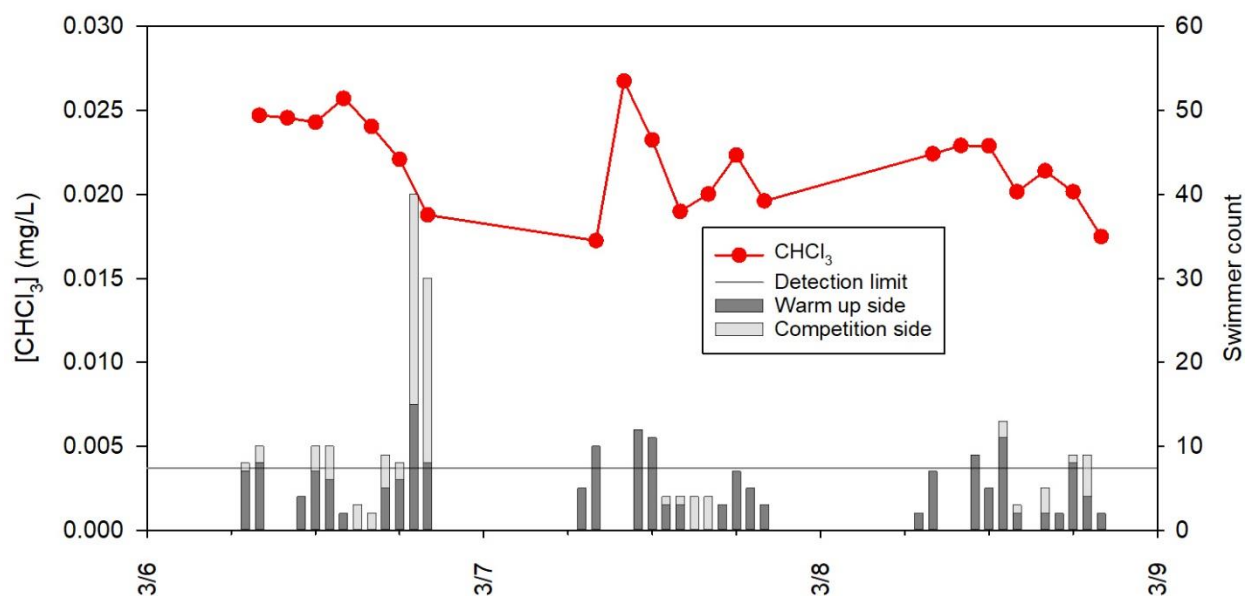


Figure 5.15. Time-course monitoring of CHCl_3 at pool facility B during regular operating hours in March 2019. Vertical bars represent the swimmer number in the pool. Horizontal line represents the detection limit.

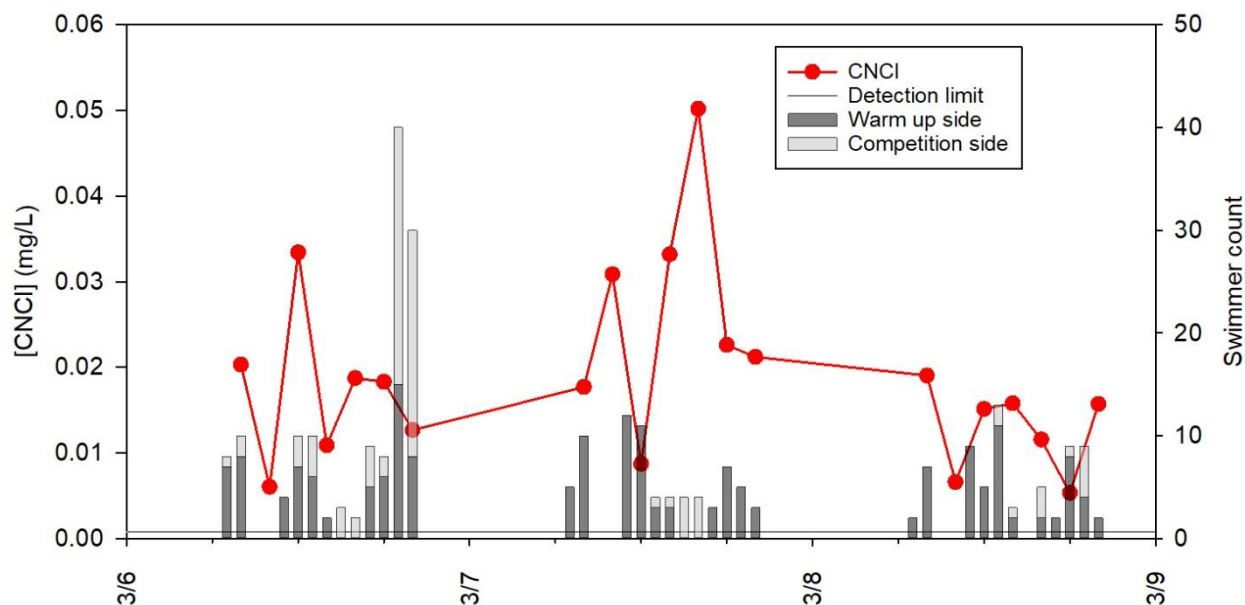


Figure 5.16. Time-course monitoring of CNCl at pool facility B during regular operating hours in March 2019. Vertical bars represent the swimmer number in the pool. Horizontal line represents the detection limit.

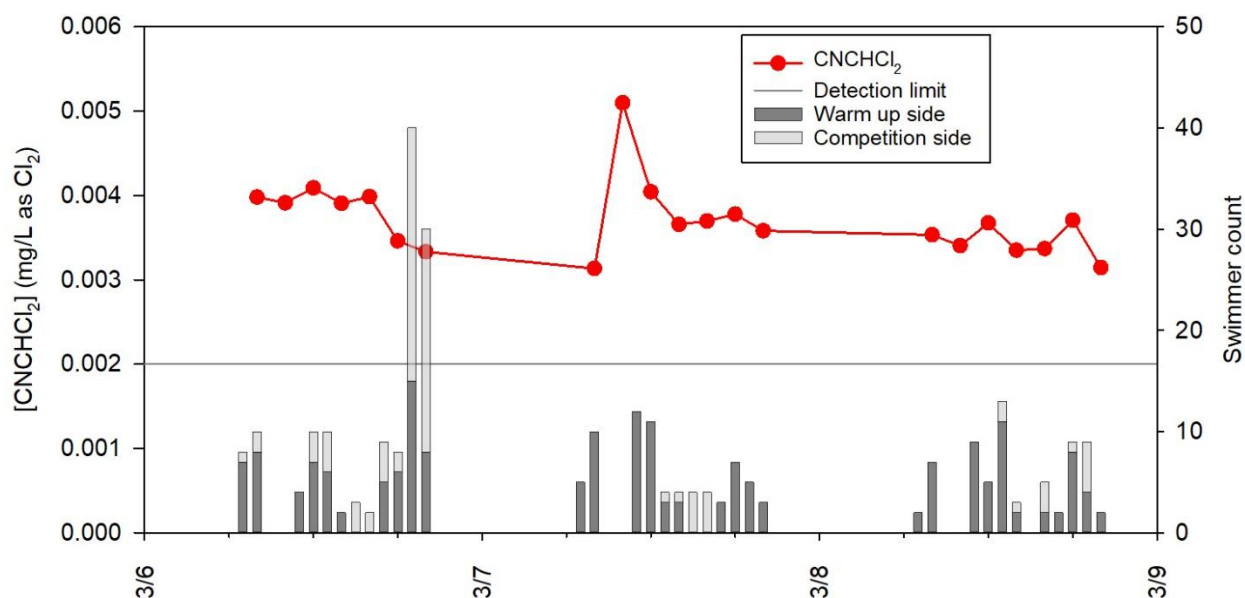


Figure 5.17. Time-course monitoring of CNCHCl_2 at pool facility B during regular operating hours in March 2019. Vertical bars represent the swimmer number in the pool. Horizontal line represents the detection limit.

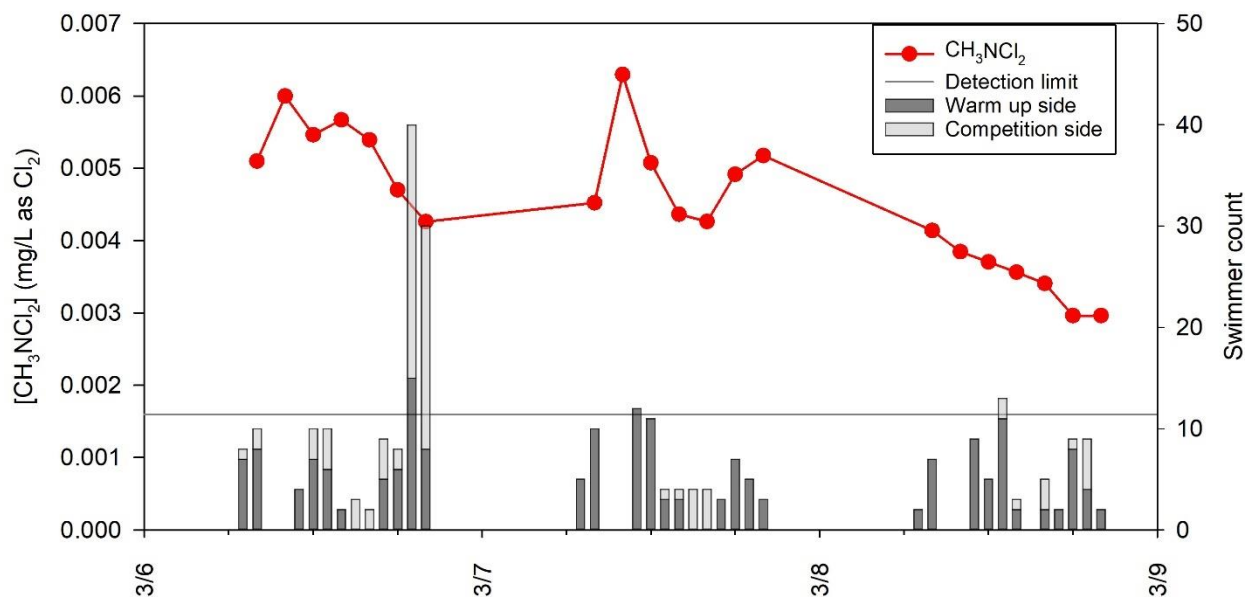


Figure 5.18. Time-course monitoring of CH_3NCl_2 at pool facility B during regular operating hours in March 2019. Vertical bars represent the swimmer number in the pool. Horizontal line represents the detection limit.

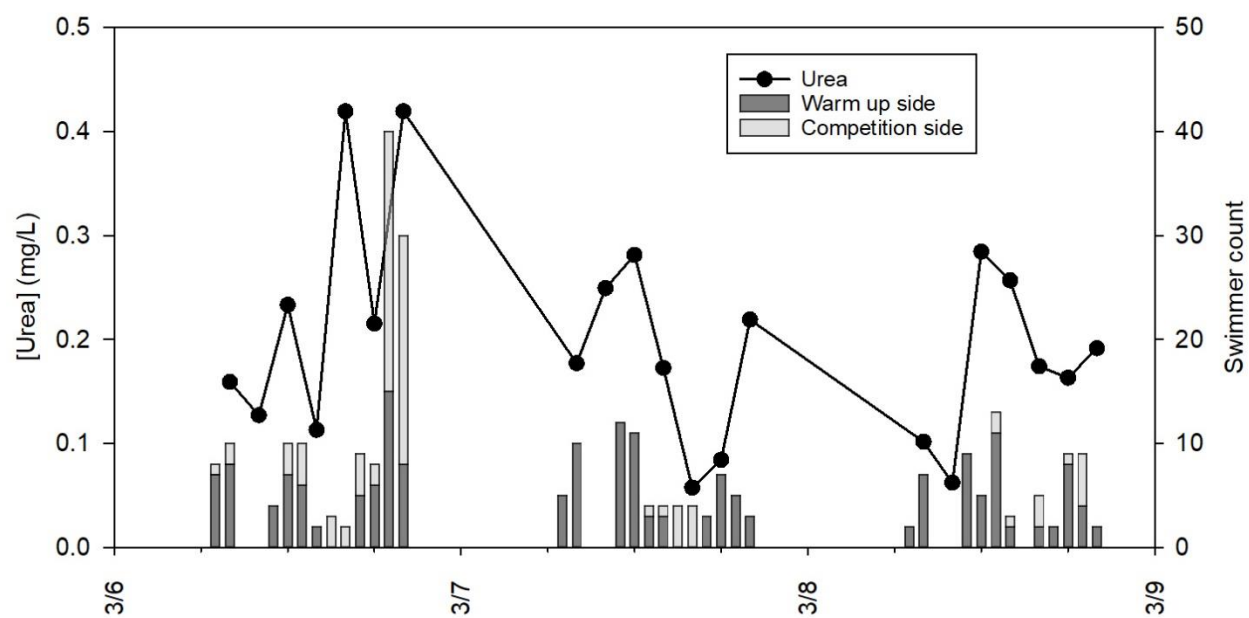


Figure 5.19. Time-course monitoring of urea at pool facility B during regular operating hours in March 2019. Vertical bars represent the swimmer number in the pool.

Time-course monitoring of gas-phase NCl_3 with relative humidity (RH) is illustrated in Figure 5.20. The gray vertical bars represent the swimmer numbers for different areas of the pool. RH measurements were all within the acceptable range (30% to 60%). Generally, concentrations of gas-phase NCl_3 were between 100 to 300 $\mu\text{g}/\text{m}^3$. Concentrations were near zero during the period from midnight to early morning of 3/8/2019. Although NEMo panel C was placed at a different height than the other two panels, the measurements from NEMo panel C were similar to those of the other two panels, thereby supporting the hypothesis of a well-mixed air space in this facility.

Time-course monitoring of gas-phase NCl_3 with gas-phase CO_2 are illustrated in Figure 5.21. Measured CO_2 concentration reached more than 600 ppm_v when there were more than 40 swimmers in the pool. Gas-phase CO_2 was usually around 400 ppm_v for panels B and C during the study period, which corresponds with CO_2 background concentration for the Northern Hemisphere from the Mauna Loa Observatory, which was slightly above 400 ppm_v at the time of this experiment (Keeling and Keeling, 2017). Maximum suggested occupational exposure limits for CO_2 for an 8-hr exposure in a working area are 5000 ppm_v as a time-weighted average from the Occupational Safety and Health Administration (OSHA, 1990).

Readings from panel A indicated CO_2 well below 300 ppm_v on 3/7/2019 and 3/8/2019, thus NEMo panel A was sent back to the manufacturer for CO_2 sensor maintenance.

The time-course behaviors of CO_2 and NCl_3 from panels B and C during this study appear to be weakly correlated at pool facility B. It was assumed that gas-phase CO_2 and NCl_3 might have high correlation in indoor pool facility as both are volatile compounds. These data suggested that any reliance on a correlation between CO_2 and NCl_3 may be affected by the number of swimmers present the pool. Specifically, the results of the February and March 2019 experiments suggest that a high correlation between CO_2 and NCl_3 may occur only when the pool is heavily occupied. In addition, the number of spectators in the pool may affect the correlation between gas-phase CO_2 and NCl_3 , thus number of people on the pool deck and in the spectator area were manually counted in subsequent swimming meets.

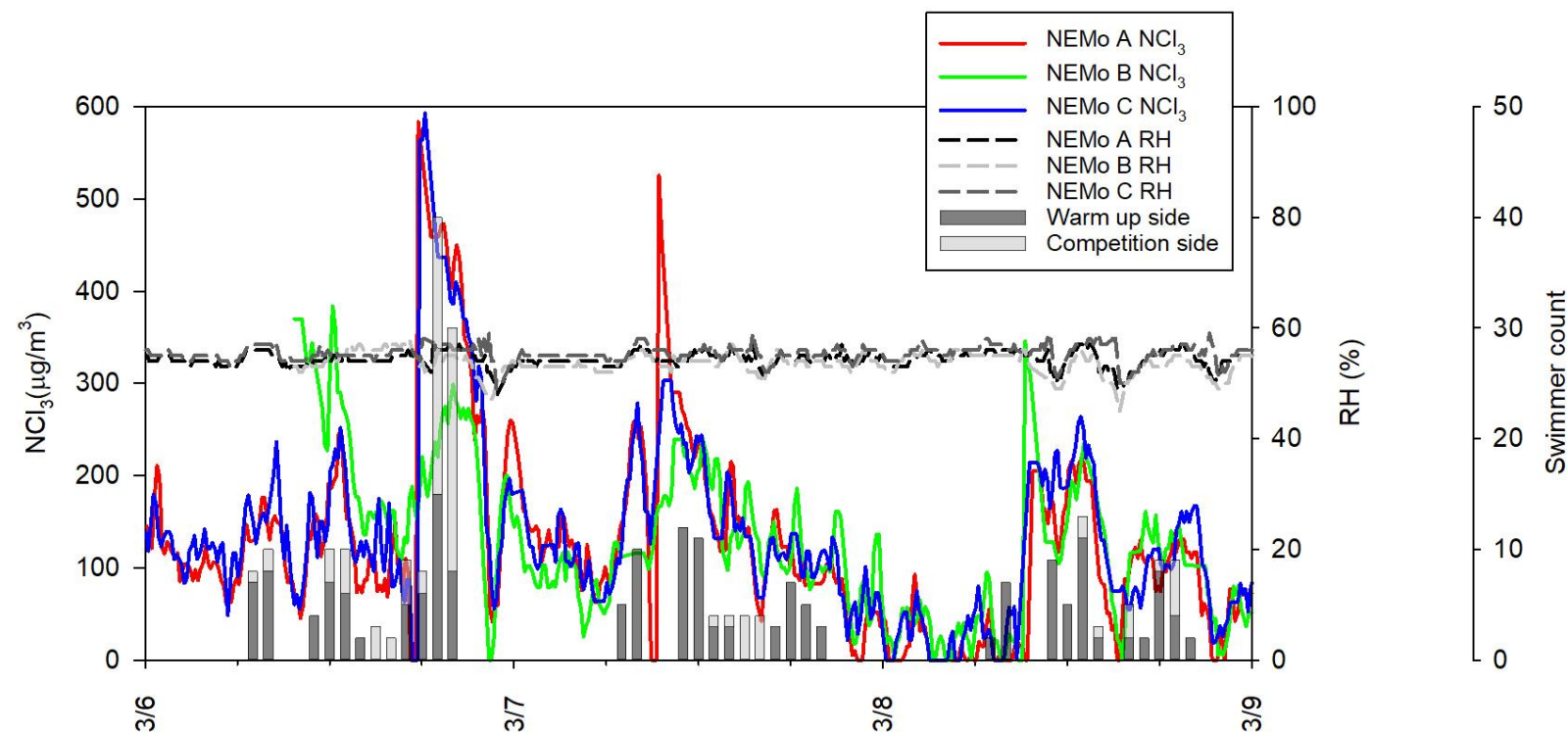


Figure 5.20. Time-course monitoring of gas-phase NCl_3 and RH measured by NEMo devices at pool facility B during regular operating hours in March 2019. Vertical bars represent the swimmer number in the pool.

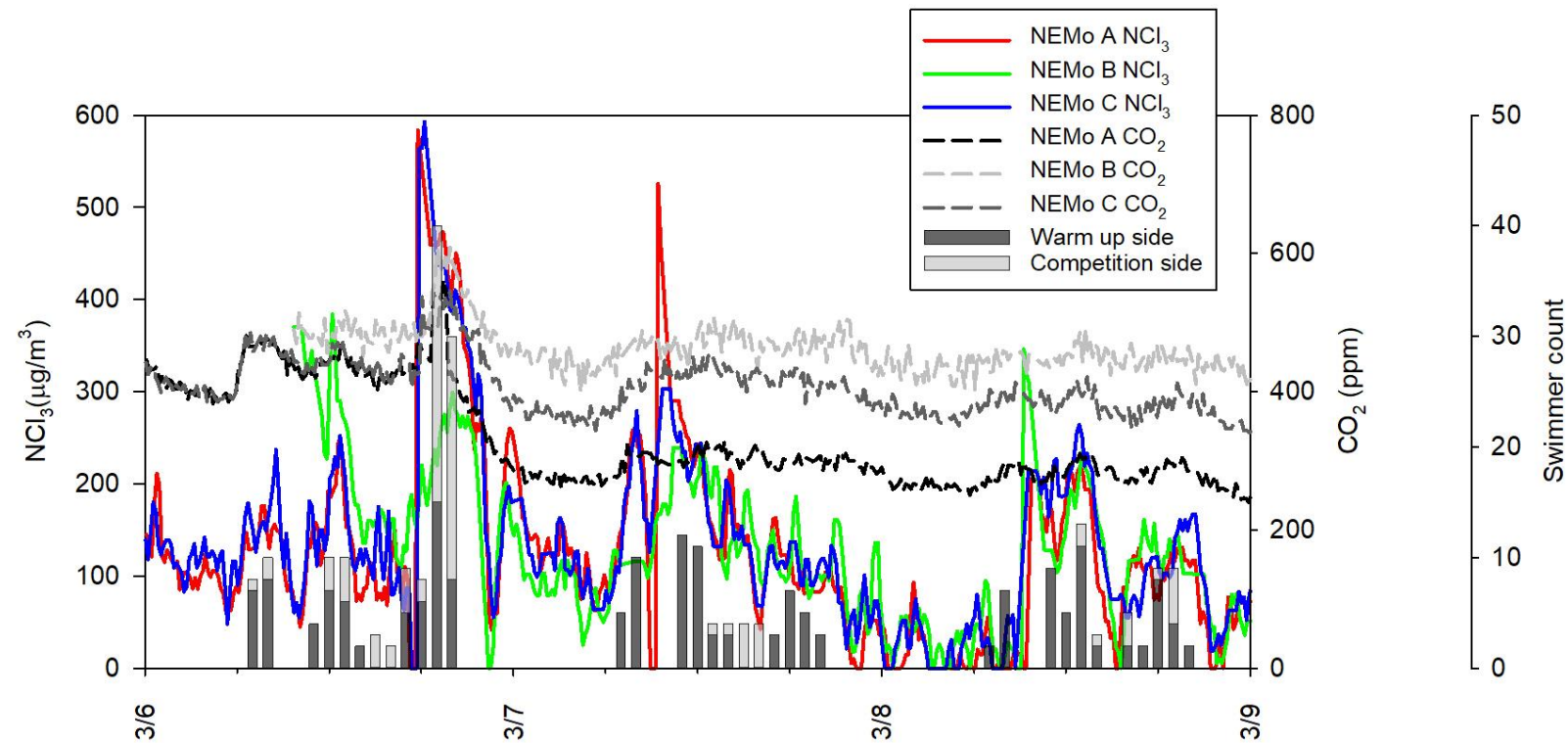


Figure 5.21. Time-course monitoring of gas-phase NCl_3 and gas-phase CO_2 measured by NEMo devices at pool facility B during regular operating hours in March 2019. Vertical bars represent the swimmer number in the pool.

5.1.3 Measurements in April 2019

Measurements were conducted during regular operating hours at pool facility B from 4/22/2019 to 4/26/2019. The study was conducted during regular operating hours to facilitate comparisons with the dynamic behavior of volatile DBPs during periods of heavy use, such as swimming meets. Also, monitoring during this period of regular use may facilitate identification of a baseline condition. During this period, the pool was used by lap swimmers, practice for competition swimming teams, and for swimming lessons. Swimmer counts were recorded hourly by pool lifeguards. Two NEMO devices were installed during this measurement and their locations around the pool area are shown in Figure 3.11.

Measurements of volatile DBPs and urea in water samples are shown in Figures 5.22-5.29. NH_2Cl and NCl_3 represented the dominant volatile DBPs in the pool. NCl_3 and CH_3NCl_2 concentrations generally increased across the experiment period. Concentrations of CHCl_3 and CNCHCl_2 were consistent during the study period.

The trends of NH_2Cl and NHCl_2 were similar, suggesting that their rates of formation and decay were similar. Their concentrations were generally lower than the February (swimming meet). The fluctuations of these measurements were likely influenced by water mixing at the sample location by swimmers and pool recirculation.

NCl_3 and CH_3NCl_2 showed generally similar patterns of behavior during this experiment, with both showing patterns of steady increase during the study period. In general terms, this implies that their rates of formation were greater than their rates of loss by volatilization.

The stable concentration of CHCl_3 suggests that its rate of formation was similar to its rate of loss. The concentrations were similar to those that were observed in March (regular hour).

The concentration of urea ranged from 0.05 to 0.2 mg/L. Urea concentrations tended to increase during the day, with the exception of 4/24/2019. A diurnal pattern of behavior was observed for the trend of urea during this study. The patterns of behavior for urea was similar in this period as in the experiment conducted under normal operating conditions in March 2019.

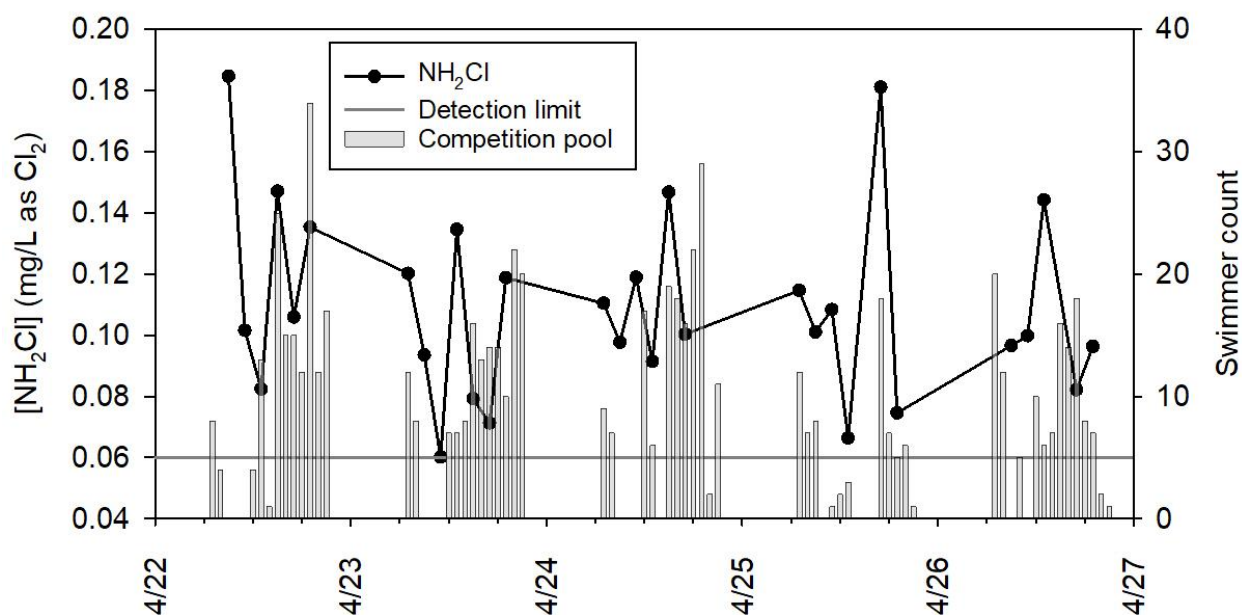


Figure 5.22. Time-course monitoring of NH_2Cl at pool facility B during regular operating conditions in April 2019. Vertical bars represent the swimmer number in the pool. Horizontal line represents the detection limit.

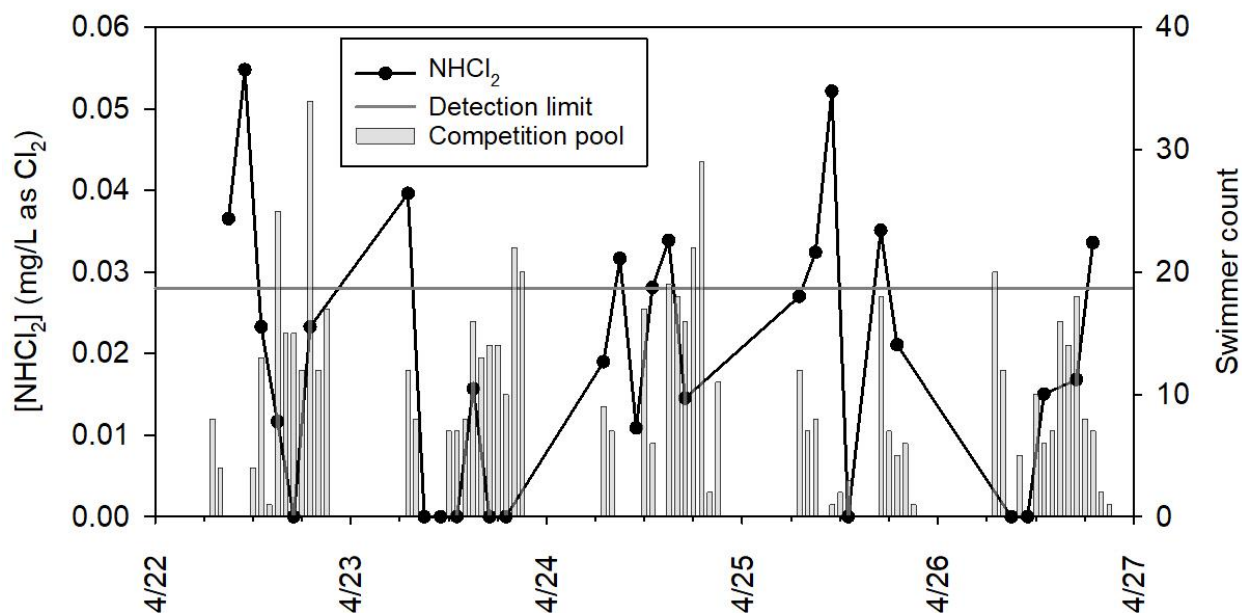


Figure 5.23. Time-course monitoring of NHCl_2 at pool facility B during regular operating conditions in April 2019. Vertical bars represent the swimmer number in the pool. Horizontal line represents the detection limit.

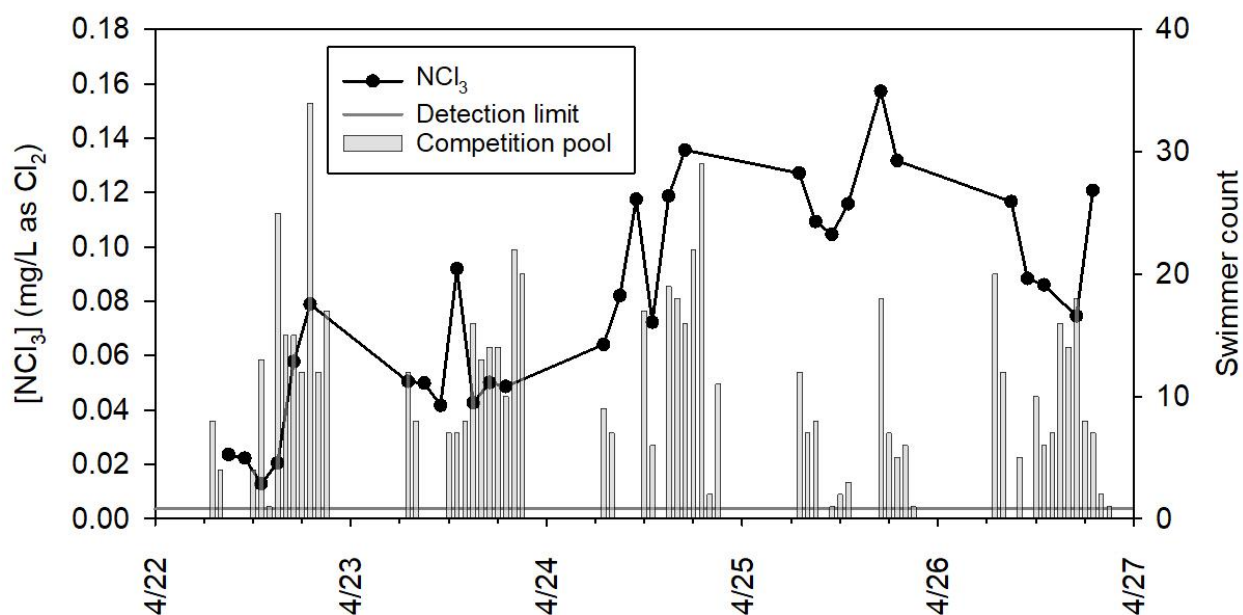


Figure 5.24. Time-course monitoring of NCl_3 at pool facility B during regular operating conditions in April 2019. Horizontal line represents the detection limit.

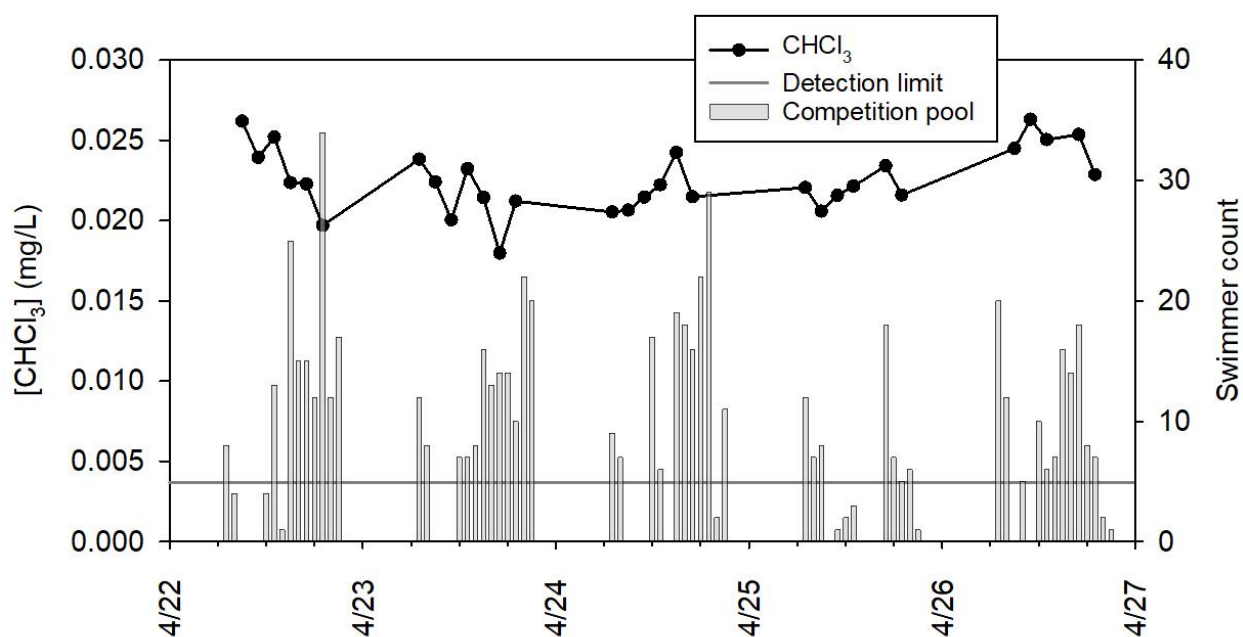


Figure 5.25. Time-course monitoring of CHCl_3 at pool facility B during regular operating conditions in April 2019. Horizontal line represents the detection limit.

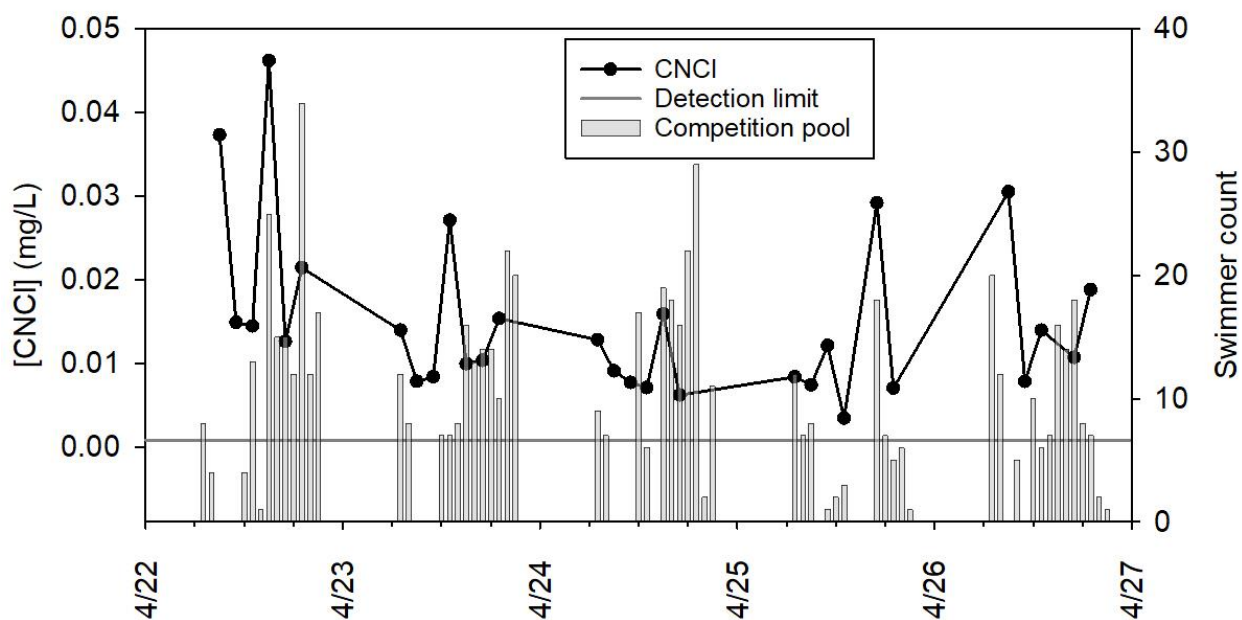


Figure 5.26. Time-course monitoring of CNCl at pool facility B during regular operating conditions in April 2019. Horizontal line represents the detection limit.

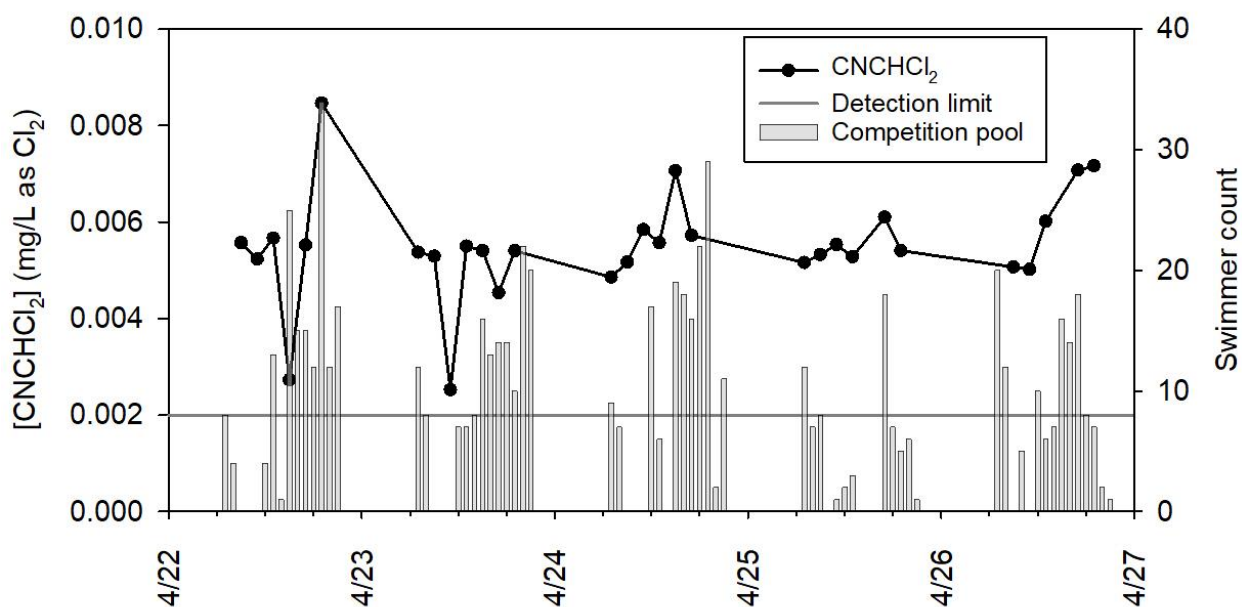


Figure 5.27. Time-course monitoring of CNCHCl_2 at pool facility B during regular operating conditions in April 2019. Horizontal line represents the detection limit.

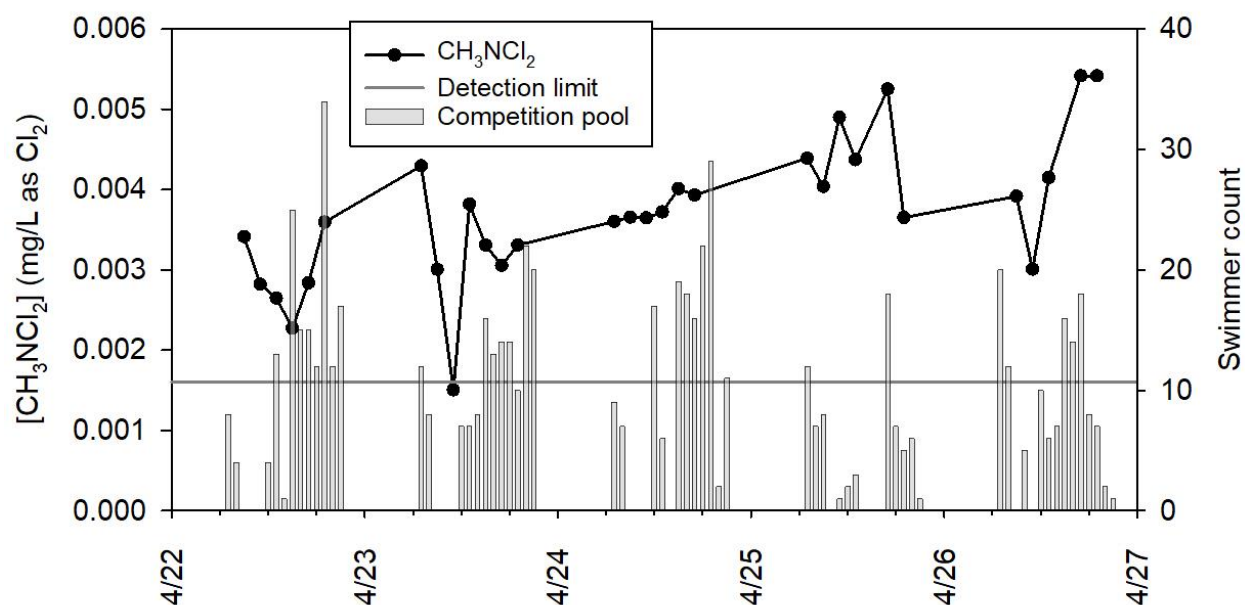


Figure 5.28. Time-course monitoring of CH_3NCl_2 at pool facility B during regular operating conditions in April 2019. Horizontal line represents the detection limit.

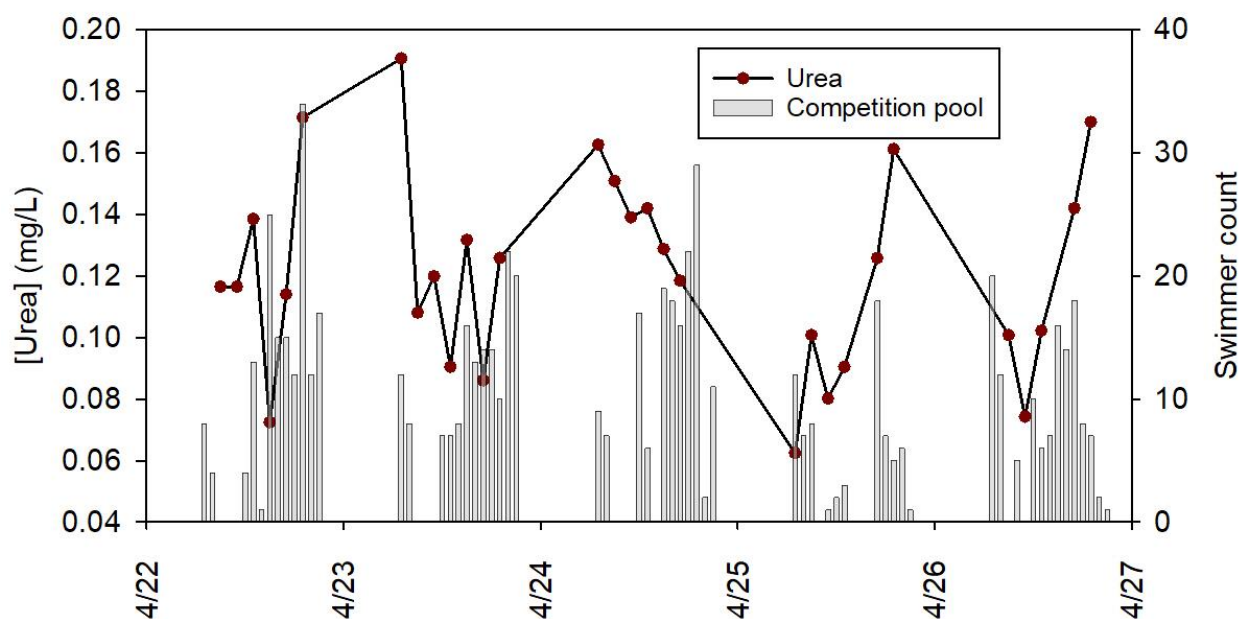


Figure 5.29. Time-course monitoring of urea at pool facility B during regular operating conditions in April 2019. Vertical bars represent the swimmer number in the pool.

Time-course monitoring of gas-phase NCl_3 with relative humidity (RH) is illustrated in Figure 5.30. The gray vertical bars represent the swimmer number at the pool facility B. RH measurements were largely within the acceptable range (30% to 60%) for the NEMo instruments.

Generally, concentrations of gas-phase NCl_3 were below $200 \mu\text{g}/\text{m}^3$, except for four occasions. Concentrations of gas-phase NCl_3 exceeded $250 \mu\text{g}/\text{m}^3$ when there were more than 20 swimmers in the pools. NEMo panels B and C showed similar trends for measured gas-phase NCl_3 concentrations during this experiment. The agreement of these measurements supports the assumption of a well-mixed air space.

In Figure 5.30, the large decrease of RH will lead to increases of reported NCl_3 concentration because the measurements of gas-phase NCl_3 concentration by the NEMo devices are sensitive to relative humidity. In addition, a peak concentration of gas-phase NCl_3 was observed early in the morning of 4/22/2019 when the recorded swimmer number was quite low. This situation could be explained as that there were group of recreational swimmers present in pool and left the pool before the lifeguards started to count swimmers on that day. Also, when I arrived pool at 7:00 am, I noticed that there were more than 40 people on the pool deck preparing to leave the pool facility.

Time-course monitoring of gas-phase NCl_3 with gas-phase CO_2 is illustrated in Figure 5.31. CO_2 measurements reached roughly 600 ppm_v when there were more than 80 swimmers in the pools. Gas-phase CO_2 was typically around 400 ppm_v for panels B and C during the study period. The time-course behaviors of CO_2 and NCl_3 from panel B and C during this study appear to be more strongly correlated than in the previous experiment. Additionally, the measurements of gas-phase CO_2 concentration were correlated to swimmer numbers.

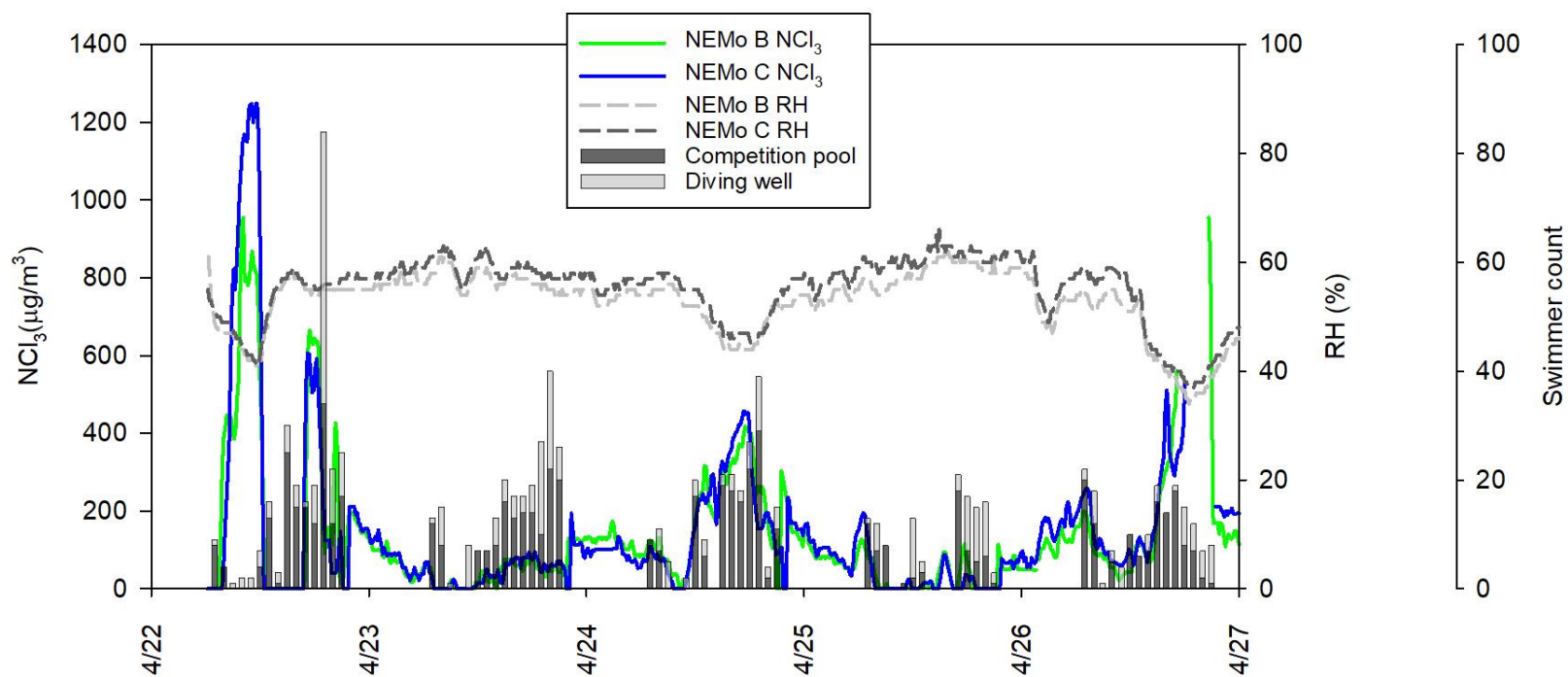


Figure 5.30. Time-course monitoring of gas-phase NCl_3 and RH measured by NEMo devices at pool facility B during regular operating hours in April 2019. Vertical bars represent the number of swimmers in the pools.

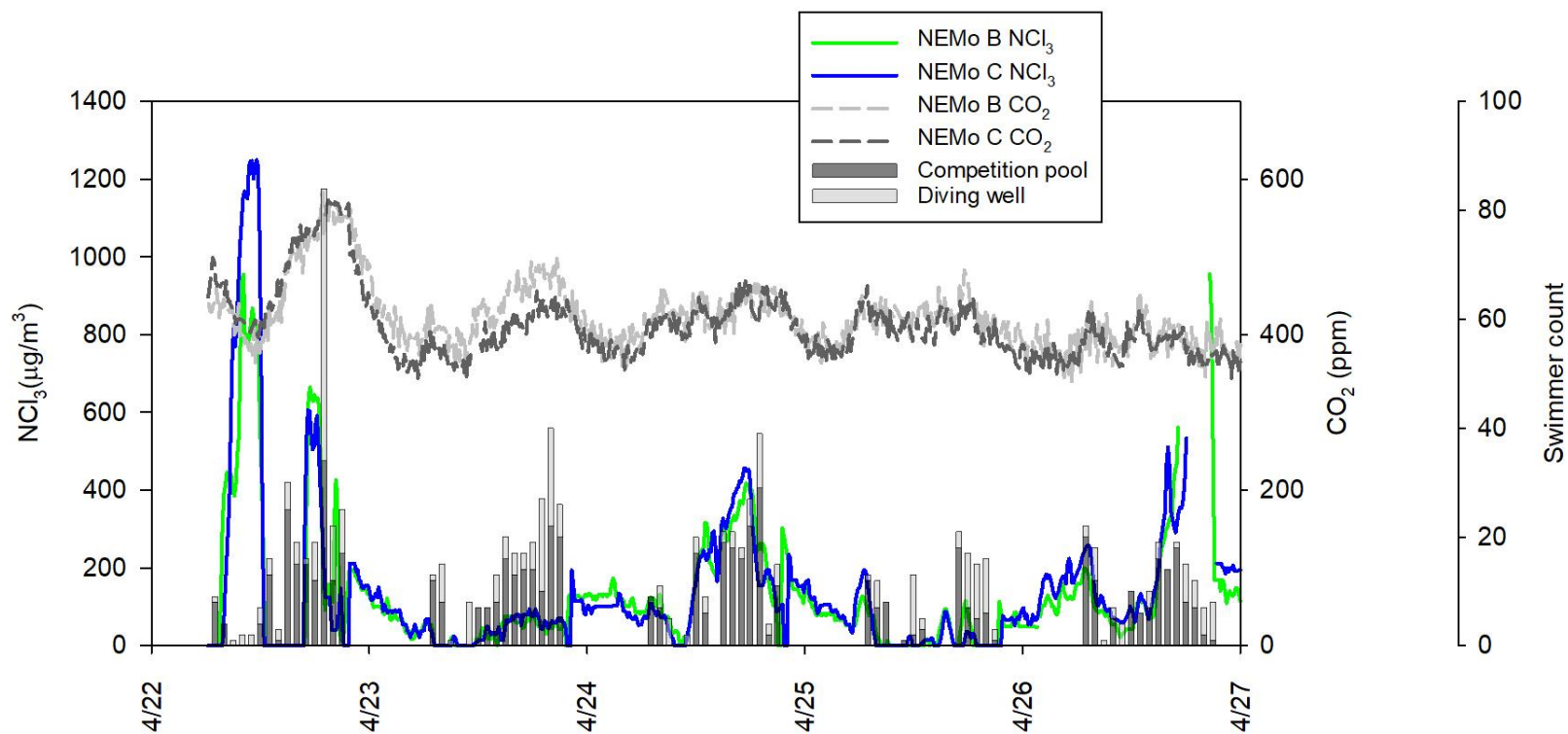


Figure 5.31. Time-course monitoring of gas-phase NCl_3 and gas-phase CO_2 measured by NEMo devices at pool facility B during regular operating hours in April 2019. Vertical bars represent the number of swimmers in the pools.

5.1.4 Measurements in June 2019

Water and air quality monitoring were conducted during a swimming meet at facility B from 6/21/2019 to 6/24/2019. Competition began Friday (6/21/2019) night and ended Sunday (6/23/2019) afternoon. The session on 6/21/2019 was held from 5:00 pm to 8:00 pm; the session on 6/22/2019 was held from 8:30 am to 6:30 pm; the session on 6/23/2019 was held from 8:00 am to 4:00 pm. Additional measurements were made one day (6/24/2019) after the meet. The meet was conducted as a long-course (50 meters) event for 8 and under children and approximately 350 swimmers participated. Water samples were collected every two hours when the facility was open from 6/21/2019 to 6/24/2019 at approximately 20 cm below the water surface at a location illustrated in Figure 3.11. Also, two NEMo devices (A and B) were installed during this meet and their locations within the pool area are illustrated in Figure 3.12.

Time-course measurements of the concentrations of free chlorine and total chlorine are illustrated in Figure 5.32. Concentrations of free chlorine ranged from 1.0 to 2.1 mg/L as Cl_2 and concentrations of total chlorine ranged from 1.3 to 2.5 mg/L as Cl_2 . The concentrations of combined chlorine (total chlorine - free chlorine) were generally close to 0.5 mg/L as Cl_2 throughout the experiment.

pH was stable during this meet as indicated in Figure 5.33 and alkalinity was stable near 100 mg/L as CaCO_3 , as shown in Figure 5.34. Aqueous-phase CO_2 concentrations were calculated from measurements of pH, alkalinity, and temperature (Tucker, 1984). As water temperature was not recorded during the study period, water temperature was assumed to be steady at 25°C throughout this experiment period; this value of water temperature is consistent with water temperature for competition pools. The trend of aqueous CO_2 concentration is illustrated in Figure 5.35. CO_2 gas is used for pH control in this pool. Variations in the concentration of liquid-phase CO_2 were believed to be attributable to: mixing behavior by the swimmers that promoted liquid to gas transfer, mixing within the pool at the location of sample collection, CO_2 injection for pH control, and respiration from swimmers and spectators.

Measurements of volatile DBPs in water samples are shown in Figures 5.36-5.42. Inorganic chloramines consistently represented the dominant volatile DBPs in the pool (specifically NH_2Cl and NCl_3). Measurements of NHCl_2 were consistently below the detection limit. Lower concentrations of NH_2Cl were observed as compared with the February study (swimming meet). The variations of NH_2Cl concentration during this study were attributed to the rates of formation

and decay, mixing behavior associated with the swimmers, liquid to gas transfer, free chlorine and mixing at the location of sample collection.

Liquid-phase concentrations of NCl_3 reached 0.18 mg/L as Cl_2 during each day of the meet. Generally, NCl_3 trended upward during the competition and decreased overnight. The factors that contributed this behavior included introduction of NCl_3 precursors into the pool by the swimmers, thereby promoting and NCl_3 formation. The rate of formation was apparently faster than the rates of decay and liquid to gas transfer. The overall trend of liquid-phase NCl_3 was opposite of the trend that was reported by Weng and Blatchley (2011), who reported measurements that were collected during a national level collegiate swimming competition. The difference of dynamic behavior could be attributed to different types (ages) of swimmers and different mixing behavior within the pool at the locations of sample collection.

Liquid-phase concentrations of CHCl_3 slowly declined during the study period, possibly because of selective removal of volatile compounds by the mixing action of swimmers that led to liquid to gas transfer or swimmer activity that led to vertical or horizontal mixing of pool water. The trend of CH_3NCl_2 concentration was similar to that of CHCl_3 . The dynamic behavior for CH_3NCl_2 in this meet was opposite to the study done by Weng and Blatchley (2011).

The concentration of CNCHCl_2 was stable throughout the meet but slowly decreased one day after the meet. The dynamic behavior suggested that rate of formation and the rates of decay and liquid to gas transfer were similar at the location of sample collection.

Time-course monitoring of concentration of urea is illustrated in Figure 5.43. The measurements of urea indicate accumulation of urea each day throughout the meet, clearly indicating the influence of swimmers. The highest concentration was observed after more than 200 swimmers got into the pool during a warm-up session. A diurnal pattern of behavior was observed for urea during this study as well. A previous study done by Weng and Blatchley (2011) reported similar behavior. The decrease of urea concentration overnight was believed to be attributable to mixing of near surface water from recirculation of the pool with deep water. A sharp decline of overall urea concentration was observed after the meet (6/24), indicating the importance of swimmer introductions of urea during the swimming meet. Subsequently, decreases of the liquid-phase concentrations of NCl_3 , CHCl_3 , CNCHCl_2 , and CH_3NCl_2 were also observed.

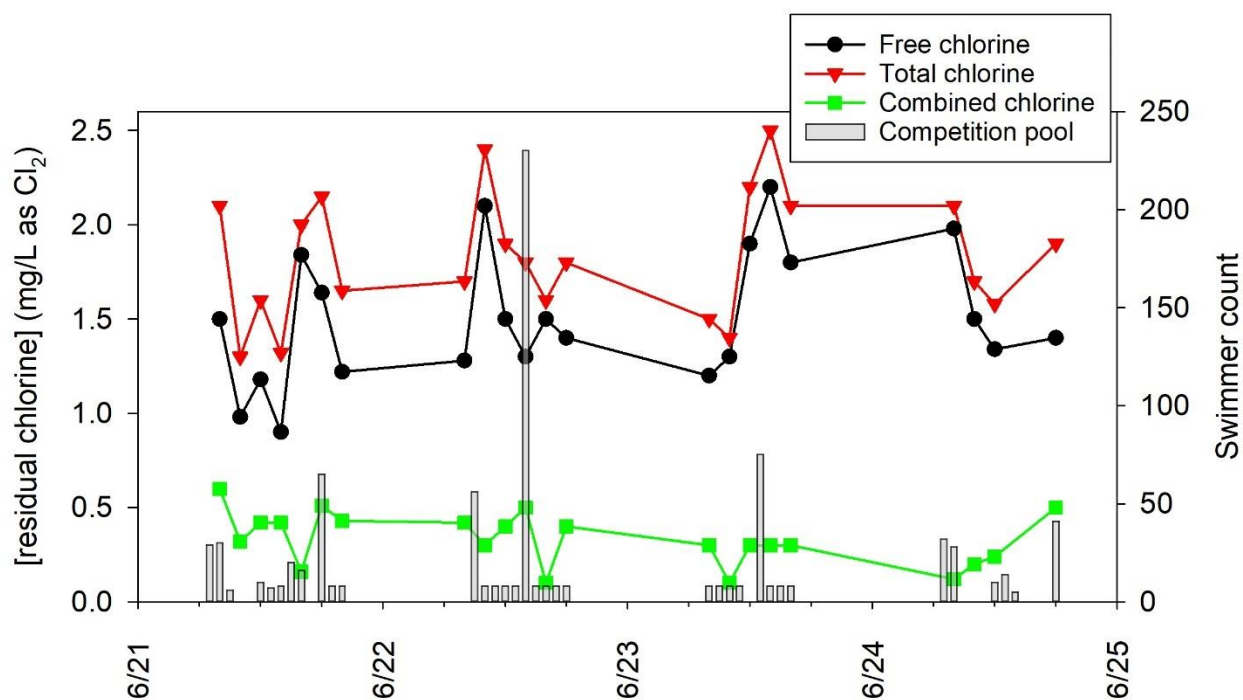


Figure 5.32. Time-course monitoring of free and total chlorine at pool facility B during swimming meet in June 2019. Vertical bars represent the number of swimmers in the pools.

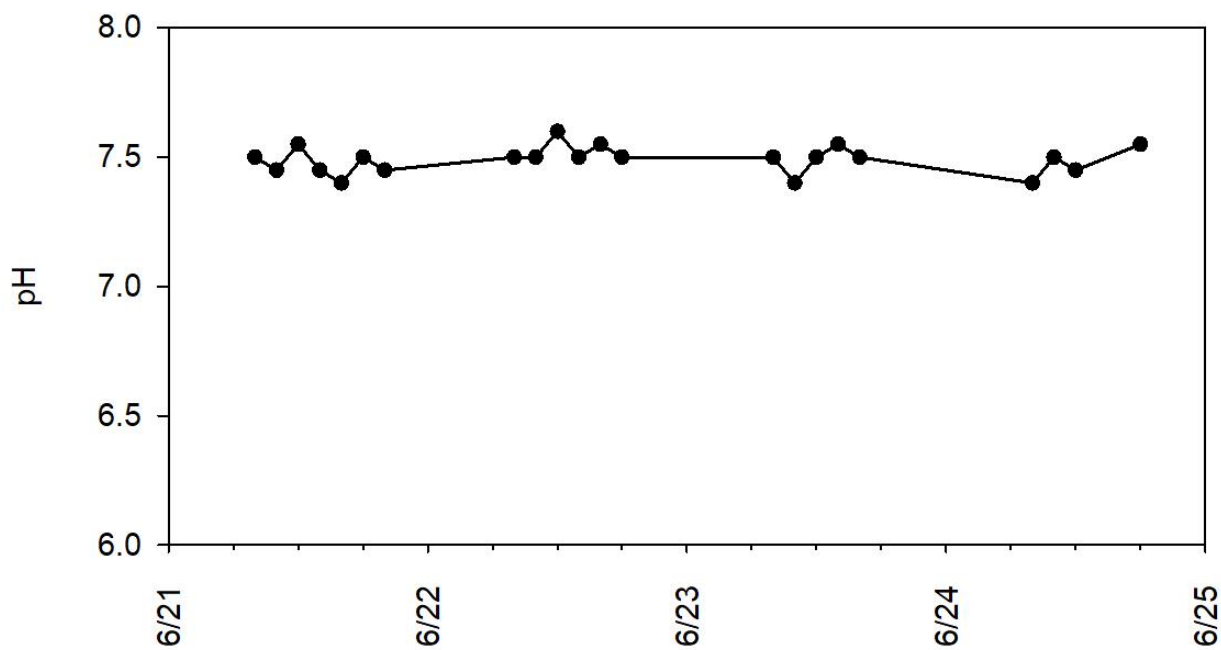


Figure 5.33. Time-course monitoring of pH at pool facility B during swimming meet in June 2019.

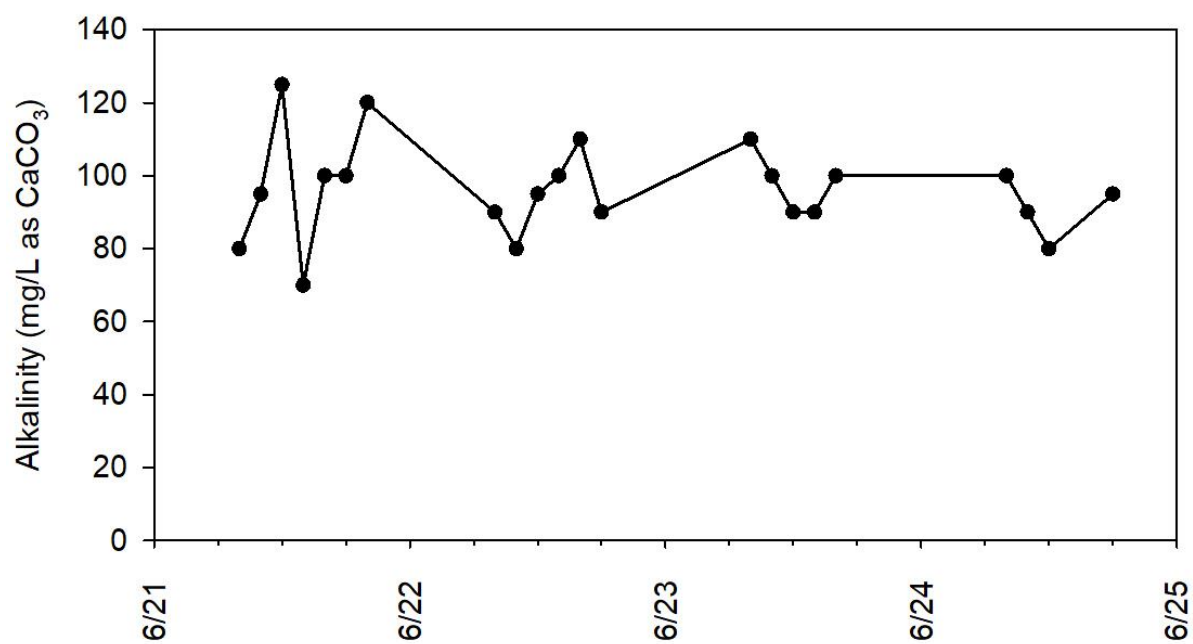


Figure 5.34. Time-course monitoring of alkalinity at pool facility B during swimming meet in June 2019.

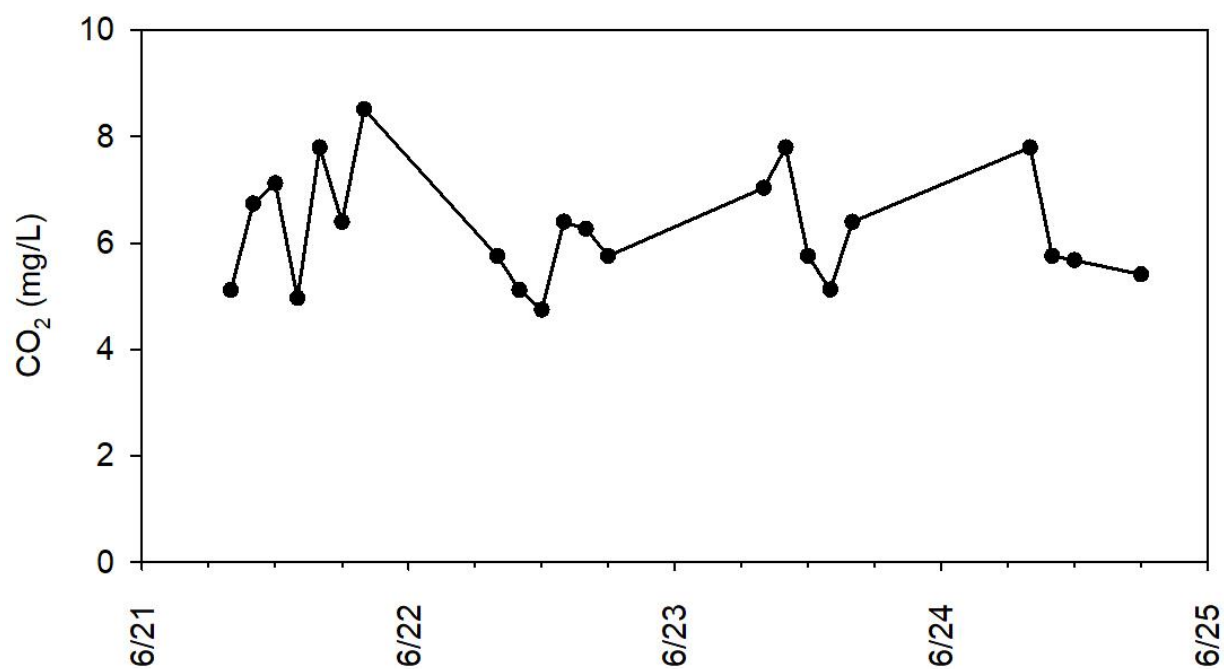


Figure 5.35. Trend of calculated aqueous-phase CO₂ at pool facility B during swimming meet in June 2019.

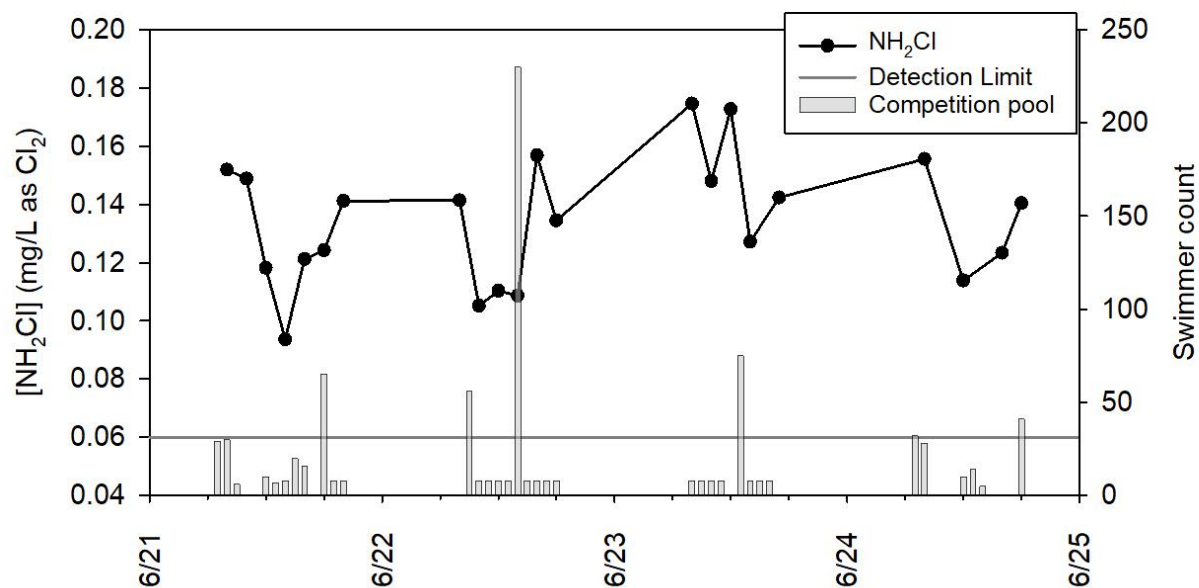


Figure 5.36. Time-course monitoring of aqueous-phase NH_2Cl at pool facility B during swimming meet in June 2019. Vertical bars represent the number of swimmers in the pools. Horizontal line represents the detection limit.

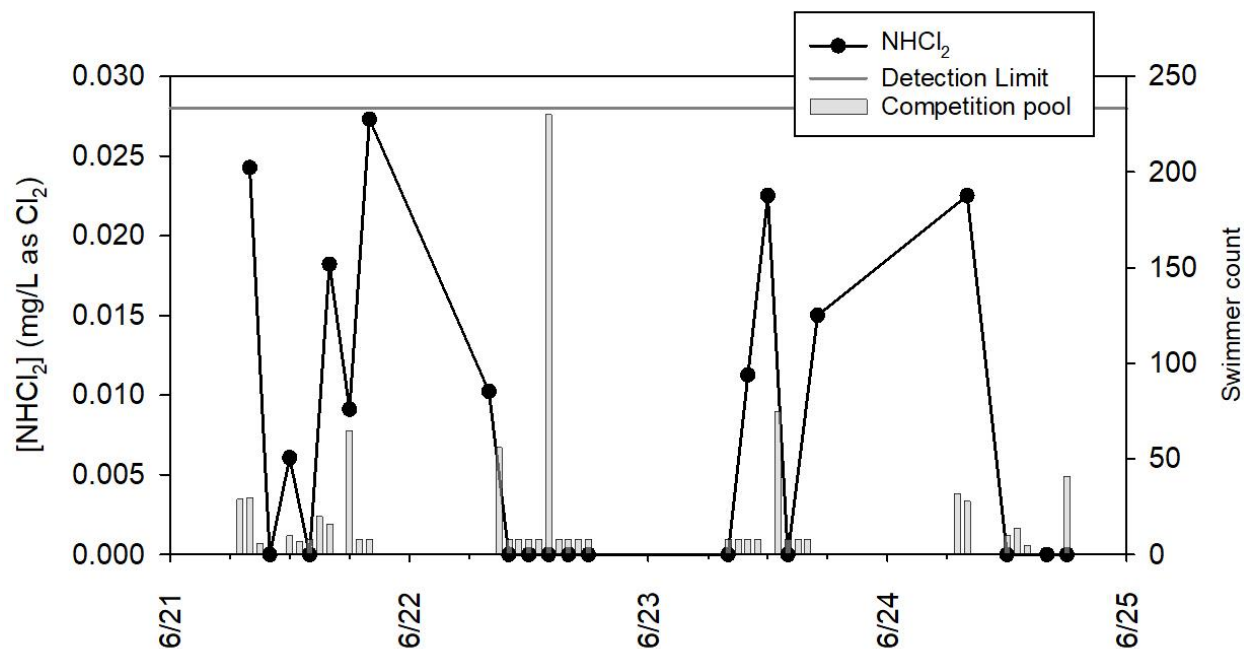


Figure 5.37. Time-course monitoring of aqueous-phase NHCl_2 at pool facility B during swimming meet in June 2019. Vertical bars represent the number of swimmers in the pools. Horizontal line represents the detection limit.

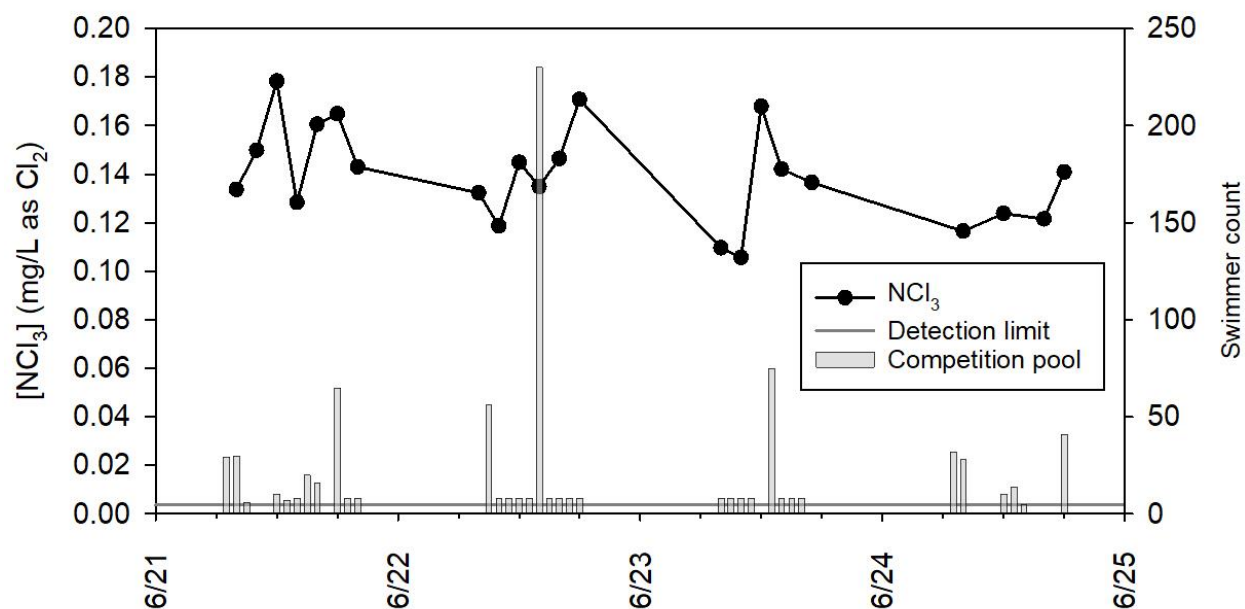


Figure 5.38. Time-course monitoring of aqueous-phase NCl_3 at pool facility B during swimming meet in June 2019. Vertical bars represent the number of swimmers in the pools. Horizontal line represents the detection limit.

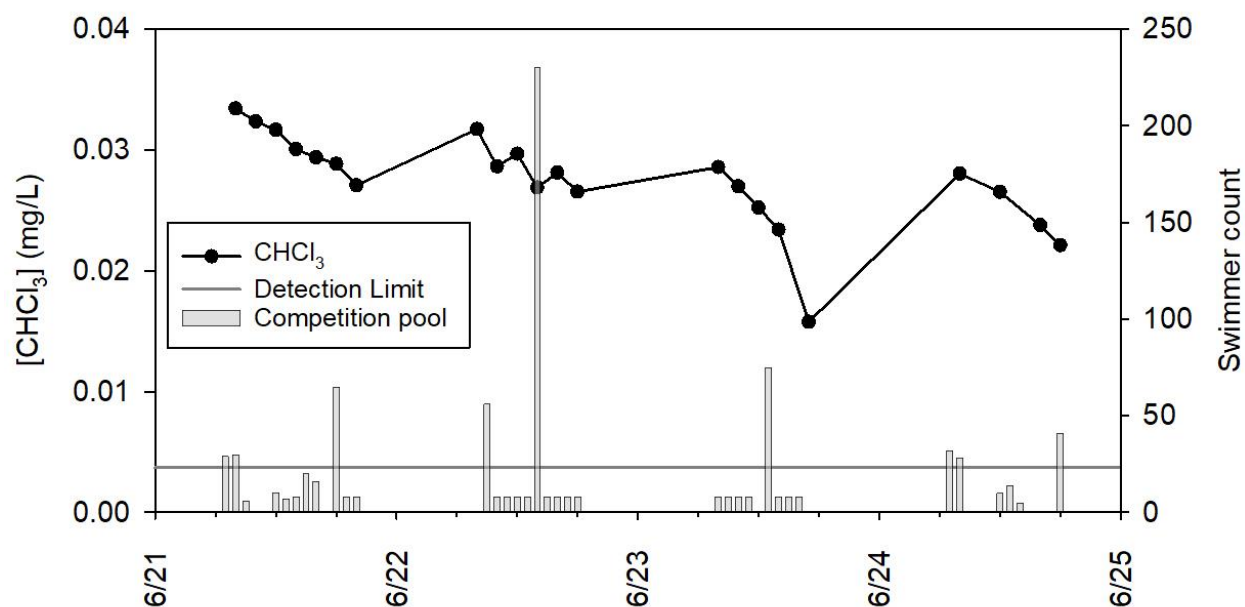


Figure 5.39. Time-course monitoring of aqueous-phase CHCl_3 at pool facility B during swimming meet in June 2019. Vertical bars represent the number of swimmers in the pools. Horizontal line represents the detection limit.

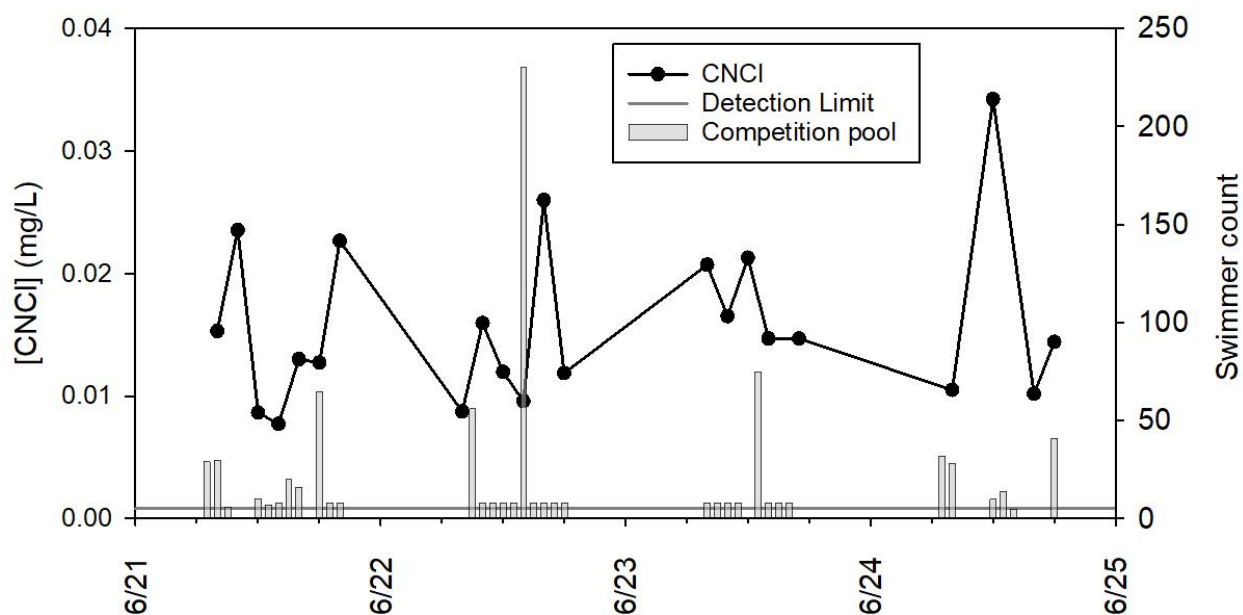


Figure 5.40. Time-course monitoring of aqueous-phase CNCl at pool facility B during swimming meet in June 2019. Vertical bars represent the number of swimmers in the pools. Horizontal line represents the detection limit.

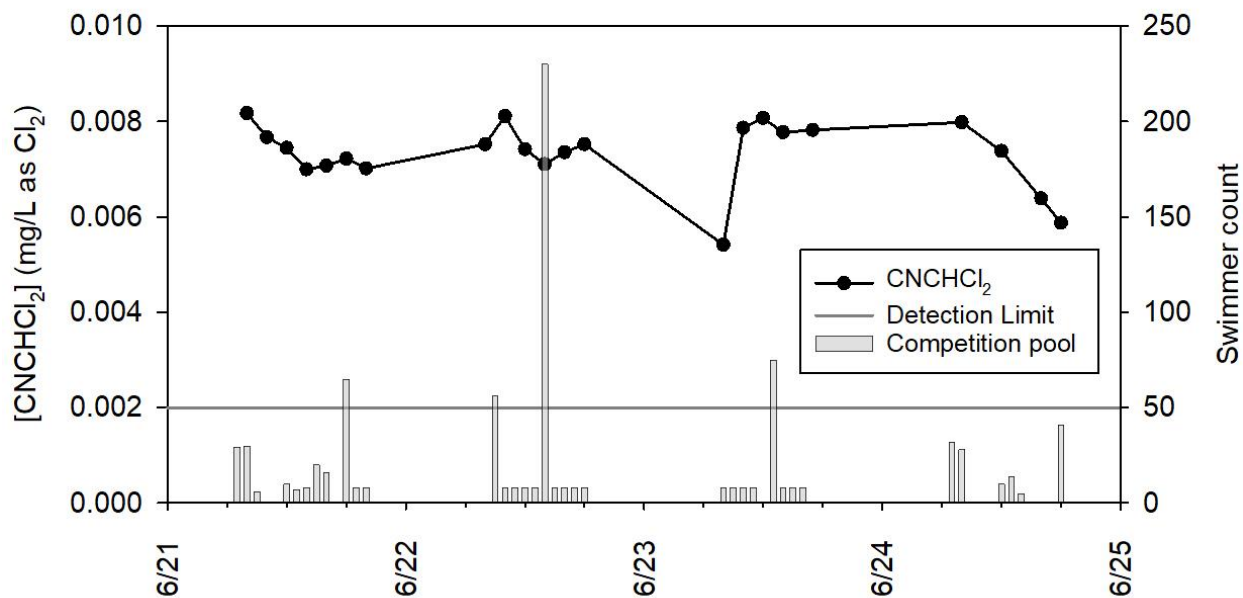


Figure 5.41. Time-course monitoring of aqueous-phase CNCHCl₂ at pool facility B during swimming meet in June 2019. Vertical bars represent the number of swimmers in the pools. Horizontal line represents the detection limit.

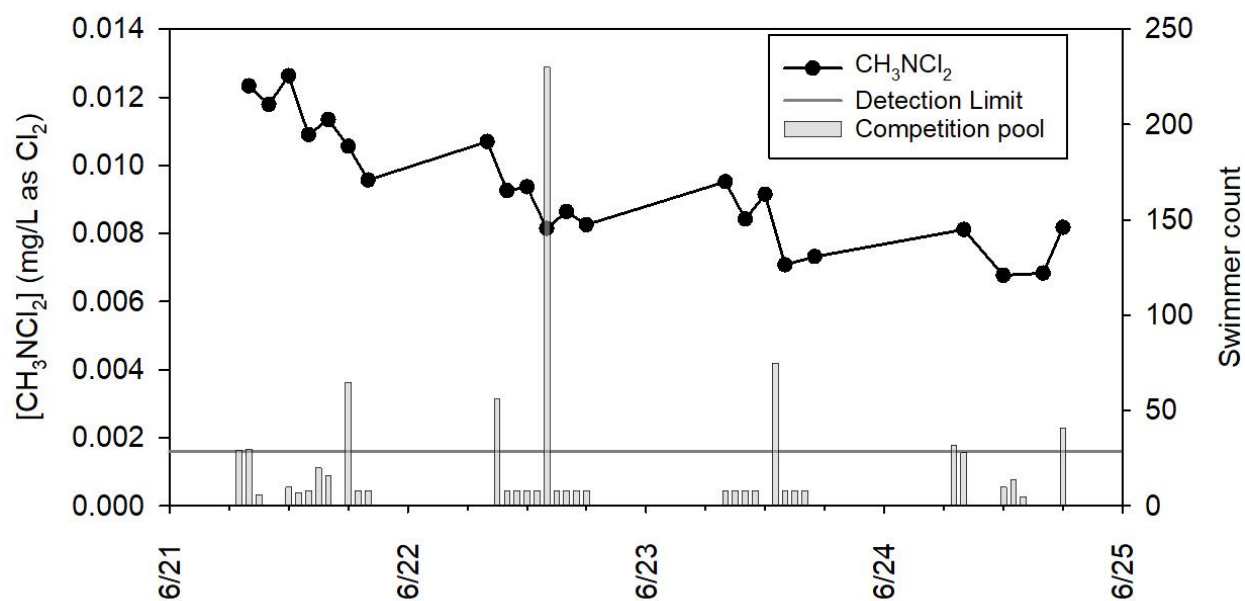


Figure 5.42. Time-course monitoring of aqueous-phase CH_3NCl_2 at pool facility B during swimming meet in June 2019. Vertical bars represent the number of swimmers in the pools. Horizontal line represents the detection limit.

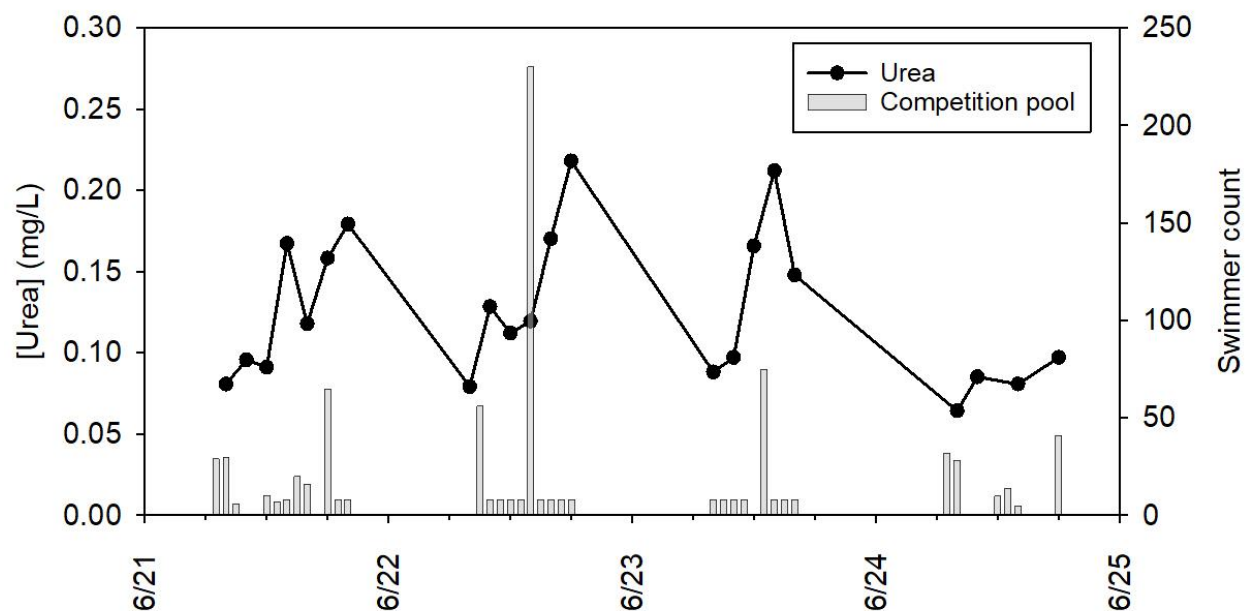


Figure 5.43. Time-course monitoring of aqueous-phase urea at pool facility B during swimming meet in June 2019. Vertical bars represent the number of swimmers in the pools.

Time-course monitoring of gas-phase NCl_3 with relative humidity (RH) is illustrated in Figure 5.44. RH values marginally exceeded 60% in both NEMo devices during this meet. As indicated previously, measurements of gas-phase NCl_3 represent underestimates when RH is above 60%. High gas-phase NCl_3 concentrations were generally observed early in each session, especially during warm-up periods, as shown in Figure 5.44. More than 100 swimmers were in the pool warming up at the beginning of each competition session. The number of swimmers present in the pool was manually counted at the top of every hour during this meet. Gas-phase NCl_3 concentrations reached as high as $800 \mu\text{g}/\text{m}^3$ in both NEMo devices. Additionally, concentrations of gas-phase NCl_3 dropped gradually after the warm-up period. Outside of the warm-up period, the concentrations of gas-phase NCl_3 were typically below $400 \mu\text{g}/\text{m}^3$ with both NEMo devices. During the overnight period when no people were in the facility, gas-phase NCl_3 was measured consistently around $100 \mu\text{g}/\text{m}^3$. We could consider that gas-phase NCl_3 reached baseline condition during the overnight period.

Results of time-course monitoring of gas-phase NCl_3 and gas-phase CO_2 by the NEMo devices are illustrated in Figure 5.45. Gas-phase CO_2 was measured as high as 1100 ppm_v from the NEMo devices during the swimming meet. Gas-phase CO_2 concentrations showed strong correlations with the number of people in the building during this meet; as many as 500 people were in the building during the meet. After the meet, CO_2 concentration dropped to around 450 ppm_v on 6/24/2019. Also, time-course trends in the gas-phase concentrations of CO_2 and NCl_3 were qualitatively similar throughout this swimming meet at facility B, as illustrated in Figure 5.45. Measurements of gas-phase NCl_3 and CO_2 from both NEMo devices were consistent with each other, thereby supporting the assumption that the air reached a well-mixed condition in this facility.

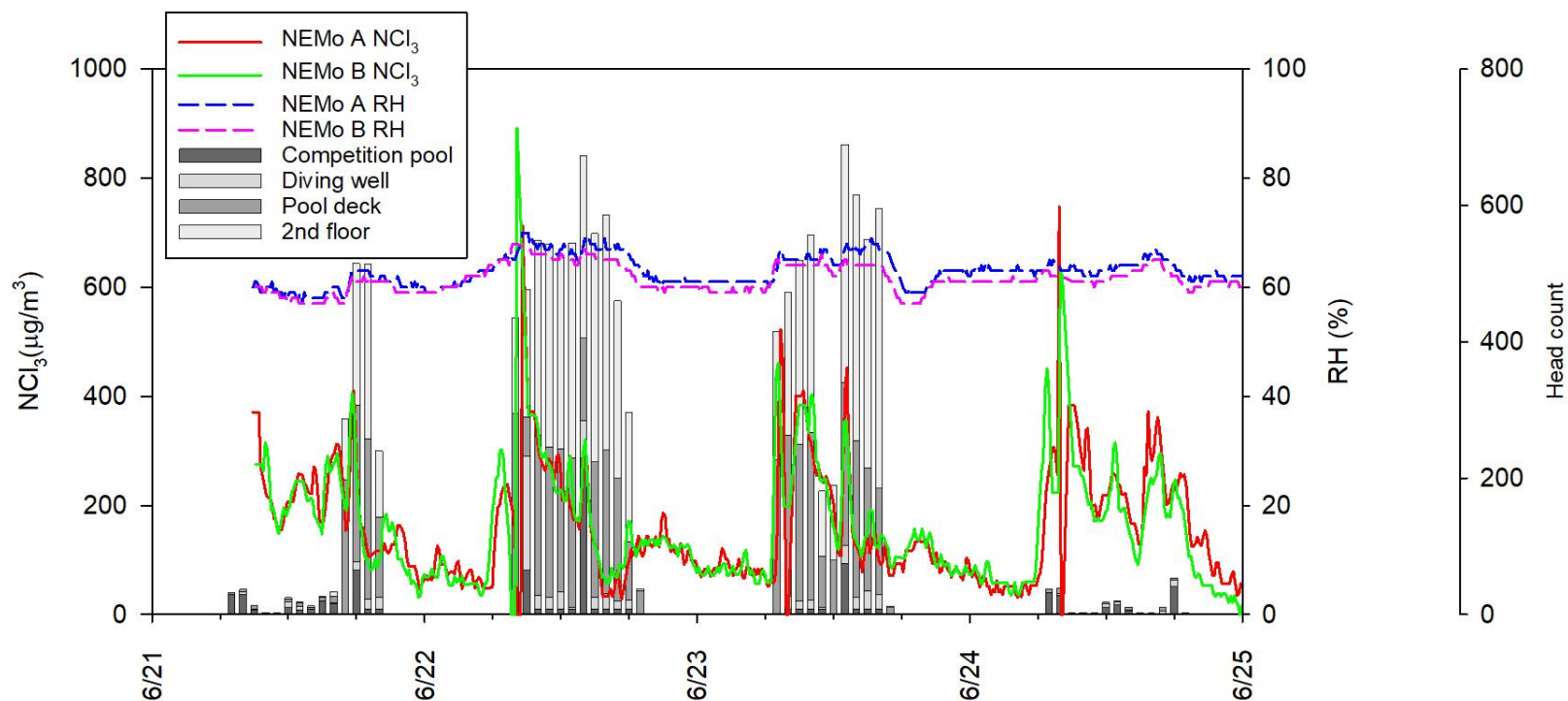


Figure 5.44. Time-course monitoring of gas-phase NCl_3 and RH, as measured by NEMo devices at pool facility B during swimming meet in June 2019. Vertical bars represent the number of people in each area of pool facility B.

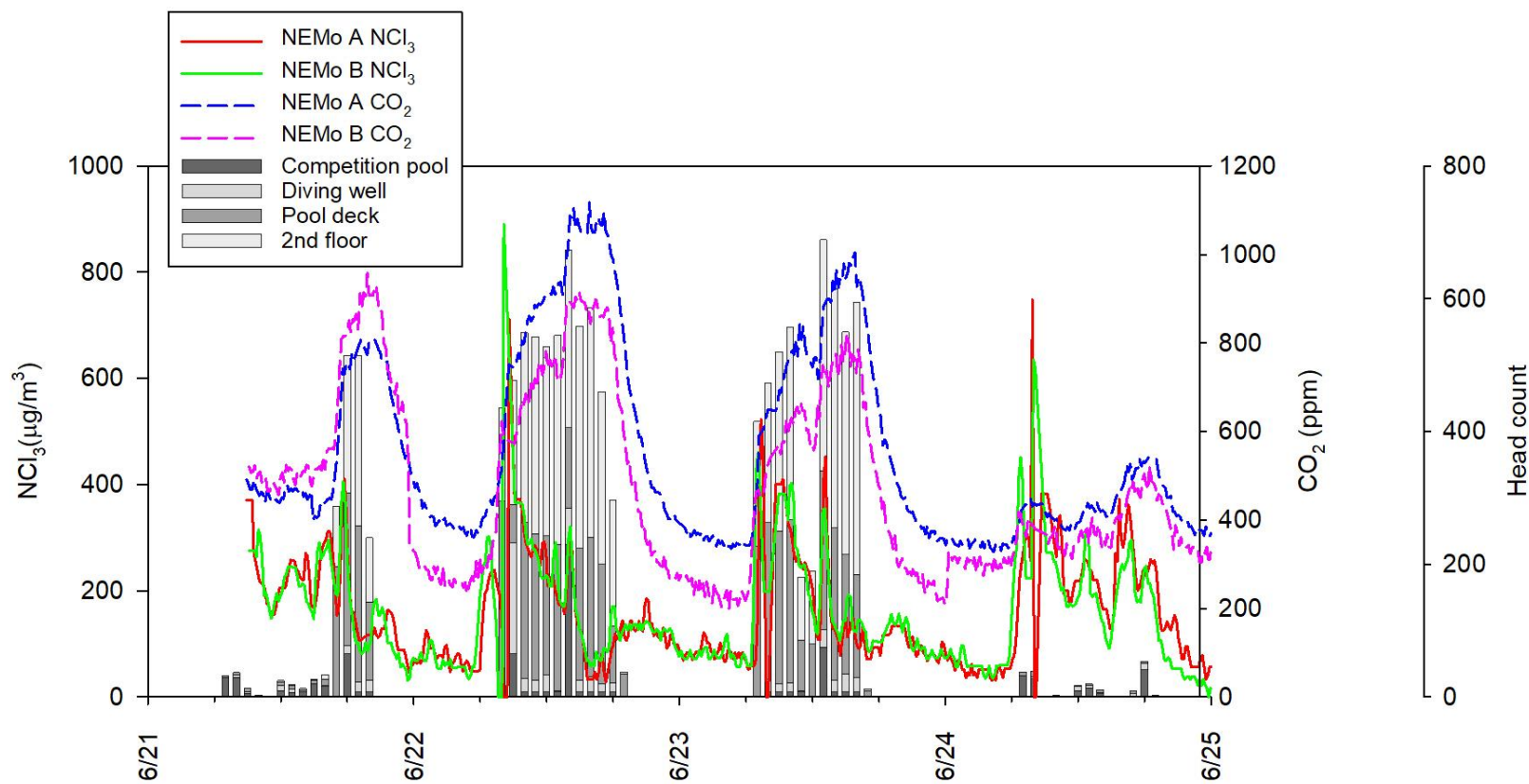


Figure 5.45. Time-course monitoring of gas-phase NCl_3 and gas-phase CO_2 , as measured by NEMo devices at pool facility B during swimming meet in June 2019. Vertical bars represent the number of people in each area of pool facility B.

5.1.5 Measurements in November 2019

Water and air quality monitoring were conducted during a swimming meet at facility B from 11/21/2019 to 11/24/2019. The meet was conducted as a short-course (25 yards) event for the period from 11/21/19-11/23/19; for the last day of the event, it was conducted as a long-course (50 meters) competition. Roughly 400 collegiate swimmers, male and female, participated in the meet. The short-course meet schedule ran from Thursday (11/21/2019) morning to Saturday (11/23/2019). The morning session each day began at 8:00 AM with a warm-up period and 10:00 AM for swim events. The evening session began at 4:30 PM with a warm-up period and 6:00 PM for swim events. On the final day of the meet (11/24/2019), long-course swimming activities involved roughly 40 swimmers and lasted from 9:00 AM to noon.

Water samples were collected every hour during the meet at 20 cm below the water surface at the location illustrated in Figure 3.13. Two NEMo devices (A and B) were installed during this meet and their locations within the pool area are illustrated in Figure 3.14.

Time-course measurements of the concentrations of free chlorine and total chlorine are illustrated in Figure 5.46. Concentrations of free chlorine ranged from 0.5 to 2.7 mg/L as Cl_2 and concentrations of total chlorine ranged from 1.0 to 3.0 mg/L as Cl_2 . The concentrations of combined chlorine (total chlorine - free chlorine) were close to 0.4 mg/L as Cl_2 throughout the experiment. The range of combined chlorine was similar to other studies conducted at this pool facility. pH ranged between 7.1 to 7.3 during this meet as indicated in Figure 5.47, while alkalinity ranged between 65 to 95 mg/L as CaCO_3 , as shown in Figure 5.48. Aqueous-phase CO_2 concentrations were calculated from measurements of pH, alkalinity, and temperature (Tucker, 1984). As water temperature was not recorded during the study period, water temperature was assumed to be 25°C throughout this experiment period. The trend of aqueous CO_2 concentration is illustrated in Figure 5.49. The aqueous CO_2 concentrations fluctuated between 8 and 12 mg/L.

The bench top MIMS system was being maintained during this experiment, thus only the portable MIMS system was available to analyze water samples throughout the swimming meet. CHCl_3 appeared to be the only volatile DBP that was measurable by the portable MIMS system (*i.e.*, present at concentrations above the limit of detection), as illustrated in Figure 5.50. Concentrations of CHCl_3 declined from day-to-day during the study period, possibly because of selective removal of volatile compounds by the mixing action of swimmers; similar behavior was observed during the June 2019 experiment. Previous studies have shown that chloroform is

produced largely by reactions between free chlorine with natural organic matter (NOM). It is also known that the precursors for fast CHCl_3 formation include compounds with resorcinol-like structures (Gallard and Von Gunten, 2002).

Time-course monitoring of the concentration of urea is illustrated in Figure 5.51. The measurements of urea indicate accumulation of urea each day throughout the meet, clearly indicating the influence of swimmers. Urea concentration decreased overnight, probably due to mixing that occurred as a result of circulation of water through the treatment system.

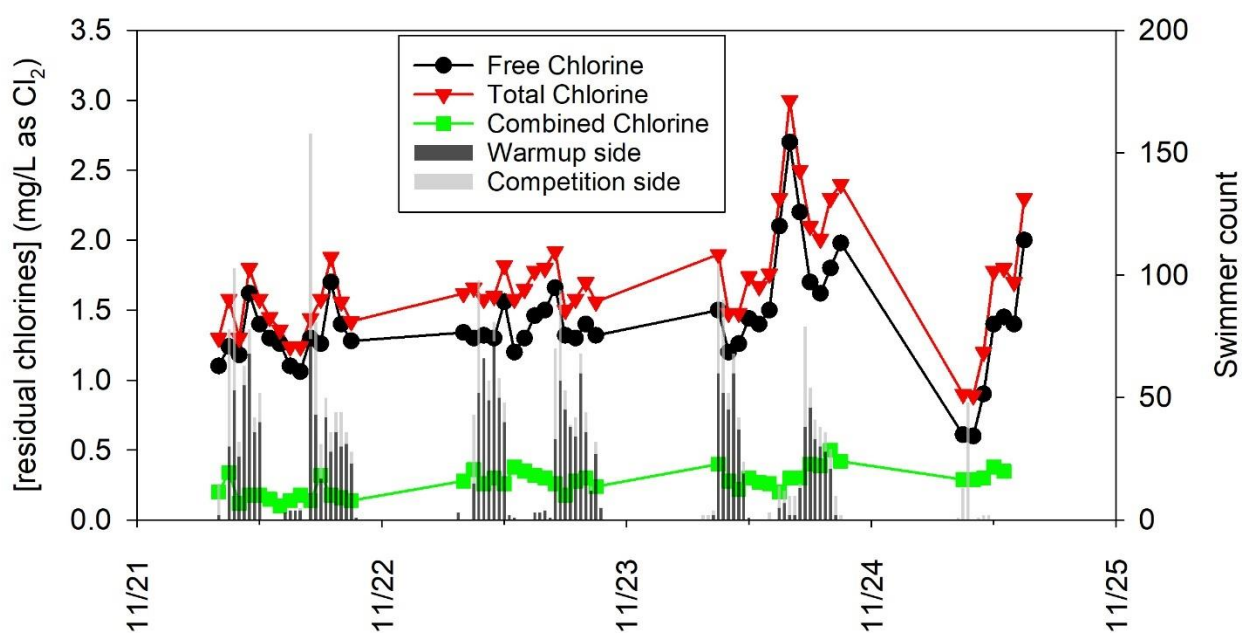


Figure 5.46. Time-course monitoring of free and total chlorine at pool facility B during swimming meet in November 2019. Vertical bars represent the number of swimmers in the pool.

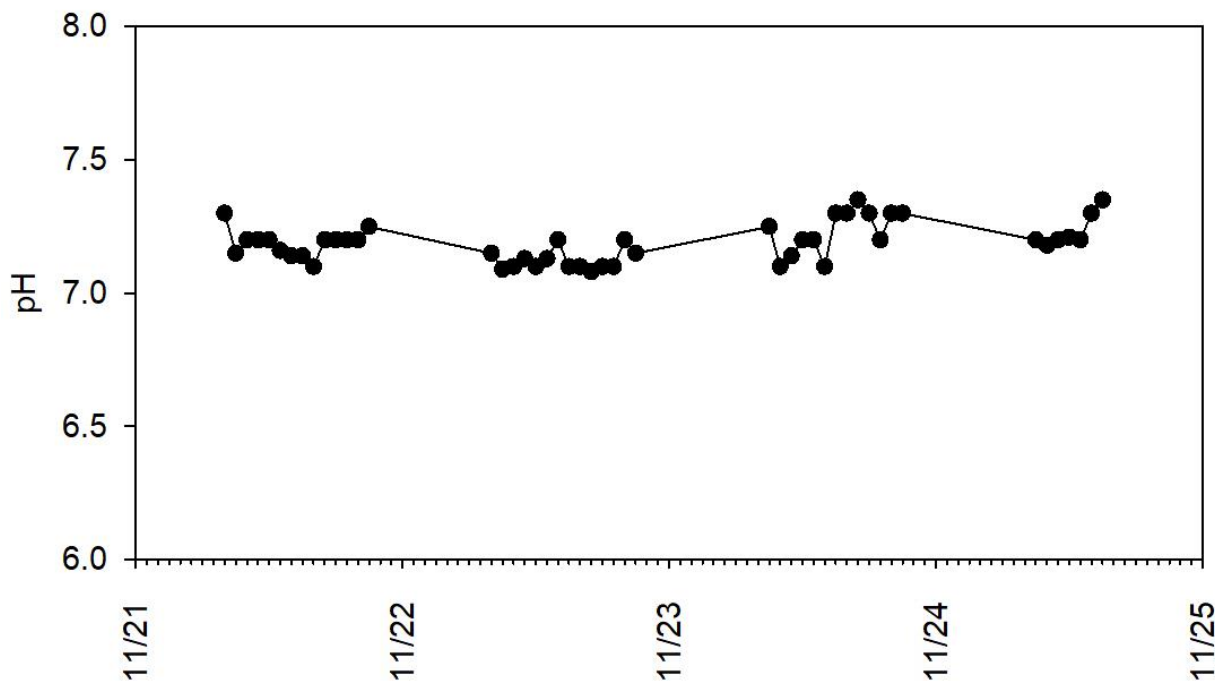


Figure 5.47. Time-course monitoring of pH at pool facility B during swimming meet in November 2019.

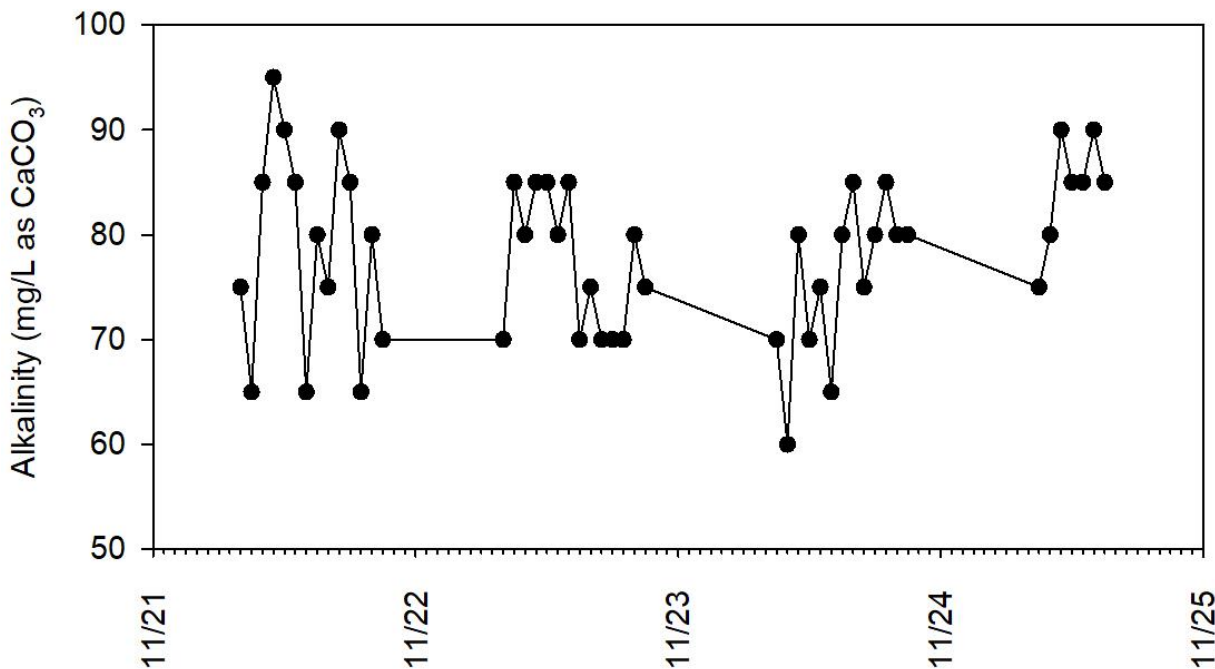


Figure 5.48. Time-course monitoring of alkalinity at pool facility B during swimming meet in November 2019.

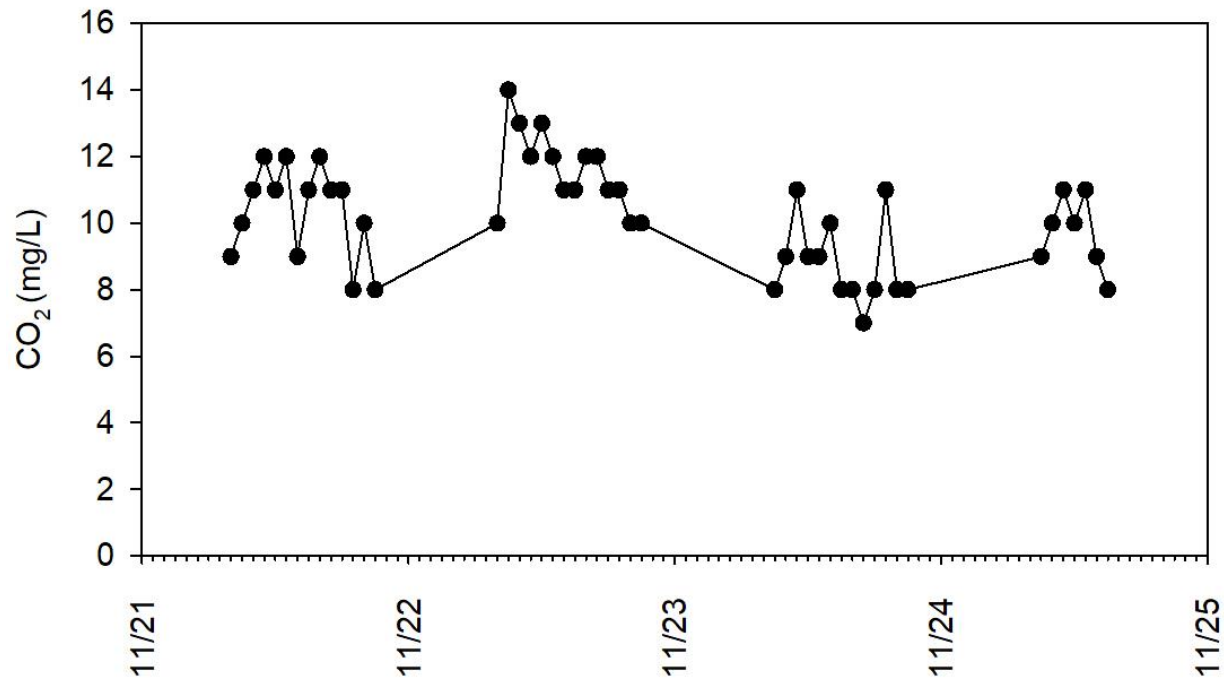


Figure 5.49. Trend of calculated aqueous-phase CO₂ at pool facility B during swimming meet in November 2019.

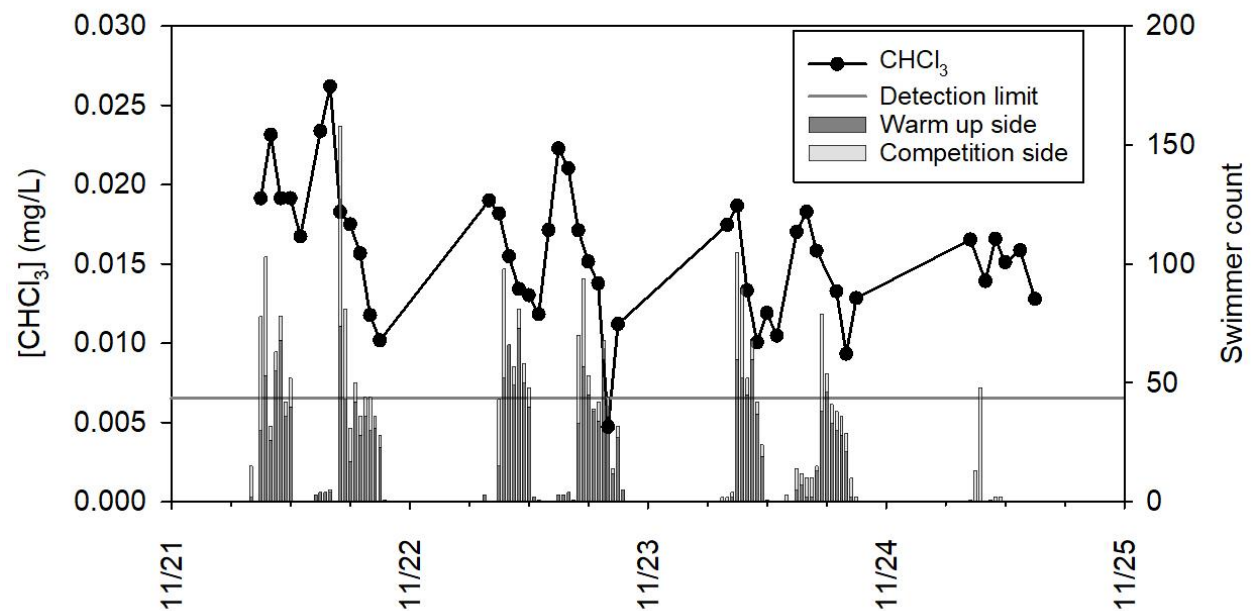


Figure 5.50. Time-course monitoring of CHCl₃ at pool facility B during swimming meet in November 2019. Vertical bars represent the number of swimmers in the pool. Horizontal line represents the detection limit.

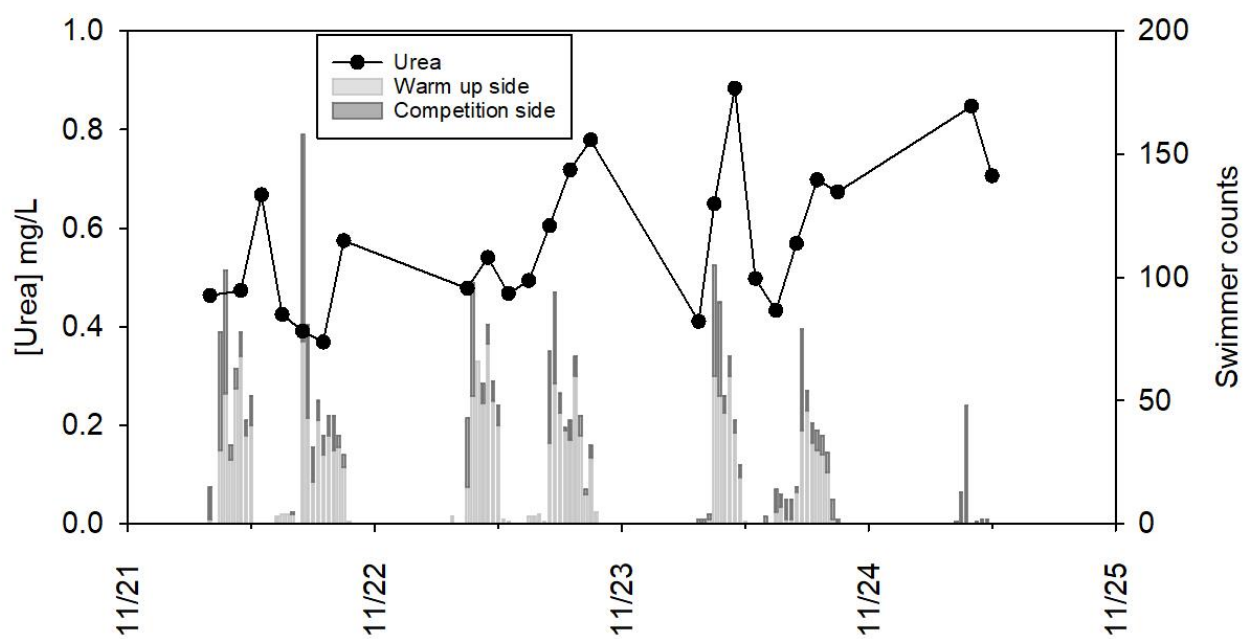


Figure 5.51. Time-course monitoring of urea at pool facility B during swimming meet in November 2019. Vertical bars represent the number of swimmers in the pool.

Time-course monitoring of gas-phase NCl_3 and relative humidity, as measured by the NEMo devices, is illustrated in Figure 5.52. RH values were marginally below 60% for both NEMo devices during this meet. As indicated previously, measurements of gas-phase NCl_3 represent underestimates when RH is above 60%. High concentrations of gas-phase NCl_3 were noticeable immediately after swimmers were present in the pool as concentrations were measured higher than $400 \mu\text{g}/\text{m}^3$ during warm-up periods when there were more than 100 swimmers in the pool at the same time. The highest gas-phase NCl_3 concentrations were observed on the third day of this meet, with measured concentrations as high as $1100 \mu\text{g}/\text{m}^3$. The number of swimmers present in the pool was manually counted by volunteers every half-hour during this meet. Concentrations of gas-phase NCl_3 dropped gradually after the warm-up period. Concentrations of gas-phase NCl_3 were mostly below $400 \mu\text{g}/\text{m}^3$ with both NEMo devices during swimming meet events, when the number of swimmers in the pool was low (8 swimmers at a time). The air flow rate was manually adjusted at 9:00 am 11/23 as swimming coaches and swimmers starting to sense that the indoor air quality was not comfortable.

Results of time-course monitoring of gas-phase NCl_3 with gas-phase CO_2 by the NEMo devices are illustrated in Figures 5.53. Gas-phase CO_2 was measured higher than 1100 ppm_v from the NEMo devices during the swimming meet. Gas-phase CO_2 concentrations also showed strong correlations with the number of people in the facility during this meet. There were more than 400 people in the facility on several occasions. The majority of people in the facility were actually on the second floor in the spectator area during the swimming meet. The number of people that were outside the pool also included swimmers resting and waiting at the pool deck as well as coaches and meet officials. These people should not affect the dynamic behavior of gas-phase NCl_3 but could affect the dynamic behavior of gas-phase CO_2 . Gas-phase CO_2 was likely transferred from liquid-phase to gas-phase by the swimmer's activity; also CO_2 was released to the air space of the pool by normal respiratory activities of the athletes and audience during the meet. Thus, number of people in the pool and outside the pool are likely to play roles in terms of gas-phase CO_2 concentration.

After the meet concluded each day, CO_2 concentration dropped immediately and approached the outside, ambient concentration. In general, time-course trends in the gas-phase concentrations of CO_2 and NCl_3 were qualitatively similar throughout this swimming meet at facility B.

During this study, a LI-830 Trace Gas Analyzer (LI-COR Biosciences, Lincoln, Nebraska) was installed to measure gas-phase CO₂ in facility B during the meet. This CO₂ monitor was able to record concentrations of gas-phase CO₂ in every 30 seconds thus it provided more detailed information regarding CO₂ dynamics than the NEMo devices, which reported gas-phase CO₂ concentrations once every 10 minutes. This analyzer was coupled with an automated switching valve system that connected Teflon tubing to 4 sampling locations including bulk air, surface air, supply air, and return air. The layout is illustrated in Figure 3.13. Samples of Bulk air were collected from 3.2 meters above the pool deck and 0.5 meters away from pool surface. Samples of surface air were collected from 0.4 meters above pool deck and 0.5 meters away from pool surface. Samples of supply air were collected from one HVAC unit. Samples of return air were measured from a return air grille. The sampling sequence was repeated as follows: return air (6 min), supply air (6 min), surface air (12 min), bulk air (12 min), surface air (12 min), and bulk air (12 min), with a full cycle of 1 hour. Additionally, the data collected in the first 2 min and last 30 seconds after the valve switch were disregarded for data analysis. This was done to mitigate the influence of the sudden pressure change on the instruments and the potential “memory effect” in the sampling system. The concentration history of gas-phase CO₂ is shown in Figure 5.54.

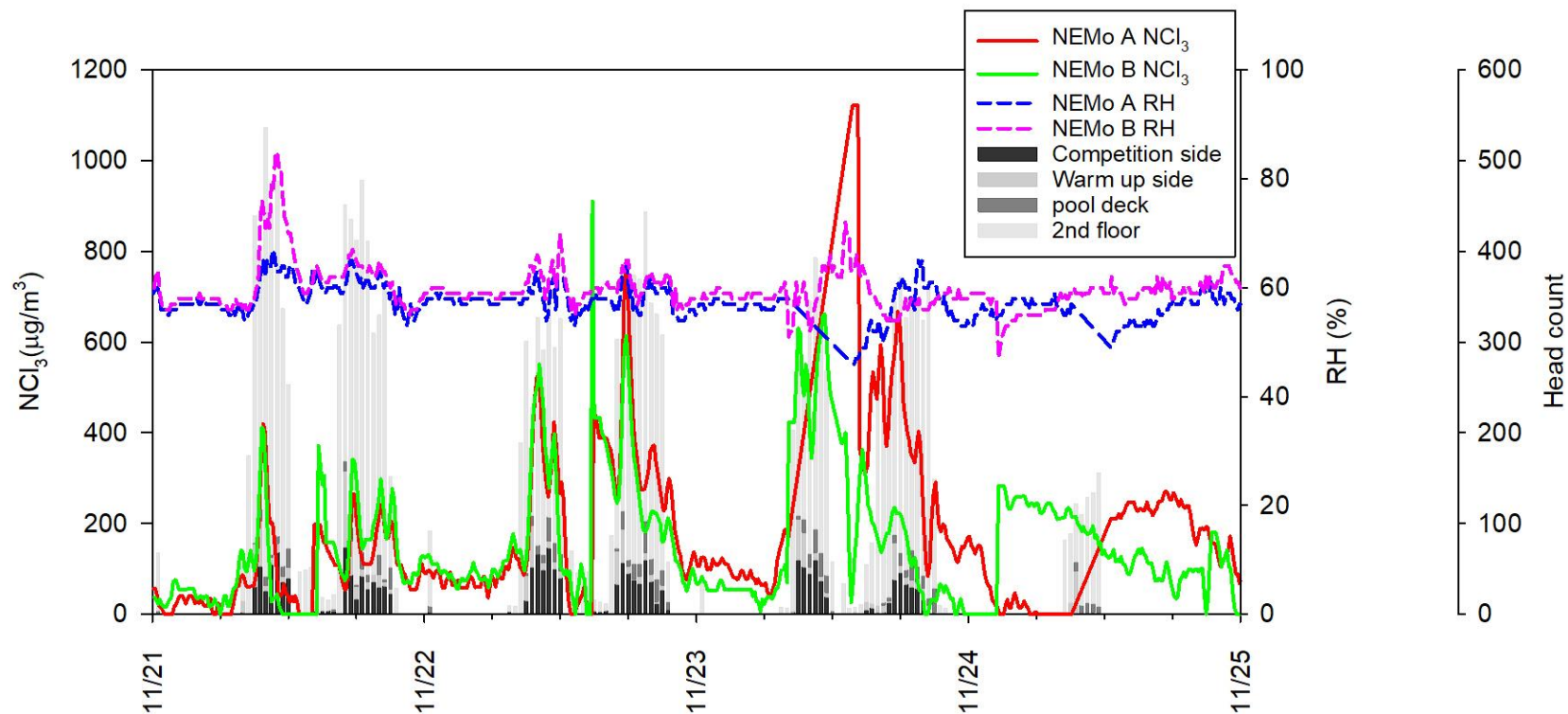


Figure 5.52. Time-course monitoring of gas-phase NCl_3 and relative humidity (RH) measured by NEMo devices at pool facility B during swimming meet in November 2019. Vertical bars represent the number of people in each area of pool facility B.

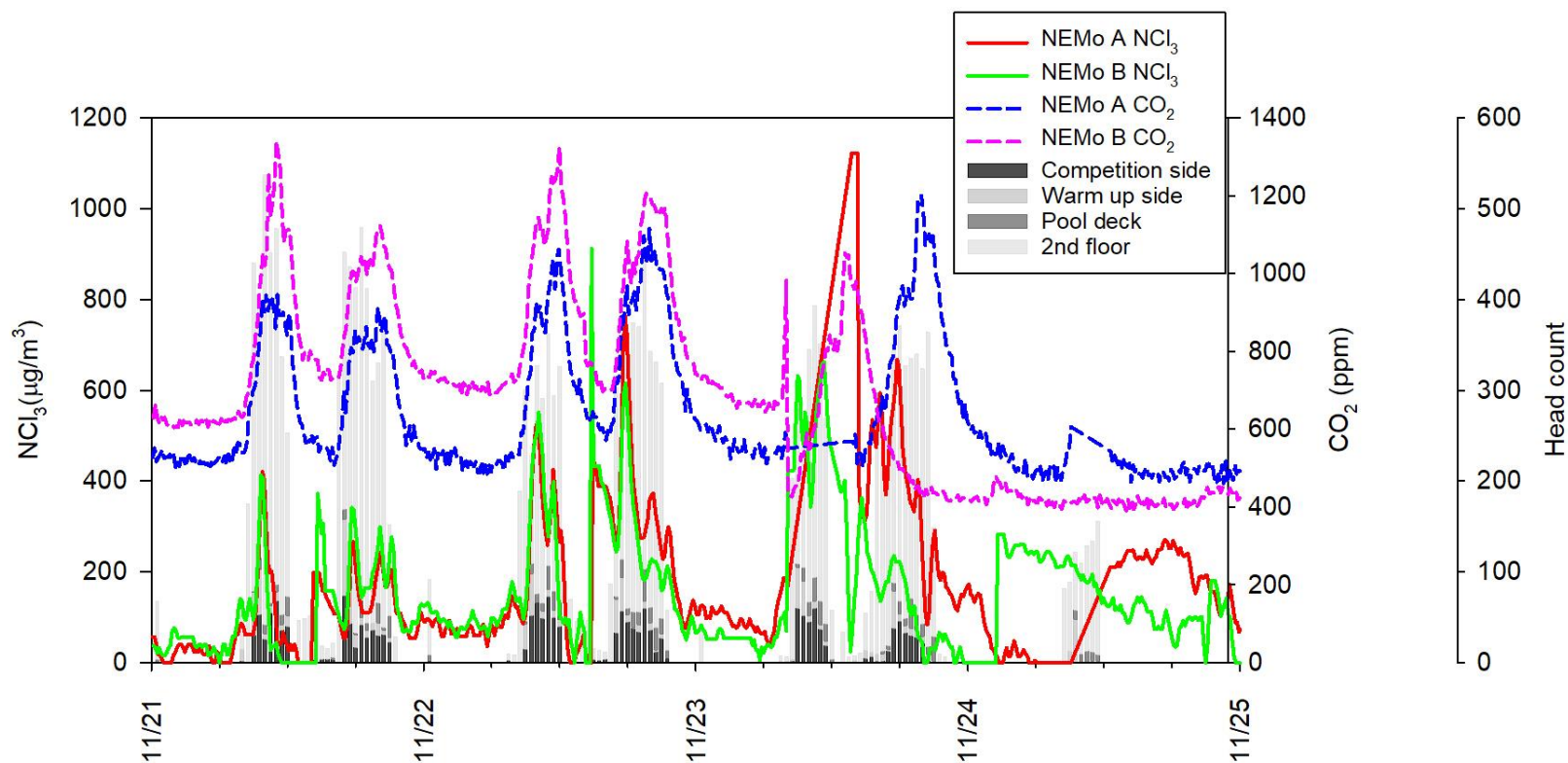


Figure 5.53. Time-course monitoring of gas-phase NCl_3 with gas-phase CO_2 measured by NEMo devices at pool facility B during swimming meet in November 2019. Vertical bars represent the number of people in each area of pool facility B.

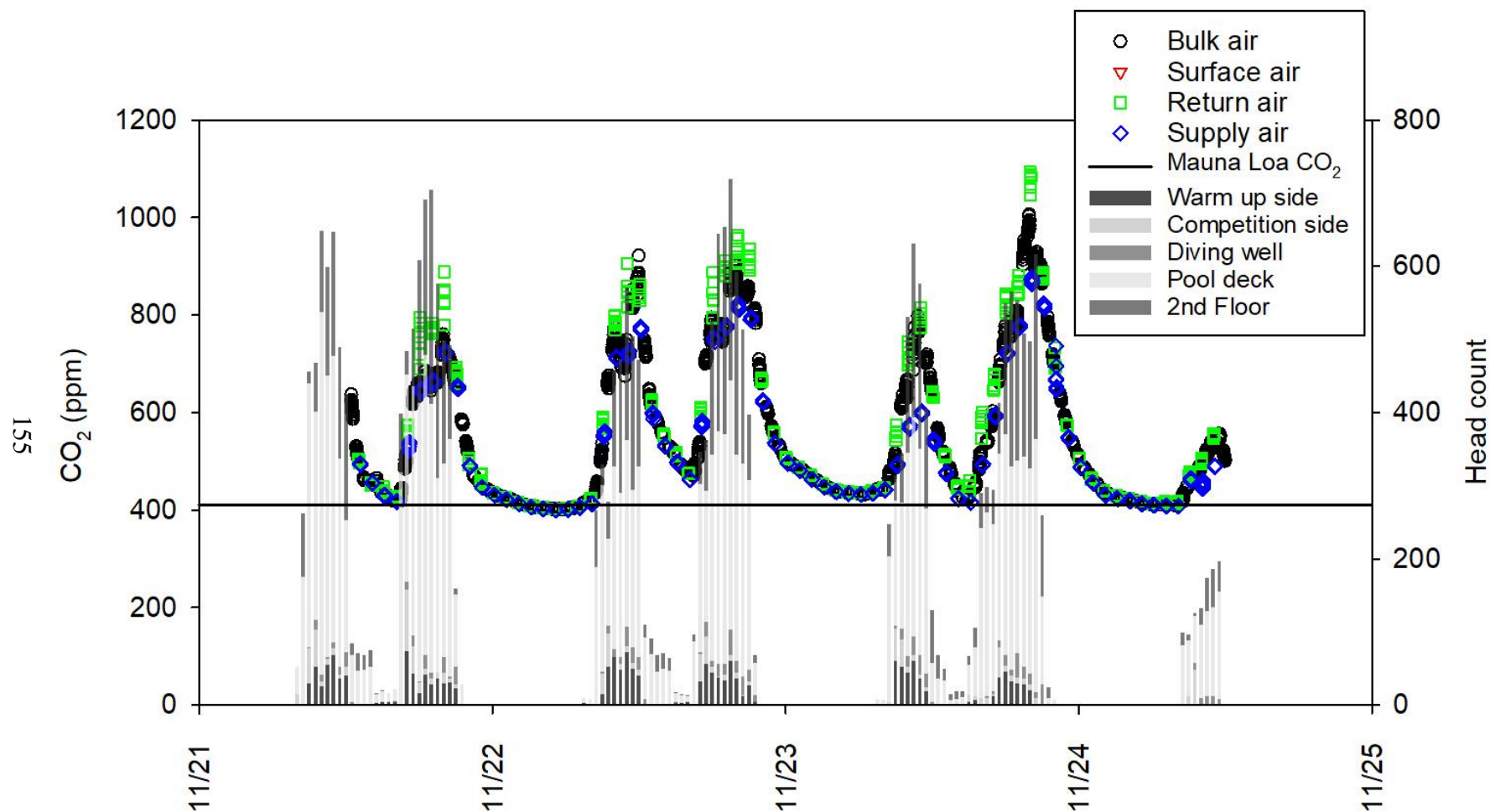


Figure 5.54. Time-course monitoring of gas-phase CO₂ measured by LI-830 Trace Gas Analyzer at pool facility B during swimming meet in November 2019. Vertical bars represent the number of people in each area of pool facility B.

5.2 Measurements at Pool facility C

Water and air quality monitoring were conducted during a swimming meet at facility C from 3/15/2019 to 3/17/2019. This meet started on Friday (3/14/2019) in the morning, but travel logistics delayed sample collection and analysis until 3/15/2019. An early competition session on 3/15/2019 was held from 7:30 AM to 12:30 PM, with a late session from 4:30 PM to 8:30 PM. Only one session was held on 3/16/2019 and 3/17/2019, with both being held from 8:30 AM to 1:00 PM. The competition was conducted as a short-course (25 yards) meet for swimmers ages 13 to 18. Approximately 300 swimmers participated in this meet. This pool was configured as two sides (warm up side and competition side), with these two spaces separated by a bulkhead. The two swimming areas were part of the same body of water. Three NEMO devices were operated during this swimming meet and their locations around the pool area are illustrated in Figure 3.10. Water samples were collected before, during, and after the swimming events each day. Water samples were collected 20 cm below the water surface at the corner of the competition side of the pool, as shown in Figure 3.10.

Time-course measurements of free chlorine and combined chlorine concentration are illustrated in Figure 5.55. Concentrations of free chlorine ranged from 1.0 to 1.7 mg/L as Cl_2 and concentrations of total chlorine ranged from 1.5 to 2.2 mg/L as Cl_2 . Estimates of combined chlorine (total chlorine – free chlorine) were generally close to 0.5 mg/L as Cl_2 but slowly increased throughout the meet. pH was stable during this meet, with measured values typically at or slightly below pH 7.5, as indicated in Figure 5.56. Concentrations of urea ranged from 0.1 to 0.3 mg/L. Concentrations of urea generally increased through the course of the meet as shown in Figure 5.57. A diurnal pattern of urea concentration was observed in this study, especially between second day and third day. The factors that may have contributed to this pattern include pool recirculation behavior, mixing behavior at the location of sample collection, and input of urea from swimmers. Concentrations of urea were similar to those measured during the June 2019 swimming meet (Figure 5.43), but were much lower than those observed during swimming meets in February 2019 (Figure 5.8) and November 2019 (Figure 5.51). The overall urea concentration will be influenced by free chlorine concentration, mixing behavior (caused by ambient water recirculation and swimmer activity), and urea input from swimmers.

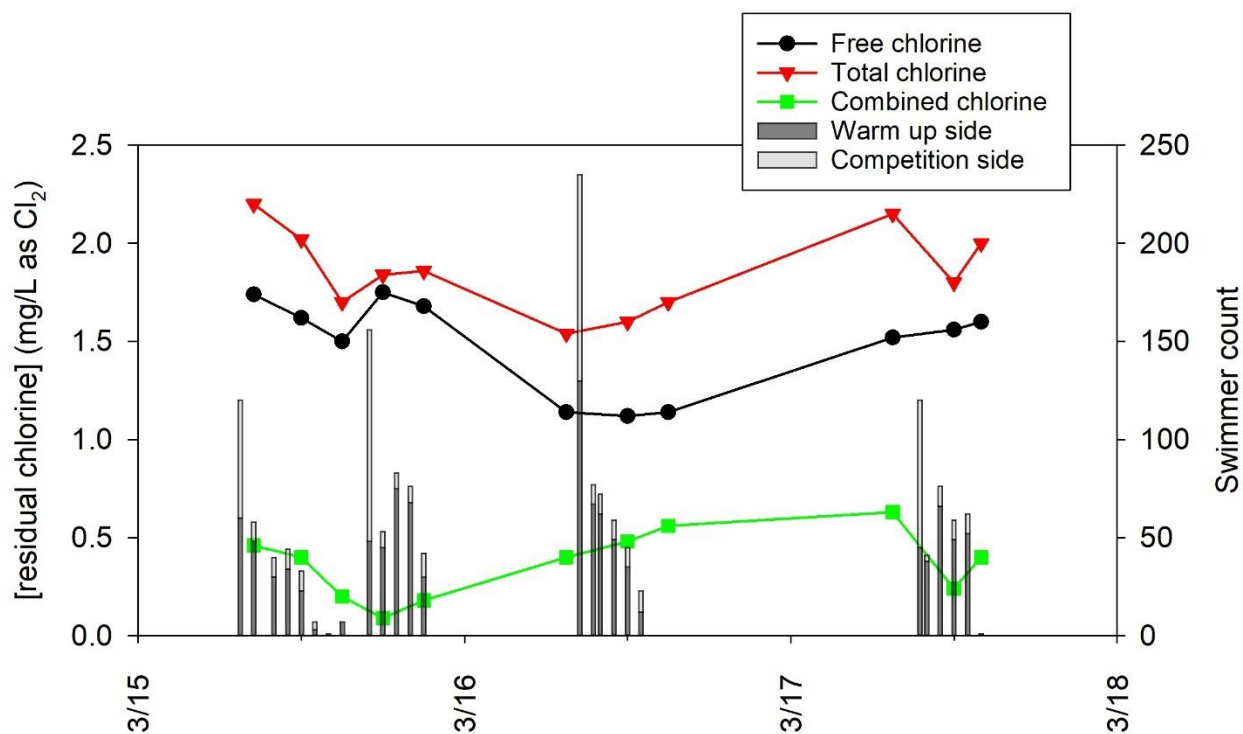


Figure 5.55. Time-course monitoring of free and total chlorine at pool facility C during swimming meet in March 2019. Vertical bars represent the number of swimmers in the pool.

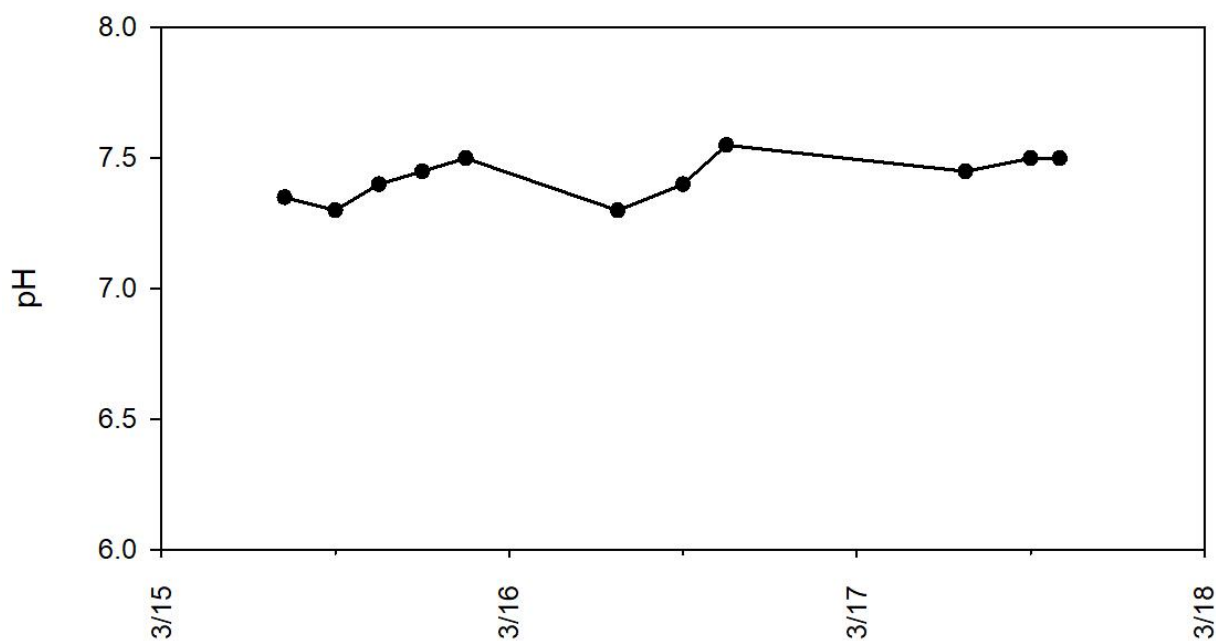


Figure 5.56. Time-course monitoring of pH at pool facility C during swimming meet in March 2019.

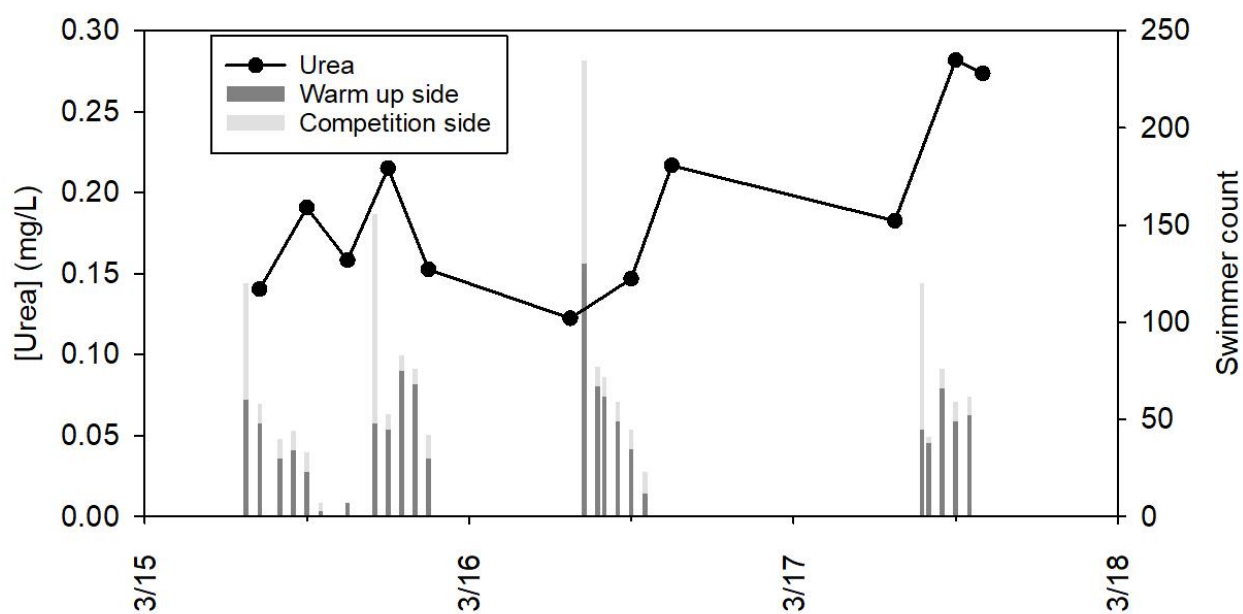


Figure 5.57. Time-course monitoring of urea at pool facility C during swimming meet in March 2019. Vertical bars represent the number of swimmers in the pool.

Time-course measurements of gas-phase NCl_3 with relative humidity (RH) are illustrated in Figure 5.58. RH values exceeded 60% for all three NEMo devices on 3/15/2019 and roughly half of 3/16/2019, but RH values reduced to below 60% on the morning of 3/16/2019. High gas-phase NCl_3 concentrations were generally observed at the beginning of each session, especially during warm-up periods when the largest number of swimmers were in the water, as shown in Figure 5.58. The number of swimmers present in the pool was manually counted at the top of every hour during this meet. Gas-phase NCl_3 concentrations reached as high as $1200 \mu\text{g}/\text{m}^3$ for all three NEMo devices. The concentration of gas-phase NCl_3 dropped sharply after each warm-up period. Outside of the warm-up period, concentrations of gas-phase NCl_3 were below $700 \mu\text{g}/\text{m}^3$ for all three NEMo devices. Generally, when swimmers were absent from the pool, the gas-phase NCl_3 was less than $200 \mu\text{g}/\text{m}^3$. This concentration may be considered as the baseline condition at this pool facility.

Time-course monitoring of gas-phase NCl_3 and gas-phase CO_2 were conducted using the NEMo devices, with results shown in Figure 5.59. Gas-phase CO_2 was observed to be as high as 1800 ppm_v for each of the NEMo devices during the swimming meet. Gas-phase CO_2 concentration showed strong correlation with the number of swimmers in the pool during this meet. However, it is possible that spectators may contribute significantly to the gas-phase CO_2 concentration in this facility. Therefore, the number of spectators in the facility and the number of people on the pool deck were counted after this meet.

A strong correlation was evident between the trends of gas-phase concentrations of CO_2 and NCl_3 throughout this swimming meet. Measurements of gas-phase NCl_3 and CO_2 concentration from all three NEMo devices around the pool facility C also suggested that the air space in this facility closely conformed to a well-mixed condition. As described previously, this has important implications with respect to the IAQ model for these facilities.

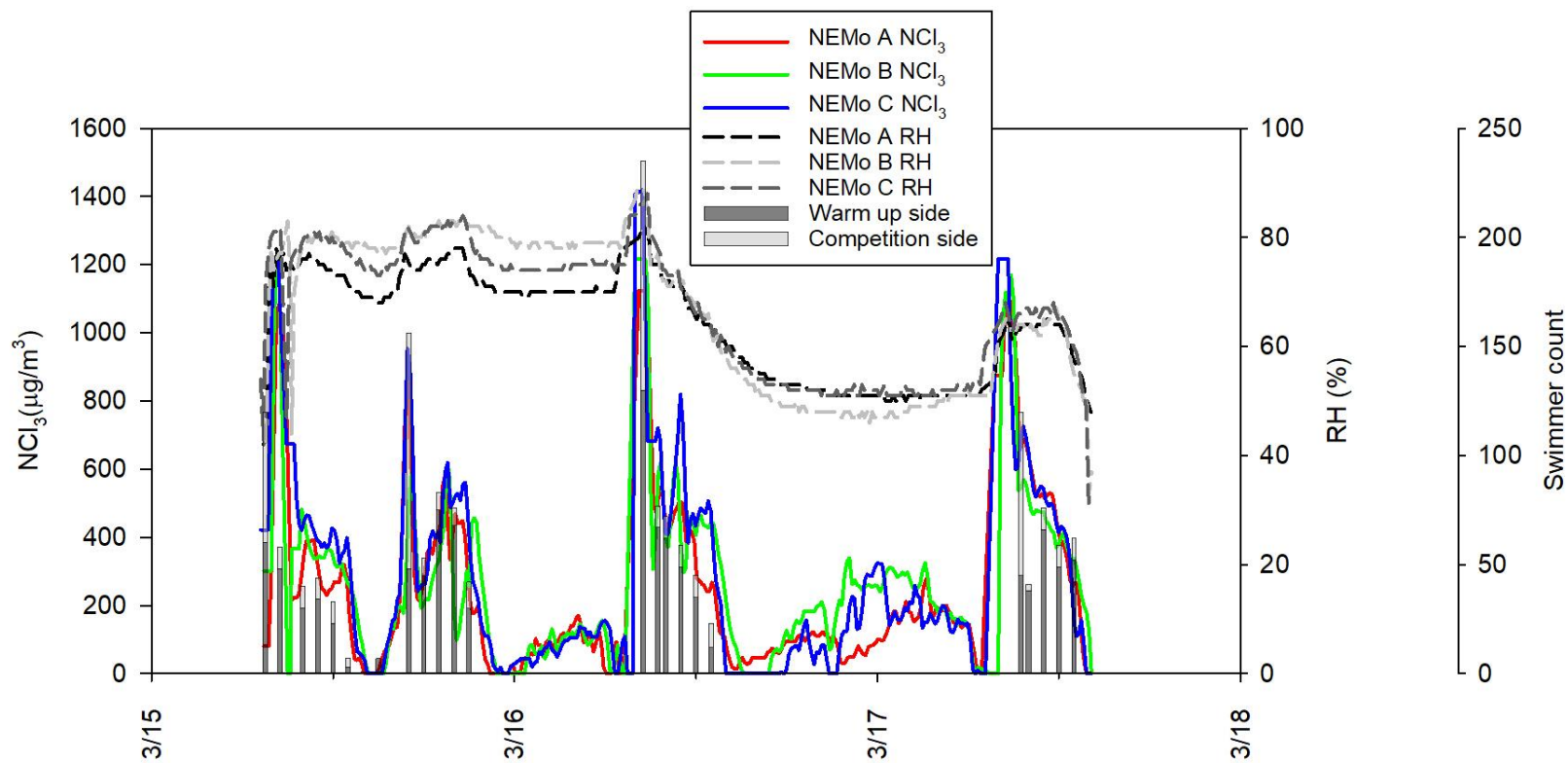


Figure 5.58. Time-course monitoring of gas-phase NCl_3 and RH measured by NEMo devices at pool facility C during swimming meet in March 2019. Vertical bars represent the swimmer number in the pool area.

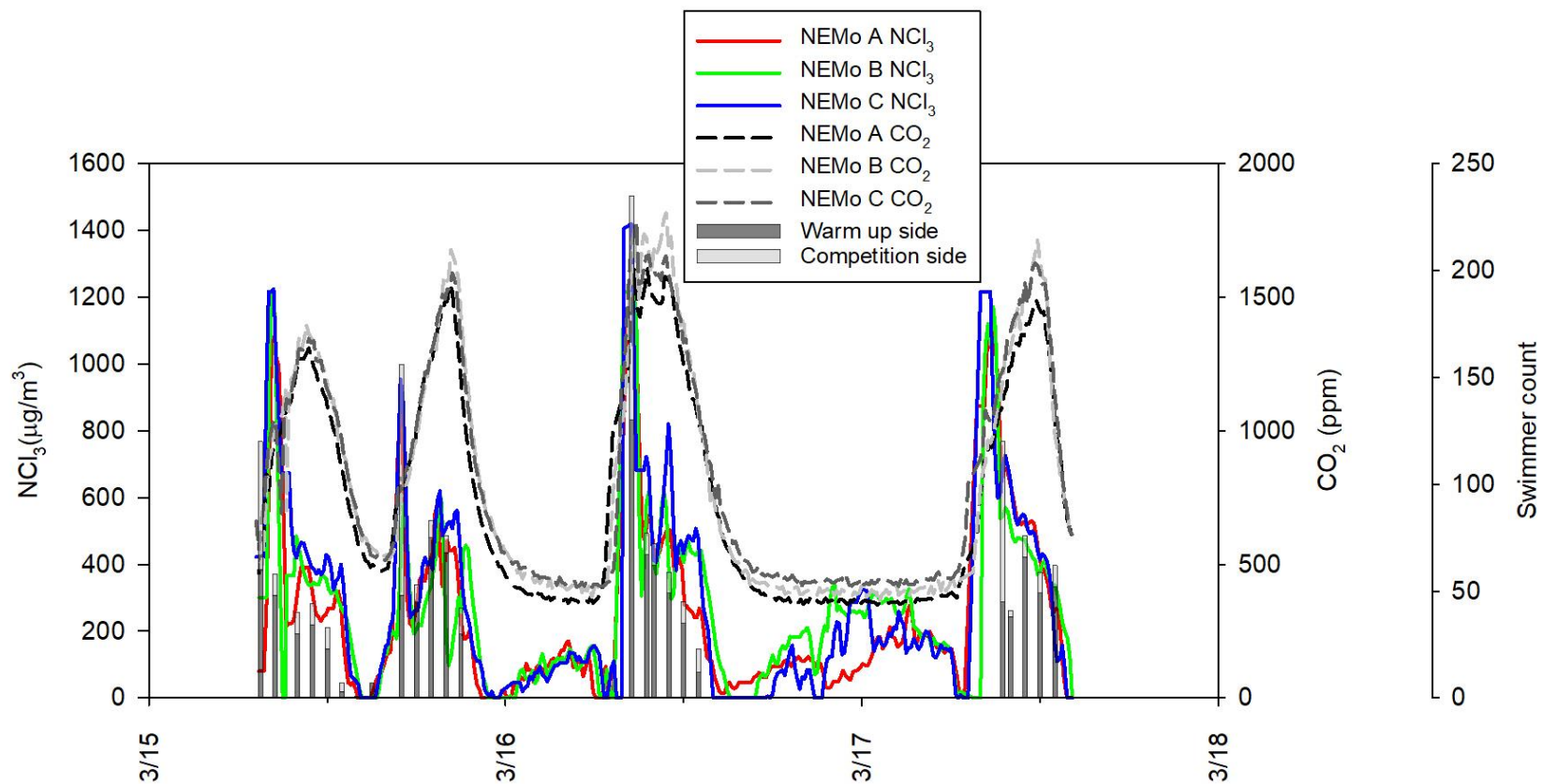


Figure 5.59. Time-course monitoring of gas-phase NCl_3 with gas-phase CO_2 measured by NEMo devices at pool facility C during swimming meet in March 2019. Vertical bars represent the swimmer number in the pool area.

5.3 Measurements at Pool facility D

Water and air quality monitoring were conducted during a swimming meet at facility D from 8/3/2019 to 8/4/2019. Events on 8/3/2019 were held from 7:00 AM to 8:00 PM and on 8/4/2019 from 7:00 AM to 7:00 PM. It was a short-course (25 yards) competition for age 14 and under swimmers. Approximately 200 swimmers participated in this swimming meet. Water samples were collected every hour during the meet. The Portable MIMS device was positioned immediately adjacent to the pool deck area to allow measurements of volatile DBPs in water samples hourly. Two NEMo devices were installed during this meet and their locations around the pool area are shown in Figure 3.13. Water samples were collected 20 cm below the water surface from a location near the center of pool, as shown in Figure 3.13.

Time-course measurements of the concentration of free chlorine and total chlorine are illustrated in Figure 5.60. Concentrations of free chlorine ranged from 1.2 to 3.5 mg/L as Cl_2 and concentrations of total chlorine ranged from 1.5 to 3.5 mg/L as Cl_2 . Higher initial free chlorine concentrations were measured at this pool facility compared with other facilities and experiment periods. Measurements of combined chlorine (total chlorine – free chlorine) were below 0.3 mg/L as Cl_2 during the majority of the meet. Concentrations of combined chlorine were in the same range as other experiment periods. pH was stable during this meet as indicated in Figure 5.61. Alkalinity was close to 100 mg/L (as CaCO_3) throughout the study period, as shown in Figure 5.62. Aqueous-phase CO_2 concentrations were calculated from pH, alkalinity, and water temperature as illustrated in Figure 5.63. As water temperature was not recorded, a water temperature of 25°C was assumed for this meet.

Measurements of volatile DBPs and urea in water samples are shown in Figures 5.64-5.66. Only NCl_3 , CHCl_3 , and CNCl were measurable (above detection limit) for water samples collected during this meet and analyzed by the portable MIMS system. Concentrations of aqueous phase NCl_3 steadily increased during both days of the competition, rising from roughly 0.1 to 0.5 mg/L as Cl_2 . This behavior suggests that its rate of formation was greater than the rate of liquid→gas transfer and its rate of decay. The decline of NCl_3 overnight may have been caused by recirculation within the pool or its decay or loss by volatilization.

Concentrations of CHCl_3 slowly decreased throughout this meet and concentrations of CNCl were relatively stable. CHCl_3 trend at this location is likely to be influenced by mixing behavior by swimmers, transport within the pool, liquid to gas transfer, and the reactions that led to its

formation and decay. The decline suggests that rate of loss was greater than rate of formation and swimmer's behavior promoted liquid to gas transfer during the swimming meet. The factors that are likely to influence the trend of CNCl concentration include free chlorine, pH, and swimmer's activity, mixing/transport within the pool, and rate of formation and decay. The initial peak of CNCl could be due to the high free chlorine concentration at the start of the meet. However, free chlorine could also promote the decay of CNCl, thereby causing the concentration of CNCl to diminish. The stable concentration suggests that rate of formation was similar to the sum of the rate of decay and liquid to gas transfer.

The concentration of urea steadily increased during the meet. Measured concentrations of urea ranged from 0.1 to 0.3 mg/L as shown in Figure 5.67. No diurnal pattern was observed during this meet. Factors that influenced this pattern are likely to have included: mixing behavior at the location of sample collection and transport within the pool.

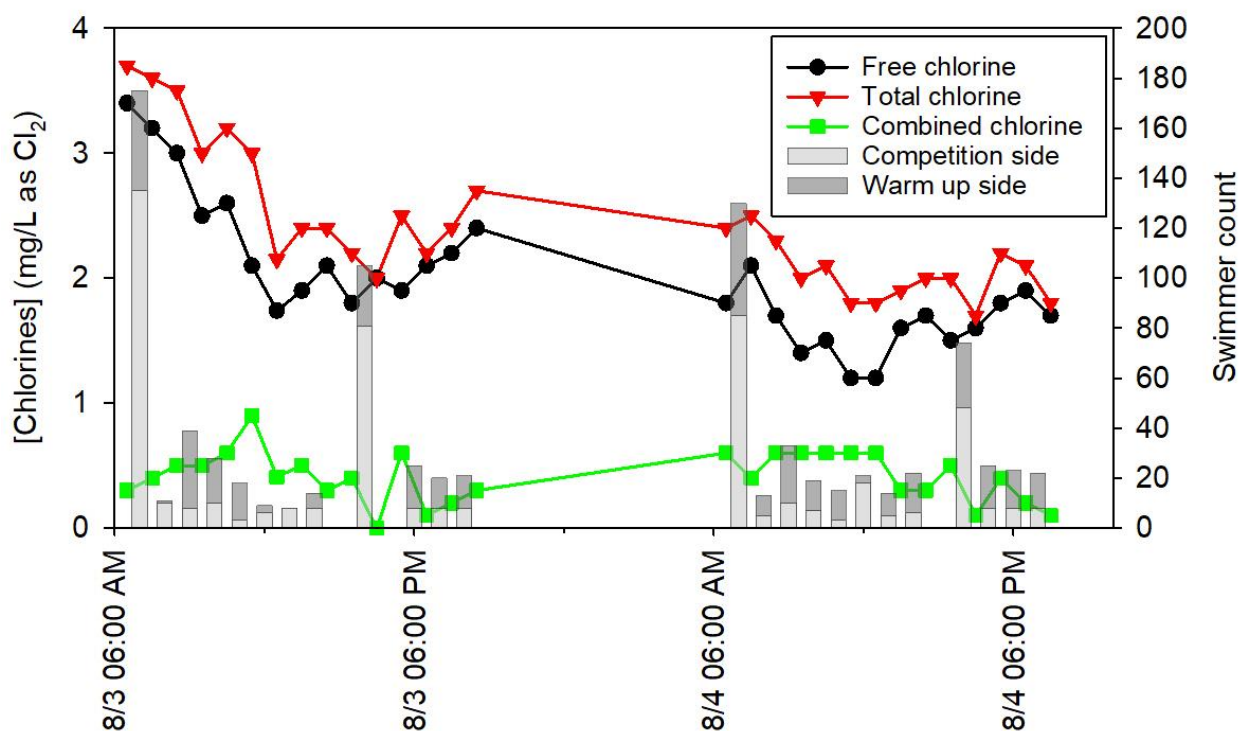


Figure 5.60. Time-course monitoring of free and total chlorine at pool facility D during swimming meet in August 2019. Vertical bars represent the number of swimmers in the pool.

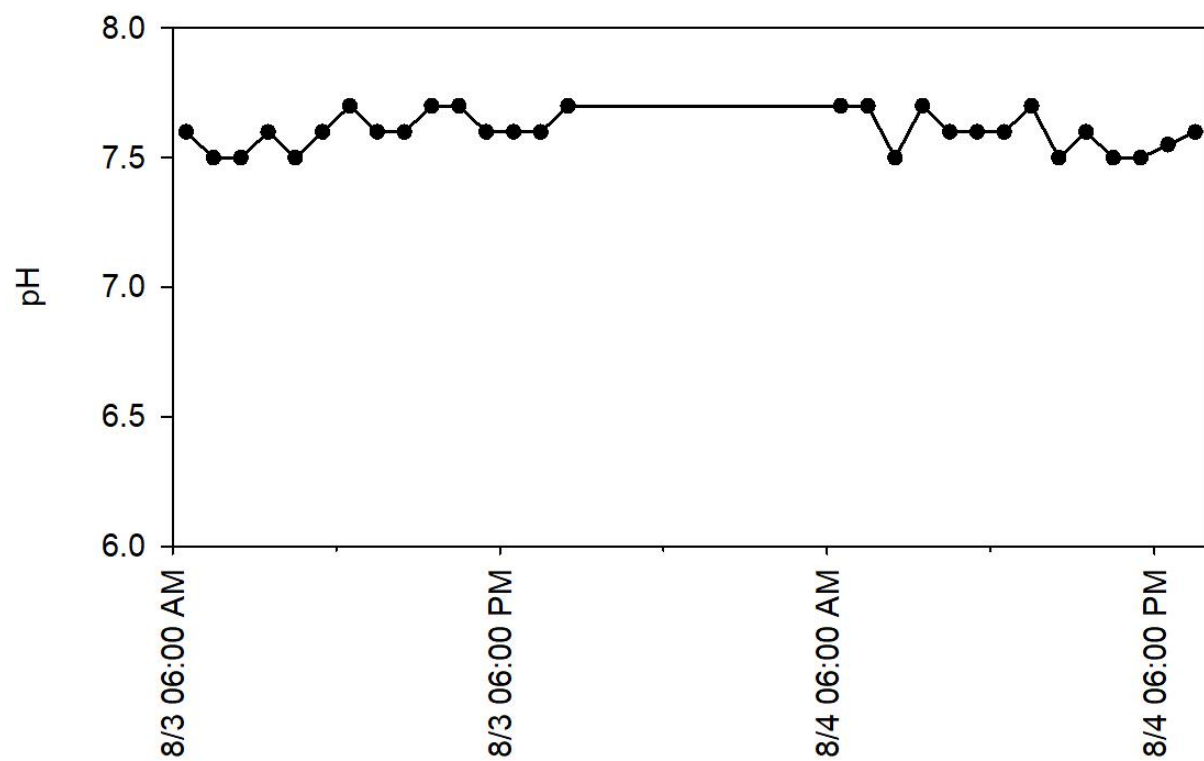


Figure 5.61. Time-course monitoring of pH at pool facility D during swimming meet in August 2019.

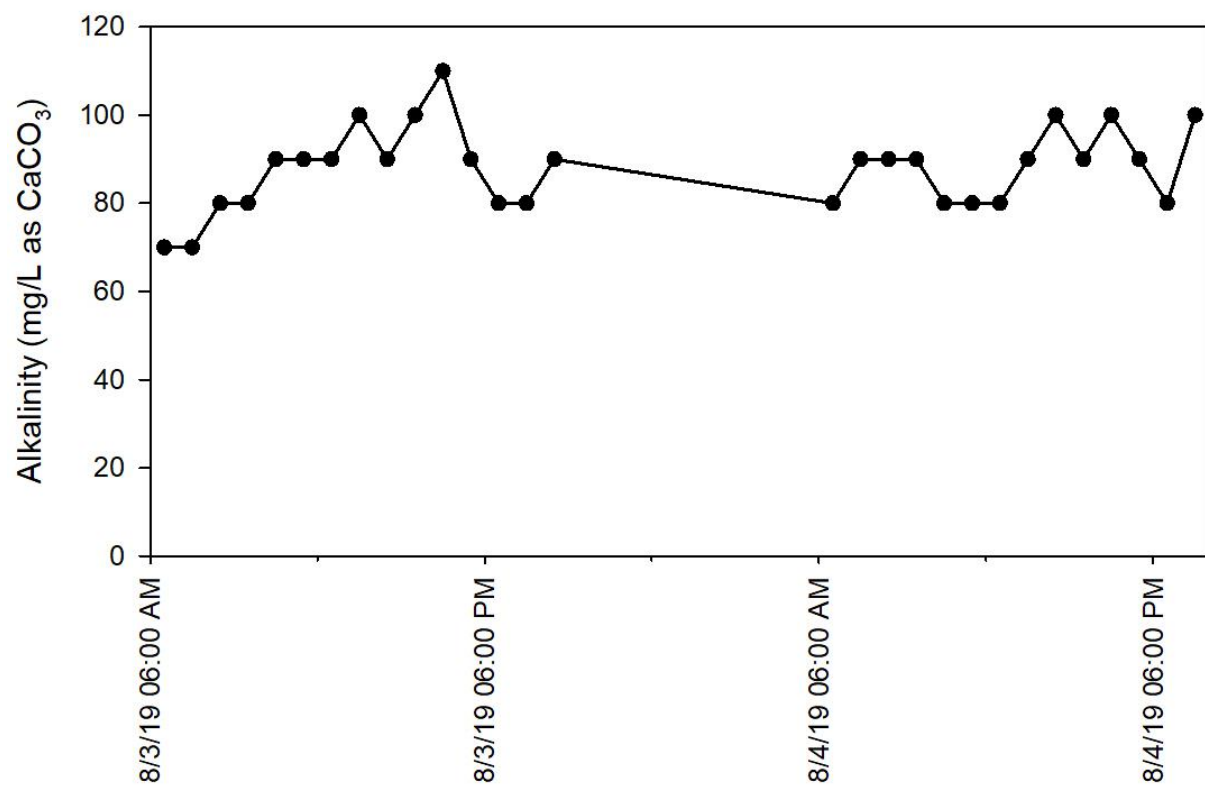


Figure 5.62. Time-course monitoring of alkalinity at pool facility D during swimming meet in August 2019.

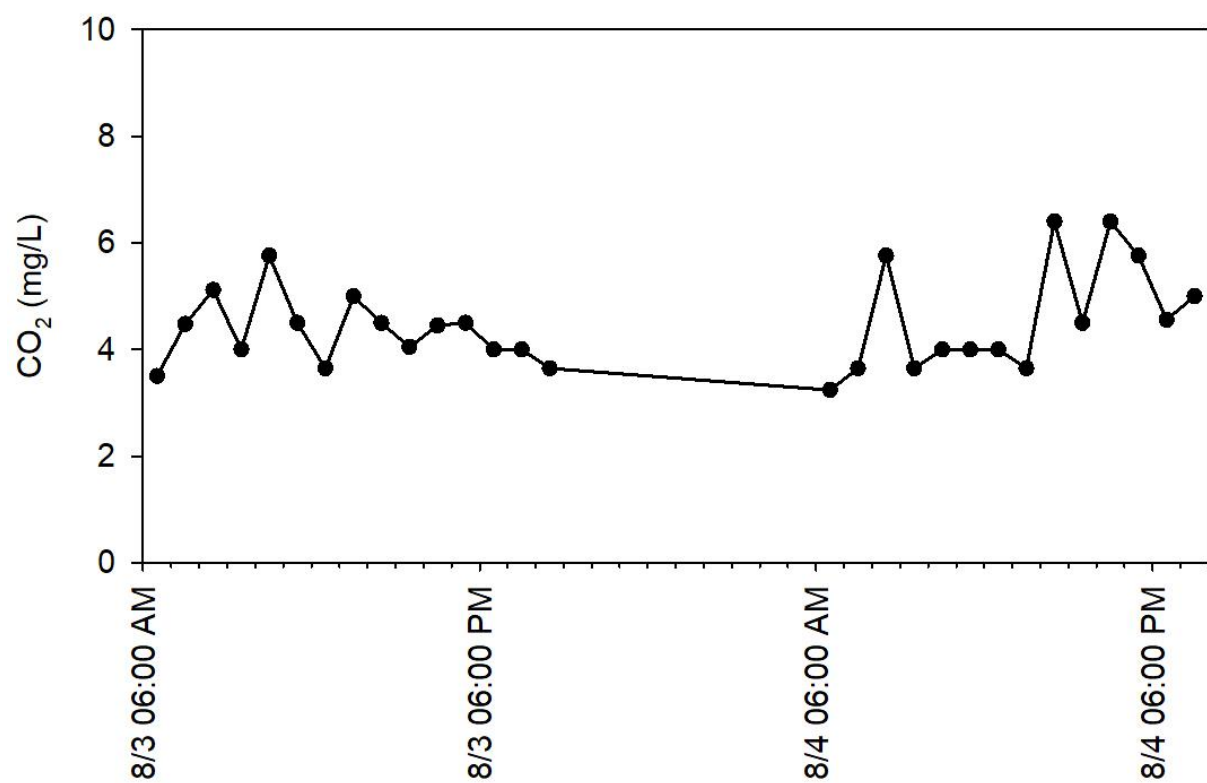


Figure 5.63. Trend of calculated aqueous-phase CO₂ at pool facility D during swimming meet in August 2019.

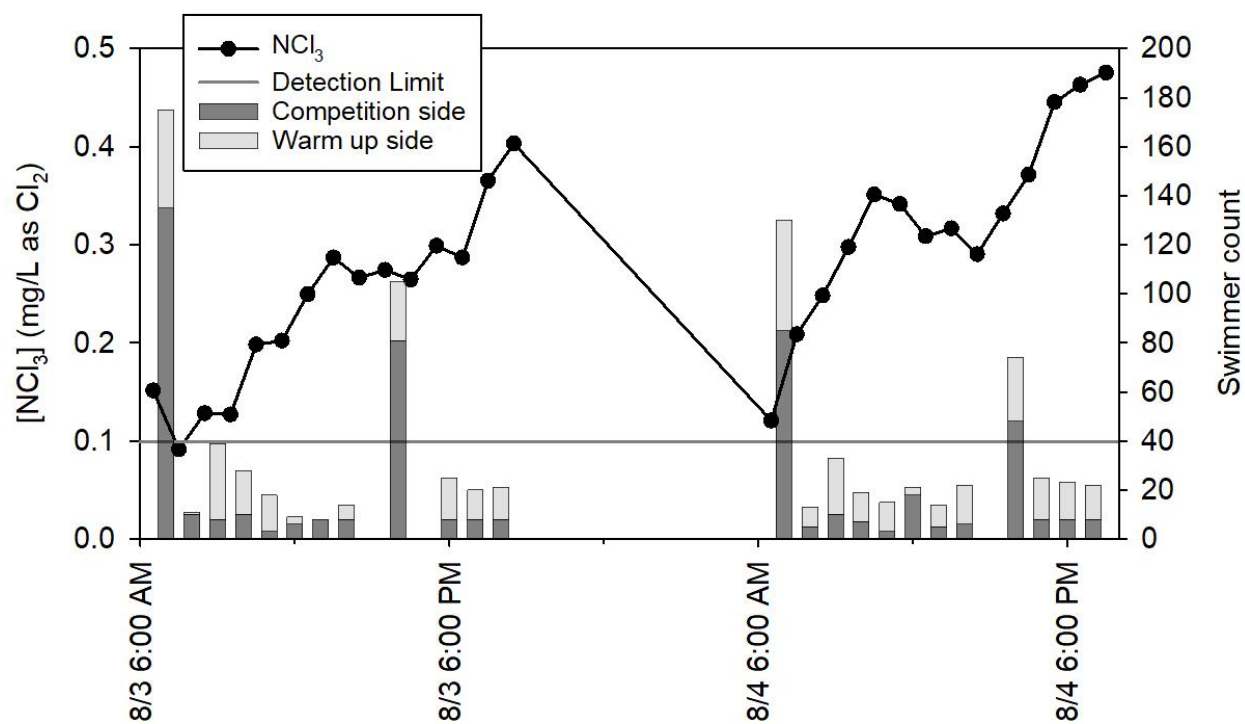


Figure 5.64. Time-course monitoring of liquid-phase NCl_3 concentration by portable MIMS at pool facility D during swimming meet in August 2019. Vertical bars represent the number of swimmers in the pool. Horizontal line represents the detection limit.

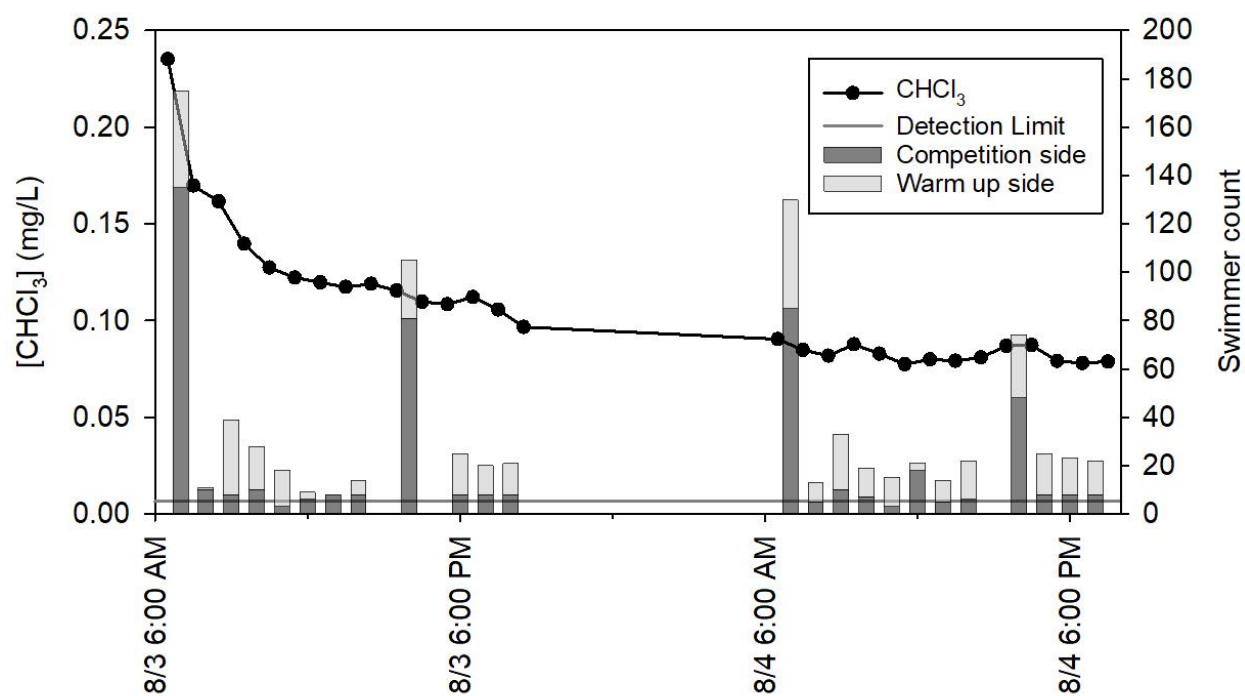


Figure 5.65. Time-course monitoring of aqueous-phase CHCl_3 by portable MIMS at pool facility D during swimming meet in August 2019. Vertical bars represent the number of swimmers in the pool. Horizontal line represents the detection limit.

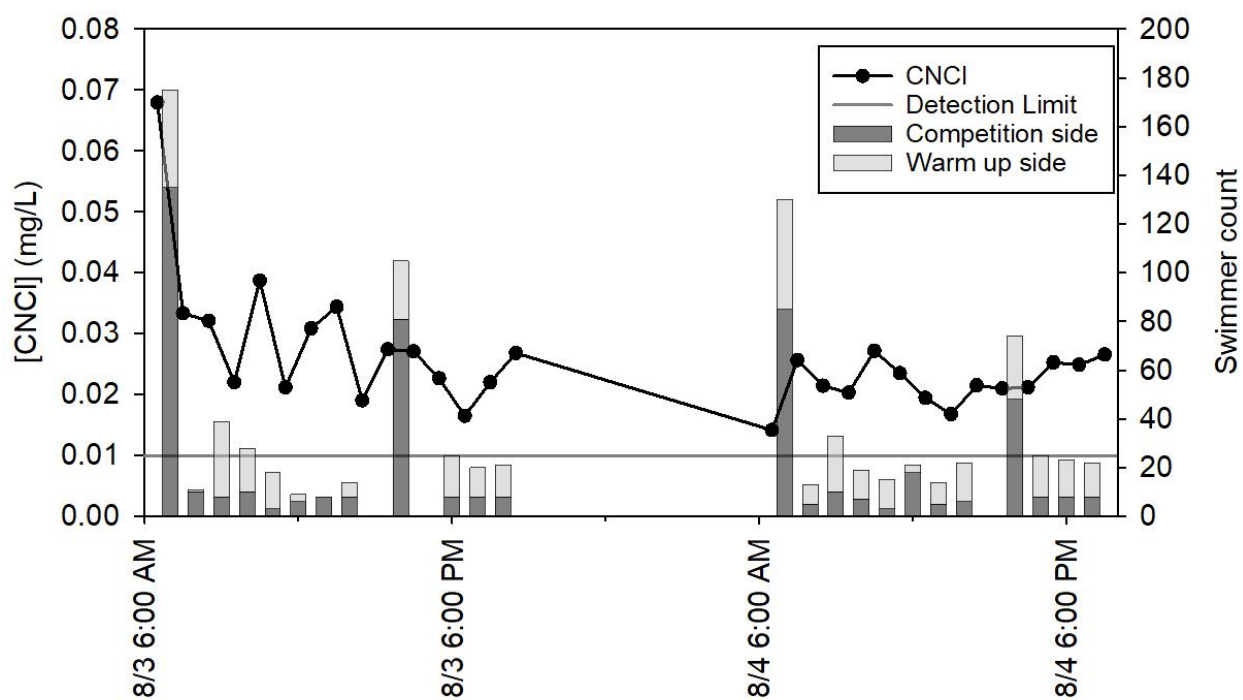


Figure 5.66. Time-course monitoring of aqueous-phase CNCI by portable MIMS device at pool facility D during swimming meet in August 2019. Vertical bars represent the number of swimmers in the pool. Horizontal line represents the detection limit.

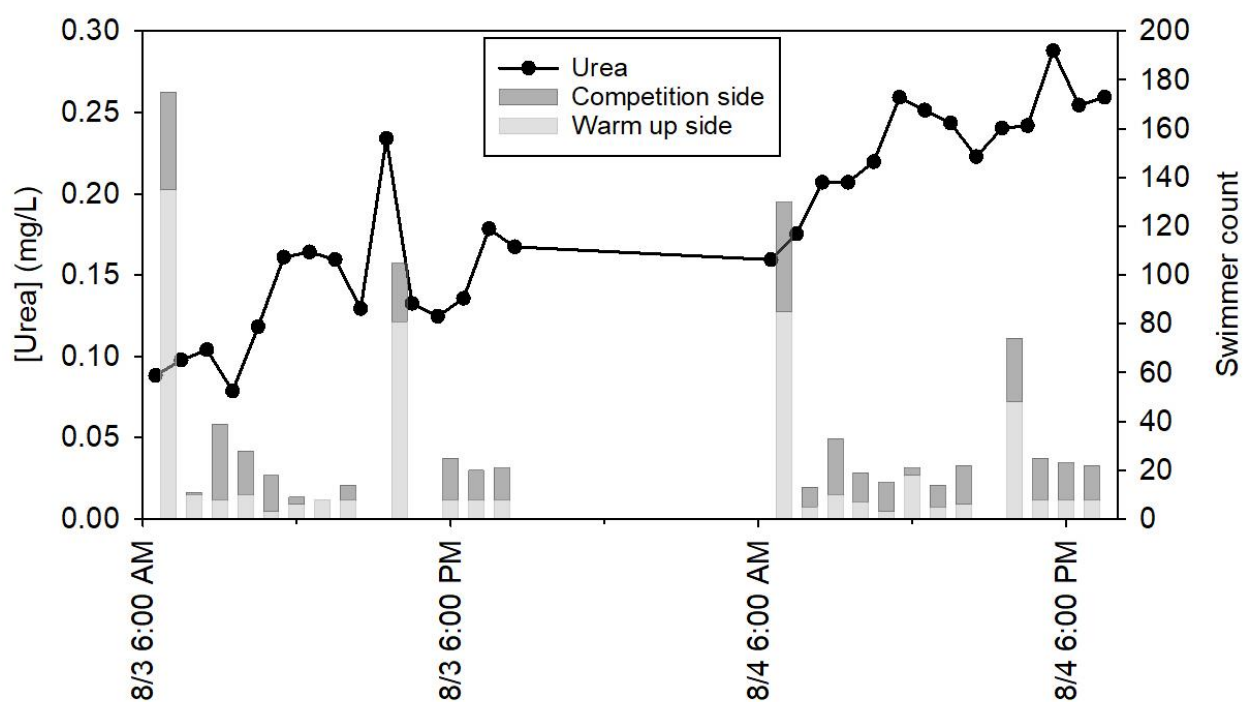


Figure 5.67. Time-course monitoring of urea at pool facility D during swimming meet in August 2019. Vertical bars represent the number of swimmers in the pool.

Time-course monitoring of gas-phase NCl_3 with relative humidity (RH) are illustrated in Figure 5.68. RH values were below 60% for both NEMo devices during the meet. High gas-phase NCl_3 concentrations were only observed during the warm-up period on the second of the day of the meet. The number of swimmers, spectators, and pool personnel at facility D were manually counted at the top of the hour during this meet. Gas-phase NCl_3 concentrations increased to roughly $700 \mu\text{g}/\text{m}^3$ for both NEMo devices. Measured concentrations of gas-phase NCl_3 were below $400 \mu\text{g}/\text{m}^3$ for the majority of the experiment for both NEMo devices. When swimmers were absent from the pool for extended periods of time (i.e., overnight, when the facility was closed), gas-phase NCl_3 was not detectable.

Results of time-course monitoring of gas-phase NCl_3 with gas-phase CO_2 by the NEMo devices are illustrated in Figure 5.69. Gas-phase CO_2 was observed as high as 1400 ppm_v from both NEMo devices during the meet. The trends for both NEMo devices were similar. Gas-phase CO_2 concentration showed a strong correlation with the number of people in this facility during the meet. As with the other experiments, a strong qualitative correlation between the time-course histories of gas-phase NCl_3 and CO_2 was observed, as illustrated in Figure 5.69. This suggests that the physical processes that are responsible for transfer of both compounds from the liquid phase to the gas phase were similar. The fact that the time-course trends for both compounds were similar also suggests that CO_2 may represent an appropriate surrogate for NCl_3 in the gas phase. The fact that the time-course histories of NCl_3 (and CO_2) as measured by two NEMo devices were quite similar also supports the assumption of a well-mixed air space in this facility.

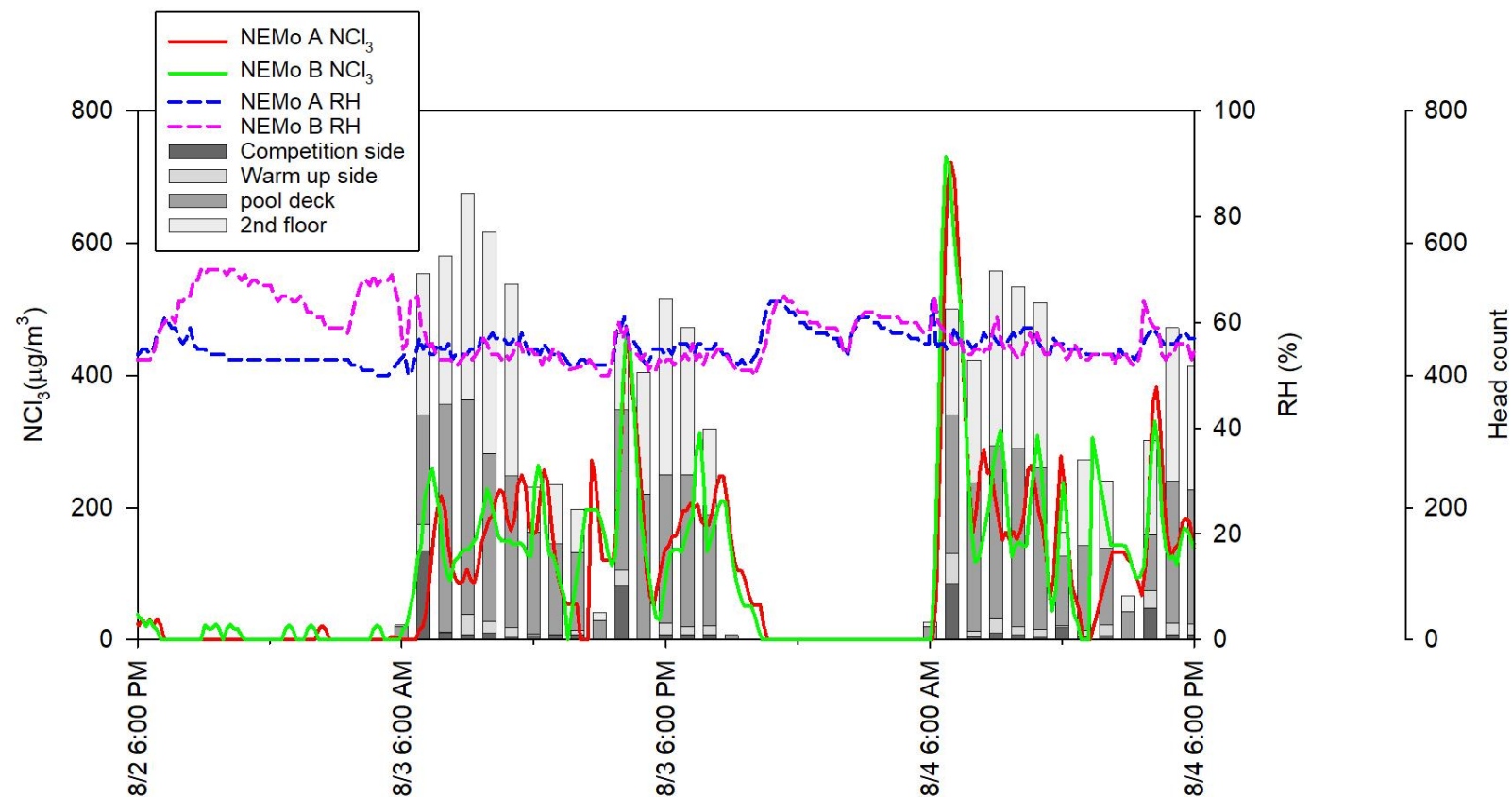


Figure 5.68. Time-course monitoring of gas-phase NCl_3 and RH measured by NEMo devices at pool facility D during swimming meet in August 2019. Vertical bars represent the number of people in each area of pool facility D.

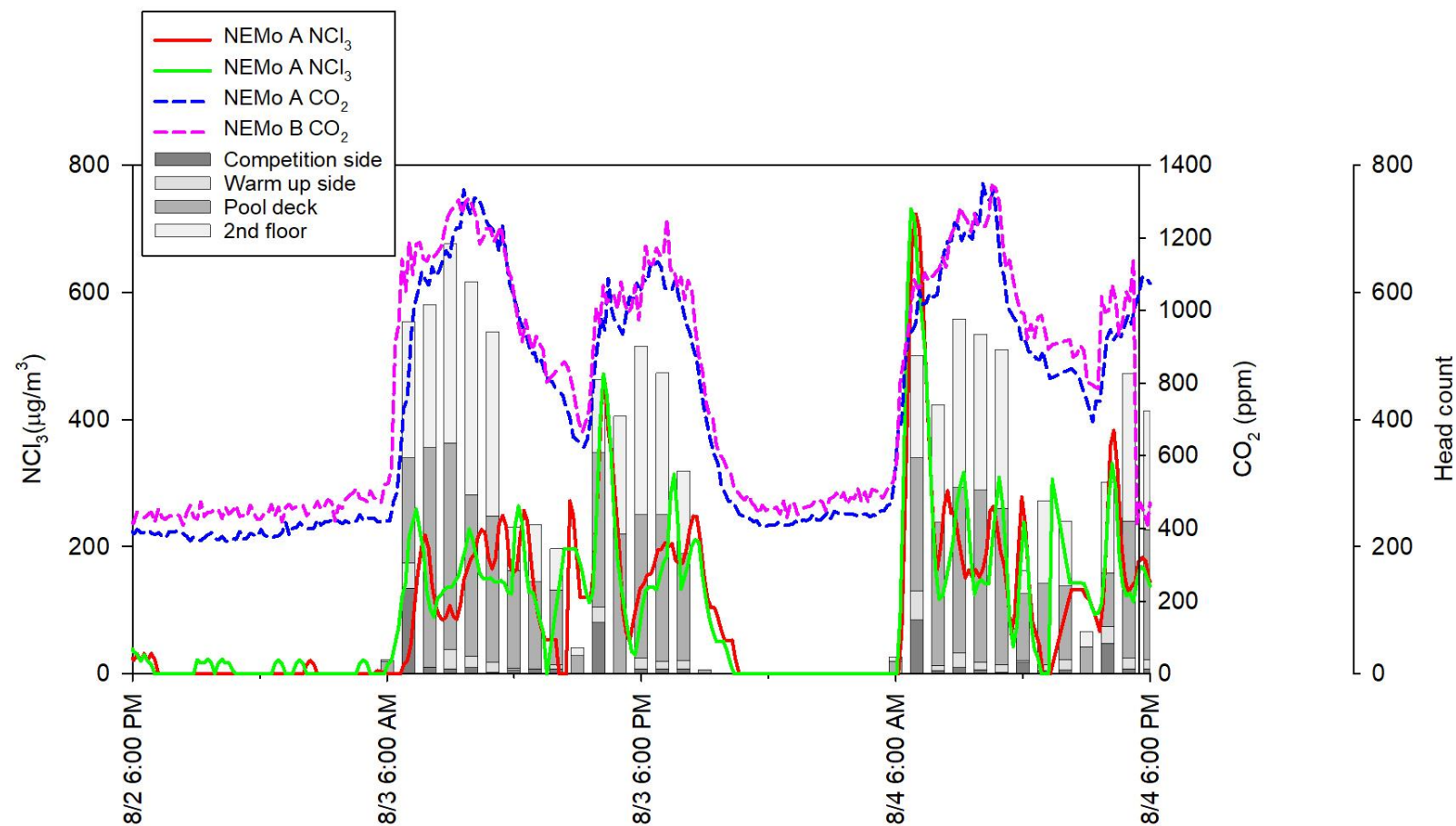


Figure 5.69. Time-course monitoring of gas-phase NCl_3 with gas-phase CO_2 measured by NEMo devices at pool facility D during swimming meet in August 2019. Vertical bars represent the number of people in each area of pool facility D.

5.4 Measurements at Pool facility E

Water and air quality monitoring were conducted during regular operating hours at facility E from 1/15/2020 to 1/19/2020. This facility held a half day swimming meet on 1/18/2020; events were held from 2:00 PM to 3:30 PM that day. The meet was a short-course (25 yards) competition for age 18 to 22 swimmers. Approximately 110 swimmers participated in this swimming meet. Water samples were collected periodically during this experiment period. The Portable MIMS device was positioned adjacent to the pool deck area to allow measurements of volatile DBPs in water samples hourly. Two NEMo devices were installed during this measurement and their locations around the pool area are shown in Figure 3.15. Water samples were collected 20 cm below the water surface from a location near the center of competition side, as shown in Figure 3.14.

Time-course measurements of the concentration of free chlorine and total chlorine are illustrated in Figure 5.70. Concentrations of free chlorine ranged from 1.1 to 1.6 mg/L as Cl_2 and concentrations of total chlorine ranged from 1.7 to 2.1 mg/L as Cl_2 . Measurements of combined chlorine (total chlorine – free chlorine) were mostly below 0.4 mg/L as Cl_2 during the study period. pH was stable at approximately 7.5 during this measurement, as indicated in Figure 5.71. Alkalinity was between 30 to 70 mg/L (as CaCO_3) during study period, as shown in Figure 5.72. Aqueous-phase CO_2 concentrations were calculated from pH, alkalinity, and water temperature, as illustrated in Figure 5.73. Water temperature was not recorded during this competition, so water temperature was assumed to be 25°C throughout the meet.

Measurements of volatile DBPs and urea in water samples are shown in Figures 5.74 and 5.75. Only CHCl_3 was measurable (above detection limit) for water samples collected during this measurement as analyzed by the portable MIMS system. Concentrations of CHCl_3 were consistent throughout this study period.

The concentrations of urea ranged from 0.05 to 0.1 mg/L during this study. Urea concentration appeared to have increased by a larger amount when the competition swimmers were in the pools, as compared to when regular swimmers were present in the pools. It was possible that more urea was brought into the pool by competition swimmers during that period. As urea reacts slowly with chlorine, it was expected to observe an increase in its concentration after a large number of swimmers were present in pool. The diurnal pattern described previously for some pools was also observed in this study period, as urea concentrations increased during the operating hours

and urea concentration decreased during the overnight period. The factors that contributed diurnal pattern include mixing and transfer within the swimming pool, swimmer's activity, and pool recirculation.

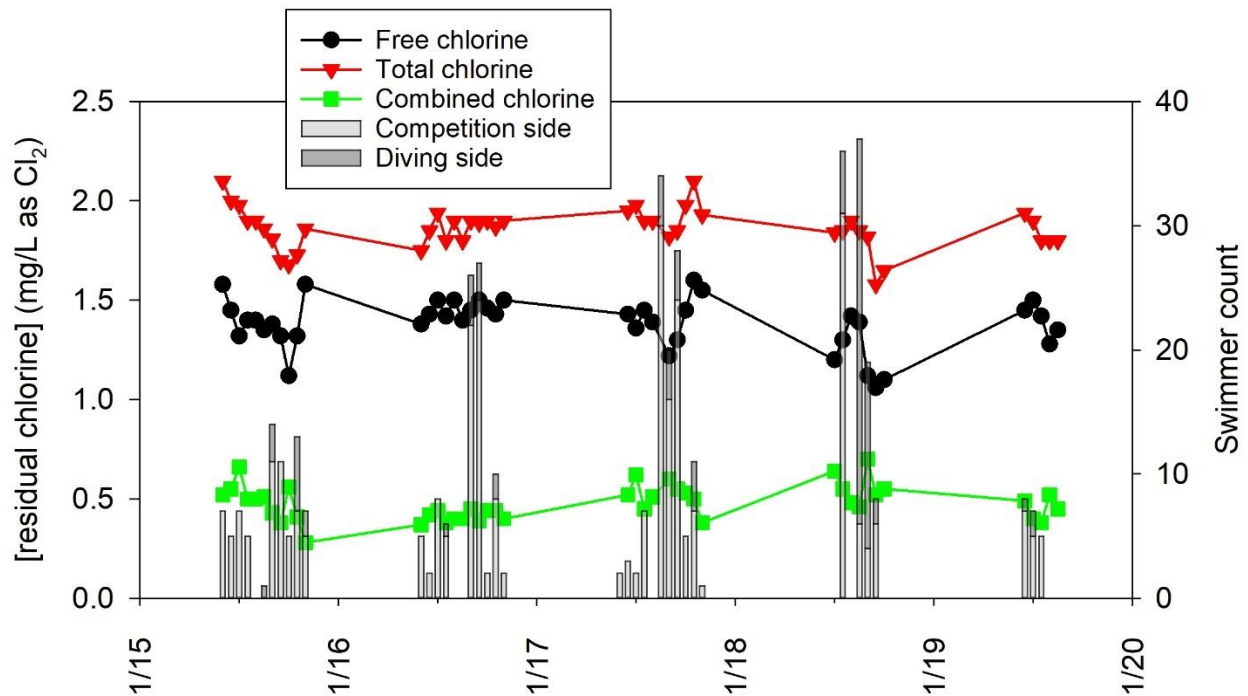
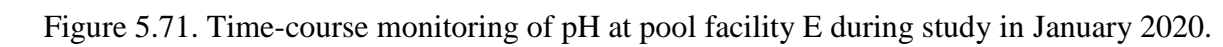
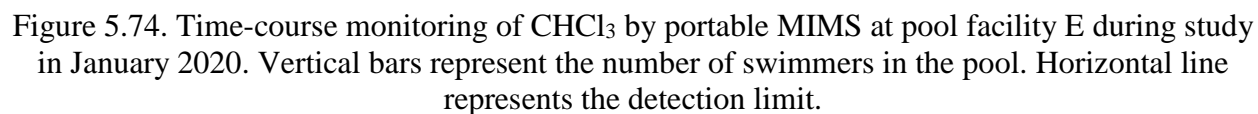
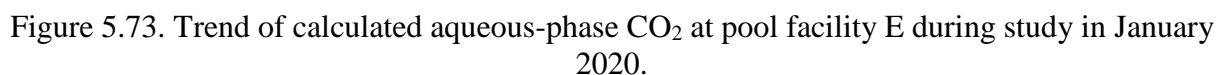


Figure 5.70. Time-course monitoring of free and total chlorine at pool facility E during study in January 2020. Vertical bars represent the number of swimmers in the pool.





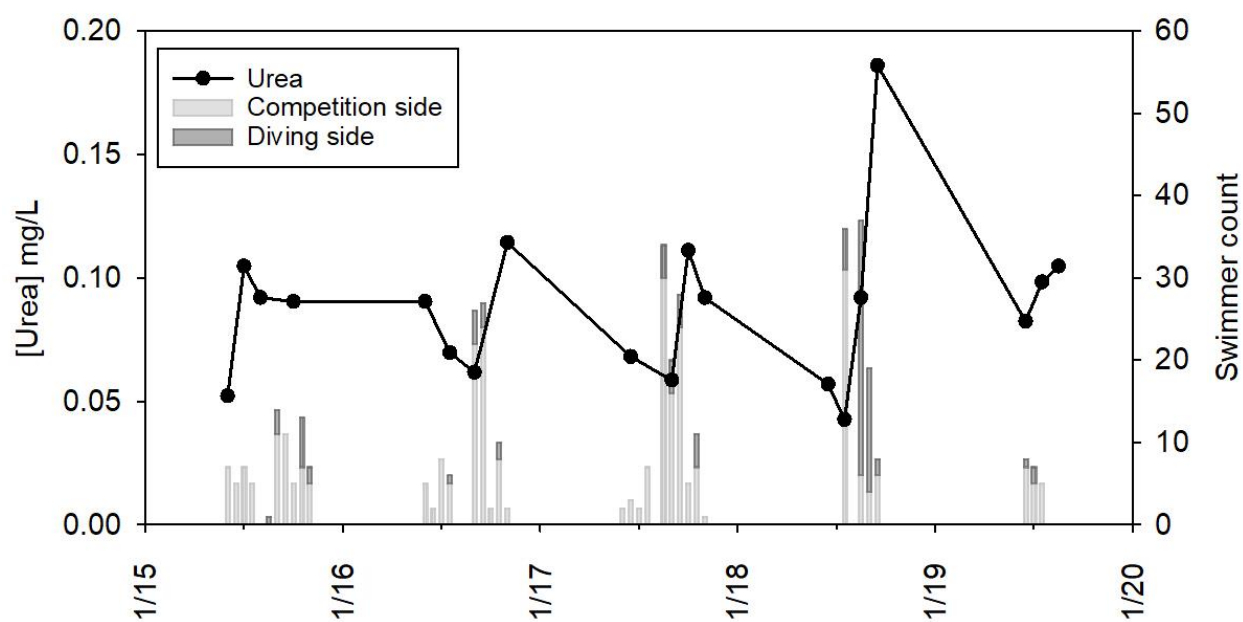


Figure 5.75. Time-course monitoring of urea at pool facility E during study in January 2020.
Vertical bars represent the number of swimmers in the pool.

Results of time-course monitoring of gas-phase NCl_3 with relative humidity (RH) are illustrated in Figure 5.76. All RH values were below 60% from both NEMo devices during the study period; however, roughly half of the measurements were below 30%. High gas-phase NCl_3 concentrations were observed when number of swimmers in the pool was large. The number of people in the pool at facility E was manually counted at the top of the hour during this study period. Swimmer counts are missing for periods when the facility was closed to the public (3:00 pm on 1/17/2020 and 11:00 am on 1/18/2020). Gas-phase NCl_3 concentrations reached as high as $1300 \mu\text{g}/\text{m}^3$ for both NEMo devices, corresponding to times immediately after large numbers of swimmers were in the pool. Measured concentrations of gas-phase NCl_3 were below $100 \mu\text{g}/\text{m}^3$ for both NEMo devices when no swimmers were present in the pool.

Time-course monitoring of gas-phase NCl_3 with gas-phase CO_2 measured by the NEMo devices are presented in Figure 5.77. Gas-phase CO_2 was observed to be as high as 1400 ppm_v from both NEMo devices during the swimming meet on 1/18/2020. Concentrations of Gas-phase CO_2 were around 700 ppm_v when swimmers were present in the pool during on other days. The trends for both NEMo devices were similar. Gas-phase CO_2 concentration showed a strong correlation with the number of people in this facility during study period. A qualitative correlation between the time-course histories of gas-phase NCl_3 and CO_2 was observed, as illustrated in Figure 5.77.

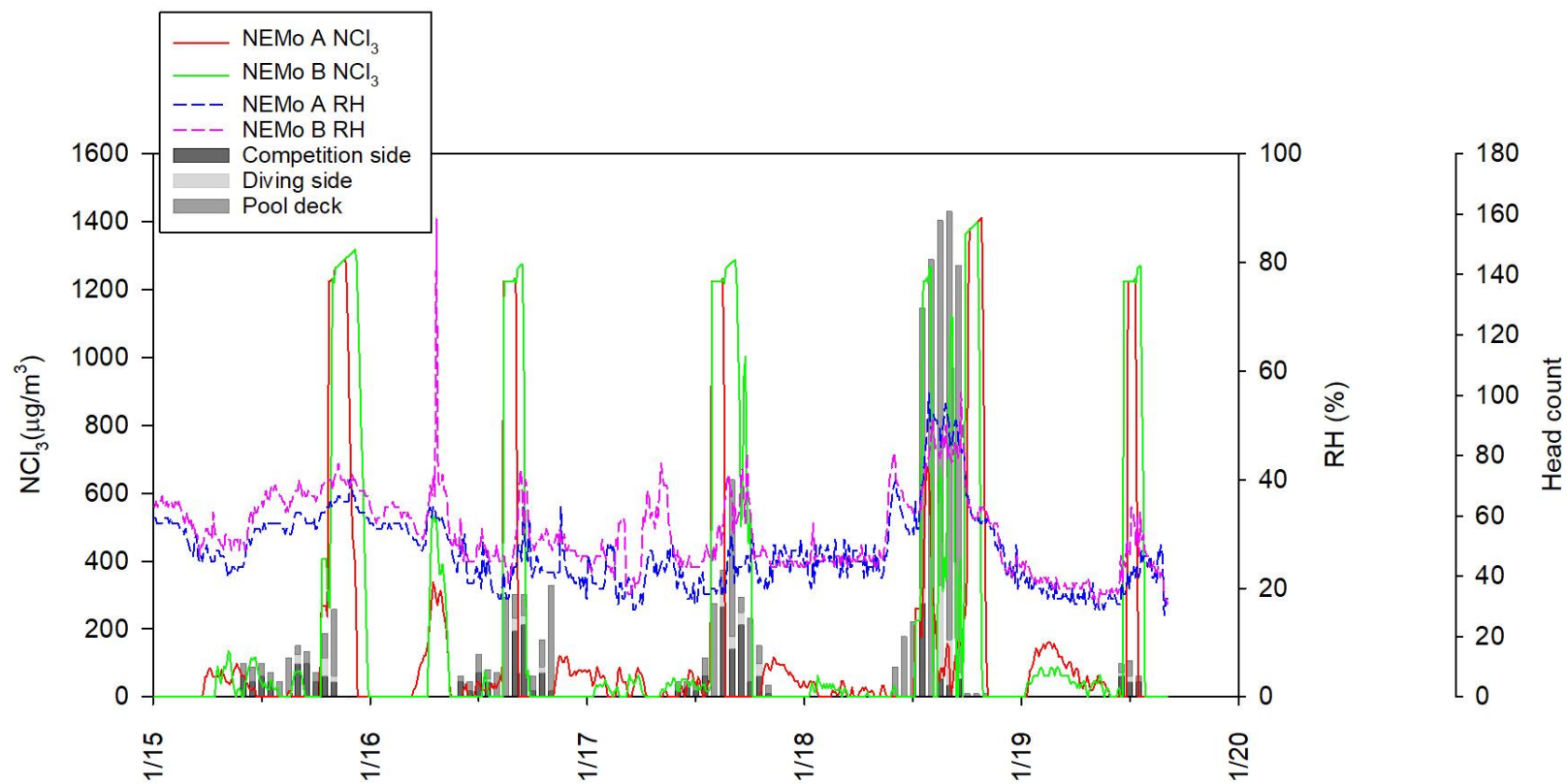


Figure 5.76. Time-course monitoring of gas-phase NCl_3 and RH measured by NEMo devices at pool facility E during study in January 2020. Vertical bars represent the number of people in each area of pool facility E.

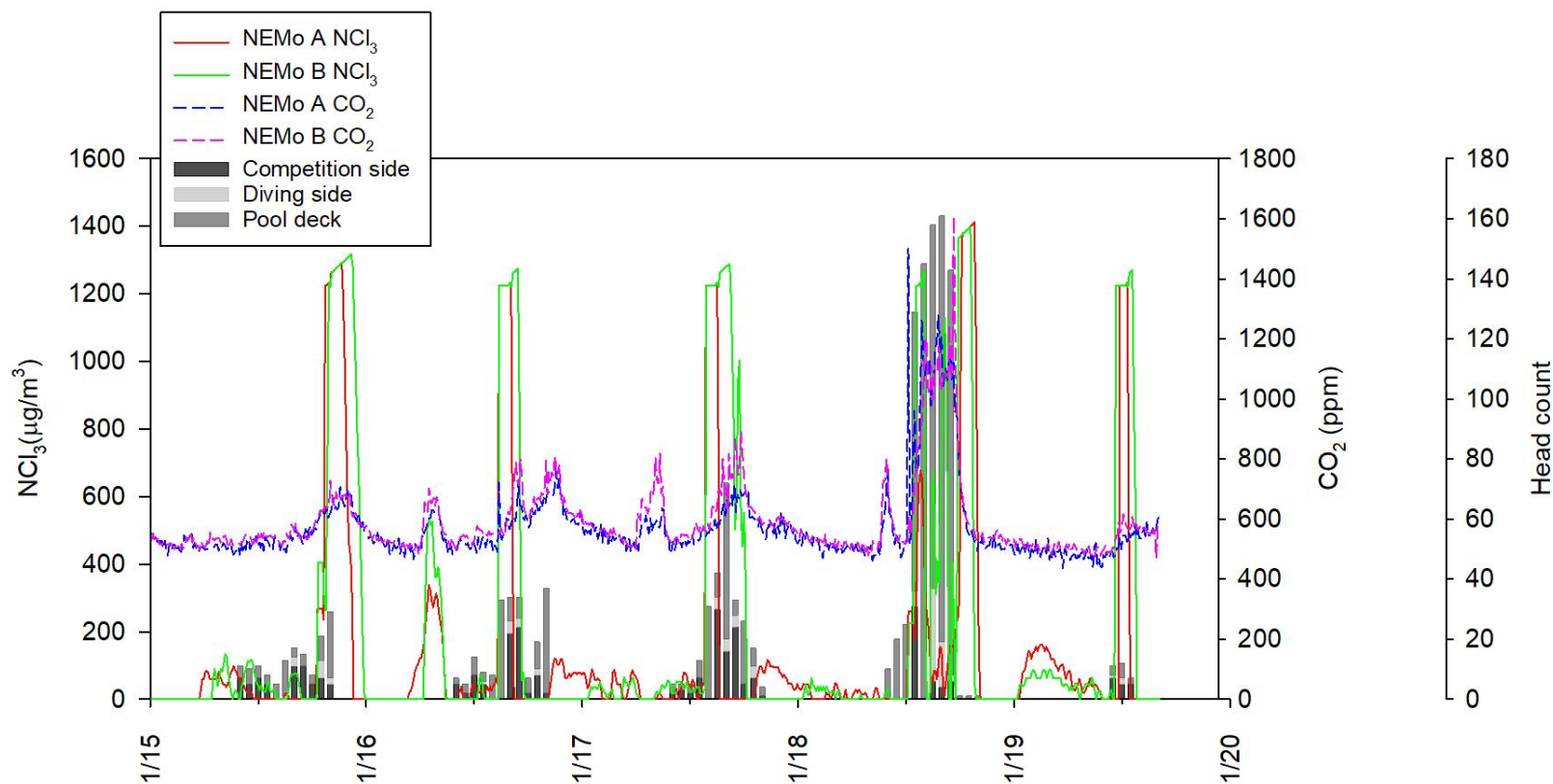


Figure 5.77. Time-course monitoring of gas-phase NCl_3 with gas-phase CO_2 measured by NEMo devices at pool facility E during study in January 2020. Vertical bars represent the number of people in each area of pool facility E.

5.5 Summary of liquid-phase volatile DBP measurements

Seven volatile DBPs were detectable in pool facilities A and B with the bench top MIMS system. It was not possible to conduct liquid-phase volatile DBPs analysis at pool facility C. NCl_3 , CHCl_3 , and CNCl were detectable during the study at pool facility D with the portable MIMS system. Only CHCl_3 was measurable during the study at pool facility E with the portable MIMS system. Comparisons of the liquid-phase concentrations of volatile DBPs measured in this study with previous studies in indoor chlorinated swimming pools are illustrated in Figure 5.78 to Figure 5.84. Concentrations of liquid-phase volatile DBPs in this study are summarized in Table 5.1.

Inorganic chloramines (NH_2Cl and NCl_3) and chloroform appeared to be the dominant volatile DBPs in pools, on the basis of liquid-phase concentrations. Similar results were observed in other studies (Weaver *et al.*, 2009; Weng and Blatchley, 2011; Zare Afifi and Blatchley, 2016). Weaver *et al.* (2009) reported that typical concentrations of NH_2Cl , NHCl_2 , and NCl_3 found in public swimming pools range from below detection limit to 1880 $\mu\text{g/L}$ as Cl_2 , below detection to 417 $\mu\text{g/L}$ as Cl_2 , and below detection limit to 377 $\mu\text{g/L}$ as Cl_2 , respectively.

Chloroform (CHCl_3) is often the dominant compound in the trihalomethane (THM) group in pool water samples (Kanan, 2010; Lahl *et al.*, 1981). Weaver *et al.* (2009) reported that chloroform concentrations in eleven chlorinated pools ranged from below detection limit to 298 $\mu\text{g/L}$. A study conducted by Bessonneau *et al.* (2011) reported measurements from 15 swimming pools in Brittany, France. They reported aqueous-phase concentrations CHCl_3 that ranged from 3.50 $\mu\text{g/L}$ to 72.6 $\mu\text{g/L}$.

A study was conducted in which material of human origin including hair, saliva, skin, urine, and a body lotion were chlorinated separately and together as mixed solutions in two water types (surface and ground water). In both waters, five different DBPs (CHCl_3 , bromodichloromethane, chloral hydrate, dichloroacetonitrile, and trichloropropane) were detected and CHCl_3 was the major product (Kim *et al.*, 2002). Several commercially available personal care products groups (deodorant/antiperspirant, sunscreen, and acne cream) have also been demonstrated to act as DBP precursors (Lee, 2016). Formation of CHCl_3 was observed after chlorination of sunscreen products. Formation of NCl_3 was observed after chlorination of deodorant/antiperspirant, sunscreen, and acne cream. Several pharmaceutical compounds and their metabolites also produced volatile DBPs after the chlorination. For instance, CHCl_3 formation was observed after chlorination of

acetaminophen, budesonide, caffeine, ibuprofen, and naproxen. Quantifiable NCl_3 was observed in chlorinated caffeine solution (Lee, 2016).

Previous research has demonstrated that CNCl and free chlorine in water samples tend to be negatively correlated (Na and Olson, 2004; Weaver et al., 2009; Zare Afifi and Blatchley, 2016). Maintaining high free residual chlorine can be used to limit the concentration of CNCl because free chlorine plays a critical role in the decay of CNCl . However, it is important to recognize that chlorine is also critical for the formation of CNCl from reactions with amino acids and uric acid (Li and Blatchley, 2007; Lian et al., 2014). At a free chlorine concentration of 0.5 mg/L (as Cl_2) at 25°C and pH=7, the half-life of CNCl in water has been reported to be roughly 60 minutes (Na and Olson, 2004). Weaver *et al.* (2009) measured CNCl in several public swimming pool water samples and the concentrations ranged from below detection limit to 194 $\mu\text{g/L}$.

Zare Afifi and Blatchley (2016) reported that aqueous CNCHCl_2 concentrations ranged from 0.67 to 30.5 $\mu\text{g/L}$ in a high school swimming pool. Lee *et al.* (2010) measured 30 public chlorinated swimming pools located in Seoul, South Korea and found that aqueous CNCHCl_2 concentrations ranged from 0.50 to 12.2 $\mu\text{g/L}$. Kanan (2010) conducted analyses on water samples from 23 indoor pools located in South Carolina, Georgia, and North Carolina in which aqueous CNCHCl_2 concentrations ranged from 4.00-47.0 $\mu\text{g/L}$.

Weaver *et al.* (2009) measured CH_3NCl_2 in several public swimming pool water samples and the concentrations ranged from below detection limit to 51.0 $\mu\text{g/L}$.

The relatively high aqueous-phase concentrations of CHCl_3 and NCl_3 that were observed at pool facility D may be due to the relatively high free chlorine concentration at the beginning of the monitoring period in August 2019. Specifically, the concentration of free chlorine was around 3.5 mg/L as Cl_2 , as shown in Figure 5.60.

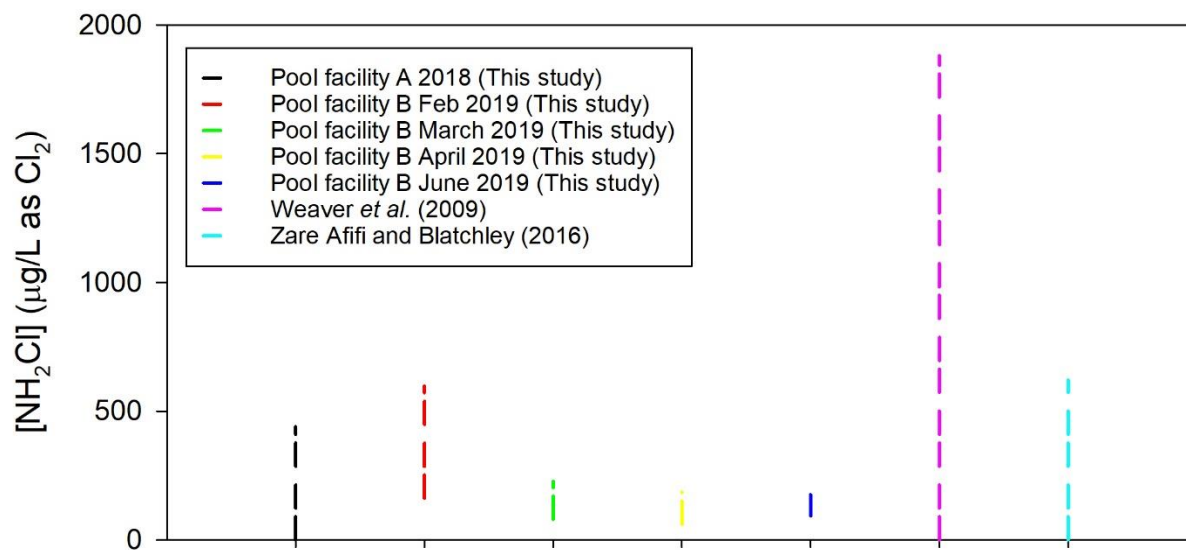


Figure 5.78. Comparison of ranges of liquid-phase NH₂Cl concentrations measured in this study with those from previous studies in chlorinated swimming pools.

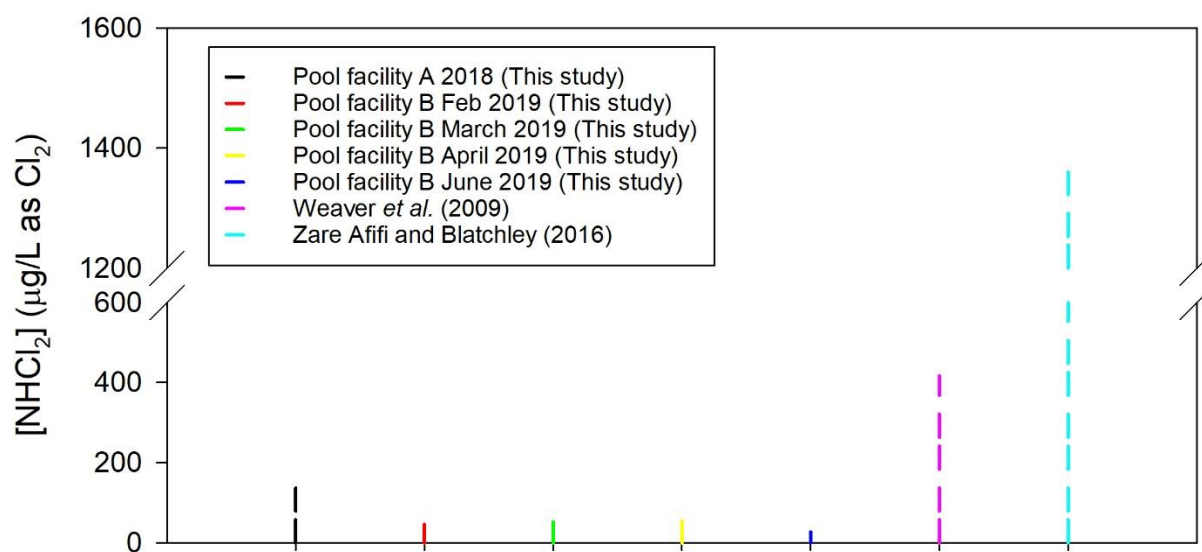


Figure 5.79. Comparison of ranges of liquid-phase NHCl₂ concentrations measured in this study with those from previous studies in chlorinated swimming pools.

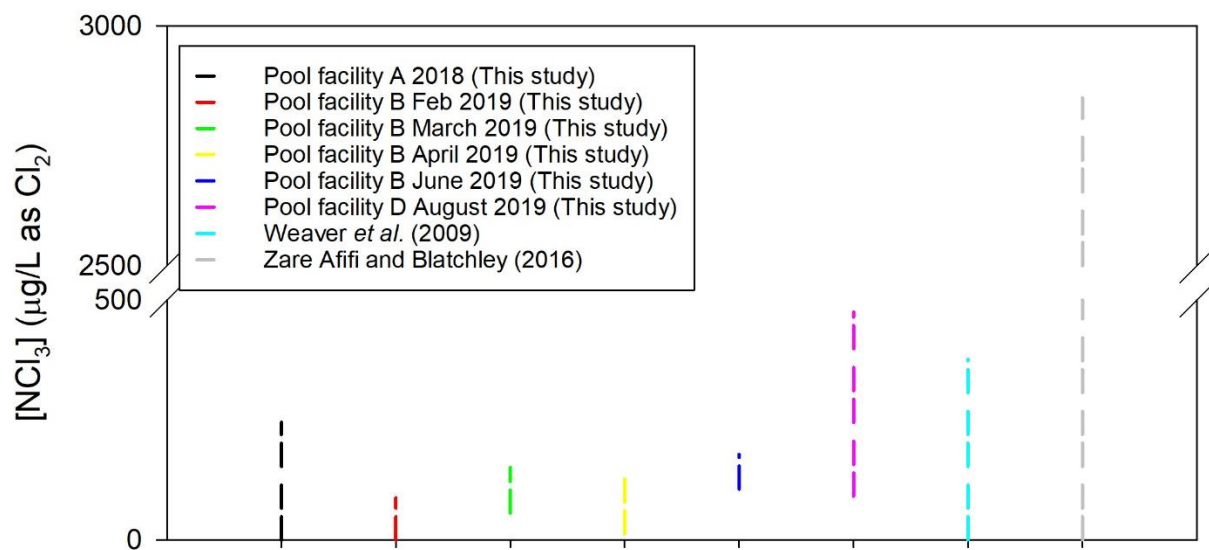


Figure 5.80. Comparison of ranges of liquid-phase NCl_3 concentrations measured in this study with those from previous studies in chlorinated swimming pools.

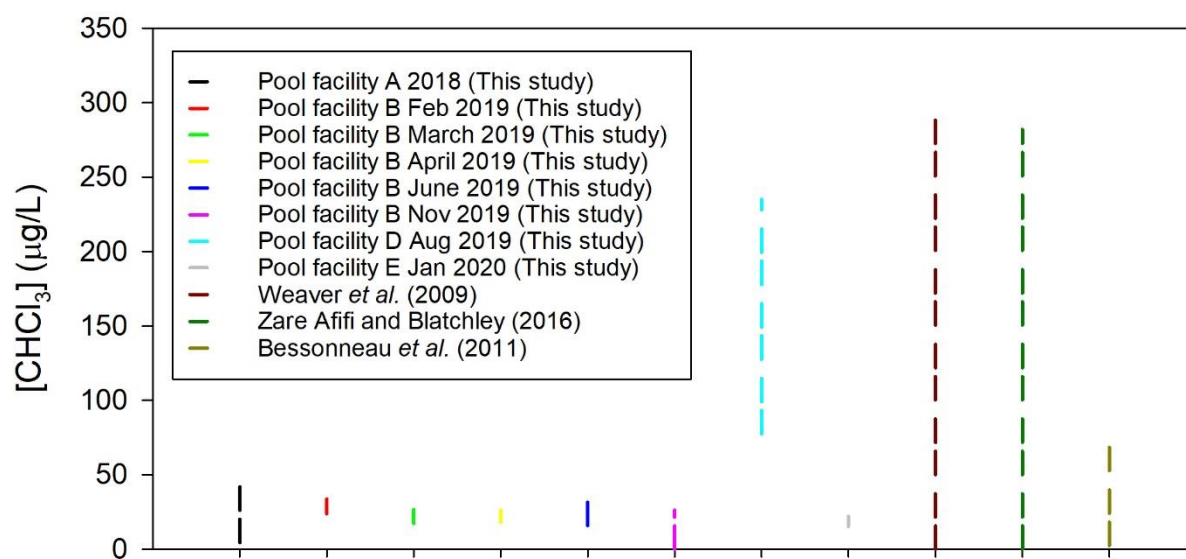


Figure 5.81. Comparison of ranges of liquid-phase CHCl_3 concentrations measured in this study with those from previous studies in chlorinated swimming pools.

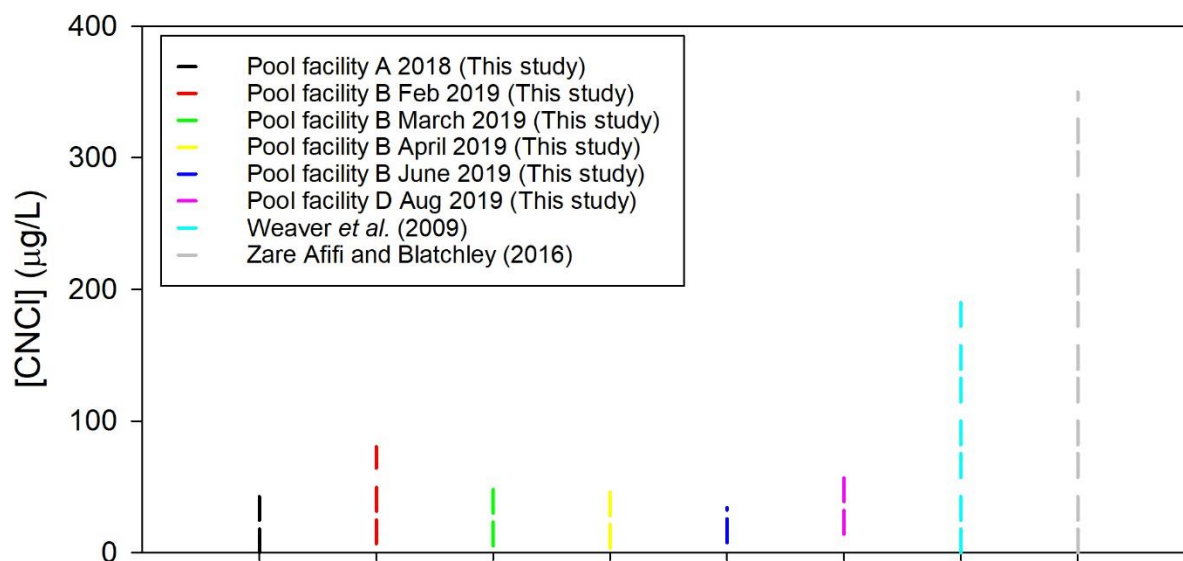


Figure 5.82. Comparison of ranges of liquid-phase CNCl concentrations measured in this study with those from previous studies in chlorinated swimming pools.

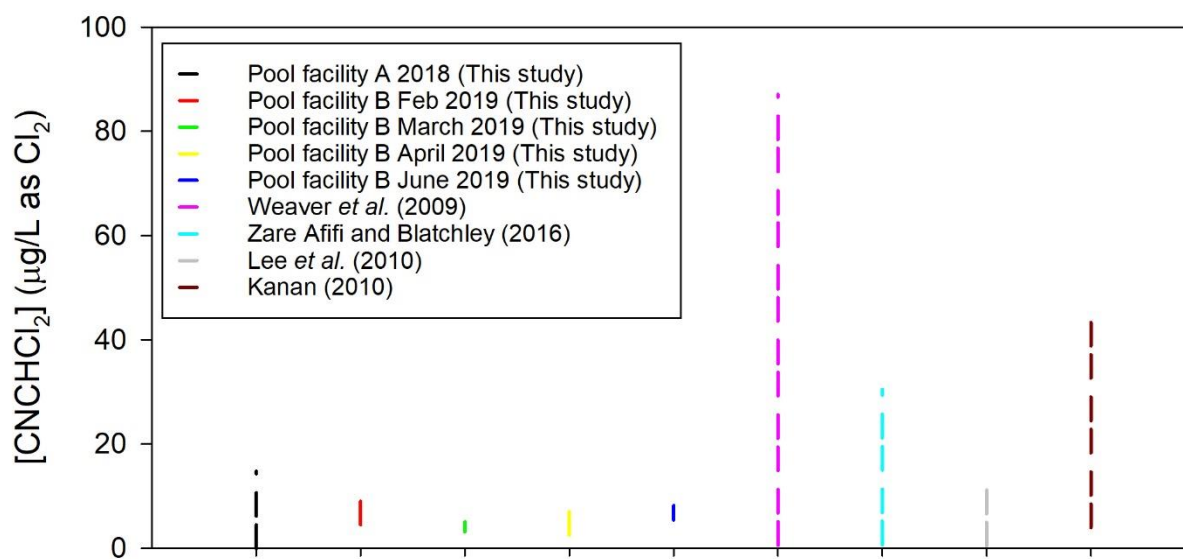


Figure 5.83. Comparison of ranges of liquid-phase CNCHCl₂ concentration measured in this study with those from previous studies in chlorinated swimming pools.

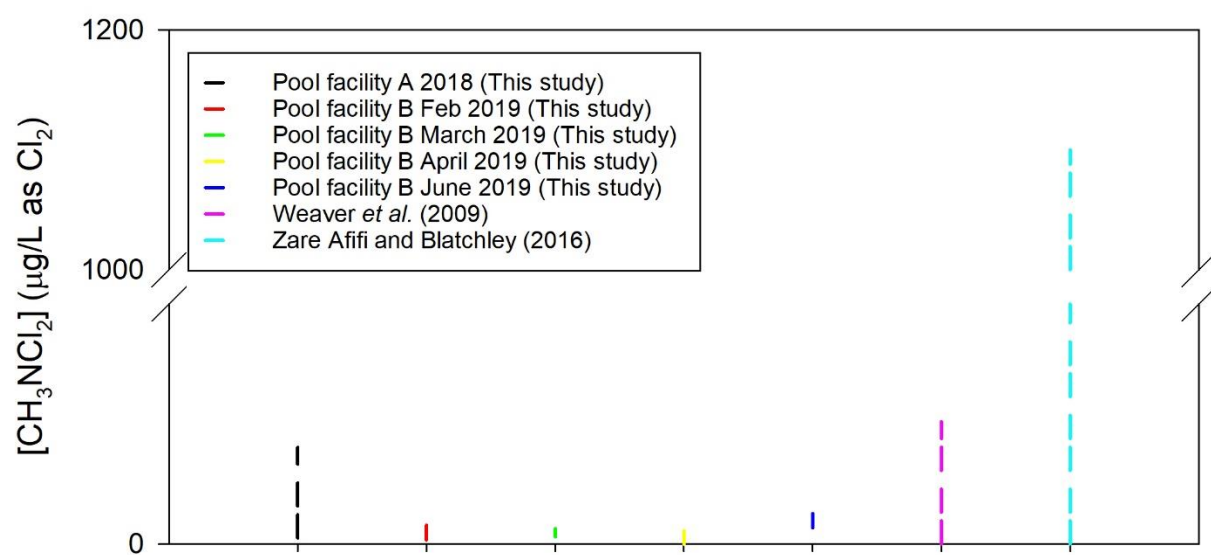


Figure 5.84. Comparison of ranges of liquid-phase CH₃NCl₂ concentrations measured in this study with those from previous studies in chlorinated swimming pools.

Table 5.1. Arithmetic mean DBP concentrations plus minimum and maximum concentration values for pool facilities A to E.

Pool facility	NH ₂ Cl (µg/L as Cl ₂)		NHCl ₂ (µg/L as Cl ₂)		NCl ₃ (µg/L as Cl ₂)		CHCl ₃ (µg/L)		CNCI (µg/L)		CNCHCl ₂ (µg/L)		CH ₃ NCl ₂ (µg/L)	
	range	mean	range	mean	range	mean	range	mean	range	mean	range	mean	range	mean
A 2018	nd-439	157	nd -183	62.3	nd -245	69.9	4.53-54.4	26.7	nd -44.6	4.17	nd-14.8	6.76	2.51-40.2	10.6
B 02/2019	162-597	290	nd-45.9	22.9	nd-88.1	50.8	23.7-33.8	28.3	6.88-80.3	32.3	4.52-10.7	7.50	1.61-7.83	5.07
B 03/2019	79.8-227	139	nd-52.3	23.7	55.5-151	106	17.2-26.7	21.9	5.31-50.2	18.7	3.13-5.10	3.71	2.96-6.30	4.56
B 04/2019	60.1-185	109	nd-54.8	19.2	12.8-157	80.5	18.0-26.3	22.5	3.38-46.2	14.9	2.53-8.47	5.49	nd-5.42	3.70
B 06/2019	93.6-175	134	nd-27.3	7.57	106-178	140	15.8-33.4	27.5	7.72-34.2	15.7	5.42-8.18	7.33	6.77-12.6	9.32
B 11/2019	nd		nd		nd		nd-26.2	15.8	nd		nd		nd	
C 03/2019	nm		nm		nm		nm		nm		nm		nm	
D 08/2019	nd		nd		91.4-475	282	77.4-235	107.4	14.1-68.0	25.9	nd		nd	
E 01/2020	nd		nd		nd		15.4-22.0	18.7	nd		nd		nd	

nd: undetectable. nm:no measurements.

As summarized in Table 5.2, correlation coefficients were calculated between measured concentrations of volatile DBPs from pool facility B. This analysis focused on pool facility B as data from this facility was more comprehensive than from other facilities. Also, this study only addressed data from the benchtop MIMS system, as the portable MIMS device was not able to measure all seven volatile DBPs consistently. The strongest correlations were observed between CHCl_3 and CNCHCl_2 , CHCl_3 and CH_3NCl_2 , as well as NCl_3 and CH_3NCl_2 .

Kim *et al.* (2002) reported that when material of human origin including hair, saliva, skin, urine, and a body lotion were chlorinated, five different DBPs including CHCl_3 , bromodichloromethane, chloral hydrate, CNCHCl_2 , and trichloropropane were detectable. The common precursors between these volatile DBPs provides a partial explanation for why they displayed relatively strong correlations. Other factors that will contribute to strong correlation include: concentration of precursors, process of formation of the compounds, as well as processes of decay and mass transfer. A study done by Wei *et al.* (2010) reported correlation coefficients between several groups of DBPs in drinking water in the distribution system in Beijing, China. They reported a Pearson correlation coefficient of 0.866 between total THM (CHCl_3 , bromodichloromethane, dibromochloromethane, and bromoform) and total HANs (CNCHCl_2 , bromochloroacetonitrile, dibromoacetonitrile, and trichloroacetonitrile).

It is also known that NCl_3 and CH_3NCl_2 share at least one common precursor, creatinine, that could potentially explain their relatively strong correlation. Creatinine is one of the most abundant nitrogenous compound by mass concentration in human sweat and urine (WHO, 2006). Li and Blatchley (2007) reported the mechanism for formation of NCl_3 and CH_3NCl_2 formation from the chlorination of creatinine.

In a recent study, carbamate insecticides have been identified as precursors of the formation of CH_3NCl_2 during chlorination in surface water (E *et al.*, 2019). Four carbamate insecticides were examined including methoymyl, carbofuran, carbaryl, and thiodicarb. CH_3NCl_2 was a common product after chlorination of these four carbamates. Moreover, chlorination of carbofuran and carbaryl yielded CHCl_3 , which may be generated from reactions between free chlorine and the aromatic structures in these carbamate compounds. The carbamate insecticides have not been reported in swimming pools to date. Thus, the high correlation between CHCl_3 and CH_3NCl_2 were not likely cause by carbamate insecticides. The strong correlation could potentially be attributed to other precursors in pool facility B that have a structure that favors formation of CHCl_3 and

CH₃NCl₂. It could also be that chlorine reacts with a wide range of compounds and that precursors to CHCl₃ and CH₃NCl₂ formation show strong positive correlations.

The slightly negative correlation between NCl₃ and CNCl was observed. It is known that high free chlorine concentration would often promote the formation of NCl₃ (Shang and Blatchley, 1999). On the other hand, high free chlorine concentration would likely promote the degradation of CNCl (Na and Olson, 2004). These reactions could potentially explain the negative correlation.

Table 5.2. Correlation matrix for DBPs in water samples collected at pool facility B.

		NH ₂ Cl	NHCl ₂	NCl ₃	CHCl ₃	CNCl	CNCHCl ₂	CH ₃ NCl ₂
NH ₂ Cl	r	1	0.375*	-0.129	0.378*	0.589*	0.361*	0.126
NHCl ₂	r		1	-0.090	-0.121	0.225*	-0.094	-0.121
NCl ₃	r			1	0.106	-0.281*	0.126	0.662*
CHCl ₃	r				1	0.307*	0.660*	0.626*
CNCl	r					1	0.269*	-0.115
CNCHCl ₂	r						1	0.521*
CH ₃ NCl ₂	r							1

r: Pearson correlation coefficient.

*: *p* value < 0.05.

5.6 Summary of gas-phase NCl_3 and CO_2 measurements

It is known that several factors may affect the concentration of DBPs in the air of indoor swimming pools, including the concentration of DBPs in the water, use of other treatment processes, including secondary oxidants and UV irradiation, the number swimmers and their hygiene habits, swimmer age and swimming intensity, water temperature, the HVAC system design and its operational characteristics, as well as the presence or absence of treatment processes for removal of DBPs from water (*e.g.*, air stripping) (Bessonneau *et al.*, 2011). A summary of gas-phase NCl_3 concentrations measured by the NEMo devices in several pool facilities is presented in Table 5.3. Two reference values have been recommended for gas-phase NCl_3 concentration in recreational pool facilities: $500 \mu\text{g}/\text{m}^3$ was established by WHO based on stationary measurements as a guideline for safe recreational water environments (WHO, 2006), while Bernard *et al.* (2006) suggested an upper limit of $300 \mu\text{g}/\text{m}^3$ in swimming pool facilities because at this value an almost immediate increase in lung epithelium permeability was observed, as evidenced by the appearance of surfactant-associated proteins as epithelial permeability markers.

Peak gas-phase NCl_3 concentrations were generally observed when large numbers of swimmers were present in the pools, with values as high as $1400 \mu\text{g}/\text{m}^3$ being observed in this work. Weng *et al.* (2011) reported a strong link between gas-phase NCl_3 concentration and bather load. An increase in bather load (swimmer number) will be accompanied by an increase in mechanical mixing of near-surface water, thereby promoting liquid→gas mass transfer of volatile compounds.

Several other studies have reported time-course measurements of gas-phase NCl_3 concentration. Zare Afifi and Blatchley (2016) reported concentrations of gas-phase NCl_3 from undetectable to $620 \mu\text{g}/\text{m}^3$, with a mean concentration of $150 \mu\text{g}/\text{m}^3$ in a high school swimming pool. Seys *et al.* (2015) measured gas-phase NCl_3 concentrations ranging from 200 to $1400 \mu\text{g}/\text{m}^3$ in a municipal swimming pool of Leopoldsburg, Belgium. Lévesque *et al.* (2015) also measured gas-phase NCl_3 at different time periods at a pool in Québec, Canada; the mean concentrations in the morning, afternoon, and night were 350, 360, and $510 \mu\text{g}/\text{m}^3$, respectively. Fornander *et al.* (2013) reported gas-phase NCl_3 concentrations ranging from 40 to $360 \mu\text{g}/\text{m}^3$ in 9 pool facilities; while the mean concentration was $200 \mu\text{g}/\text{m}^3$. Nordberg *et al.* (2012) also investigated human exposure to gas-phase NCl_3 in two groups of people (random swimmers (group A) and pool workers (group B)). At the time of their exposure, mean gas-phase NCl_3 concentration for non-

regular swimmers was $23 \mu\text{g}/\text{m}^3$ and mean gas-phase NCl_3 concentration for pool workers was $19 \mu\text{g}/\text{m}^3$. Generally, the reported gas-phase NCl_3 measurements in previous studies varied over wide ranges as illustrated in Figure 5.85. Reported gas-phase concentrations were related to the liquid phase free chlorine concentration, numbers of bathers, and HVAC system characteristics (Bessonneau et al., 2011).

In this study, high concentrations of gas-phase NCl_3 were observed during swimming meets. During regular operation periods, the highest measurement was around $600 \mu\text{g}/\text{m}^3$ in March 2019 at pool facility B in November 2019. In the same venue, the highest concentration of gas-phase NCl_3 was $1122 \mu\text{g}/\text{m}^3$ during a swimming meet.

In addition, the type of swimmers also affected the concentration of gas-phase NCl_3 . For competitions involving collegiate and junior high swimmers, gas-phase NCl_3 concentration reached as high as $1400 \mu\text{g}/\text{m}^3$. On the other hand, the highest gas-phase NCl_3 measured during a swimming competition for age 14 and under children was $731 \mu\text{g}/\text{m}^3$ at pool facility D in August 2019. This behavior is consistent with the greater amount of mechanical mixing that would be expected from older, more advanced swimmers, as compared to younger swimmers. Stronger water mixing would likely promote the liquid→gas mass transfer and lead to higher peak NCl_3 in the air.

Table 5.3. The Arithmetic mean gas-phase NCl_3 concentrations plus minimum and maximum concentration values for pool facility B to E.

Pool Facility	NEMo A ($\mu\text{g}/\text{m}^3$)		NEMo B ($\mu\text{g}/\text{m}^3$)		NEMo C ($\mu\text{g}/\text{m}^3$)	
	range	mean	range	mean	range	mean
B 02/2019	nd-699	178	nd-673	169	nd-687	147
B 03/2019	nd-584	122	nd-384	128	nd-593	132
B 04/2019	nm		nd-956	216	nd-1250	200
B 06/2019	nd-748	159	nd-891	156	nm	
B 11/2019	nd-1122	165	nd-912	153	nm	
C 03/2019	nd-1124	249	nd-1217	270	nd-1420	285
D 08/2019	nd-723	102	nd-731	103	nm	
E 01/2020	nd-1411	140	nd-1400	204	nm	

nd: undetectable. nm: no measurements.

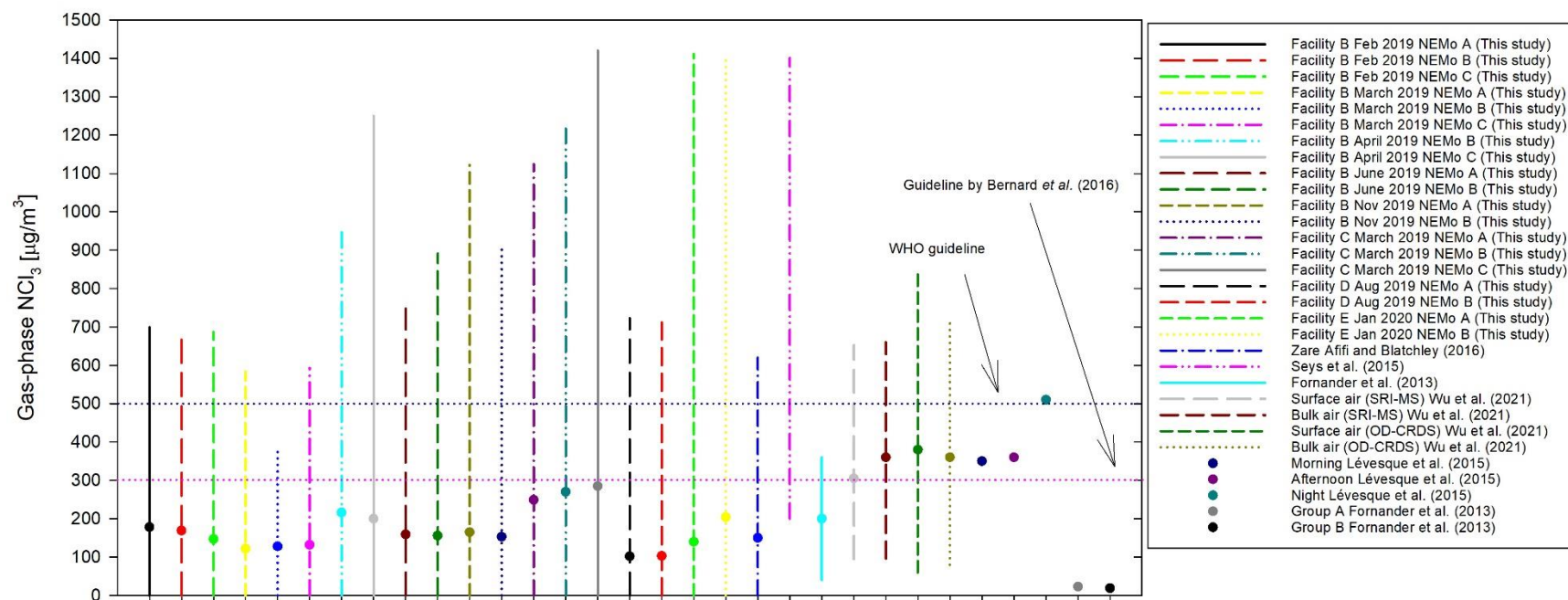


Figure 5.85. Comparison of the ranges of gas-phase NCl_3 concentration measured in this study with previous studies in chlorinated swimming pools. Colored vertical lines represent the concentration ranges of measured gas-phase NCl_3 in each study. Colored circles represent the mean concentration of gas-phase NCl_3 in each study. Horizontal dark blue dotted line represents the guideline level of gas-phase NCl_3 recommended by WHO (2006). Horizontal pink dotted line represents the guideline level of gas-phase NCl_3 recommended by Bernard (2006).

From Figures 5.31, 5.53, 5.59, and 5.69, the trends of NCl_3 and CO_2 appeared to follow each other, thus linear correlations between NCl_3 and CO_2 concentrations and dynamics were investigated. Pearson correlation coefficients were calculated for the measurements of NCl_3 with CO_2 concentrations for each NEMo device. The calculated correlation coefficients are summarized in Table 5.4.

Only weak ($0 \leq r \leq 0.3$) and moderate ($0.3 \leq r \leq 0.7$) linear relationships were observed between NCl_3 and CO_2 . It is known that the concentration of gas-phase NCl_3 is strongly influenced by bather loading (Weng et al., 2011; Zare Afifi and Blatchley, 2016).

Table 5.4. The correlation coefficients between NCl_3 and CO_2 in each NEMo devices.

Pool Facility	NEMo A NCl_3 v.s CO_2	NEMo B NCl_3 v.s CO_2	NEMo C NCl_3 v.s CO_2
B 02/2019	$r = 0.308^*$	$r = 0.348^*$	$r = 0.445^*$
B 03/2019	$r = 0.396^*$	$r = 0.591^*$	$r = 0.634^*$
C 03/2019	$r = 0.640^*$	$r = 0.559^*$	$r = 0.663^*$
B 04/2019	nm	$r = 0.077$	$r = 0.094^*$
B 06/2019	$r = 0.186^*$	$r = 0.298^*$	nm
D 08/2019	$r = 0.687^*$	$r = 0.626^*$	nm
B 11/2019	$r = 0.405^*$	$r = 0.198^*$	nm
E 01/2020	$r = 0.159^*$	$r = 0.364^*$	nm

r: Correlation coefficients.

*: p value < 0.05 .

nm: no measurements.

6. PHASE 3 (IAQ MODEL)

6.1 Derivation of the governing equations

An IAQ model for gas-phase NCl_3 was developed based on mass-balance principles, as shown in Equation 3.15 (copied below) and as described in section 3.3.2.

$$\forall_g \frac{dC_g}{dt} = Q_g C_{g,in} - Q_g C_g + \Phi_B + \sum_{i=1}^n \Phi_{S,i} \quad (\text{eq. 3.15})$$

Where,

\forall_g = volume of gas phase (air volume in indoor pool facility).

C_g = concentration of contaminant (NCl_3) in air space, and leaving air space.

t = time.

Q_g = volumetric flow rate of air into (and out of) the air space.

$C_{g,in}$ = concentration of contaminant (NCl_3) in outside air entering the air space.

Φ_B = (net) rate of mass transfer of contaminant (NCl_3) from liquid→gas under baseline conditions.

$\Phi_{S,i}$ = (net) rate of mass transfer of contaminant (NCl_3) from liquid→gas attributable to i^{th} swimmer.

n = number of swimmers.

For the specific case of NCl_3 , we can assume that $C_{g,in} = 0$, because outside air that is brought into the studied systems was assumed to be “clean,” in terms of gas-phase NCl_3 (*i.e.*, it does not contain NCl_3). Two-film theory was used to calculate Φ_B and $\Phi_{S,i}$ by multiplying the flux terms by an appropriate gas:liquid interfacial area. For the baseline condition, the relevant area was the total surface area of the studied pool. Φ_B was calculated as shown in equation 6.1. When swimmers are present in the pool, each swimmer will impart mechanical mixing energy on the water (and air) in the immediate vicinity of the gas:liquid interface. That mixing energy will promote transfer of volatile compounds across the air:water interface from an area surrounding the swimmer. $\Phi_{S,i}$ was calculated as described in equation 6.2.

$$\Phi_B = K_l A (C_l - C_l^*) \quad (\text{eq. 6.1})$$

Where,

K_l : mass-transfer coefficient based on liquid phase measurements.

A : total surface area of the swimming pool.

C_l : liquid-phase concentration of volatile compound (NCl_3).

C_l^* : liquid-phase concentration of volatile compound (NCl_3) that would be in equilibrium with the gas phase.

$$\Phi_{S,i} = K_{l,i} A_i (C_l - C_l^*) \quad (\text{eq. 6.2})$$

Where,

$K_{l,i}$: overall mass-transfer coefficient based on liquid phase measurements for the i^{th} swimmer.

A_i : area disturbed by the i^{th} swimmer.

When applying equations 6.1 and 6.2, it was assumed that the liquid-phase concentration of volatile compound that would be in equilibrium with the gas phase was negligibly small as compared with C_l and could be ignored. This assumption was based on the fact that measured gas-phase concentrations of volatile DBPs are typically about 1% of their respective equilibrium values (Weng et al., 2011). Specifically, the reported gas-phase concentrations of volatile DBPs in indoor pool facilities are typically on the order of 1% of their equilibrium values. This means that $C_l \gg C_l^*$ for most (if not all) volatile DBPs in indoor pool facilities. Also, it was assumed that mixing and transport behavior delivered by each swimmer was independent and therefore additive. Therefore, the net mass-transfer caused by a group of n swimmers was expressed as equation 6.3.

$$\Phi_S = \sum_{i=1}^n \Phi_{S,i} = \sum_{i=1}^n K_{l,i} A_i C_l \quad (\text{eq. 6.3})$$

After further examination, it was discovered that $K_{l,i}$ could not be estimated for each swimmer. Similarly, it was not possible to accurately measure A_i for each swimmer, independently. As an alternative to estimating these parameters independently for each swimmer,

calculations were based on the summation of $K_{l,i}A_i$. As such, equation 4.3 was transformed to equation 6.4:

$$\sum_{i=1}^n K_{l,i}A_iC_l = nK_l'C_l \quad (\text{eq. 6.4})$$

Where,

n : number of swimmers.

K_l' : effective mass transfer coefficient (equal to $\sum_{i=1}^n K_{l,i}A_i$).

C_l : liquid-phase concentration of volatile compound.

Based on the limitations described above, the IAQ model for NCl_3 was simplified, as shown in equation 6.5.

$$V_g \frac{dC_g}{dt} = -Q_gC_g + K_lAC_l + nK_l'C_l \quad (\text{eq. 6.5})$$

A similar approach was used to develop an IAQ model for CO_2 . However, the assumption of negligibly equilibrium liquid-phase CO_2 was not applicable for the CO_2 model. In addition, some modifications were required because CO_2 is present in the atmosphere naturally. Ambient CO_2 is brought into each pool facility by its HVAC system. Also, humans exhale CO_2 . Respiration/emission rates of CO_2 for swimmers are also likely to differ from lifeguards, pool workers, and spectators. Extra terms were added to the general governing equation, as shown in equation 6.6.

$$V_g \frac{dC_g}{dt} = Q_gC_{g,in} - Q_gC_g + K_lA(C_l - C_l^*) + nK_l'(C_l - C_l^*) + nemCO_2' + NemCO_2 \quad (\text{eq. 6.6})$$

Where,

$C_{g,in}$: concentration of gas-phase CO_2 in outside air entering the air space.

C_l^* : equilibrium concentration of liquid-phase CO_2 .

n : number of swimmers.

$emCO_2'$: CO_2 emission rate by swimmers.

N : number of non-swimmers.

$emCO_2$: CO_2 emission rate by non-swimmers.

Equations 6.5 and 6.6 were applied under the assumption that liquid-phase concentrations of NCl_3 and CO_2 changed linearly (with time) between measured values in pool water samples, and that the pools were each well-mixed. For the time being, it is not possible to accurately simulate DBP or CO_2 formation dynamics in pool water because the kinetics of many of the participating reactions are undefined. CO_2 gas is also used in many pools for pH control. At present, it is not possible to accurately simulate the dynamics of liquid-phase CO_2 concentrations in pools. Also, it is important to point out that swimmers likely exhale CO_2 under water. The behavior will potentially lead to transfer of gas-phase CO_2 into water. However, the CO_2 model described herein did not account for this CO_2 source. This approach was used for two reasons. First, the exhaled gas bubbles that are released from swimmers to water are likely to be fairly large. Second, the coarse bubbles that are released to the air are generated immediately below the air:water interface. Some of the exhaled CO_2 from swimmers who are swimming freestyle, butterfly, or breaststroke will be emitted above water surface; less of the exhaled CO_2 from backstroker was released underwater. To simplify the model, this study assumed that all exhaled CO_2 from swimmers was released to the gas-phase.

6.2 Estimation of parameters

The parameters included in equations 6.5 and 6.6 can be either measured or estimated. \forall_g was estimated from building drawings, based on the physical dimensions of the air space. Q_g was calculated from measured air velocity as a function of damper opening setting and the cross-sectional dimensions of the inlet duct for the pool facility, as described in 3.24. Gas-phase NCl_3 was measured by NEMo devices, while liquid-phase NCl_3 was quantified by MIMS. Surface area was calculated based on the measured dimensions of the pool surface. The number of swimmers was recorded hourly during each sampling period. For equation 6.5, dividing both sides of the equation by \forall_g and doing a little rearranging, the governing equation can be presented as equation 6.7.

$$\frac{dC_g}{dt} + \frac{Q_g}{\forall_g} C_g = K_l \frac{A}{\forall_g} C_l + \frac{n}{\forall_g} K' C_l \quad (\text{eq. 6.7})$$

Equation 6.7 can be rearranged and presented in finite difference form as equation 6.8 below.

$$\Delta C_g = \frac{\Delta t}{V_g} (-Q_g C_g) + \frac{\Delta t}{V_g} (K_l A C_l) + \frac{\Delta t}{V_g} (n K' C_l) \quad (\text{eq. 6.8})$$

At steady-state ($\frac{dC_g}{dt} = 0$), with no swimmers in the pool ($n = 0$), equation 6.7 will reduce to equation 6.9.

$$\frac{Q_g}{V_g} C_{g,ss} = K_l \frac{A}{V_g} C_{l,ss} \quad (\text{eq. 6.9})$$

Where,

Q_g = steady-state air flow rate (flow rate when no people are in the pool facility).

$C_{g,ss}$ = steady-state concentration of NCl_3 in the gas phase (concentration when no swimmers were present in the pool).

$C_{l,ss}$ = steady-state concentration of NCl_3 in the liquid phase (concentration when no swimmers were present in the pool).

If steady-state concentrations in both phases are achieved (probably early morning after an extend period of no use of the pool), it is then possible to rearrange equation 6.9 to develop an estimate of the value of K_l , as described by equation 6.10.

$$K_l = \frac{Q_g C_{g,ss}}{A C_{l,ss}} \quad (\text{eq. 6.10})$$

The only remaining unresolved term in equation 6.5 was K' . Equation 6.8 describes the incremental changes in C_g that took place in each time step of a monitoring period. By extension, this information can be used to simulate the time-course behavior of C_g for a monitoring period:

$$C_g(t + \Delta t) = C_g(t) + \Delta C_g \quad (\text{eq. 6.11})$$

A regression model was used to estimate K' by least-squares fitting of equation 6.11 to the time-course measurements of gas-phase NCl_3 concentration. It is important to reiterate that linear

interpolation was used to simulate liquid-phase NCl_3 concentration. In other words, the value of liquid-phase NCl_3 concentration used in the simulations was estimated by linear interpolation between measured values of liquid-phase NCl_3 concentration. This approach was applied because concentrations of gas-phase NCl_3 were reported every 10 minutes during the entire sampling periods, yet water samples were collected and analyzed approximately every 2 hours when pool facility was open to public; water samples were not collected or analyzed when the pool facility was closed. This process represents a source of error in application of the model.

For equation 6.6, many of the input parameters were also measurable, including V_g , Q_g , C_l , n and N . At steady-state, with no people in the pool, equation 6.6 will reduce to equation 6.12.

$$Q_g(C_{g,ss} - C_{g,in}) = K_l A(C_{l,ss} - C_l^*) \quad (\text{eq. 6.12})$$

Where,

Q_g = steady-state air flow rate (flow rate when no people are in the pool facility).

$C_{g,ss}$ = steady-state concentration of CO_2 in the gas phase (concentration when no people were present in the pool facility).

$C_{g,in}$ = concentration of CO_2 in the air that is brought into the pool facility (this concentration was assumed to be equal to the value reported at the Mauna Loa observatory at the time of these experiments (410 ppm_v), which was converted to mass concentration based on the ideal gas law).

$C_{l,ss}$ = steady-state concentration of CO_2 in the liquid-phase (concentration when no people were present in the pool facility).

C_l^* = equilibrium concentration of CO_2 in the liquid-phase (concentration when no people were present in the pool facility). Calculated by application of Henry's law to measured values of CO_2 concentration in air above the pool.

Algebraic rearrangement of equation 6.12 yields equation 6.13, which was used to estimate the value of K_l for CO_2 .

$$K_l = \frac{Q_g(C_{g,ss} - C_{g,in})}{A(C_{l,ss} - C_l^*)} \quad (\text{eq. 6.13})$$

The term $emCO_2$ was calculated based on reported respiration rates for humans. This calculation was based on several reported values, as illustrated in equation 6.14. First, humans exhale a CO_2 at a concentration of 4~5% in each breath (Taucher et al., 1996). Tidal volume represents the volume of air that moves in or out of the lungs with each respiratory cycle. Typical tidal volumes for healthy adult males at rest are roughly 500 mL and approximately 400 mL for an average healthy female (Hallett and Ashurst, 2019). The typical breathing frequency in normal humans is within the range of 10 to 20 breaths per minute (Russo et al., 2017). Thus, $emCO_2$ was calculated as follows:

$$emCO_2 = 450 \frac{mL}{breath} \times 4.5\% \times 15 \frac{breath}{minute} = 304 \frac{mL}{minute} = 18240 \frac{mL}{hour} = 32600 \frac{mg}{hour} \quad (\text{eq. 6.14})$$

For each of the terms in equation 6.14 (tidal volume, CO_2 concentration, breathing frequency), a mean value was applied. In addition, these values were assumed to apply generally to all non-swimmers who were present in the facility. The selection of mean values was intended to provide an estimate of the CO_2 emission rate for the non-swimmers that were present in the facility, but also represents a source of error in application of the CO_2 model.

For $emCO_2'$, the respiratory pattern of swimmers was characterized by the tidal volume associated with spontaneous breathing exercise (Rodríguez, 2000). The measurements of breathing frequency during all-out front crawl, backstroke, or breast stroke swimming in trained swimmers has been reported to be between 39 to 57 breaths per minute and reports of tidal volume have ranged between 1.43 to 3.54 Liters (Bonen et al., 1980; Holmér et al., 1974a, 1974b; Magel and Faulkner, 1967; Rodríguez, 2000). Thus, $emCO_2'$ was calculated as illustrated in equation 6.15:

$$emCO_2' = 2000 \frac{mL}{breath} \times 4.5\% \times 48 \frac{breath}{minute} = 4320 \frac{mL}{minute} = 324000 \frac{mL}{hour} = 470000 \frac{mg}{hour} \quad (\text{eq. 6.15})$$

6.3 Results of NCl_3 IAQ model

Estimates of mass transfer coefficients for NCl_3 at Pool Facility B were developed by fitting of the IAQ model to data from experiments that were conducted in March, April, and June 2019. The fitting was conducted by identifying the K' value that yielded the minimum value of residual

sum of the square (RSS) errors of (measured gas-phase NCl_3 concentration – model gas-phase NCl_3 concentration). As described above, linear interpolation was used to estimate liquid-phase NCl_3 concentrations; this interpolation approach was applied because liquid-phase NCl_3 concentration was measured less frequently than gas-phase NCl_3 concentration. Similarly, the number of swimmers in the pool was manually counted only every top of the hour; for purposes of these simulations, the number of swimmers in the pool was assumed to be constant for each one-hour period.

A sample spreadsheet from NEMo A, as applied to the March 2019 study data for pool facility B to estimate K_l , is presented in Appendix A. Specific input parameters used in the spreadsheet are listed in Table 6.1. Fitting curves of RSS versus K' for each NEMo device data set are shown in Figures 6.1 to Figure 6.7.

Table 6.2 provides a summary of the values of the best-fit mass transfer coefficients for these data sets. The results of K_l multiplied by pool surface area are also shown in Table 6.2 because mass transfer coefficients are sometimes reported as the product $K_l A$. The lower steady-state concentrations of liquid-phase NCl_3 during April experiments caused values of $K_l A$ for the April study to be larger than those from other experiments, as shown in Table 6.2. Generally, K' values were similar during March and April studies as both were collected during regular operation hours. The difference of K' among the March, April, and June experiments was mainly attributed to differences in the ages of the swimmers from these experiments. Specifically, the March and April data sets were collected during a period of normal operations, when the majority of swimmers were adult recreational lap swimmers. In contrast, the data from the June 2019 experiment was collected during a swimming competition for children at age 8 and under.

For comparison, reported values of K_l for other air:water systems are as follows. For still ponds and pools that are included in indoor air spaces, reported estimates of K_l ranged from: $1.8 \times 10^{-4} \frac{m}{hr} \leq K_l \leq 5.63 \times 10^{-3} \frac{m}{hr}$ (Guo and Roache, 2003). It is important to point out that these values were developed for stagnant bodies of water. For surface waters that move (*e.g.*, rivers, estuaries), reported estimates are larger. For example, reported estimates of K_l for PCB air:water exchange in the New York-New Jersey Harbor Estuary were: $0.0013 \frac{m}{hr} \leq K_l \leq 0.015 \frac{m}{hr}$ (Totten et al., 2001). The estimates of K_l in this study are within the range of values reported for this estuary. In addition, Schwarzenbach *et al.* (2003) reported a calculated liquid-phase mass transfer

coefficient for NCl_3 of $0.0216 \frac{m}{hr}$ for an unused pool, based on the Deacon's boundary layer theory, which is slightly higher than the values observed this study.

Table 6.1. Input parameters used in NCl_3 IAQ model spreadsheet.

Parameter	Units	Explanation
Δt	hour	Time gradient
$C_g \text{ NCl}_3$	mg/m^3	Concentration of measured gas-phase NCl_3
$C_l \text{ NCl}_3$	mg/L	Concentration of measured liquid-phase NCl_3
n Swimmer		Swimmer count
V_g	m^3	Representative value of air volume above the studied facility
Q_g	m^3/hour	Measurement of air flow rate
A	m^2	Representative value of pool surface area of studied pool
K_l	m/hour	See equation 6.10
delta C_g	mg/m^3	Gas-phase NCl_3 concentration gradient. See equation 6.8

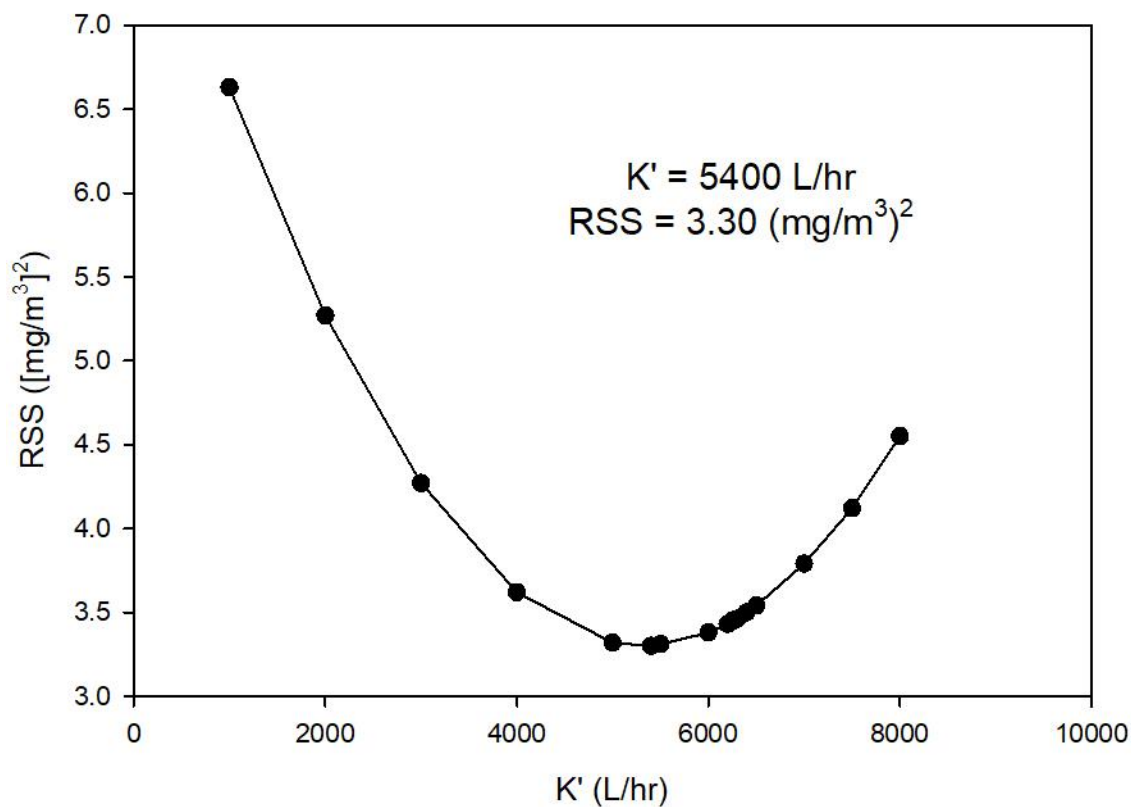


Figure 6.1. Fitting curve of the selection for best-fit value of K' from NEMo A from March 2019 study at pool facility B. RSS = Residual sum of (measured gas-phase NCl_3 concentration – model gas-phase NCl_3 concentration)². K' = liquid to gas phase of NCl_3 mass transfer coefficient.

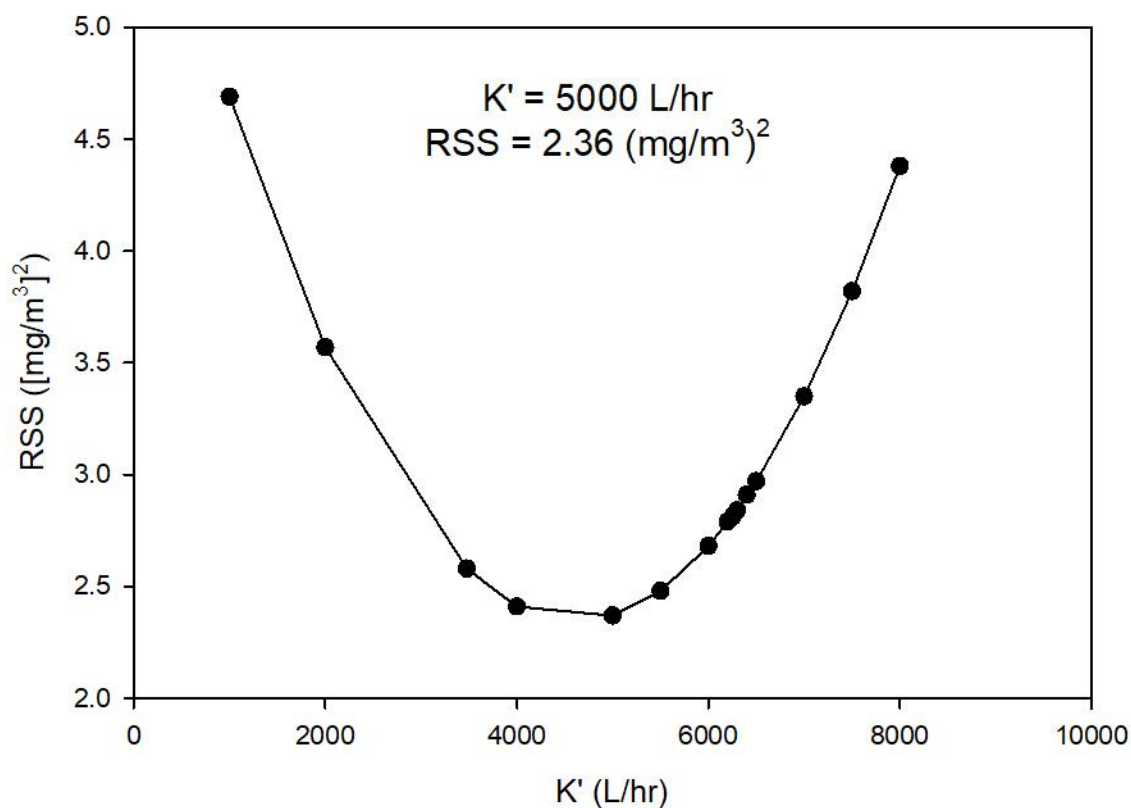


Figure 6.2. Fitting curve of the selection for best-fit value of K' from NEMo B from March 2019 study at pool facility B. RSS = Residual sum of (measured gas-phase NCl_3 concentration – model gas-phase NCl_3 concentration)². K' = liquid to gas phase of NCl_3 mass transfer coefficient.

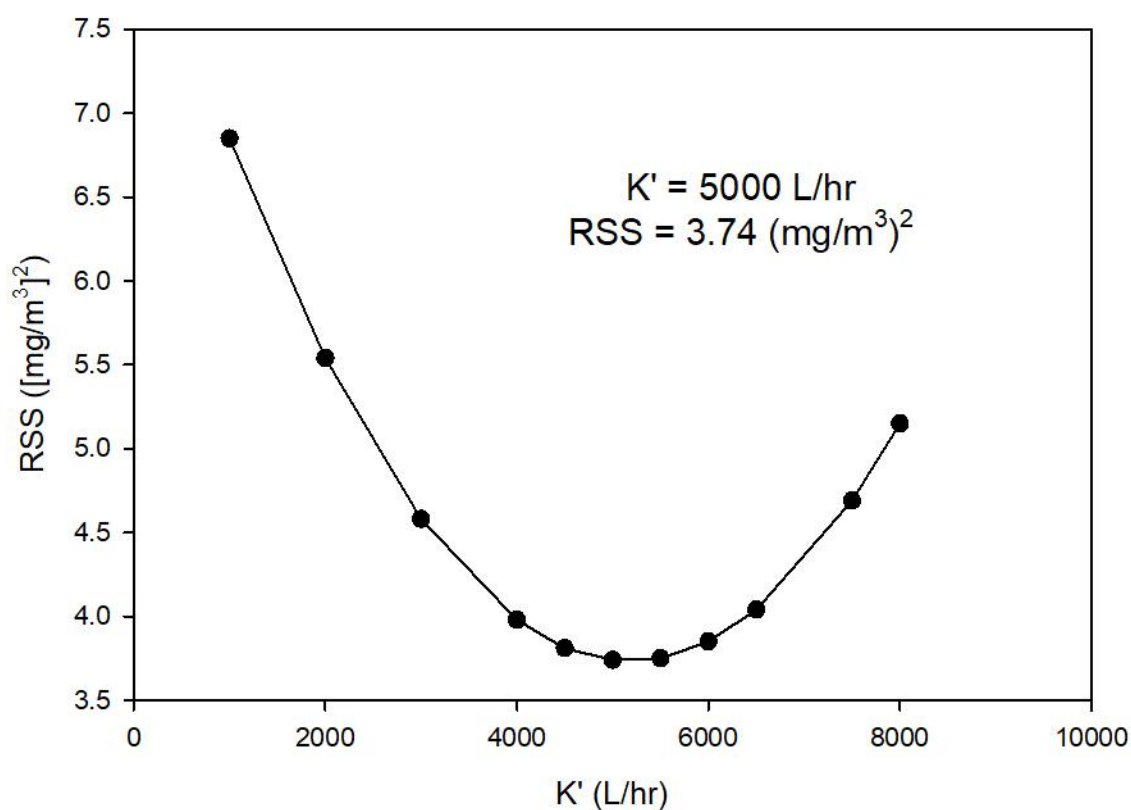


Figure 6.3. Fitting curve of the selection for best-fit value of K' from NEMo C from March 2019 study at pool facility B. RSS = Residual sum of (measured gas-phase NCl_3 concentration – model gas-phase NCl_3 concentration) 2 . K' = liquid to gas phase of NCl_3 mass transfer coefficient.

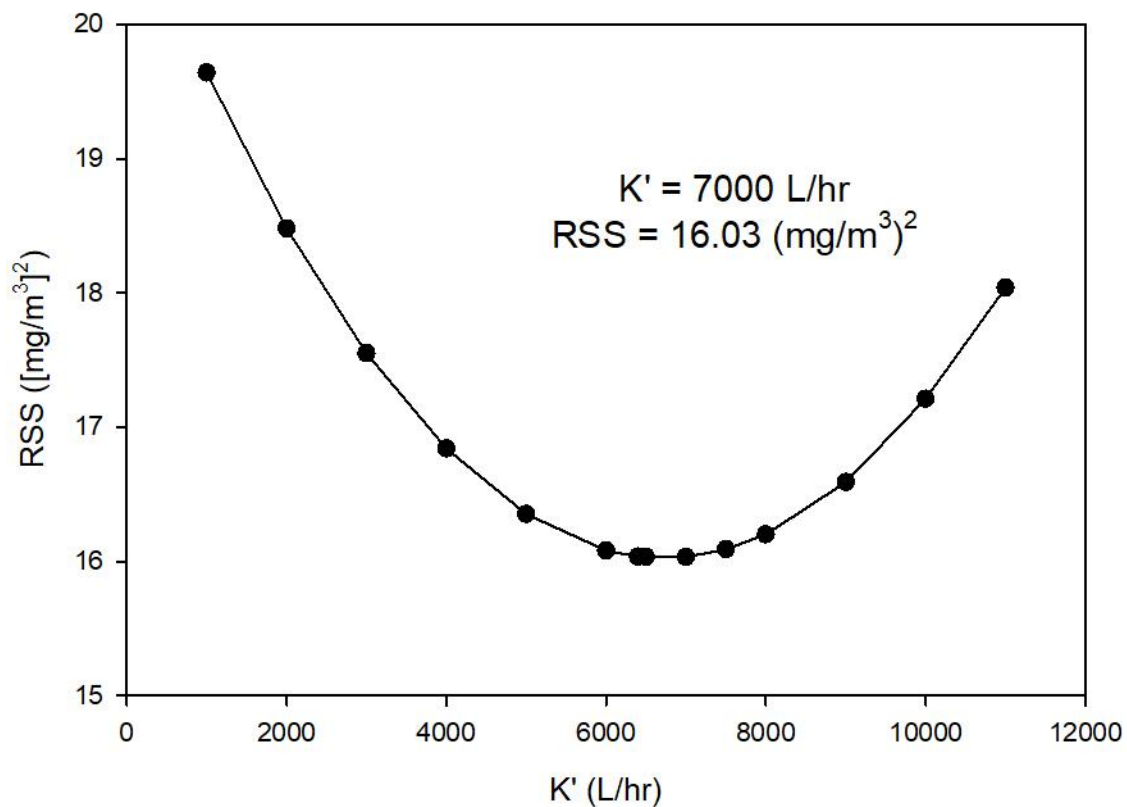


Figure 6.4. Fitting curve of the selection for best-fit value of K' from NEMo B from April 2019 study at pool facility B. RSS = Residual sum of (measured gas-phase NCl_3 concentration – model gas-phase NCl_3 concentration)². K' = liquid to gas phase of NCl_3 mass transfer coefficient.

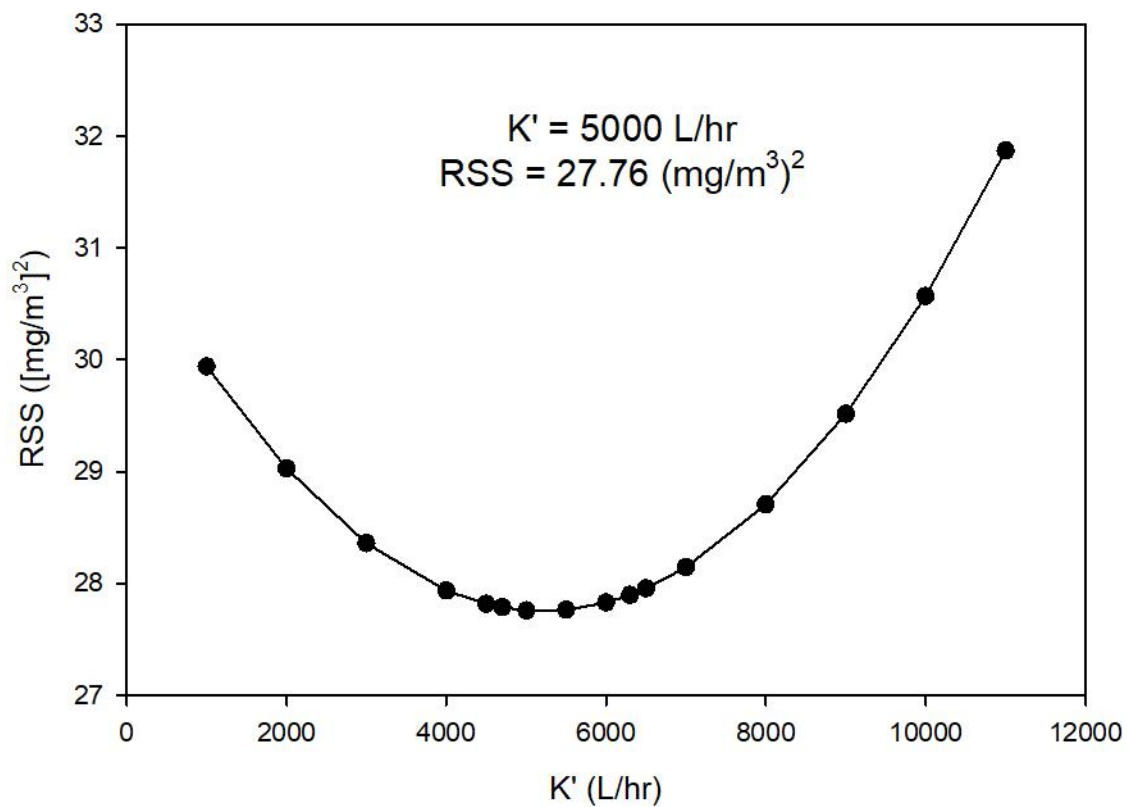


Figure 6.5. Fitting curve of the selection for best-fit value of K' from NEMo C from April 2019 study at pool facility B. RSS = Residual sum of (measured gas-phase NCl_3 concentration – model gas-phase NCl_3 concentration)². K' = liquid to gas phase of NCl_3 mass transfer coefficient.

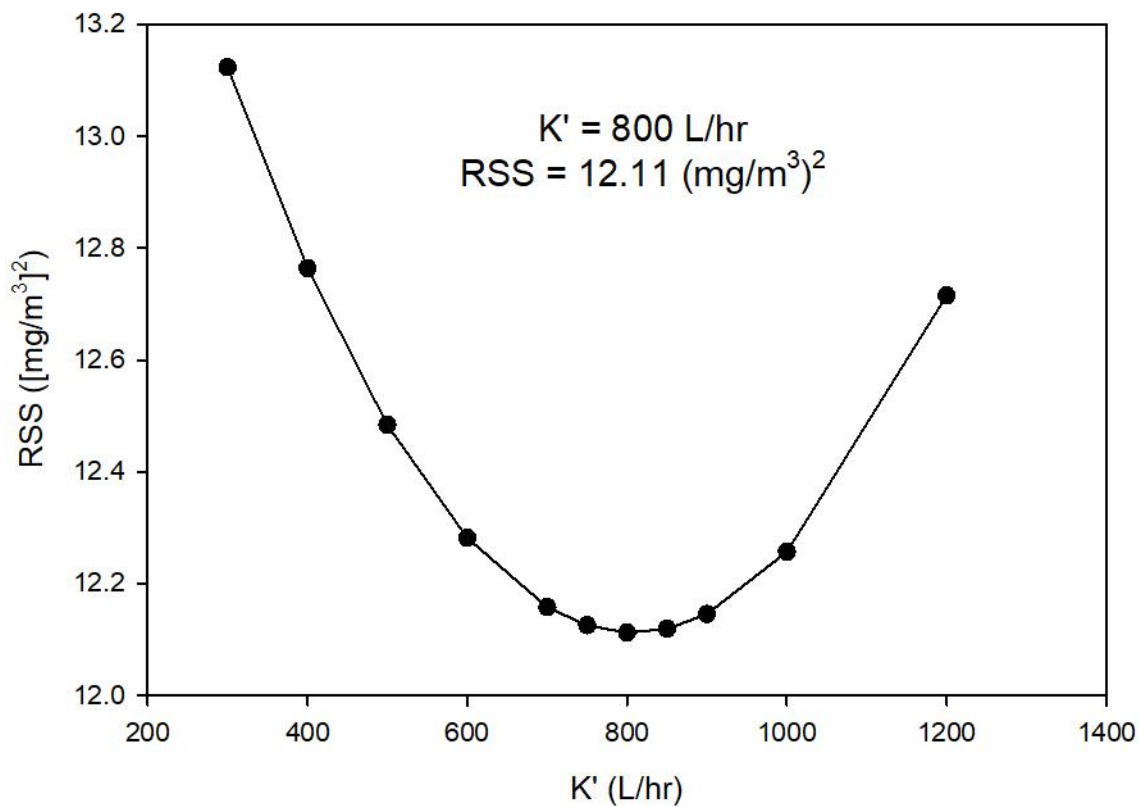


Figure 6.6. Fitting curve of the selection for best-fit value of K' from NEMo A from June 2019 study at pool facility B. RSS = Residual sum of (measured gas-phase NCl_3 concentration – model gas-phase NCl_3 concentration)². K' = liquid to gas phase of NCl_3 mass transfer coefficient.

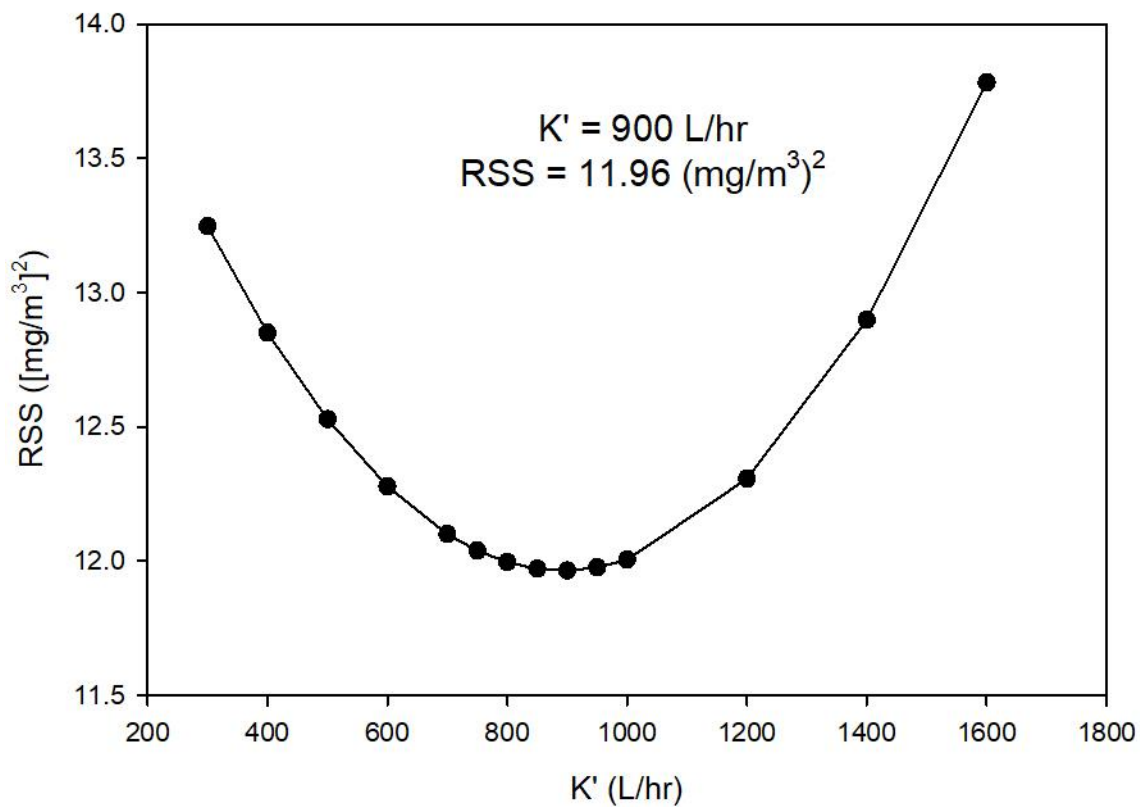


Figure 6.7. Fitting curve of the selection for best-fit value of K' from NEMo B from June 2019 study at pool facility B. RSS = Residual sum of (measured gas-phase NCl_3 concentration – model gas-phase NCl_3 concentration) 2 . K' = liquid to gas phase of NCl_3 mass transfer coefficient.

Table 6.2. Summary of conditions of each experiment and corresponding estimates of mass transfer coefficients for NCl_3 .

Pool facility B	Date	Type of swimmer	Age of swimmers	K_l (m/hour)	$K_l A$ (m ³ /hour)	K' (m ³ /hour)	RSS ((mg/m ³) ²)
March NEMo A	3/6/2019 to	Daily lap swimmers	Adults	0.0024	4.07	5.40	3.30
March NEMo B	3/8/2019			0.0022	3.64	5.00	2.36
March NEMo C		Swim team practice	College students	0.0023	3.86	5.00	3.74
April NEMo B	4/22/2019 to	Daily lap swimmers	Adults	0.0077	11.5	7.00	16.0
April NEMo C	4/26/2019			0.0069	12.9	5.00	27.8
		Swim team practice	College students				
June NEMo A	6/21/2019 to	Age group swimmers	8 and under	0.0022	3.67	0.80	12.1
June NEMo B	6/24/2019			0.0017	2.76	0.90	12.0

A: studied pool surface area is 1670 m²

The model was applied with the estimated values of mass transfer coefficients to simulate the dynamic behavior of gas-phase NCl_3 concentration for each of the experiments. These simulations were developed using the measured (interpolated) values liquid-phase NCl_3 , swimmer counts, and air flow rate. The simulation results for facility B for March 2019 are illustrated in Figures 6.8 to 6.10. The simulation results for facility B for April 2019 are illustrated in Figures 6.11 and 6.12. The March and April 2019 experiments were both conducted during regular operation hours. The pool was used by recreational lap swimmers, swimming practice, and for swimming lessons during these experiment periods.

A source of error in the application of the model for simulations of IAQ dynamics during these periods was that only single values of the mass transfer coefficients were applied for each experiment. It is clear that K' will be different when a pool is occupied by swimmers of different ages and different activity levels. Figures 6.8 to 6.12 indicate that the timing and magnitude of the simulated peaks of gas-phase NCl_3 concentration were similar to the measured timing and magnitudes of these peaks; however, differences in these values are also clearly evident in the figures. It is clear that swimmer number is a critical factor in governing IAQ in indoor pool facilities. Previous experimental measurements and modeling simulations have also supported the importance of the link between swimmer number and IAQ (Gérardin et al., 2015; Tsamba et al., 2020; Weng et al., 2011; Wu et al., 2021).

An important application of this model is for prediction of how often and how long gas-phase NCl_3 will exceed the guideline upper limits of 0.3 mg/m^3 (Bernard et al., 2006) or 0.5 mg/m^3 (WHO, 2006). Some deviations between model and measurement were evident in these results, but the model predictions were generally similar to measurements from these experiments.

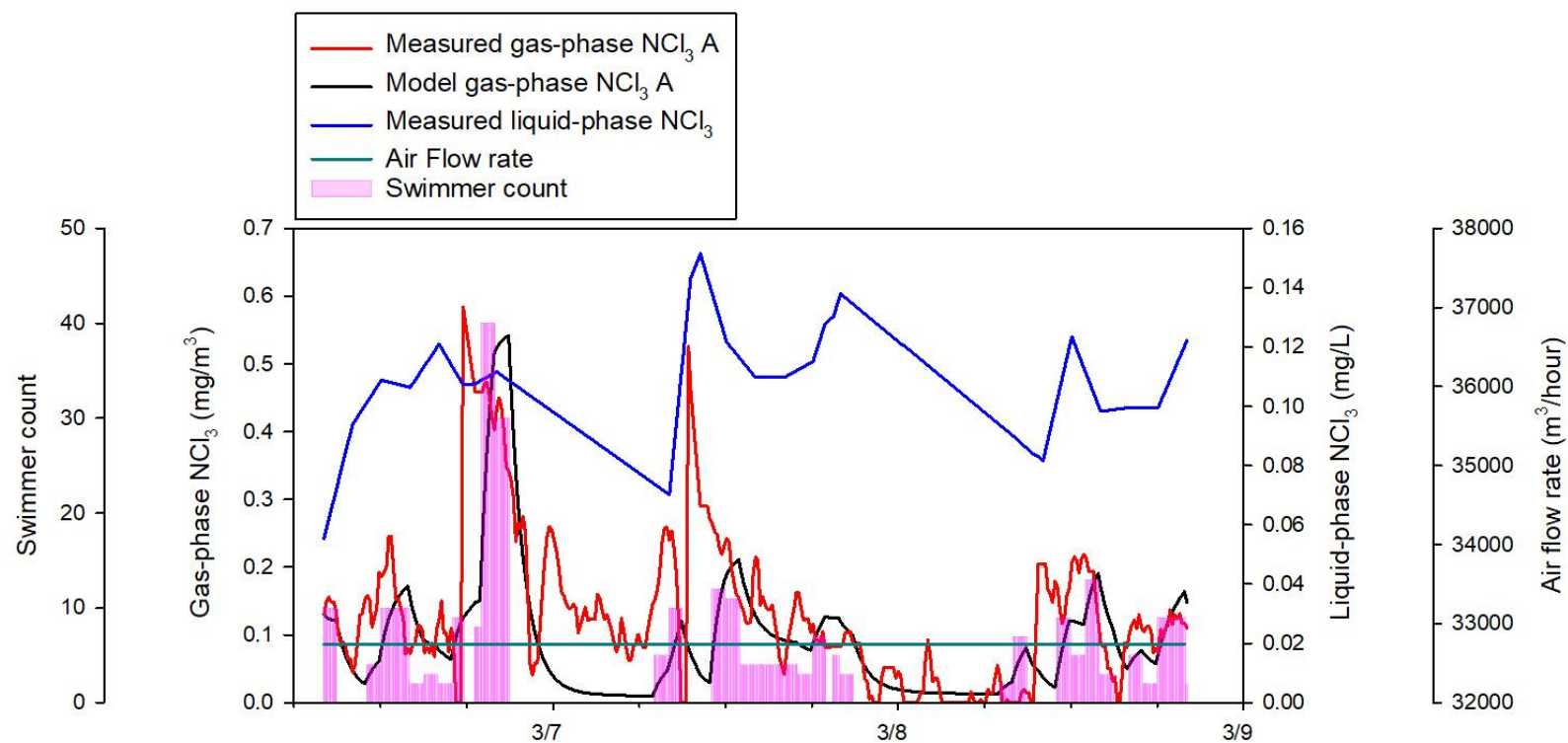


Figure 6.8. Time-course monitoring of gas-phase NCl_3 by NEMo device A and liquid-phase NCl_3 with model gas-phase NCl_3 , and trend of air flow rate in pool facility B during experiment in March 2019. Vertical bars represent the number of swimmers in pool facility B.

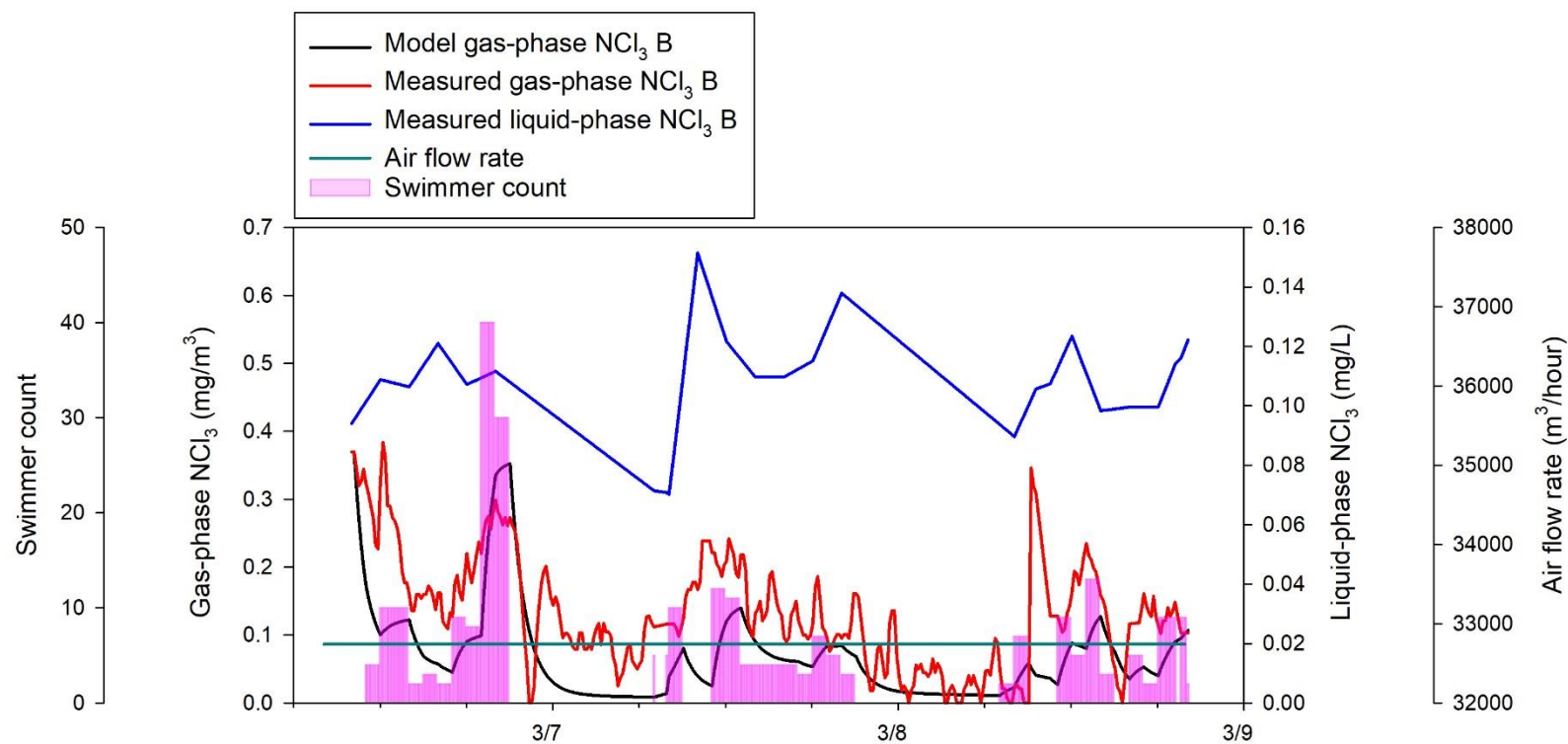


Figure 6.9. Time-course monitoring of gas-phase NCl_3 by NEMo device B and liquid-phase NCl_3 with model gas-phase NCl_3 , and trend of air flow rate in pool facility B during experiment in March 2019. Vertical bars represent the number of swimmers in pool facility B.

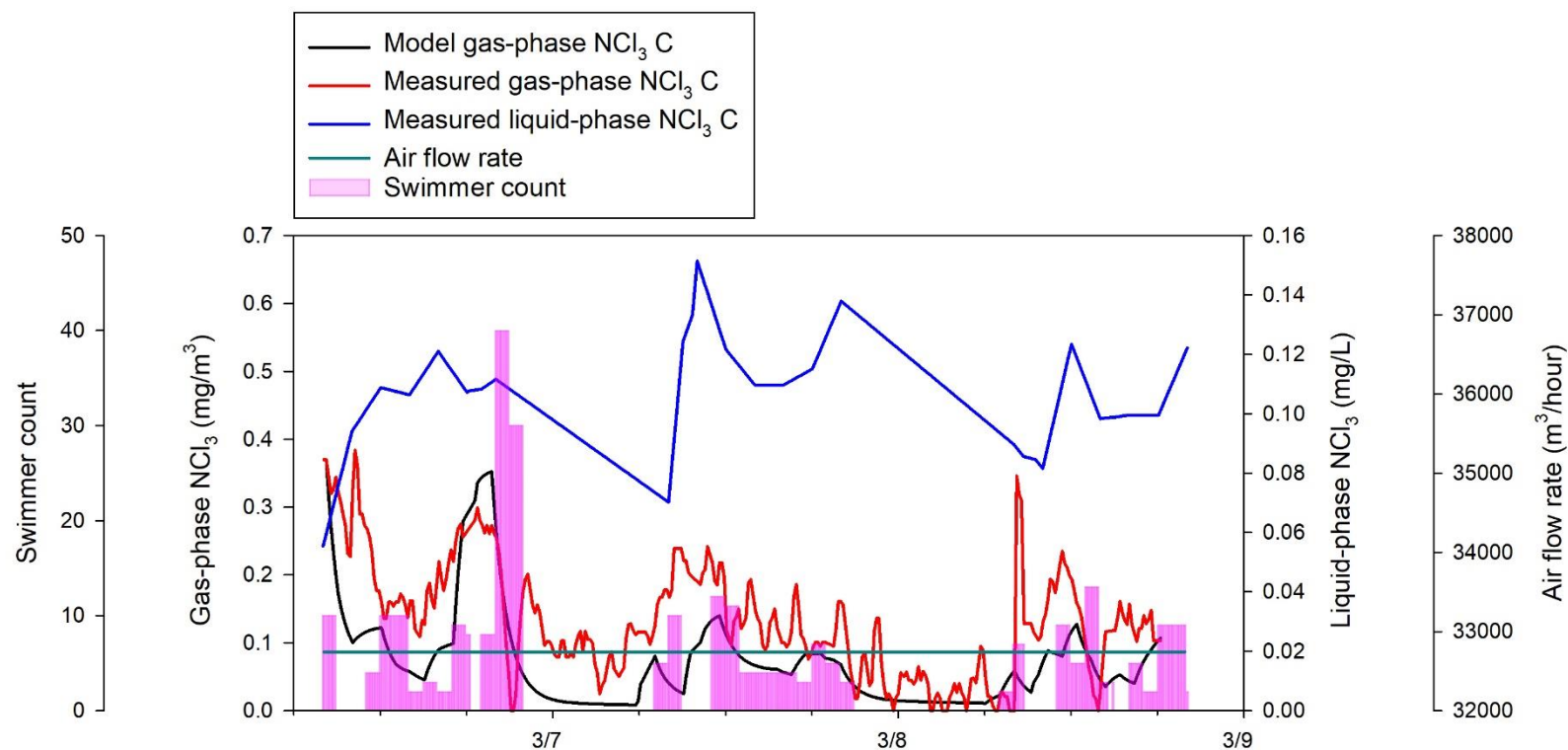


Figure 6.10. Time-course monitoring of gas-phase NCl_3 by NEMo device C and liquid-phase NCl_3 with model gas-phase NCl_3 , and trend of air flow rate in pool facility B during experiment in March 2019. Vertical bars represent the number of swimmers in pool facility B.

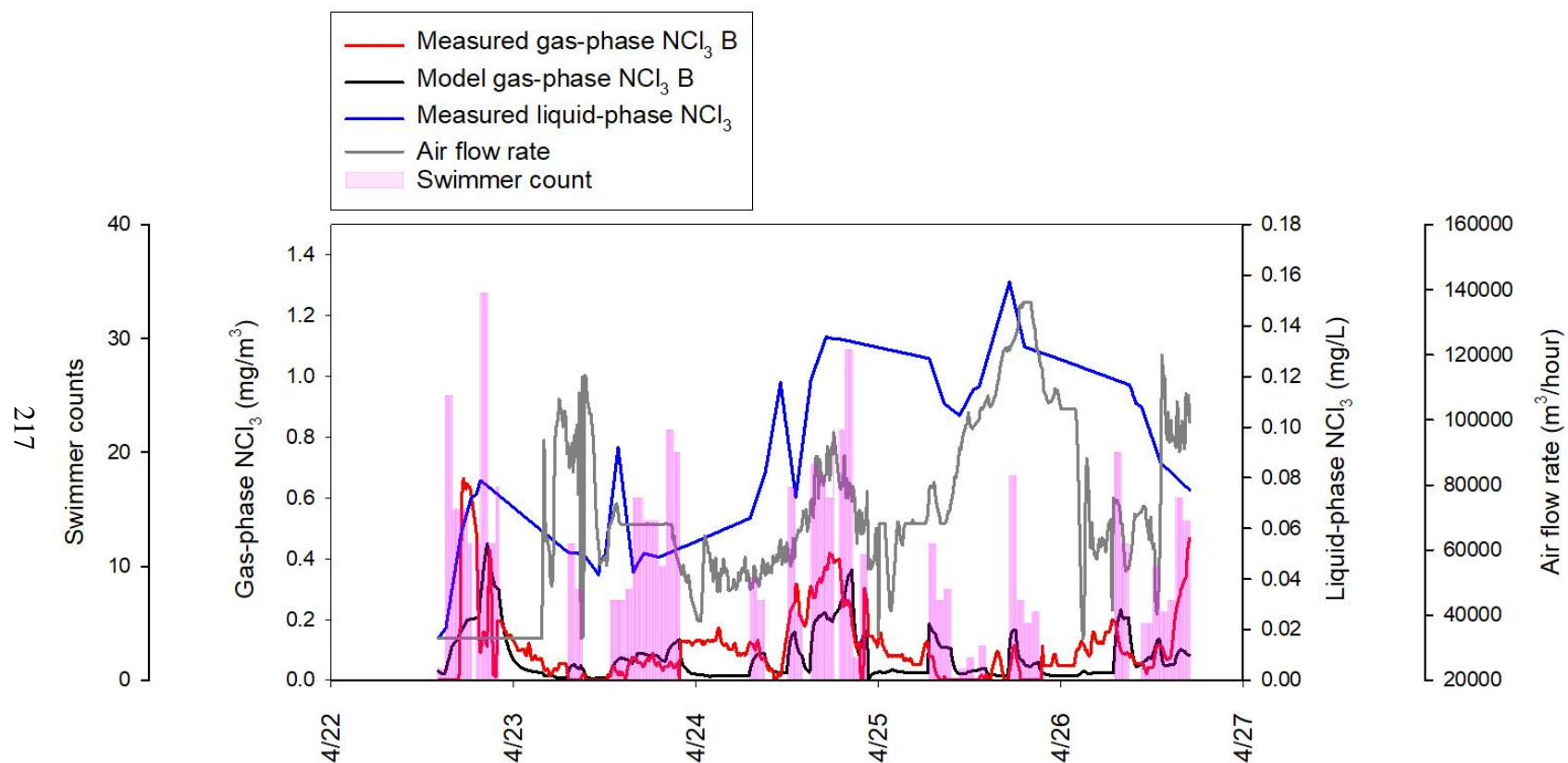


Figure 6.11. Time-course monitoring of gas-phase NCl_3 by NEMo device C and liquid-phase NCl_3 with model gas-phase NCl_3 , and trend of air flow rate in pool facility B during experiment in April 2019. Vertical bars represent the number of swimmers in pool facility B.

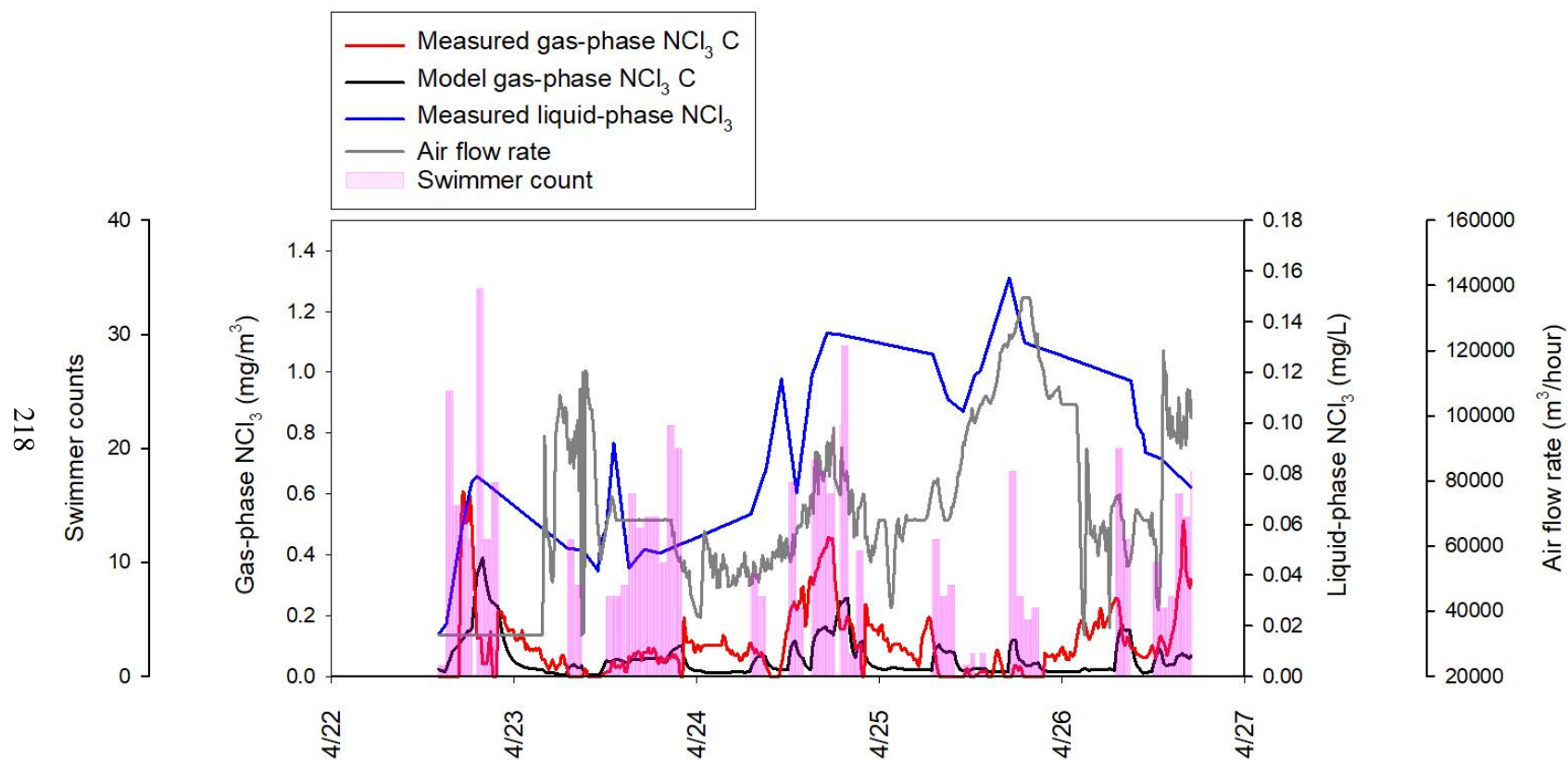


Figure 6.12. Time-course monitoring of gas-phase NCl_3 by NEMo device C and liquid-phase NCl_3 with model gas-phase NCl_3 , and trend of air flow rate in pool facility B during experiment in April 2019. Vertical bars represent the number of swimmers in pool facility B.

Measurements and simulations of gas-phase NCl_3 dynamic behavior at facility B in June 2019 are presented in Figures 6.13 and 6.14. This experiment was conducted during a swimming meet for 8 and under children in which approximately 350 swimmers participated. Both figures indicate that model predictions of gas-phase NCl_3 were similar to the data, but with an apparent lag. As air flow rate in pool facility B was essentially constant and low during this experiment, it is likely that the delay was caused by the low air flow rate for this NCl_3 IAQ simulation. Also, the model predictions of local peak concentrations were not always correct. Further study will be necessary to more completely define the effects of various types of swimmer activity on liquid→gas transfer dynamics. Specifically, it is expected that mechanical mixing of water will vary among activity types, such as competition events, warm-up or warm-down, and the age of the swimmer.

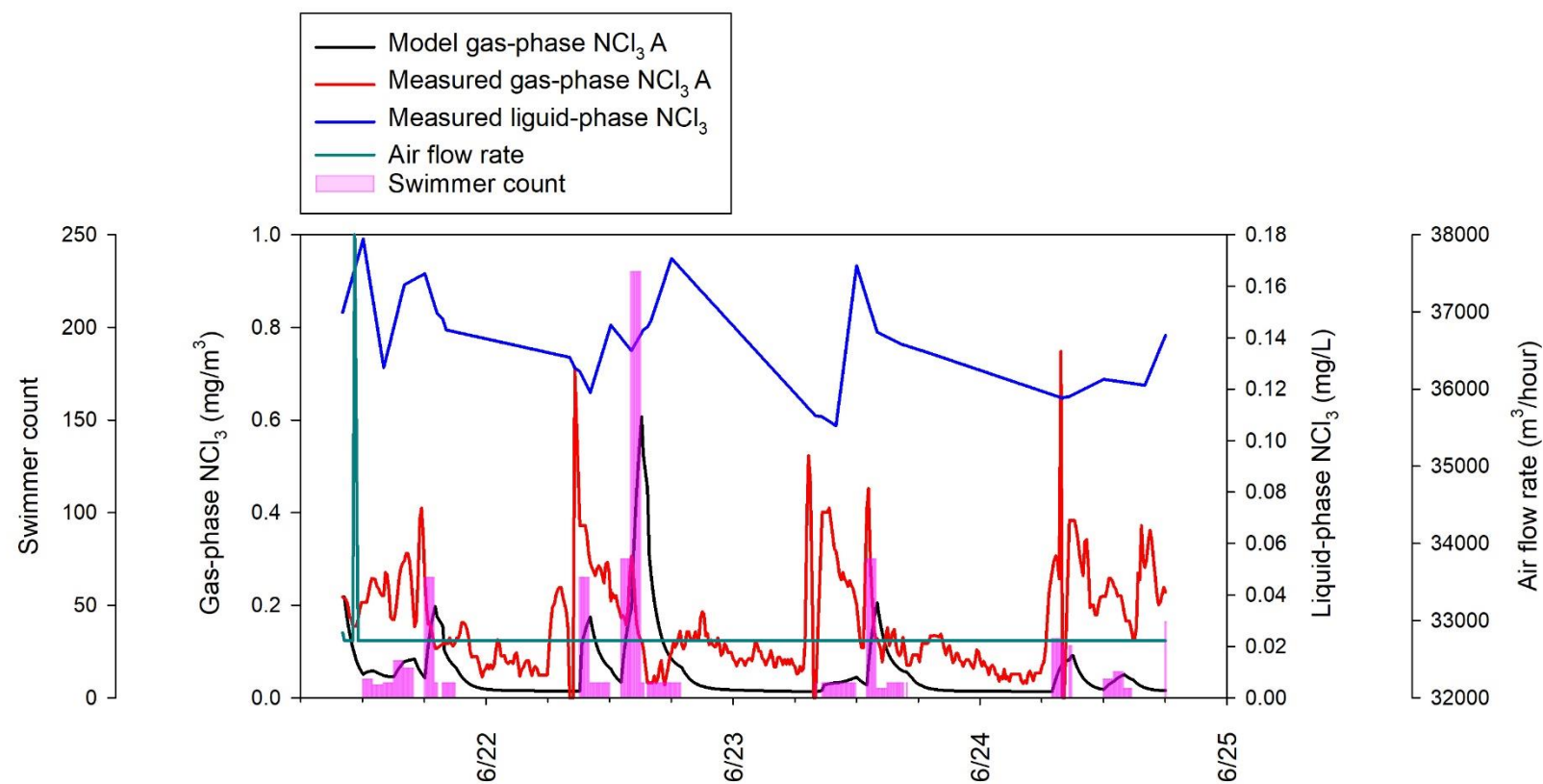


Figure 6.13. Time-course monitoring of gas-phase NCl_3 by NEMo device A and liquid-phase NCl_3 with model gas-phase NCl_3 , and trend of air flow rate in pool facility B during study in June 2019. Vertical bars represent the number of swimmers in pool facility B.

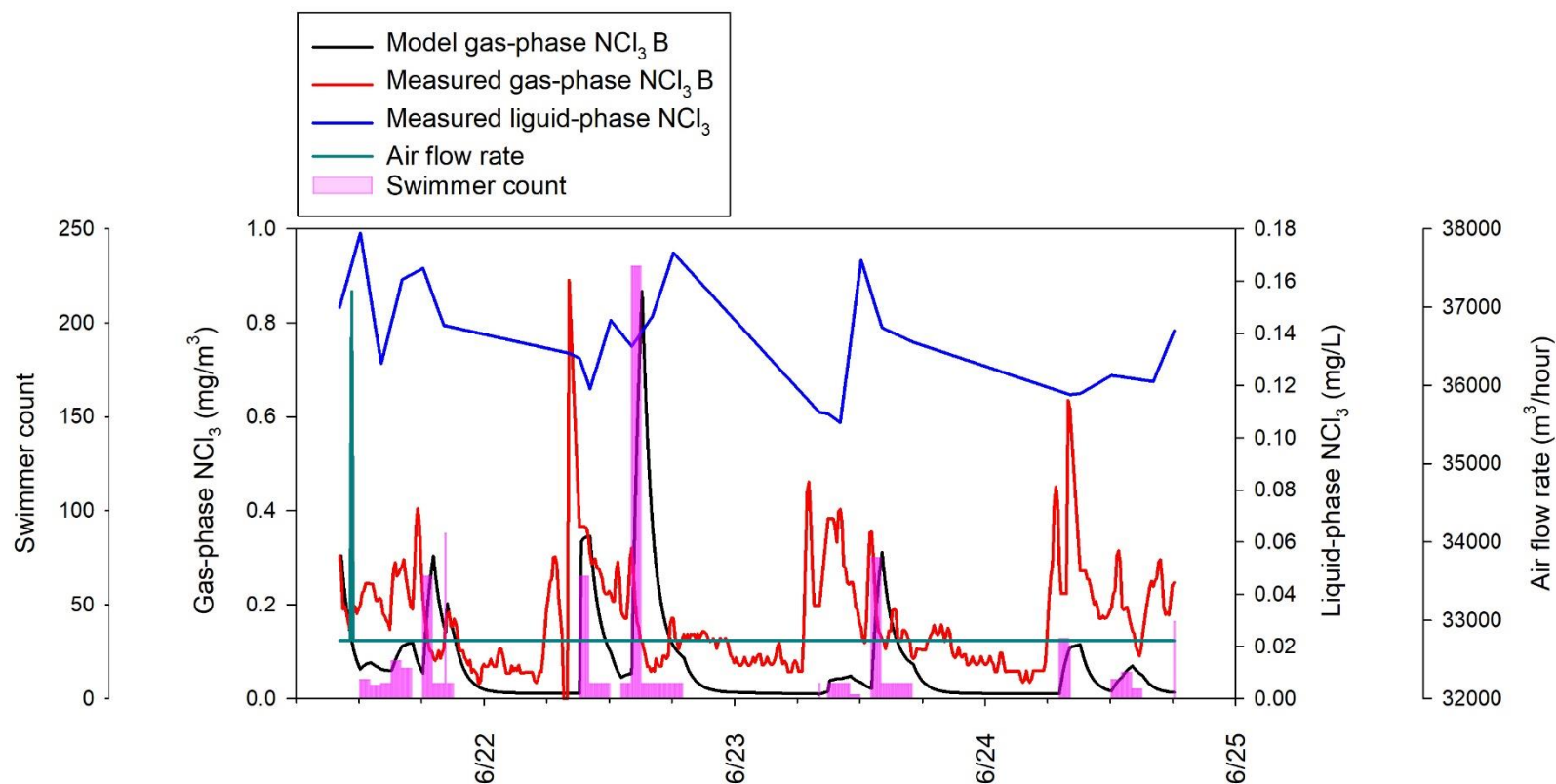


Figure 6.14. Time-course monitoring of gas-phase NCl_3 by NEMo device B and liquid-phase NCl_3 with model gas-phase NCl_3 , and trend of air flow rate in pool facility B during study in June 2019. Vertical bars represent the number of swimmers in pool facility B.

Gas-phase NCl_3 models will be useful as a tool to provide guidance for pool operators. For example, these models could be useful for prediction of circumstances that will result in the concentration of gas-phase NCl_3 exceeding guidance values, such as the upper limits of 0.3 mg/m^3 (Bernard et al., 2006) or 0.5 mg/m^3 (WHO, 2006). Pool operators could adjust the air handling units to alter the air change rate in the pool facility beforehand, thereby maintaining gas-phase NCl_3 concentrations below the target value.

Two-film theory suggests that liquid-phase concentration of NCl_3 is a driving factor for liquid-phase to gas-phase mass transfer. Therefore, it may be possible to mitigate transfer of NCl_3 to air by inclusion of a process modifications to reduce liquid-phase NCl_3 concentration. This could be accomplished by inclusion of an air stripping system into the pool water treatment process. Air stripping is a process in which volatile compounds are brought into contact with clean air, thereby promoting transfer from liquid-phase into gas-phase in a controlled manner. With proper installation of such a system, it may be possible to vent volatile compounds directly to outdoor air, rather than to the air space above a pool. This approach recognizes that most of the volatile DBPs like NCl_3 that are contained in a swimming pool facility are likely to form in the water. Previous studies have demonstrated the effectiveness of air stripping systems for removal of liquid-phase NCl_3 from pool water (Gérardin and Héry, 2005; Tardif et al., 2017). Such a system could be appropriate to augment ventilation. However, air stripping systems will consume energy, both by the pumping and ventilation requirements of the system, and by promotion of heat transfer from water (Tsamba et al., 2020). Also, off-gas treatment may be required (Huang and Shang, 2006). Another concern is stripping of desirable chemicals, such as CO_2 (pH control) which could affect pool water chemistry.

Acknowledgement of model limitations is important for proper interpretation of model predictions. Some model limitations are directly attributable to model assumptions. For example, the assumptions of well-mixed air and water will not apply strictly to pool facilities. Another limitation of this study was the frequency and location of liquid-phase NCl_3 measurements. In most experiments, liquid-phase NCl_3 was measured once every two hours from a single location. For application to the IAQ model, linear interpolation was applied to simulate liquid-phase NCl_3 dynamics. In addition, swimmer number was recorded only at the top of the hour, but for the model it was assumed that swimmer count was constant for the entire hour. Another limitation was the assumption of a single value of each mass transfer coefficient being used to describe dynamics

during an entire experiment. It is likely that mass transfer behavior will vary with the type of swimming activity, the age and physical strength of the swimmer, and the intensity of their effort. All of these factors will contribute to variability in mass transfer behavior.

6.4 Results of CO₂ IAQ model

Data from the June 2019 and November 2019 experiments at Pool facility B were used to develop the CO₂ IAQ model. Linear interpolation was used to estimate air flow rate for the November experiments; this interpolation approach was applied because gas-phase CO₂ concentration was measured every 30 seconds by LI-COR CO₂ analyzer and air flow rate was reported every 5 minutes. Similarly, the number of swimmers in the pool was manually counted only every top of the hour; for purposes of these simulations, the number of swimmers in the pool was assumed to be constant for each one-hour period. Specifically, fitting of the model to the data from these experiments was conducted to identify values of K' that minimized the residual sum of the square (RSS) error between the measured gas-phase CO₂ concentration and model predicted gas-phase CO₂ concentration. A sample spreadsheet from process is presented in Appendix B. Specific input parameters used in the spreadsheet are illustrated in Table 6.3.

The estimation of the mass transfer coefficients for the baseline conditions was conducted based on measured concentrations of liquid-phase and gas-phase CO₂. Application of the best-fit values of K' for the June 2019 and November 2019 study periods are presented in Figure 6.15 and Figure 6.16, respectively. The conditions of the experiments and estimated values of K_l and K' are summarized in Table 6.4. The K' of zero for the June 2019 study indicated that liquid to gas transfer of CO₂ was negligible for this event. The main control factors were indicated to be human respiration and input of indoor/outdoor air. The estimate of K' for CO₂ for the November 2019 experiment was slightly higher than K' values estimated for NCl₃, as illustrated in Table 6.2.

The measurements and model gas-phase CO₂ concentrations at facility B for the June 2019 experiment are presented in Figure 6.17. The swimming competition involved children aged 8 and under. The model generally provides a good fit to the data, but it appeared to over-predict two peaks of CO₂ on 6/22. The main reason for the overpredicting is believed to be due to the swimmer's exhalation. The model assumed CO₂ exhaled by swimmers would be released entirely into the air space. This assumption will result in an overestimate of the CO₂ contribution by the swimmer's exhalation.

The measurements and model gas-phase CO₂ concentrations at facility B for the November 2019 experiment are presented in Figure 6.18. This experiment was conducted during a swimming meet for collegiate athletes. The graph illustrates a good fit of the model to the data. This suggests that the CO₂ IAQ model may be more appropriate for strong adult swimmers, as opposed to youth swimmers, because liquid→gas transfer is likely to be more important for these stronger swimmers. In all, both CO₂ IAQ model applications indicated general agreement between measured and modeled CO₂ concentrations; however, clear deviations between measurements and model predictions were also evident.

Limitations of this IAQ model were similar to those of the NCl₃ models. For example, the assumptions of well-mixed air and water are not strictly correct for pool facilities, though some measurements support this assumption. Time-course concentrations of liquid-phase CO₂ were calculated from pH and alkalinity measurements that were conducted every hour. In turn, linear interpolation was applied to simulate liquid-phase CO₂ concentrations at times between these measurements. In addition, swimmer number was recorded only every hour; for the model, swimmer count was assumed to be constant for each corresponding one-hour period. This model also assumes all exhaled CO₂ by swimmers is released to the air instead of remaining in the water.

Table 6.3. Input parameters used in CO₂ IAQ model spreadsheet.

Parameter	Units	Explanation
Δt	hour	Time gradient
$C_g \text{ CO}_2$	mg/m ³	Concentration of measured gas-phase CO ₂
$C_l \text{ CO}_2$	mg/L	Concentration of measured liquid-phase CO ₂
$C_l \text{ CO}_2^*$	mg/L	Equilibrium concentration of liquid-phase CO ₂
n Swimmer		Swimmer count
N people		Number of non-swimmers
\forall_g	m ³	Representative value of air volume above the studied facility
Q_g	m ³ /hour	Measurement of air flow rate
A	m ²	Representative value of pool surface area of studied pool
K_l	m/hour	See equation 6.12
delta C_g	mg/m ³	Gas-phase CO ₂ concentration gradient. See equation 6.6
$C_{g,in}$	mg/m ³	Concentration of outdoor gas-phase CO ₂
emCO ₂	mg/hr	Emission rate for non-swimmers. See equation 6.13
emCO _{2X}	mg/hr	Emission rate for swimmer. See equation 6.14

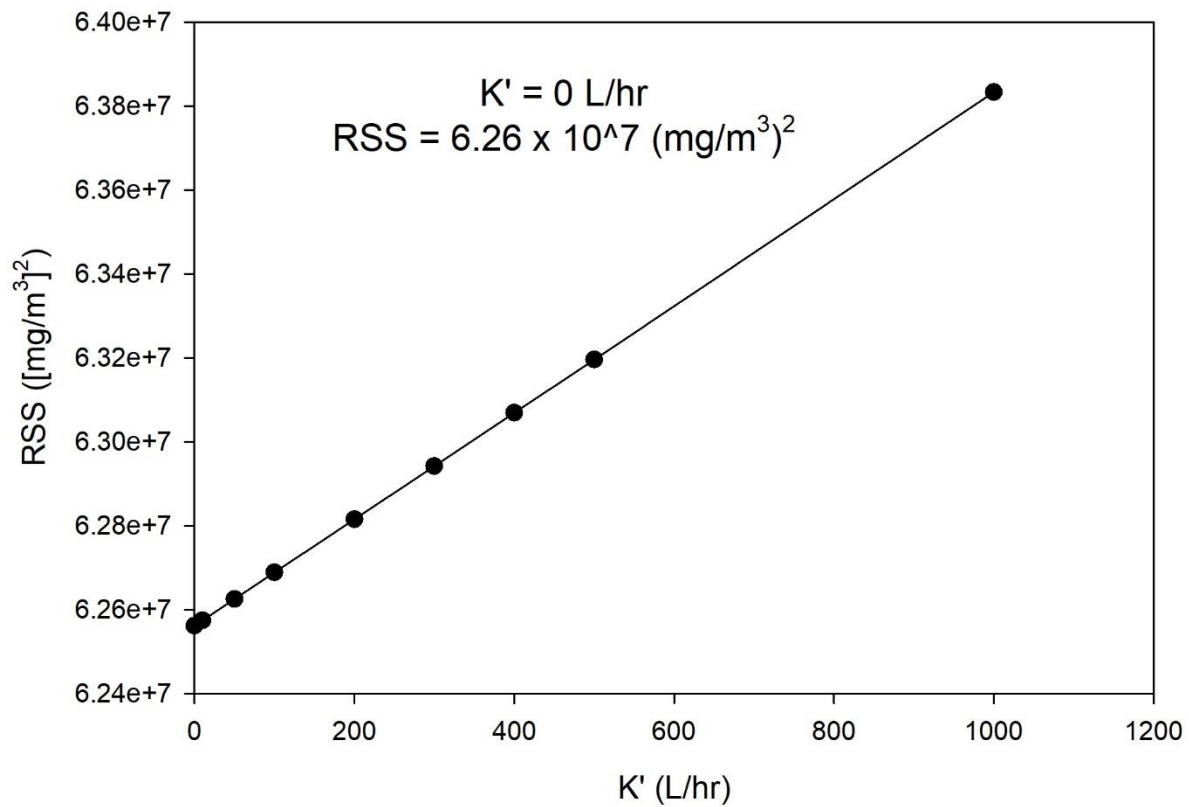


Figure 6.15. Fitting curve of the selection for best-fit value of K' from NEMo A for June 2019 study at pool facility B. RSS = Residual sum of the (measured gas-phase CO₂ concentration – model gas-phase CO₂ concentration)². K' = liquid to gas phase of CO₂ mass transfer coefficient.

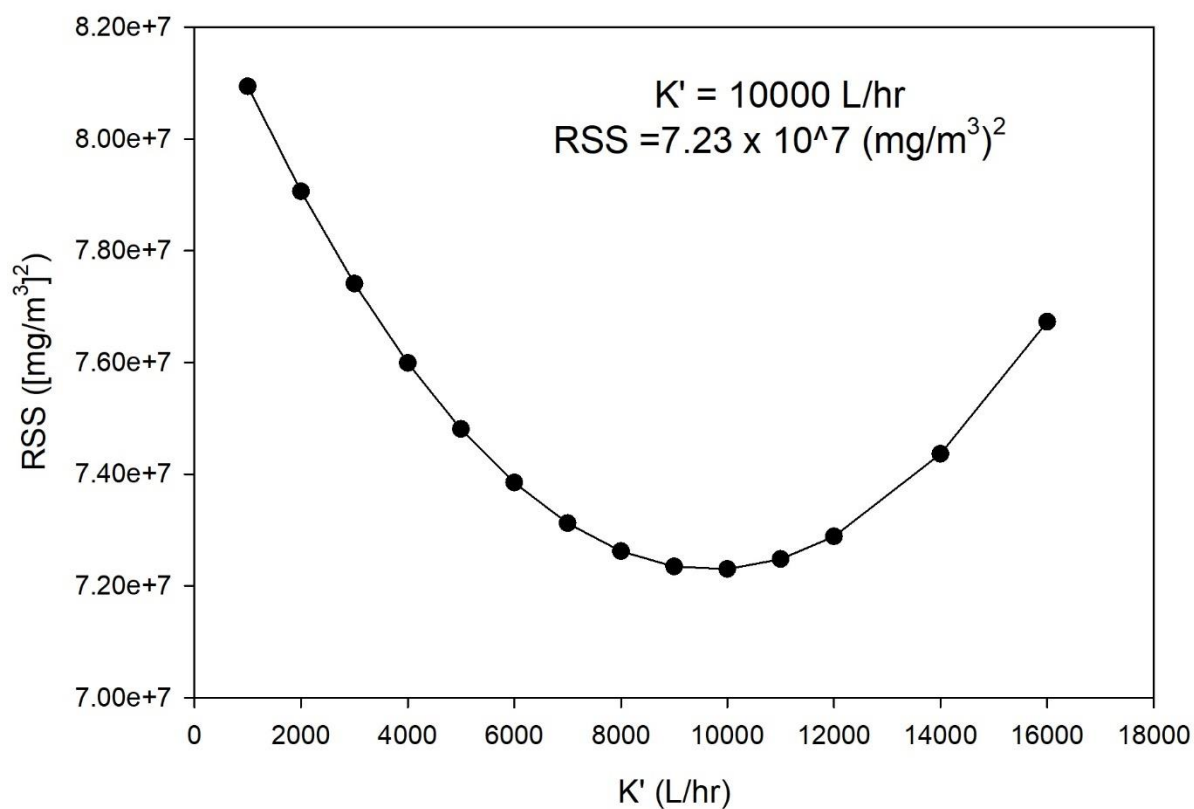


Figure 6.16. Fitting curve for selection of best-fit value of K' from LI-COR CO_2 analyzer for November 2019 study at pool facility B. RSS = Residual sum of the (measured gas-phase CO_2 concentration – model gas-phase CO_2 concentration)². K' = liquid to gas phase of CO_2 mass transfer coefficient.

Table 6.4. Calculated and estimated liquid-phase mass transfer coefficients of CO₂ for Facility B during the June 2019 and November 2019 experiments.

	Date	Type of swimmer	Age of swimmers	K_l (m/hour)	$K_l A$ (m ³ /hour)	K' (m ³ /hour)	RSS ((mg/m ³) ²)
NEMo A	6/21/2019 to 6/24/2019	Age group swimmers	8 and under	0.045	75.2	0	6.26E+07
LI-COR CO ₂ analyzer	11/21/2019 to 11/24/2019	Collegiate athletic	College students	0.051	85.2	10	7.23E+07

A: studied pool surface area is 1670 m²

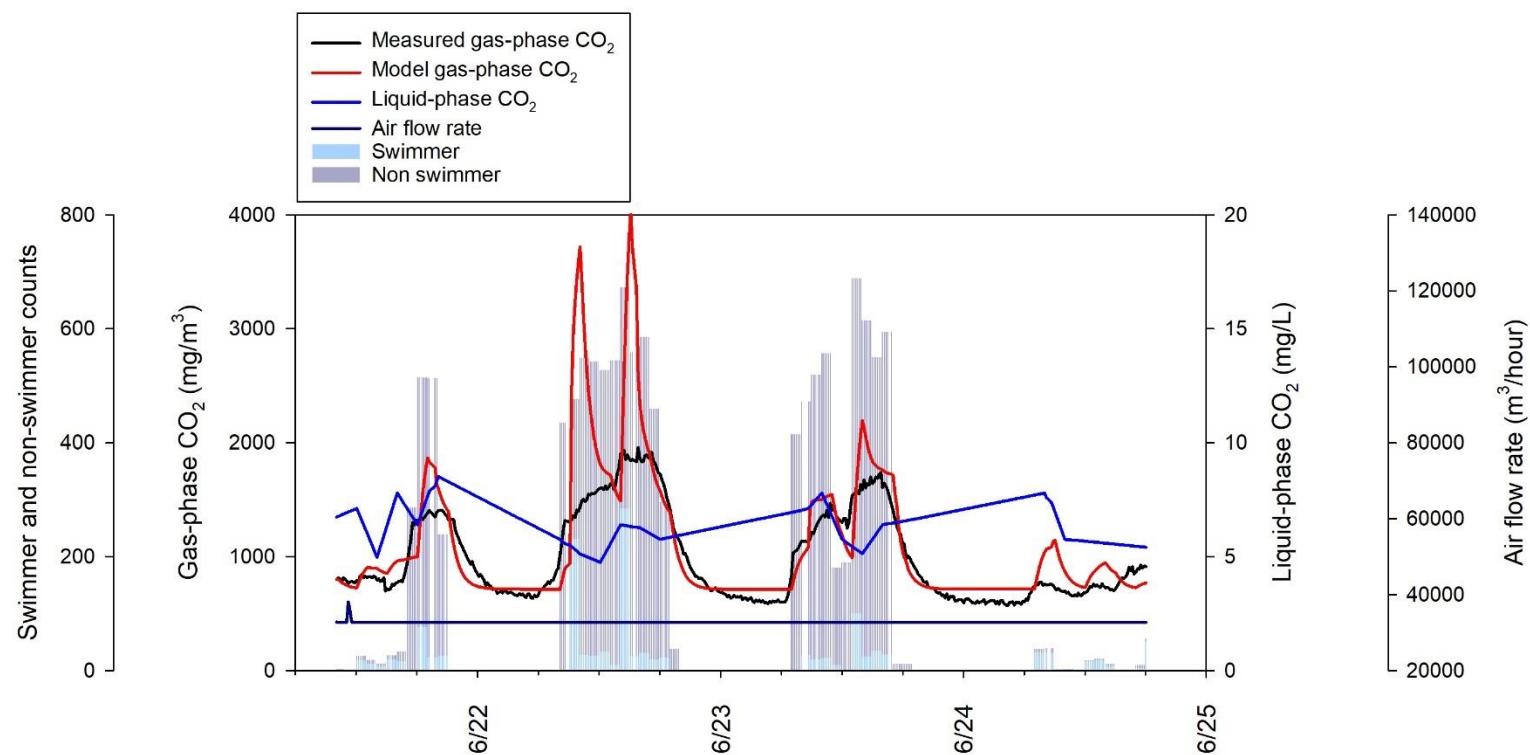


Figure 6.17. Time-course monitoring of gas-phase CO₂ by NEMo A and liquid-phase CO₂ with model gas-phase CO₂, and trend of air flow rate in pool facility B during study in June 2019. Vertical bars represent the number of swimmers and non-swimmer in pool facility B.

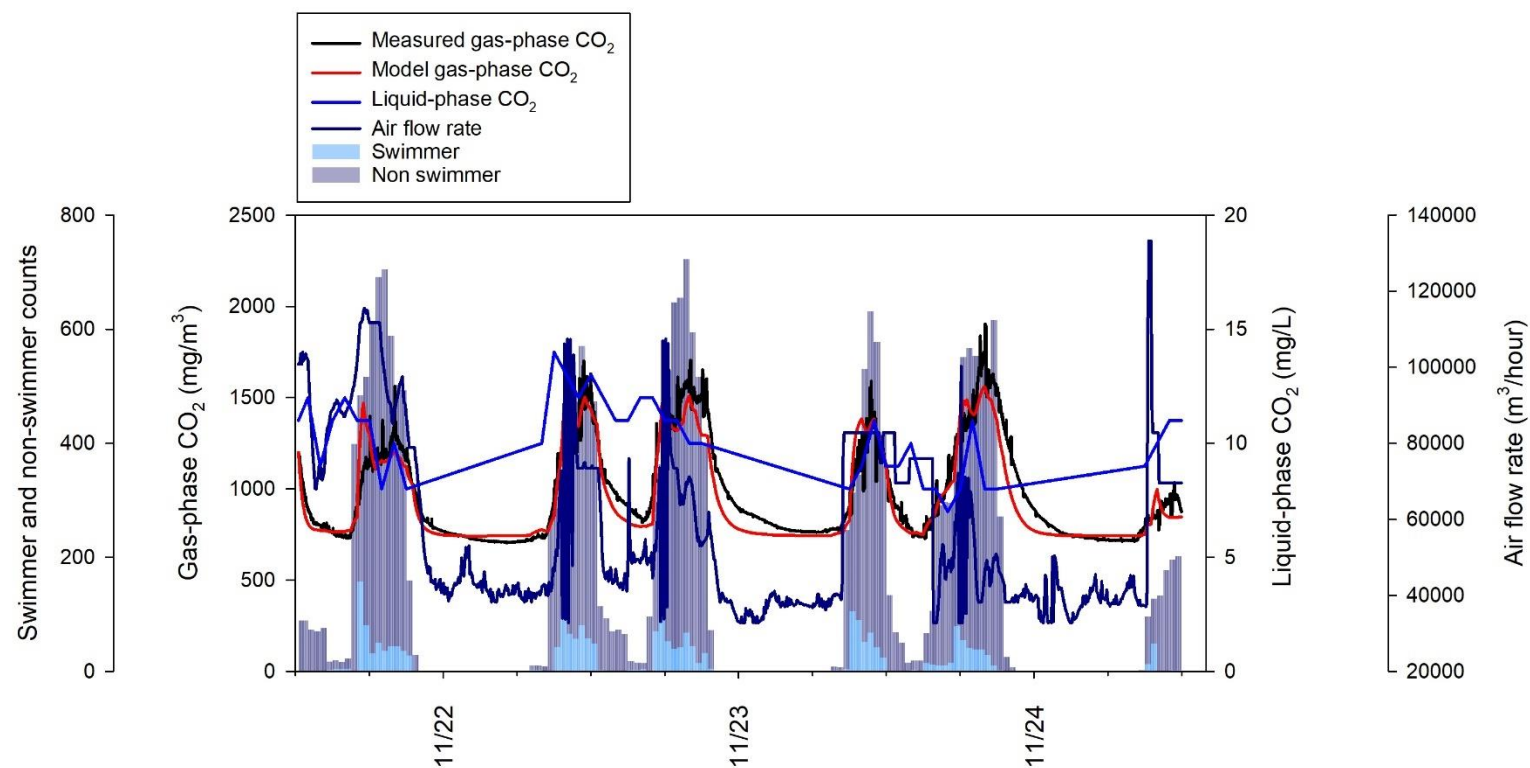


Figure 6.18. Time-course monitoring of gas-phase CO₂ by LI-COR CO₂ analyzer and liquid-phase CO₂ with model gas-phase CO₂, and trend of air flow rate in pool facility B during study in November 2019. Vertical bars represent the number of swimmers and non-swimmer in pool facility B.

One of the motivations for applying the IAQ model to simulate CO₂ dynamics was to explore the possibility of using gas-phase CO₂ as a surrogate for gas-phase NCl₃ in swimming pool facilities. A number of factors contributed to this idea, including that there are many inexpensive, commercially available CO₂ sensors that could be used to monitor IAQ monitor in pool facilities. However, there are important limitations that accompany this approach. Of particular importance is the fact that gas-phase NCl₃ is entirely attributable to transfer from the liquid phase, while gas-phase CO₂ will enter the air space in a pool facility by transfer from the liquid phase, by respiration of swimmers and non-swimmers in the facility, and from ambient outdoor air.

The measured gas-phase CO₂, modeled gas-phase CO₂, and measured gas-phase NCl₃ from NEMo B for the June 2019 and November 2019 experiment periods are illustrated in Figures 6.19 and 6.20, respectively. For Figure 6.20, peaks of model gas-phase CO₂ generally coincide with the measurements of gas-phase NCl₃. These results support the use of gas-phase CO₂ as a surrogate for the gas-phase NCl₃. However, in Figure 6.19, the trend of measured/model NCl₃ did not match up with measured/model CO₂ as well. This is believed to be largely due to the contribution from swimmer's activity.

The NCl₃ IAQ model was developed based on dynamic behavior attributed to swimmers, but the CO₂ IAQ model for June 2019 experiment indicated that liquid→gas transfer of CO₂ promoted by mechanical mixing of youth (age 8 and under) swimmers was negligible ($K' = 0$). It is believed that the mechanical mixing initiated by these young swimmers was insufficient to promote quantifiable liquid→gas transfer of CO₂. This phenomenon may represent a limitation on the use of gas-phase CO₂ as a surrogate for gas-phase NCl₃ in indoor swimming pool facility. However, it is worth noting that the worst IAQ is likely to occur at times when large numbers of adult swimmers are in a pool, so gas-phase CO₂ may still be worth considering as a surrogate for gas-phase NCl₃ for these conditions.

To date, only two sets of gas-phase CO₂ data have been collected to develop the CO₂ IAQ model. Additional experiments involving time-course measurements of gas-phase CO₂ and NCl₃ concentrations will be required to further examine the application of gas-phase CO₂ as surrogate for gas-phase NCl₃.

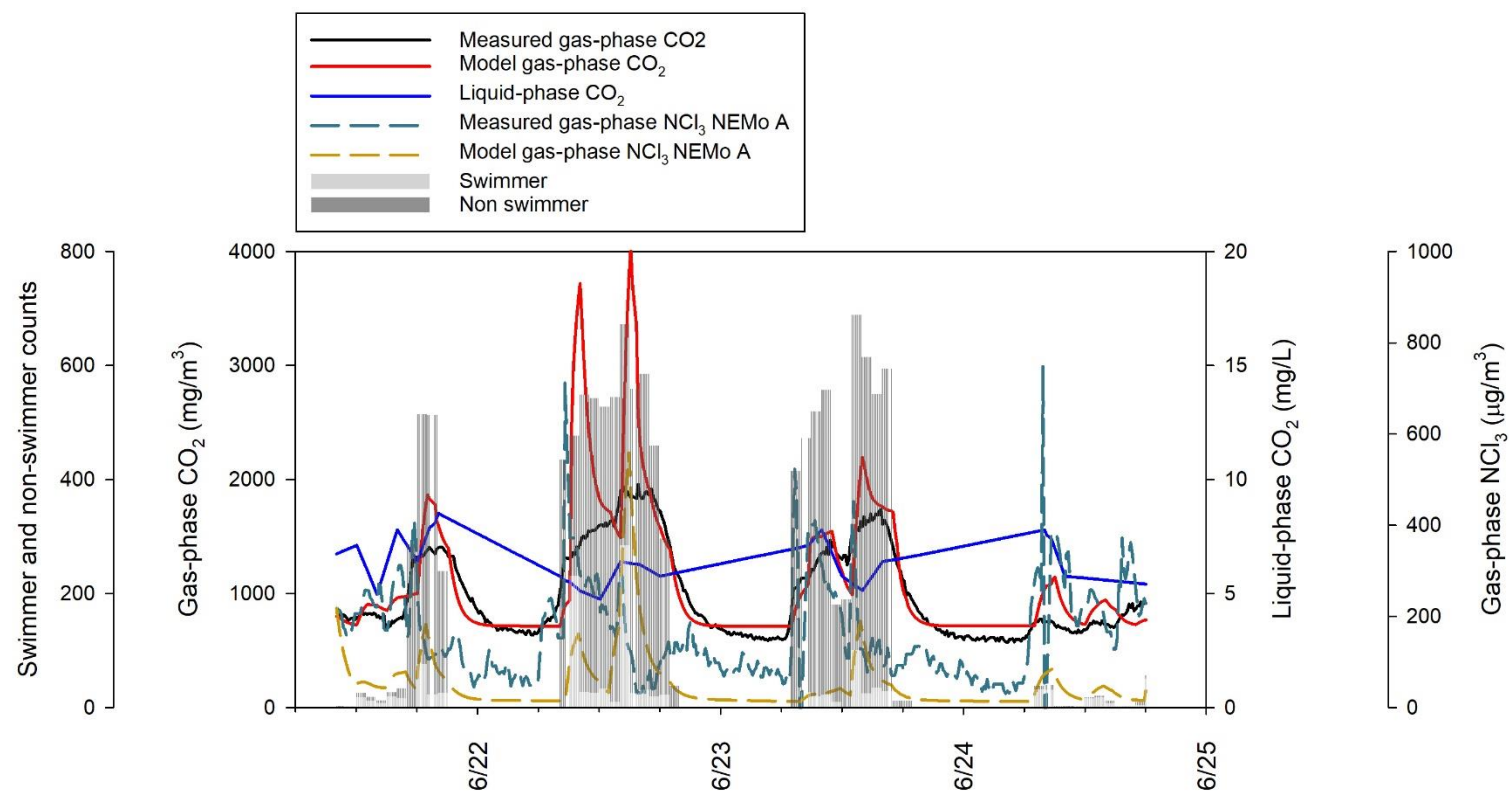


Figure 6.19. Time-course monitoring of gas-phase CO₂ by NEMo A and liquid-phase CO₂ with model gas-phase CO₂ in pool facility B during study in June 2019. Vertical bars represent the number of swimmers and non-swimmer in pool facility B. Gray dash line represents the gas-phase NCl₃ measurement by NEMo A and green dash line represent the model gas-phase NCl₃ from NEMo A.

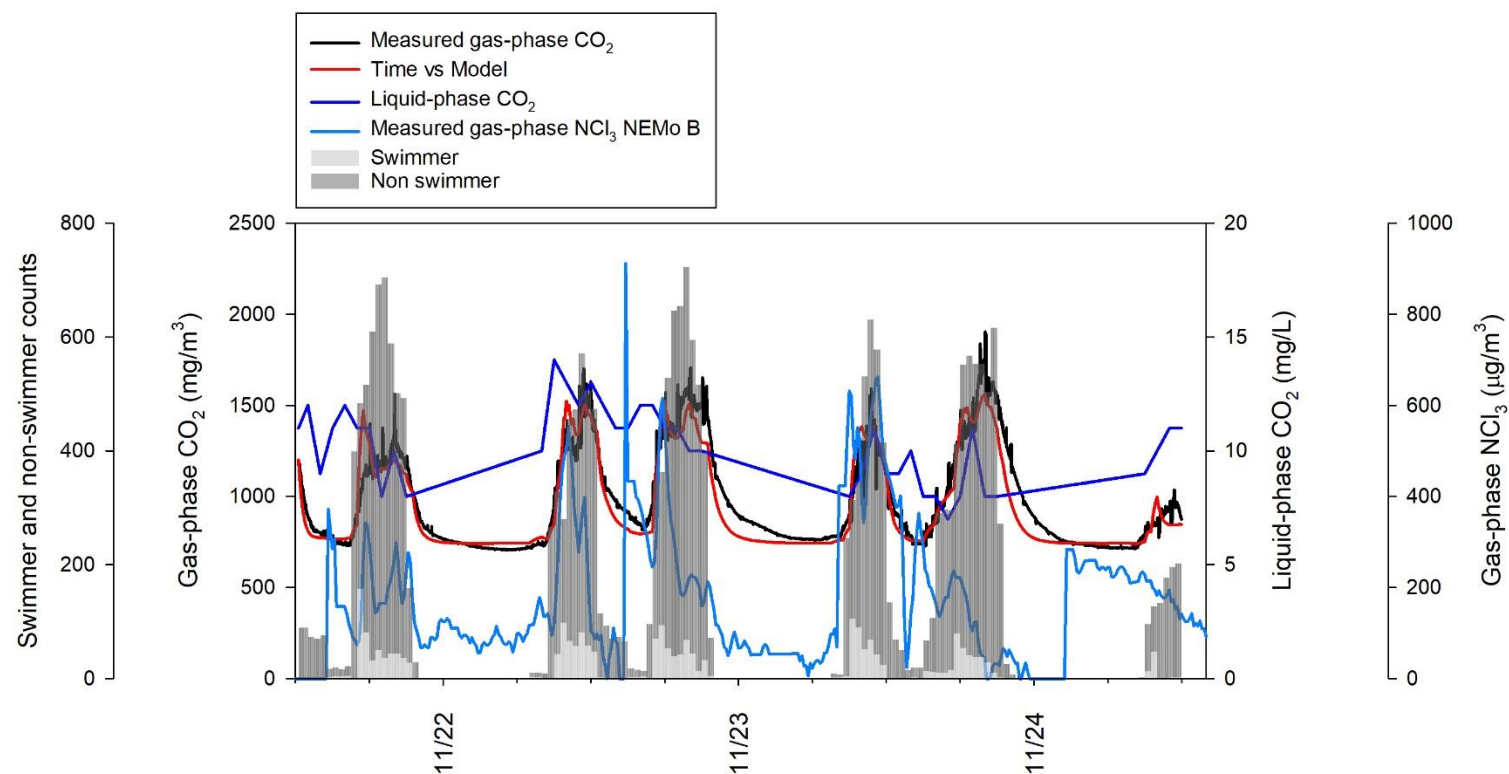


Figure 6.20. Time-course monitoring of gas-phase CO_2 by LI-COR CO_2 analyzer and liquid-phase CO_2 with model gas-phase CO_2 in pool facility B during study in November 2019. Vertical bars represent the number of swimmers and non-swimmer in pool facility B. Pink line represents the gas-phase NCl_3 measurement by NEMo B device.

7. SUMMARY AND CONCLUSIONS

The phase 1 project involved experiments that were used to characterize the responses of water chemistry to changes in water treatment methods. Seven volatile disinfection by-products (DBPs) and urea were measured throughout study period. A new air quality monitoring device (NEMo) was installed in the pool at a fixed location to collect air quality parameters as well.

After application of secondary oxidizers, reductions of free chlorine and total chlorine in the swimming pool water were observed while maintaining essentially constant ORP, as compared with prior operating conditions. A decrease in the concentration of combined chlorine was evident after addition of the secondary oxidant and activator. CNCl concentration was reduced substantially after addition of the oxidizers. The concentrations of NCl₃, CHCl₃, and CNCHCl₂ declined after introduction of the secondary oxidizers. The degradation of these compounds apparently depended on the presence of the secondary oxidant, as increases of the concentrations of these DBPs were seen once the secondary oxidant feed rate was reduced. The addition of the activator also resulted in small reductions of the concentrations of several volatile DBPs including NCl₃, CNCl, and CNCHCl₂. The introduction of the activator in the pool also diminished the concentration of urea. Secondary oxidizers coupled with the activator could be an effective treatment process to limit the accumulation of DBPs and their precursors in swimming pools.

The phase 2 study involved experiments to examine how the characteristics of water treatment systems, swimmer activity, and HVAC system design and operation affected indoor air quality. Measurements of water and air quality were conducted before, during, and after periods of swimming meets at four indoor pool facilities. Water samples were collected to examine changes of pH, free and total chlorine, alkalinity, urea, and seven volatile DBPs. Air quality was monitored using multiple NEMo devices.

Eight experiment periods were examined among the four swimming pool facilities between February 2019 and January 2020. pH and alkalinity were generally stable during swimming meets. NH₂Cl, NHCl₂, NCl₃, and chloroform were the dominant volatile DBPs in pools, in terms of mass or molar concentration; this observation was consistent with previous studies. In general, liquid-phase NCl₃ concentration tended to be higher at the end of the swim meet than at earlier times, probably because of introduction of NCl₃ precursors by swimmers. Liquid-phase concentrations of chloroform were generally stable throughout the swimming meets. No clear time-course trend

for the concentrations of the other volatile DBPs emerged during these experiments. The kinetics and mechanisms of volatile DBP formation have been partially defined in the literature, but insufficient information exists to accurately simulate the dynamics of volatile DBP formation in pools. Urea concentration tended to increase in pool water during the swimming meets, indicating that urea and other DBP precursors were introduced to the pool water by swimmers during swimming meets. Diurnal changes in urea concentration were also observed, which were probably attributable to mixing behavior in pools in combination with the activity of swimmers. This observation is consistent with previous investigations.

The measurements collected with the NEMo devices confirmed the effects of swimmers on the concentrations of gas-phase NCl_3 and CO_2 , especially during swimming meets. Peak gas-phase NCl_3 concentrations were observed when large numbers of swimmer were present in the pools; measured gas-phase concentrations were as high as $1400 \mu\text{g}/\text{m}^3$. The measured gas-phase NCl_3 concentration often exceeded the suggested upper limits of $300 \mu\text{g}/\text{m}^3$ or $500 \mu\text{g}/\text{m}^3$ during swimming meets, especially during and immediately after warm-up periods, when the largest numbers of swimmers were in the pool. Concentrations of gas-phase NCl_3 rarely exceeded $300 \mu\text{g}/\text{m}^3$ during regular hours of operation. A strong link between gas-phase NCl_3 concentration and bather load was confirmed. Also, concentrations of gas-phase NCl_3 were often undetectable when pool facilities were closed. This supports the hypothesis of swimmer impact on air quality in pool facilities. In addition, the type of swimmers will influence the transfer of volatile compounds, such as NCl_3 , from water to air in pool facilities. Measurements conducted during collegiate and junior high swimming meets indicated gas-phase NCl_3 concentrations as high as $1400 \mu\text{g}/\text{m}^3$. On the other hand, the highest gas-phase NCl_3 concentration was about half this value when a similar number of younger children was actively swimming in the pool. This suggests that elite swimmers are likely to impose stronger mixing dynamics on water, which in turn will result in promotion of liquid→gas mass transfer and lead to higher peak NCl_3 in the air.

Phase 3 of the study involved the development of IAQ models for gas-phase NCl_3 and CO_2 . Models were developed by application of a conventional mass balance approach coupled with two-film theory. Several assumptions were made to simplify the model. Measurements from Phase 2 of the study at pool facility B were used to develop estimates of key parameters for the governing mass balance equation.

Mass transfer coefficients were obtained through regression analysis of the governing mass balance equation. The models were used to simulate the dynamics of gas-phase NCl_3 during regular operating hours in April 2019. In addition, the model was used to simulate the dynamics of gas-phase NCl_3 during a swimming meet that was held at the same facility June 2019. In general, the model predictions illustrated the contributions of swimmer activity to liquid→gas mass transfer, but deviations between model predictions and measurements were evident, both in terms of peak gas-phase NCl_3 concentration and timing of the peaks.

Several sources of error were identified for the model, many of which were linked to model assumptions. Among these were the assumptions that water and air were well-mixed in the pool facility. Despite the limitations of these models, the NCl_3 model may be useful as a tool to examine the effects of process changes on IQ dynamics in pool facilities. Pool operators could adjust air handling units to prevent gas-phase NCl_3 from exceeding guidance values. Air-stripping systems could also be included as part of water treatment as a means of reducing the liquid-phase concentrations of volatile DBPs, including NCl_3 .

The IAQ model for gas-phase CO_2 also showed positive results. However, further examination is required to justify the use of gas-phase CO_2 as surrogate for gas-phase NCl_3 , especially during periods that involve low CO_2 mass transfer from liquid→gas phases, such as during an age-group swimming meet involving young children or when a pool is minimally occupied. In order to have use the CO_2 IAQ model to forecast concentrations of gas-phase NCl_3 , additional experiments will be needed to consolidate this observation.

Although gas-phase NCl_3 and gas-phase CO_2 models presented in this study only describe the situations for a single indoor swimming pool, they represent a first step to extend this approach to different swimming pools. Additional experiments should be conducted to provide more information and consolidate the model assumptions proposed in this study. Further work should be conducted to assess the sources of error in models and to apply the models to other settings. During the experiment period, water samples were not collected when facilities were closed to the public. Linear interpolation was applied to simulate liquid-phase concentrations between consecutive measurements (last measurement before facility closed and first measurement when facility open). Future experiments should include measurements to define the liquid-phase concentration during the overnight period. Also, water samples were collected approximately every 2 hours when the facility was open. Linear interpolation was also applied between

consecutive liquid-phase measurements to allow time-agreement with the gas-phase measurements, which were reported every 10 minutes. In the future, water samples should be collected and analyzed more frequently to reduce or eliminate the use of linear interpolation.

In addition, the validity of the well-mixed assumptions for the gas and liquid phases should be examined. For this investigation, air quality monitors were placed at two or three fixed locations in the pool facility and water samples were collected from a single, fixed location. It would be beneficial to increase the number of sampling locations to allow further examination of the assumption of well-mixed conditions. Furthermore, only one volatile DBP (NCl_3) was measured in the gas phase during this study. Measurements of gas and liquid phase concentrations of other volatile DBPs would allow for a more thorough characterization of IAQ dynamics in indoor swimming pool facilities.

REFERENCES

- American Water Works Association (AWWA), 1999. Water quality and treatment: a handbook of community water supplies, 5th ed, McGraw-Hill handbooks. McGraw-Hill, New York.
- APHA-AWWA-WEF, 1998. Standard Methods for the Examination of Water and Wastewater, 20th ed. Washington. DC.
- Bätjer, K., Cetinkaya, M., Düszen, J.v, Gabel, B., Lahl, U., Stachel, B., Thiemann, W., 1980. Chloroform emission into urban atmosphere. *Chemosphere* 9, 311–316.
- Beech, J.A., Diaz, R., Ordaz, C., Palomeque, B., 1980. Nitrates, chlorates and trihalomethanes in swimming pool water. *Am. J. Public Health* 70, 79–82.
- Bernard, A., Carbonnelle, S., deBurbure, C., Michel, O., Nickmilder, M., 2006. Chlorinated Pool Attendance, Atopy, and the Risk of Asthma during Childhood. *Environ. Health Perspect.* 114, 1567–1573. <https://doi.org/10.1289/ehp.8461>
- Bernard, A., Carbonnelle, S., Dumont, X., Nickmilder, M., 2007. Infant Swimming Practice, Pulmonary Epithelium Integrity, and the Risk of Allergic and Respiratory Diseases Later in Childhood. *Pediatrics* 119, 1095 LP – 1103.
- Bernard, A., Carbonnelle, S., Michel, O., Higuët, S., deBurbure, C., Buchet, J.-P., Hermans, C., Dumont, X., Doyle, I., 2003. Lung hyperpermeability and asthma prevalence in schoolchildren: unexpected associations with the attendance at indoor chlorinated swimming pools. *Occup. Environ. Med.* 60, 385 LP – 394.
- Bessonneau, V., Derbez, M., Clément, M., Thomas, O., 2011. Determinants of chlorination by-products in indoor swimming pools. *Int. J. Hyg. Environ. Health* 215, 76–85. <https://doi.org/10.1016/j.ijheh.2011.07.009>
- Blatchley Ernest R., Cheng, M., 2010. Reaction Mechanism for Chlorination of Urea. *Environ. Sci. Technol.* 44, 8529–8534.
- Blatchley III, E.R., Cheng, M., 2010. Reaction Mechanism for Chlorination of Urea. *Environ. Sci. Technol.* 44, 8529–8534.
- Bonen, A., Wilson, B.A., Yarkony, M., Belcastro, A.N., 1980. Maximal oxygen uptake during free, tethered, and flume swimming. *J. Appl. Physiol.* 48, 232–235. <https://doi.org/10.1152/jappl.1980.48.2.232>
- Boorman, G.A., 1999. Drinking water disinfection byproducts: review and approach to toxicity evaluation. *Environ. Health Perspect.* 107, 207–217.

- Bowen, A.B., Kile, J.C., Otto, C., Kazerouni, N., Austin, C., Blount, B.C., Wong, H.-N., Beach, M.J., Fry, A.M., 2007. Outbreaks of Short-Incubation Ocular and Respiratory Illness Following Exposure to Indoor Swimming Pools. *Environ. Health Perspect.* 115, 267–271. <https://doi.org/10.1289/ehp.9555>
- Bullock, G., 2003. Disinfection of Swimming Pool Water.
- Carbonnelle, S., Francaux, M., Doyle, I., Dumont, X., Burbure, C.de, Morel, G., Michel, O., Bernard, A., 2002. Changes in serum pneumoproteins caused by short-term exposures to nitrogen trichloride in indoor chlorinated swimming pools. *Biomarkers* 7, 464–478.
- Centers for Disease Control and Prevention and U.S. Department of Housing and Urban Development, 2006. Healthy Housing Reference Manual. Atlanta, GA.
- Chrostowski, P.C., Foster, S.A., 2004. Swimming Pool Shock Treatment. *J. Environ. Health* 66, 26–27.
- Chu, H., Nieuwenhuijsen, M.J., 2002. Distribution and determinants of trihalomethane concentrations in indoor swimming pools. *Occup. Environ. Med.* 59, 243–247.
- Chu, T.-S., Cheng, S.-F., Wang, G.-S., Tsai, S.-W., 2013. Occupational exposures of airborne trichloramine at indoor swimming pools in Taipei. *Sci. Total Environ.* 461–462, 317–322. <https://doi.org/10.1016/J.SCITOTENV.2013.05.012>
- Craik, S.A., Weldon, D., Finch, G.R., Bolton, J.R., Belosevic, M., 2001. Inactivation of cryptosporidium parvum oocysts using medium- and low-pressure ultraviolet radiation. *Water Res.* 35, 1387–1398. [https://doi.org/10.1016/S0043-1354\(00\)00399-7](https://doi.org/10.1016/S0043-1354(00)00399-7)
- Dang, B., Chen, L., Mueller, C., Dunn, K.H., Almaguer, D., Roberts, J.L., Otto, C.S., 2010. Ocular and Respiratory Symptoms Among Lifeguards at a Hotel Indoor Waterpark Resort. *J. Occup. Environ. Med.* 52, 207–213.
- Davey, N.G., Krogh, E.T., Gill, C.G., 2011. Membrane-introduction mass spectrometry (MIMS). *TrAC Trends Anal. Chem.* 30, 1477–1485.
- DeLaat, J., Feng, W., Freyfer, D.A., Dossier-Berne, F., 2011. Concentration levels of urea in swimming pool water and reactivity of chlorine with urea. *Water Res.* 45, 1139–1146. <https://doi.org/10.1016/J.WATRES.2010.11.005>
- E, Y., Yang, Q., Guo, Y., Lian, L., Li, J., Blatchley, E.R., 2019. CH₃NCl₂ Formation from Chlorination of Carbamate Insecticides. *Environ. Sci. Technol.* 53, 13098–13106. <https://doi.org/10.1021/acs.est.9b03891>
- Erdinger, L., Kirsch, F., Sonntag, H.G., 1997. Potassium as an indicator of anthropogenic contamination of swimming pool water. *Int. J. Hyg. Environ. Med.* 200, 297–308.
- Ethera, 2018. Trichloramine monitor NEMo TC [WWW Document]. URL <http://www.etheralabs.com/en/trichloramine-monitor>

- Fantuzzi, G., Righi, E., Predieri, G., Giacobazzi, P., Petra, B., Aggazzotti, G., 2012. Airborne trichloramine (NCl₃) levels and self-reported health symptoms in indoor swimming pool workers: dose-response relationships. *J. Expo. Sci. Environ. Epidemiol.* 23, 88.
- Font-Ribera, L., Kogevinas, M., Schmalz, C., Zwiener, C., Marco, E., Grimalt, J.O., Liu, J., Zhang, X., Mitch, W., Critelli, R., Naccarati, A., Heederik, D., Spithoven, J., Arjona, L., deBont, J., Gracia-Lavedan, E., Villanueva, C.M., 2016. Environmental and personal determinants of the uptake of disinfection by-products during swimming. *Environ. Res.* 149, 206–215. <https://doi.org/10.1016/j.envres.2016.05.013>
- Font-Ribera, L., Kogevinas, M., Zock, J.-P., Gómez, F.P., Barreiro, E., Nieuwenhuijsen, M.J., Fernandez, P., Lourencetti, C., Pérez-Olabarría, M., Bustamante, M., Marcos, R., Grimalt, J.O., Villanueva, C.M., 2010. Short-Term Changes in Respiratory Biomarkers after Swimming in a Chlorinated Pool. *Environ. Health Perspect.* 118, 1538–1544.
- Fornander, L., Ghafouri, B., Lindahl, M., Graff, P., 2013. Airway irritation among indoor swimming pool personnel: trichloramine exposure, exhaled NO and protein profiling of nasal lavage fluids. *Int. Arch. Occup. Environ. Health* 86, 571–580. <https://doi.org/10.1007/s00420-012-0790-4>
- Gallard, H., VonGunten, U., 2002. Chlorination of natural organic matter: Kinetics of chlorination and of THM formation. *Water Res.* 36, 65–74. [https://doi.org/10.1016/S0043-1354\(01\)00187-7](https://doi.org/10.1016/S0043-1354(01)00187-7)
- Gérardin, F., Cloteaux, A., Midoux, N., 2015. Modeling of variations in nitrogen trichloride concentration over time in swimming pool water. *Process Saf. Environ. Prot.* 94, 452–462. <https://doi.org/10.1016/j.psep.2014.10.004>
- Gérardin, F., Héry, M., 2005. Effects of nitrogen trichloride stripping on air quality in indoor swimming pools.
- Glauner, T., Waldmann, P., Frimmel, F.H., Zwiener, C., 2005. Swimming pool water—fractionation and genotoxicological characterization of organic constituents. *Water Res.* 39, 4494–4502.
- Goodman, M., Hays, S., 2008. Asthma and Swimming: A Meta-Analysis. *J. Asthma* 45, 639–647.
- Gordon, S.M., Brinkman, M.C., Ashley, D.L., Blount, B.C., Lyu, C., Masters, J., Singer, P.C., 2006. Changes in Breath Trihalomethane Levels Resulting from Household Water-Use Activities. *Environ. Health Perspect.* 114, 514–521.
- Griffiths, T., 2003. *The Complete Swimming Pool Reference*, 2nd Editio. ed. Sagamore Publishing.
- Gunkel, K., Jessen, H.-J., 1986. Untersuchungen über den Harnstoffeintrag in das Badewasser. *Acta Hydrochim. Hydrobiol.* 14, 451–461.
- Guo, F., 2017. Development of a model for controlling indoor air quality.

- Guo, Z., Roache, N.F., 2003. Overall Mass Transfer Coefficient for Pollutant Emissions from Small Water Pools under Simulated Indoor Environmental Conditions. *Ann. Occup. Hyg.* 47, 279–286. <https://doi.org/10.1093/annhyg/meg035>
- Hallett, S., Ashurst, J.V., 2019. Physiology, tidal volume. StatPearls [Internet].
- Hansen, K.M.S., Willach, S., Antoniou, M.G., Mosbæk, H., Albrechtsen, H.-J., Andersen, H.R., 2012. Effect of pH on the formation of disinfection byproducts in swimming pool water - Is less THM better? *Water Res.* 46, 6399–6409. <https://doi.org/10.1016/J.WATRES.2012.09.008>
- Héry, M., Hecht, G., Gerber, J.M., Gender, J.C., Hubert, G., Rebuffaud, J., 1995. Exposure to Chloramines in the Atmosphere of Indoor Swimming Pools. *Ann. Occup. Hyg.* 39, 427–439.
- Héry, M., Hecht, G., Gerber, J.M., Gendre, J.C., Hubert, G., Rebuffaud, J., 1995. Exposure to chloramines in the atmosphere of indoor swimming pools. *Ann. Occup. Hyg.* 39, 427–439. [https://doi.org/10.1016/0003-4878\(95\)00013-5](https://doi.org/10.1016/0003-4878(95)00013-5)
- Hijnen, W.A.M., Beerendonk, E.F., Medema, G.J., 2006. Inactivation credit of UV radiation for viruses, bacteria and protozoan oocysts in water: A review. *Water Res.* 40, 3–22. <https://doi.org/10.1016/J.WATRES.2005.10.030>
- Holmér, I., Lundin, A., Eriksson, B.O., 1974a. Maximum oxygen uptake during swimming and running by elite swimmers. *J. Appl. Physiol.* 36, 711–714. <https://doi.org/10.1152/jappl.1974.36.6.711>
- Holmér, I., Stein, E.M., Saltin, B., Ekblom, B., Astrand, P.O., 1974b. Hemodynamic and respiratory responses compared in swimming and running. *J. Appl. Physiol.* 37, 49–54. <https://doi.org/10.1152/jappl.1974.37.1.49>
- Holzwarth, G., Balmer, R.G., Soni, L., 1984. The fate of chlorine and chloramines in cooling towers Henry's law constants for flashoff. *Water Res.* 18, 1421–1427. [https://doi.org/10.1016/0043-1354\(84\)90012-5](https://doi.org/10.1016/0043-1354(84)90012-5)
- Huang, J.-C., Shang, C., 2006. Advanced Physicochemical Treatment Processes, in: Wang, L.K., Hung, Y.-T., Shammas, N.K. (Eds.), Humana Press, Totowa, NJ, pp. 47–79. https://doi.org/10.1007/978-1-59745-029-4_2
- Isaac, R.A., Morris, J.C., 1980. Water Chlorination Environmental Impact, Vol.3, Ann Arbor. ed. Ann Arbor, MI.
- Jacobs, J.H., Spaan, S., vanRooy, G.B.G.J., Meliefste, C., Zaat, V.A.C., Rooyackers, J.M., Heederik, D., 2007. Exposure to trichloramine and respiratory symptoms in indoor swimming pool workers. *Eur. Respir. J.* 29, 690–8. <https://doi.org/10.1183/09031936.00024706>
- Jafvert, C.T., Valentine, R.L., 1992. Reaction scheme for the chlorination of ammoniacal water. *Environ. Sci. Technol.* 26, 577–586.

- Jensen, J.N., Johnson, J.D., 1990. Interferences by monochloramine and organic chloramines in free available chlorine methods. 2. N, N-Diethyl-p-phenylenediamine. *Environ. Sci. Technol.* 24, 985–990.
- Johnson, R.C., Cooks, R.G., Allen, T.M., Cisper, M.E., Hemberger, P.H., 2000. Membrane introduction Mass Spectrometry: Trends and applications. *Mass Spectrom. Rev.* 19, 1–37.
- Jolley, R.L., Carpenter, J.H., 1983. Review of the chemistry and environmental fate of reactive oxidant species in chlorinated water. *Water chlorination Environ. impact Heal. Eff.* 4.
- Judd, S.J., Black, S.H., 2000. Disinfection by-product formation in swimming pool waters: a simple mass balance. *Water Res.* 34, 1611–1619.
- Judd, S.J., Bullock, G., 2003. The fate of chlorine and organic materials in swimming pools. *Chemosphere* 51, 869–879.
- Judd, S.J., Jeffrey, J.A., 1995. Trihalomethane formation during swimming pool water disinfection using hypobromous and hypochlorous acids. *Water Res.* 29, 1203–1206.
- Kanan, A., 2010. Occurrence and formation of disinfection by-products in indoor swimming pools water. Clemson University.
- Kaydos-Daniels, S.C., Beach, M.J., Shwe, T., Magri, J., Bixler, D., 2008. Health effects associated with indoor swimming pools: A suspected toxic chloramine exposure. *Public Health* 122, 195–200. <https://doi.org/10.1016/J.PUHE.2007.06.011>
- Keeling, R.F., Keeling, C.D., 2017. Atmospheric Monthly In Situ CO₂ Data-Mauna Loa Observatory, Hawaii [WWW Document]. Scripps CO₂ Progr. data. UC San Diego Libr. Digit. Collect. URL <https://doi.org/10.6075/J08W3BHW> (accessed 3.10.21).
- Ketola, R.A., Kotiaho, T., Cisper, M.E., Allen, T.M., 2002. Environmental applications of membrane introduction mass spectrometry. *J. Mass Spectrom.* 37, 457–476.
- Kim, H., Shim, J., Lee, S., 2002. Formation of disinfection by-products in chlorinated swimming pool water. *Chemosphere* 46, 123–130.
- Kotiaho, T., Lister, A.K., Hayward, M.J., Cooks, R.G., 1991. On-line monitoring of chloramine reactions by membrane introduction mass spectrometry. *Talanta* 38, 195–200.
- Lahl, U., Bätjer, K., Düszel, J.V., Gabel, B., Stachel, B., Thiemann, W., 1981. Distribution and balance of volatile halogenated hydrocarbons in the water and air of covered swimming pools using chlorine for water disinfection. *Water Res.* 15, 803–814. [https://doi.org/10.1016/0043-1354\(81\)90133-0](https://doi.org/10.1016/0043-1354(81)90133-0)
- Lee, C., Choi, W., Kim, Y.G., Yoon, J., 2005. UV Photolytic Mechanism of N-Nitrosodimethylamine in Water: Dual Pathways to Methylamine versus Dimethylamine. *Environ. Sci. Technol.* 39, 2101–2106. <https://doi.org/10.1021/es0488941>

- Lee, J., Jun, M.-J., Lee, Man-Ho, Lee, Min-Hwan, Eom, S.-W., Zoh, K.-D., 2010. Production of various disinfection byproducts in indoor swimming pool waters treated with different disinfection methods. *Int. J. Hyg. Environ. Health* 213, 465–474. <https://doi.org/10.1016/J.IJHEH.2010.09.005>
- Lee, L.T., 2016. Fate and Behavior of Pharmaceuticals and Personal Care Products In Chlorinated Swimming Pools. Purdue University.
- Lévesque, B., Ayotte, P., LeBlanc, A., Dewailly, E., Prud'Homme, D., Lavoie, R., Allaire, S., Levallois, P., 1994. Evaluation of dermal and respiratory chloroform exposure in humans. *Environ. Health Perspect.* 102, 1082–1087.
- Lévesque, B., Vézina, L., Gauvin, D., Leroux, P., 2015. Investigation of Air Quality Problems in an Indoor Swimming Pool: A Case Study. *Ann. Occup. Hyg.* 59, 1085–1089.
- Li, J., Blatchley III, E.R., 2007. Volatile Disinfection Byproduct Formation Resulting from Chlorination of Organic–Nitrogen Precursors in Swimming Pools. *Environ. Sci. Technol.* 41, 6732–6739.
- Lian, L., E, Y., Li, J., Blatchley III, E.R., 2014. Volatile Disinfection Byproducts Resulting from Chlorination of Uric Acid: Implications for Swimming Pools. *Environ. Sci. Technol.* 48, 3210–3217.
- Lindstrom, A.B., Pleil, J.D., Berkoff, D.C., 1997. Alveolar breath sampling and analysis to assess trihalomethane exposures during competitive swimming training. *Environ. Health Perspect.* 105, 636–642.
- Loos, R., Barceló, D., 2001. Determination of haloacetic acids in aqueous environments by solid-phase extraction followed by ion-pair liquid chromatography–electrospray ionization mass spectrometric detection. *J. Chromatogr. A* 938, 45–55.
- Magel, J.R., Faulkner, J.A., 1967. Maximum oxygen uptakes of college swimmers. *J. Appl. Physiol.* 22, 929–933. <https://doi.org/10.1152/jappl.1967.22.5.929>
- Magos, L., 1987. C. Lentner (ed.). *Geigy Scientific Tables*, 8th edition. Vol. 1. Units of Measurement. Body Fluids. Composition of the Body. Nutrition. 1981, 298 pp. Vol. 2. Introduction to Statistics. Statistical Tables. Mathematical Formulae. 1982, 241 pp. Vol. 3. *Physi. J. Appl. Toxicol.* 7, 413.
- Massin, N., Bohadana, A.B., Wild, P., Héry, M., Toamain, J.P., Hubert, G., 1998. Respiratory symptoms and bronchial responsiveness in lifeguards exposed to nitrogen trichloride in indoor swimming pools. *Occup. Environ. Med.* 55, 258–263.
- Morris, J.C., 1967. *Principles and Applications of Water Chemistry*, Wiley. ed. New York.
- Na, C., Olson, T.M., 2004. Stability of Cyanogen Chloride in the Presence of Free Chlorine and Monochloramine. *Environ. Sci. Technol.* 38, 6037–6043.

- Nguyen, T.H., Chevallier, E., Garcia, J., Nguyen, T.D., Laurent, A.M., Beaubestre, C., Karpe, P., Tran-Thi, T.H., 2013. Innovative colorimetric sensors for the detection of nitrogen trichloride at ppb level in swimming pools. *Sensors Actuators, B Chem.* 187, 622–629. <https://doi.org/10.1016/j.snb.2013.07.041>
- NIOSH, 2003. Cyanogen Chloride: Systemic Agent [WWW Document]. URL http://www.cdc.gov/niosh/ershdb/emergencyresponsecard_29750039.html
- Nordberg, G.F., Lundstrom, N.-G., Forsberg, B., Hagenbjork-Gustafsson, A., Lagerkvist, B.J., Nilsson, J., Svensson, M., Blomberg, A., Nilsson, L., Bernard, A., Dumont, X., Bertilsson, H., Eriksson, K., 2012. Lung function in volunteers before and after exposure to trichloramine in indoor pool environments and asthma in a cohort of pool workers. *BMJ Open* 2, e000973. <https://doi.org/10.1136/bmjopen-2012-000973>
- NSPF, 2006. Certified Pool-Spa Operator Handbook: National Swimming Pool Foundation.
- Nuckols, J.R., Ashley, D.L., Lyu, C., Gordon, S.M., Hinckley, A.F., Singer, P., 2005. Influence of Tap Water Quality and Household Water Use Activities on Indoor Air and Internal Dose Levels of Trihalomethanes. *Environ. Health Perspect.* 113, 863–870.
- Nweke, A., Scully, F.E., 1989. Stable N-chloroaldehydes and other products of the chlorination of isoleucine in model solutions and in a wastewater. *Environ. Sci. Technol.* 23, 989–994. <https://doi.org/10.1021/es00066a010>
- Osgood, C., Sterling, D., 1991. Dichloroacetonitrile, a by-product of water chlorination, induces aneuploidy in *Drosophila*. *Mutat. Res. Toxicol.* 261, 85–91.
- OSHA, 1990. Sampling and Analytical Methods. Carbon Dioxide In Workplace Atmospheres, Occupational Safety and Health Administration.
- Parrat, J., Donzé, G., Iseli, C., Perret, D., Tomicic, C., Schenk, O., 2012. Assessment of Occupational and Public Exposure to Trichloramine in Swiss Indoor Swimming Pools: A Proposal for an Occupational Exposure Limit. *Ann. Occup. Hyg.* 56, 264–277.
- Plewa, M.J., Wagner, E.D., Mitch, W.A., 2011. Comparative Mammalian Cell Cytotoxicity of Water Concentrates from Disinfected Recreational Pools. *Environ. Sci. Technol.* 45, 4159–4165.
- Pool Water Treatment Advisory Group, 2016. Code of Practice for Swimming Pool Water.
- Prescott, L.M., Jones, M.E., 1969. Modified methods for the determination of carbamyl aspartate. *Anal. Biochem.* 32, 408–419. [https://doi.org/10.1016/S0003-2697\(69\)80008-4](https://doi.org/10.1016/S0003-2697(69)80008-4)
- Reckhow, D.A., MacNeill, A.L., Platt, T.L., McClellan, J.N., 2001. Formation and degradation of dichloroacetonitrile in drinking waters. *J. Water Supply Res. Technol. - Aqua* 50, 1–13.
- Reid, E.E., 1940. The War Gases: Chemistry and Analysis (Sartori, Mario). *J. Chem. Educ.* 17, 199.

- Richardson, S.D., Plewa, M.J., Wagner, E.D., Schoeny, R., DeMarini, D.M., 2007. Occurrence, genotoxicity, and carcinogenicity of regulated and emerging disinfection by-products in drinking water: A review and roadmap for research. *Mutat. Res. Mutat. Res.* 636, 178–242.
- Rodríguez, F., 2000. Maximal oxygen uptake and cardiorespiratory response to maximal 400-m free swimming, running and cycling tests in competitive swimmers. *J. Sports Med. Phys. Fitness* 40, 87–95.
- Russo, M.A., Santarelli, D.M., O'Rourke, D., 2017. The physiological effects of slow breathing in the healthy human. *Breathe* 13, 298 LP – 309. <https://doi.org/10.1183/20734735.009817>
- Sander, R., 1999. Compilation of Henry's Law Constants for Inorganic and Organic Species of Potential Importance in Environmental Chemistry (Version 3).
- Schmalz, C., Frimmel, F.H., Zwiener, C., 2011. Trichloramine in swimming pools – Formation and mass transfer. *Water Res.* 45, 2681–2690. <https://doi.org/10.1016/J.WATRES.2011.02.024>
- Schwarzenbach, R.P., Gschwend, P.M., Imboden, D.M., 2003. Environmental organic chemistry. John Wiley & Sons.
- Seys, S.F., Feyen, L., Keirsbilck, S., Adams, E., Dupont, L.J., Nemery, B., 2015. An outbreak of swimming-pool related respiratory symptoms: An elusive source of trichloramine in a municipal indoor swimming pool. *Int. J. Hyg. Environ. Health* 218, 386–391. <https://doi.org/10.1016/j.ijheh.2015.03.001>
- Shang, C., Blatchley III, E.R., 1999. Differentiation and Quantification of Free Chlorine and Inorganic Chloramines in Aqueous Solution by MIMS. *Environ. Sci. Technol.* 33, 2218–2223.
- Shang, C., Gong, W.-L., Blatchley III, E.R., 2000. Breakpoint Chemistry and Volatile Byproduct Formation Resulting from Chlorination of Model Organic-N Compounds. *Environ. Sci. Technol.* 34, 1721–1728.
- Sivey, J.D., Roberts, A.L., 2012. Assessing the Reactivity of Free Chlorine Constituents Cl₂, Cl₂O, and HOCl Toward Aromatic Ethers. *Environ. Sci. Technol.* 46, 2141–2147. <https://doi.org/10.1021/es203094z>
- Snyder, M.P., Margerum, D.W., 1982. Kinetics of chlorine transfer from chloramine to amines, amino acids, and peptides. *Inorg. Chem.* 21, 2545–2550. <https://doi.org/10.1021/ic00137a005>
- Soltani, A., Sousaraei, A., Mirarab, M., Balakheyli, H., 2015. Interaction of CNCl molecule and single-walled AlN nanotubes using DFT and TD-DFT calculations. *J. Saudi Chem. Soc.*
- Spengler, J.D., Samet, J.M., McCarthy, J.F., 2001. Indoor Air Quality Handbook. McGraw-Hill Education, New York.
- Srinivasan, A., Chowdhury, P., Viraraghavan, T., 2008. Air Stripping in Industrial Waste Water Treatment.

- Tanaka, H., Bassett, D.R.J., Howley, E.T., Thompson, D.L., Ashraf, M., Rawson, F.L., 1997. Swimming training lowers the resting blood pressure in individuals with hypertension. *J. Hypertens.* 15, 651–657.
- Tardif, R., Rodriguez, M., Catto, C., Charest-Tardif, G., Simard, S., 2017. Concentrations of disinfection by-products in swimming pool following modifications of the water treatment process: An exploratory study. *J. Environ. Sci.* 58, 163–172. <https://doi.org/10.1016/J.JES.2017.05.021>
- Taucher, J., Hansel, A., Jordan, A., Lindinger, W., 1996. Analysis of compounds in human breath after ingestion of garlic using proton-transfer-reaction mass spectrometry. *J. Agric. Food Chem.* 44, 3778–3782.
- Thickett, K.M., McCoach, J.S., Gerber, J.M., Sadhra, S., Burge, P.S., 2002. Occupational asthma caused by chloramines in indoor swimming-pool air. *Eur. Respir. J.* 19, 827–832.
- Totten, L.A., Brunciak, P.A., Gigliotti, C.L., Dachs, J., Glenn, Nelson, E.D., Eisenreich, S.J., 2001. Dynamic Air–Water Exchange of Polychlorinated Biphenyls in the New York–New Jersey Harbor Estuary. *Environ. Sci. Technol.* 35, 3834–3840. <https://doi.org/10.1021/es010791k>
- Tsamba, L., Correc, O., Couzinet, A., 2020. +Chlorination by-products in indoor swimming pools: Development of a pilot pool unit and impact of operating parameters. *Environ. Int.* 137, 105566. <https://doi.org/10.1016/j.envint.2020.105566>
- Tucker, C.S., 1984. Carbon dioxide in TL Wellborn, Jr. and JR MacMillan (eds.) For fish farmers 84-2, Mississippi Co-operative Extension Service.
- U.S EPA, 2014. An Introduction to Indoor Air Quality (IAQ). Volatile Organic Compounds (VOCs).
- U.S EPA, 2009a. Drinking Water Standards and Health Advisories Table [WWW Document]. URL <https://www3.epa.gov/region9/water/drinking/files/dwshat-v09.pdf>
- U.S EPA, 2009b. National primary drinking water regulations.
- U.S EPA, 2006. National Primary Drinking Water Regulations: Stage 2 Disinfectants and Disinfection Byproducts Rule. (EPA-HQ-OW-2002-0043). Publication date 4th January, 2006, Federal Register 71.
- Uyan, Z.S., Carraro, S., Piacentini, G., Baraldi, E., 2009. Swimming pool, respiratory health, and childhood asthma: Should we change our beliefs? *Pediatr. Pulmonol.* 44, 31–37.
- Villanueva, C.M., Cantor, K.P., Grimalt, J.O., Malats, N., Silverman, D., Tardon, A., Garcia-Closas, R., Serra, C., Carrato, A., Castaño-Vinyals, G., Marcos, R., Rothman, N., Real, F.X., Dosemeci, M., Kogevinas, M., 2007. Bladder Cancer and Exposure to Water Disinfection By-Products through Ingestion, Bathing, Showering, and Swimming in Pools. *Am. J. Epidemiol.* 165, 148–156.

- Wahman, D.G., 2018. Web-Based Applications to Simulate Drinking Water Inorganic Chloramine Chemistry. *J. Am. Water Works Assoc.* 110, E43–E61. <https://doi.org/10.1002/awwa.1146>
- Weaver, W.A., Li, J., Wen, Y., Johnston, J., Blatchley, M.R., Blatchley III, E.R., 2009. Volatile disinfection by-product analysis from chlorinated indoor swimming pools. *Water Res.* 43, 3308–3318.
- Wei, J., Ye, B., Wang, W., Yang, L., Tao, J., Hang, Z., 2010. Spatial and temporal evaluations of disinfection by-products in drinking water distribution systems in Beijing, China. *Sci. Total Environ.* 408, 4600–4606. <https://doi.org/10.1016/j.scitotenv.2010.06.053>
- Weisel, C.P., Richardson, S.D., Nemery, B., Aggazzotti, G., Baraldi, E., Blatchley, E.R., Blount, B.C., Carlsen, K.-H., Eggleston, P.A., Frimmel, F.H., Goodman, M., Gordon, G., Grinshpun, S.A., Heederik, D., Kogevinas, M., LaKind, J.S., Nieuwenhuijsen, M.J., Piper, F.C., Sattar, S.A., 2009. Childhood Asthma and Environmental Exposures at Swimming Pools: State of the Science and Research Recommendations. *Environ. Health Perspect.* 117, 500–507.
- Weng, S., 2013. The dynamics of volatile disinfection byproducts in indoor, chlorinated swimming pools. Dissertations.
- Weng, S., Blatchley III, E.R., 2011. Disinfection by-product dynamics in a chlorinated, indoor swimming pool under conditions of heavy use: National swimming competition. *Water Res.* 45, 5241–5248.
- Weng, S., Li, J., Blatchley, E.R., 2012. Effects of UV254 irradiation on residual chlorine and DBPs in chlorination of model organic-N precursors in swimming pools. *Water Res.* 46, 2674–2682. <https://doi.org/10.1016/J.WATRES.2012.02.017>
- Weng, S., Weaver, W.A., Zare Afifi, M., Blatchley, T.N., Cramer, J.S., Chen, J., Blatchley, E.R., 2011. Dynamics of gas-phase trichloramine (NCl₃) in chlorinated, indoor swimming pool facilities. *Indoor Air* 21, 391–399. <https://doi.org/10.1111/j.1600-0668.2011.00710.x>
- Whitaker, H.J., Nieuwenhuijsen, M.J., Best, N.G., 2003. The relationship between water concentrations and individual uptake of chloroform: a simulation study. *Environ. Health Perspect.* 111, 688–694.
- White, G.C., 1999. The handbook of chlorination and alternative disinfectants, John Wiley & Sons, Inc., New York. [https://doi.org/10.1016/S1074-9098\(00\)00062-9](https://doi.org/10.1016/S1074-9098(00)00062-9)
- WHO, 2017. Guidelines for drinking-water quality, 4th edition, incorporating the 1st addendum, WHO. World Health Organization.
- WHO, 2006. Guidelines for Safe Recreational Water Environments, swimming pools and similar environments. Geneva.
- Wu, T., Földes, T., Lee, L.T., Wagner, D.N., Jiang, J., Tasoglou, A., Boor, B.E., Blatchley, E.R., 2021. Real-Time Measurements of Gas-Phase Trichloramine (NCl₃) in an Indoor Aquatic Center. *Environ. Sci. Technol.* 55, 8097–8107. <https://doi.org/10.1021/acs.est.0c07413>

- Zare Afifi, M., Blatchley, E.R., 2016. Effects of UV-based treatment on volatile disinfection byproducts in a chlorinated, indoor swimming pool. *Water Res.* 105.
- Zare Afifi, M., Blatchley, E.R. 3rd, 2015. Seasonal dynamics of water and air chemistry in an indoor chlorinated swimming pool. *Water Res.* 68, 771–783. <https://doi.org/10.1016/j.watres.2014.10.037>
- Zwiener, C., Richardson, S.D., DeMarini, D.M., Grummt, T., Glauner, T., Frimmel, F.H., 2007. Drowning in Disinfection Byproducts? Assessing Swimming Pool Water. *Environ. Sci. Technol.* 41, 363–372.

APPENDIX A. SAMPLE SPREAD SHEET FOR NCL₃ MODEL

Time	Δt (hr)	C_s NCl ₃ (mg/m ³)	C_l NCl ₃ (mg/L)	n Swimmer	∇_s (m ³)	Q_s (m ³ /hr)	A (m ²)	K_l (m/hr)
3/6/2019 8:05	0.00E+00	1.30E-01	5.55E-02	10	3.68E+04	3.27E+04	1.67E+03	2.44E-03
3/6/2019 8:15	1.67E-01	1.50E-01	5.87E-02	10	3.68E+04	3.27E+04	1.67E+03	2.44E-03
3/6/2019 8:25	1.67E-01	1.56E-01	6.19E-02	10	3.68E+04	3.27E+04	1.67E+03	2.44E-03
3/6/2019 8:35	1.67E-01	1.49E-01	6.51E-02	10	3.68E+04	3.27E+04	1.67E+03	2.44E-03
3/6/2019 8:45	1.67E-01	1.49E-01	6.83E-02	10	3.68E+04	3.27E+04	1.67E+03	2.44E-03
3/6/2019 8:55	1.67E-01	1.36E-01	7.16E-02	10	3.68E+04	3.27E+04	1.67E+03	2.44E-03
3/6/2019 9:05	1.67E-01	1.03E-01	7.48E-02	0	3.68E+04	3.27E+04	1.67E+03	2.44E-03
3/6/2019 9:15	1.67E-01	8.40E-02	7.80E-02	0	3.68E+04	3.27E+04	1.67E+03	2.44E-03
3/6/2019 9:25	1.67E-01	9.00E-02	8.12E-02	0	3.68E+04	3.27E+04	1.67E+03	2.44E-03
3/6/2019 9:35	1.67E-01	8.40E-02	8.44E-02	0	3.68E+04	3.27E+04	1.67E+03	2.44E-03
3/6/2019 9:45	1.67E-01	6.40E-02	8.76E-02	0	3.68E+04	3.27E+04	1.67E+03	2.44E-03
3/6/2019 9:55	1.67E-01	6.50E-02	9.08E-02	0	3.68E+04	3.27E+04	1.67E+03	2.44E-03
3/6/2019 10:05	1.67E-01	4.50E-02	9.41E-02	0	3.68E+04	3.27E+04	1.67E+03	2.44E-03
3/6/2019 10:15	1.67E-01	5.80E-02	9.53E-02	0	3.68E+04	3.27E+04	1.67E+03	2.44E-03
3/6/2019 10:25	1.67E-01	9.10E-02	9.65E-02	0	3.68E+04	3.27E+04	1.67E+03	2.44E-03
3/6/2019 10:35	1.67E-01	1.30E-01	9.78E-02	0	3.68E+04	3.27E+04	1.67E+03	2.44E-03
3/6/2019 10:45	1.67E-01	1.31E-01	9.90E-02	0	3.68E+04	3.27E+04	1.67E+03	2.44E-03
3/6/2019 10:55	1.67E-01	1.51E-01	1.00E-01	0	3.68E+04	3.27E+04	1.67E+03	2.44E-03
3/6/2019 11:05	1.67E-01	1.58E-01	1.01E-01	4	3.68E+04	3.27E+04	1.67E+03	2.44E-03
3/6/2019 11:15	1.67E-01	1.51E-01	1.03E-01	4	3.68E+04	3.27E+04	1.67E+03	2.44E-03
3/6/2019 11:25	1.67E-01	1.12E-01	1.04E-01	4	3.68E+04	3.27E+04	1.67E+03	2.44E-03
3/6/2019 11:35	1.67E-01	1.25E-01	1.05E-01	4	3.68E+04	3.27E+04	1.67E+03	2.44E-03
3/6/2019 11:45	1.67E-01	1.39E-01	1.06E-01	4	3.68E+04	3.27E+04	1.67E+03	2.44E-03
3/6/2019 11:55	1.67E-01	1.92E-01	1.08E-01	4	3.68E+04	3.27E+04	1.67E+03	2.44E-03
3/6/2019 12:05	1.67E-01	1.86E-01	1.09E-01	10	3.68E+04	3.27E+04	1.67E+03	2.44E-03

Continued

Time	$nK'C_i \Delta t/V_g$	$Q_g C_g \Delta t/V_g$	$K_L A C_i \Delta t/V_g$	ΔC_g	$K' \text{ (L/hr)}$	Model $C_g \text{ (mg/m}^3\text{)}$	RSS	Sum of RSS
3/6/2019 8:05	0.00E+00	0.00E+00	0.00E+00	0.00E+00	5.40E+03	1.30E-01	0.00E+00	1.1207E-01
3/6/2019 8:15	1.44E-02	1.93E-02	1.08E-03	-3.84E-03		1.26E-01	5.69E-04	
3/6/2019 8:25	1.52E-02	1.87E-02	1.14E-03	-2.43E-03		1.24E-01	1.04E-03	
3/6/2019 8:35	1.60E-02	1.84E-02	1.20E-03	-1.22E-03		1.23E-01	7.02E-04	
3/6/2019 8:45	1.67E-02	1.82E-02	1.26E-03	-1.91E-04		1.22E-01	7.12E-04	
3/6/2019 8:55	1.75E-02	1.82E-02	1.32E-03	6.84E-04		1.23E-01	1.69E-04	
3/6/2019 9:05	0.00E+00	1.83E-02	1.38E-03	-1.69E-02		1.06E-01	9.73E-06	
3/6/2019 9:15	0.00E+00	1.58E-02	1.44E-03	-1.43E-02		9.18E-02	6.08E-05	
3/6/2019 9:25	0.00E+00	1.36E-02	1.50E-03	-1.21E-02		7.97E-02	1.07E-04	
3/6/2019 9:35	0.00E+00	1.18E-02	1.56E-03	-1.03E-02		6.94E-02	2.13E-04	
3/6/2019 9:45	0.00E+00	1.03E-02	1.62E-03	-8.69E-03		6.07E-02	1.08E-05	
3/6/2019 9:55	0.00E+00	9.02E-03	1.68E-03	-7.34E-03		5.34E-02	1.35E-04	
3/6/2019 10:05	0.00E+00	7.93E-03	1.74E-03	-6.19E-03		4.72E-02	4.76E-06	
3/6/2019 10:15	0.00E+00	7.01E-03	1.76E-03	-5.25E-03		4.19E-02	2.58E-04	
3/6/2019 10:25	0.00E+00	6.23E-03	1.78E-03	-4.44E-03		3.75E-02	2.86E-03	
3/6/2019 10:35	0.00E+00	5.57E-03	1.81E-03	-3.76E-03		3.37E-02	9.27E-03	
3/6/2019 10:45	0.00E+00	5.01E-03	1.83E-03	-3.18E-03		3.05E-02	1.01E-02	
3/6/2019 10:55	0.00E+00	4.54E-03	1.85E-03	-2.69E-03		2.79E-02	1.52E-02	
3/6/2019 11:05	9.94E-03	4.14E-03	1.87E-03	7.68E-03		3.55E-02	1.50E-02	
3/6/2019 11:15	1.01E-02	5.28E-03	1.90E-03	6.68E-03		4.22E-02	1.18E-02	
3/6/2019 11:25	1.02E-02	6.27E-03	1.92E-03	5.83E-03		4.80E-02	4.09E-03	
3/6/2019 11:35	1.03E-02	7.14E-03	1.94E-03	5.11E-03		5.32E-02	5.16E-03	
3/6/2019 11:45	1.04E-02	7.89E-03	1.97E-03	4.49E-03		5.77E-02	6.62E-03	
3/6/2019 11:55	1.05E-02	8.56E-03	1.99E-03	3.97E-03		6.16E-02	1.70E-02	
3/6/2019 12:05	2.67E-02	9.15E-03	2.01E-03	1.95E-02		8.11E-02	1.10E-02	

APPENDIX B. SAMPLE SPREAD SHEET FOR CO₂ MODEL

Time	Δt (hr)	$C_g \text{ CO}_2$ (mg/m ³)	$C_l \text{ CO}_2^*$ (mg/L)	ΔC_g	$C_l \text{ CO}_2$ (mg/L)	$C_l(\text{actual-equilibrium})$	n Swimmer	N people
11/21/2019 12:14:15	0.00E+00	1.20E+03	9.99E-01	0.00E+00	1.10E+01	1.00E+01	0	89
11/21/2019 12:14:45	8.33E-03	1.18E+03	9.99E-01	-2.00E+01	1.10E+01	1.00E+01	0	89
11/21/2019 12:15:15	8.33E-03	1.19E+03	9.90E-01	4.90E+00	1.10E+01	1.00E+01	0	89
11/21/2019 12:15:45	8.33E-03	1.19E+03	9.82E-01	3.55E+00	1.10E+01	1.01E+01	0	89
11/21/2019 12:16:15	8.33E-03	1.19E+03	9.74E-01	-4.58E+00	1.10E+01	1.01E+01	0	89
11/21/2019 12:16:45	8.33E-03	1.19E+03	9.66E-01	6.01E+00	1.11E+01	1.01E+01	0	89
11/21/2019 12:17:15	8.33E-03	1.18E+03	9.58E-01	-8.29E+00	1.11E+01	1.01E+01	0	89
11/21/2019 12:17:45	8.33E-03	1.18E+03	9.51E-01	-1.56E+00	1.11E+01	1.01E+01	0	89
11/21/2019 12:18:15	8.33E-03	1.18E+03	9.43E-01	3.37E+00	1.11E+01	1.01E+01	0	89
11/21/2019 12:18:45	8.33E-03	1.18E+03	9.36E-01	-6.50E+00	1.11E+01	1.02E+01	0	89
11/21/2019 12:19:15	8.33E-03	1.18E+03	9.29E-01	-1.87E+00	1.11E+01	1.02E+01	0	89
11/21/2019 12:19:45	8.33E-03	1.17E+03	9.22E-01	-2.96E+00	1.11E+01	1.02E+01	0	89
11/21/2019 12:20:15	8.33E-03	1.17E+03	9.15E-01	-4.90E+00	1.11E+01	1.02E+01	0	89
11/21/2019 12:20:45	8.33E-03	1.17E+03	9.09E-01	7.68E-01	1.11E+01	1.02E+01	0	89
11/21/2019 12:21:15	8.33E-03	1.14E+03	9.02E-01	-2.57E+01	1.12E+01	1.03E+01	0	89
11/21/2019 12:21:45	8.33E-03	1.14E+03	8.96E-01	-5.48E+00	1.12E+01	1.03E+01	0	89
11/21/2019 12:22:15	8.33E-03	1.14E+03	8.90E-01	4.66E+00	1.12E+01	1.03E+01	0	89
11/21/2019 12:22:45	8.33E-03	1.14E+03	8.84E-01	-7.26E+00	1.12E+01	1.03E+01	0	89
11/21/2019 12:23:15	8.33E-03	1.13E+03	8.78E-01	-7.04E+00	1.12E+01	1.03E+01	0	89

Continued

Time	emCO ₂ (mg/hr)	NemCO ₂	emCO _{2x} (mg/hr)	nemCO _{2x}	V _g (m ³)	Q _g (m ³ /hr)	A (m ²)	K _i (m/hr)	C _{g,in} (mg/m ³)
11/21/2019 12:14:15	3.26E+04	2.90E+06	4.70E+05	0	3.68E+04	1.01E+05	1.67E+03	5.15E-02	7.25E+02
11/21/2019 12:14:45	3.26E+04	2.90E+06	4.70E+05	0	3.68E+04	1.01E+05	1.67E+03	5.15E-02	7.25E+02
11/21/2019 12:15:15	3.26E+04	2.90E+06	4.70E+05	0	3.68E+04	1.01E+05	1.67E+03	5.15E-02	7.25E+02
11/21/2019 12:15:45	3.26E+04	2.90E+06	4.70E+05	0	3.68E+04	1.01E+05	1.67E+03	5.15E-02	7.25E+02
11/21/2019 12:16:15	3.26E+04	2.90E+06	4.70E+05	0	3.68E+04	1.01E+05	1.67E+03	5.15E-02	7.25E+02
11/21/2019 12:16:45	3.26E+04	2.90E+06	4.70E+05	0	3.68E+04	1.01E+05	1.67E+03	5.15E-02	7.25E+02
11/21/2019 12:17:15	3.26E+04	2.90E+06	4.70E+05	0	3.68E+04	1.01E+05	1.67E+03	5.15E-02	7.25E+02
11/21/2019 12:17:45	3.26E+04	2.90E+06	4.70E+05	0	3.68E+04	1.01E+05	1.67E+03	5.15E-02	7.25E+02
11/21/2019 12:18:15	3.26E+04	2.90E+06	4.70E+05	0	3.68E+04	1.01E+05	1.67E+03	5.15E-02	7.25E+02
11/21/2019 12:18:45	3.26E+04	2.90E+06	4.70E+05	0	3.68E+04	1.01E+05	1.67E+03	5.15E-02	7.25E+02
11/21/2019 12:19:15	3.26E+04	2.90E+06	4.70E+05	0	3.68E+04	1.01E+05	1.67E+03	5.15E-02	7.25E+02
11/21/2019 12:19:45	3.26E+04	2.90E+06	4.70E+05	0	3.68E+04	1.01E+05	1.67E+03	5.15E-02	7.25E+02
11/21/2019 12:20:15	3.26E+04	2.90E+06	4.70E+05	0	3.68E+04	1.01E+05	1.67E+03	5.15E-02	7.25E+02
11/21/2019 12:20:45	3.26E+04	2.90E+06	4.70E+05	0	3.68E+04	1.01E+05	1.67E+03	5.15E-02	7.25E+02
11/21/2019 12:21:15	3.26E+04	2.90E+06	4.70E+05	0	3.68E+04	1.01E+05	1.67E+03	5.15E-02	7.25E+02
11/21/2019 12:21:45	3.26E+04	2.90E+06	4.70E+05	0	3.68E+04	1.02E+05	1.67E+03	5.15E-02	7.25E+02
11/21/2019 12:22:15	3.26E+04	2.90E+06	4.70E+05	0	3.68E+04	1.02E+05	1.67E+03	5.15E-02	7.25E+02
11/21/2019 12:22:45	3.26E+04	2.90E+06	4.70E+05	0	3.68E+04	1.02E+05	1.67E+03	5.15E-02	7.25E+02
11/21/2019 12:23:15	3.26E+04	2.90E+06	4.70E+05	0	3.68E+04	1.02E+05	1.67E+03	5.15E-02	7.25E+02

Continued

Time	$nK'(C_i - C_i^*) \Delta t / V_g$	$Q_g C_g^* \Delta t / V_g$	$K_L A (C_i - C_i^*) \Delta t / V_g$	$Q_g C_{g,in}^* \Delta t / V_g$	$n^* \text{emCO}_{2X}^* \Delta t / V_g$	$N^* \text{emCO}_2^* \Delta t / V_g$	delta C_g
11/21/2019 12:14:15	0	0.00E+00	0.00E+00	0.00E+00	0	0.00E+00	0.00E+00
11/21/2019 12:14:45	0	2.75E+01	1.95E-01	1.66E+01	0	6.58E-01	0.00E+00
11/21/2019 12:15:15	0	2.75E+01	1.96E-01	1.66E+01	0	6.58E-01	-1.00E+01
11/21/2019 12:15:45	0	2.72E+01	1.96E-01	1.66E+01	0	6.58E-01	-1.00E+01
11/21/2019 12:16:15	0	2.70E+01	1.96E-01	1.66E+01	0	6.58E-01	-9.81E+00
11/21/2019 12:16:45	0	2.68E+01	1.97E-01	1.66E+01	0	6.58E-01	-9.58E+00
11/21/2019 12:17:15	0	2.66E+01	1.97E-01	1.66E+01	0	6.58E-01	-9.35E+00
11/21/2019 12:17:45	0	2.63E+01	1.97E-01	1.66E+01	0	6.58E-01	-9.13E+00
11/21/2019 12:18:15	0	2.61E+01	1.98E-01	1.66E+01	0	6.58E-01	-8.92E+00
11/21/2019 12:18:45	0	2.59E+01	1.98E-01	1.66E+01	0	6.58E-01	-8.71E+00
11/21/2019 12:19:15	0	2.57E+01	1.98E-01	1.66E+01	0	6.58E-01	-8.50E+00
11/21/2019 12:19:45	0	2.55E+01	1.99E-01	1.66E+01	0	6.58E-01	-8.30E+00
11/21/2019 12:20:15	0	2.53E+01	1.99E-01	1.66E+01	0	6.58E-01	-8.11E+00
11/21/2019 12:20:45	0	2.52E+01	2.00E-01	1.66E+01	0	6.58E-01	-7.92E+00
11/21/2019 12:21:15	0	2.51E+01	2.00E-01	1.67E+01	0	6.58E-01	-7.76E+00
11/21/2019 12:21:45	0	2.50E+01	2.00E-01	1.67E+01	0	6.58E-01	-7.60E+00
11/21/2019 12:22:15	0	2.49E+01	2.01E-01	1.68E+01	0	6.58E-01	-7.44E+00
11/21/2019 12:22:45	0	2.48E+01	2.01E-01	1.68E+01	0	6.58E-01	-7.29E+00
11/21/2019 12:23:15	0	2.47E+01	2.01E-01	1.68E+01	0	6.58E-01	-7.14E+00

Continued

Time	K' (L/hr)	Model C _s (mg/m ³)	RSS	Sum of RSS
11/21/2019 12:14:15	1.00E+04	1.20E+03	0.00E+00	7.23E+07
11/21/2019 12:14:45		1.20E+03	4.00E+02	
11/21/2019 12:15:15		1.19E+03	2.57E+01	
11/21/2019 12:15:45		1.18E+03	7.25E+01	
11/21/2019 12:16:15		1.17E+03	1.89E+02	
11/21/2019 12:16:45		1.16E+03	8.60E+02	
11/21/2019 12:17:15		1.15E+03	9.23E+02	
11/21/2019 12:17:45		1.14E+03	1.44E+03	
11/21/2019 12:18:15		1.13E+03	2.52E+03	
11/21/2019 12:18:45		1.13E+03	2.75E+03	
11/21/2019 12:19:15		1.12E+03	3.49E+03	
11/21/2019 12:19:45		1.11E+03	4.15E+03	
11/21/2019 12:20:15		1.10E+03	4.58E+03	
11/21/2019 12:20:45		1.09E+03	5.83E+03	
11/21/2019 12:21:15		1.09E+03	3.41E+03	
11/21/2019 12:21:45		1.08E+03	3.67E+03	
11/21/2019 12:22:15		1.07E+03	5.28E+03	
11/21/2019 12:22:45		1.06E+03	5.28E+03	
11/21/2019 12:23:15		1.06E+03	5.30E+03	